technische universität
dortmund

mpi
dortmund

Knock off and on:
a novel approach to autophagy modulation

Dissertation

Zur Erlangung des akademischen Grades
eines Doktors der Naturwissenschaften der
Fakultät für Chemie an der Technischen Universität Dortmund

angefertigt am

Max-Planck Institut für molekulare Physiologie
in Dortmund

vorgelegt von

Laura Kristin Klewer

Juni 2017

Die vorliegende Arbeit wurde in der Zeit von September 2012 bis Juni 2017 am Max-Planck-Institut für molekulare Physiologie in Dortmund unter der Anleitung von Dr. Yao-Wen Wu und Prof. Dr. Roger Goody durchgeführt.

1. Gutachter: Prof. Dr. Roger Goody
2. Gutachter: Prof. Dr. Philippe Bastiaens

In the context of this thesis the following articles were accepted for publication:

S. Voss, **L. Klewer**, and Y.-W.Wu. Chemically induced dimerization: reversible and spatiotemporal control of protein function in cells. *Curr Opin Chem Biol*, 28:194201, 2015.

L. Klewer and Y.-W.Wu. Knock off and on - A novel Approach to Autophagy Modulation. *In preparation.*

Contents

Abbreviations **vii**

Summary **viii**

Zusammenfassung **x**

1 Introduction **1**
1.1 Autophagy: An Overview . . . 1
1.1.1 Regulation of Autophagy . . . 2
1.1.2 Autophagosome Formation and Maturation . . . 3
1.1.3 Studying Self-Digestion: Autophagy Modulation . . . 8
1.2 Inducible Dimerization . . . 10
1.2.1 Chemically Inducible Dimerization . . . 10
1.2.2 Photoinducible Dimerization Systems . . . 16
1.2.3 Optogenetic Dimerization Systems . . . 19
1.2.4 Biological Applications of Inducible Dimerization Systems . . . 22

2 Materials and Methods **28**
2.1 Materials . . . 28
2.1.1 Chemicals . . . 28
2.1.2 Enzymes and Standards . . . 29
2.1.3 Cell Culture Media and Reagents . . . 30
2.1.4 Antibodies . . . 30
2.1.5 Kits . . . 31
2.1.6 Consumables . . . 31
2.1.7 Instruments . . . 32
2.1.8 Bacterial Strains . . . 33
2.1.9 Eucaryotic Cell Lines . . . 33
2.1.10 Buffers and Growth Media . . . 34
2.1.11 Expression Plasmids . . . 36
2.2 Methods . . . 38
2.2.1 Methods in Molecular Biology . . . 38
2.2.2 Methods in Cell Biology . . . 42
2.2.3 Biochemical Methods . . . 46
2.2.4 Microscopy . . . 49

3 Results and Discussion **52**

3.1 Establishing the Knock Off and On Strategy . . . 52
3.1.1 Knock Off Induces Translocalization of Exogenous PI3K Prey Proteins . . . 53
3.1.2 Knock Off Induces Mislocalization of Endogenous PI3K Prey Proteins . . . 55
3.1.3 Nanobodies as Bait in the Knock Off and On System . . . 58
3.2 Modulation of Autophagosome Formation with Knock Off and On . . . 60
3.2.1 Perturbation of PI3K Proteins Impairs Autophagosome Formation . . . 61
3.2.2 Dynamics of Autophagosome Formation . . . 64
3.2.3 Dynamics of Autophagosome Formation and Maturation . . . 67
3.3 UVRAGs Function in Autophagy . . . 70
3.3.1 Generation of an UVRAG-specific Beclin1 . . . 71
3.3.2 Generation of an Atg14L-specific Beclin1 . . . 74
3.3.3 UVRAGs Function in Autophagosome Formation and Maturation . . . 74
3.4 Spatial Organization of Autophagosome Biogenesis . . . 80

4 Conclusions and Perspectives **84**

Appendices **110**

List of Abbreviations

ddH_2O	Double-distilled Water
E.coli	*Escherichia coli*
ActA	Listerial Actin A
AMP	Adenosine Monophosphate
AMPK	AMP-Activated Protein Kinase
Atg	Autophagy Related Gene
ATP	Adenosine Triphosphate
BATS	Barkor/Atg14L Autophagosome Targeting Sequence
Bcl-2	B-Cell Lymphoma 2
BG	Benzylguanine
BLUF	Blue-Light-Using FAD
BME	β-Mercaptoethanol
cAMP	Cyclic Adenosine Monophosphate
Cb5	Cytochrome b5
CIB1	Cryptochrome-Interacting Basic-Helix-Loop-Helix 1
CID	Chemically Induced Dimerization
COP1	Constitutively Morphogenetic 1
DEACM	[7-(Diethylamino)Coumarin-4-yl]Methyl
Deptor	DEP-Domain-Containing mTOR-Interacting Protein
DFCP1	Double FYVE-Containing Protein 1
DMEM	Dulbecco's Modified Eagle Medium
DMNB	4,5-Dimethoxy-2-Nitrobenzyl
DMNPP	2-(4,5-Dimethoxy-2-Nitrophenyl) Propyl
DMSO	Dimethyl Sulfoxide
DNA	Deoxyribonucleic Acid
DPBS	Dulbecco's Phosphate Buffered Saline
EBSS	Earl's Balanced Salt Solution
EDTA	Ethylenediaminetetraacetic Acid
EGFP	Enhanced Green Fluorescent Protein
ER	Endoplasmatic Reticulum
ERGIC	ER-Golgi Intermediate Compartment
ERGIC53	ER-Golgi intermediate compartment 53 kDa protein
Erk	Extracellular-Signal-Regulated Kinase
FACS	Fluorescence–activated Cell Sorting
FAD	Flavin Adenine Dinucleotide
FBS	Fetal Bovine Serum

FIP200	Focal Adhesion Kinase Family-Interacting Protein 200 kDa
FKBP12	FK506-Binding Protein of Size 12 kD
FKF1	Flavin-Binding Kelch Repeat F-Box 1
FMN	Flavin Mononucleotide
GA	Gibberellic Acid
GABARAP	Gamma-Aminobutyrate Receptor-Associated Protein
GAP	GTPase-Activating Protein
GEF	Guanine Nucleotide Exchange Factor
GI	Gigenta
GPCR	G-Protein-Coupled Receptors
GR	Glucocorticoid Receptor
GTP	Guanosine Triphosphate
GYT	Glycerol Yeast Extract Tryptone
HA	Human Influenza Hemagglutinin
hAGT	O^6-Alkylguanine-DNA Alkyltransferase
HBSS	Hank's Balanced Salt Solution
HDAC6	Histone Deacetylase 6
HEK	Human Embryonic Kidney
HeLa	Henrietta Lacks
HOPS	Homotypic Fusion and Vacuolar Protein Sorting
KRas	Kirsten Rat Sarcoma
LB	Lysogeny broth
LC3	Light Chain 3
LIR	LC3-Interacting Region
LITEs	Light-Inducible Transcriptional Effectors
LKB1	Liver Kinase B1
LOV	Light-Oxygen-Voltage
MCF7	Michigan Cancer Foundation-7
MEME	Minimum Essential Medium Eagle
MeNPOC	α-Methyl-6-Nitropiperonyloxycarbonyl
MeNV	Methyl-6-Nitroveratryl
mLST8	mTOR-Associated Protein LST8
mTOR	Mammalian Target of Rapamycin
NaCl	Sodium Chloride
NBR1	Neighbor of BRCA1 Gene 1 Protein
NDP52	Nuclear Domain 10 Protein 52
NO	Nitric Oxide
NVOC	2-(4,5-Dimethoxy-2-Nitrophenyl) Propyl
OATL1	Ornithine Aminotransferase-Like 1
OD	Optical Density
PAS	Period-ARNT-Singleminded
PCR	Polymerase Chain Reaction

PDK1	Phosphoinositide-Dependent Kinase 1
PEG	Polyethylenglycol
PFA	Paraformaldehyde
PI3K	Phosphoinositide 3-Kinase
PI3KC1a	Phosphatidylinositol-3-OH kinase
PIF	Phytochrome-Interacting Factors
PIP_3	Phosphatidylinositol(3,4,5)-Trisphosphate
PRAS40	Proline-Rich Akt Substrate of 40 kDa
PYL	PYR1-like
PYR	Pyrabactin Resistance
Rag	Ras-Related GTP-Binding Protein
Raptor	Regulatory Associated Protein of mTOR
RCAR	Regulatory Component of the ABA Receptor
rcf	Relative Centrifugal Force
Rheb	Ras Homolog Enriched in Brain
RIPA	Radioimmunoprecipitation Assay
rpm	Rounds per Minute
SAP	Shrimp Alkaline Phosphatase
SDS	Sodium Dodecylsulphate
SLC	Solute Carrier
SLF	Synthetic Ligand of FKBP
SNARE	Soluble N-ethylmaleimide-Sensitive Factor-Attachment Protein Receptor
SQSTM1	Sequestosome-1
TBST	Tris-buffered saline with Tween
TECPR1	Tectonin β-Propeller Repeat-Containing Protein 1
TGN	Trans-Golgi Network
TMP	Trimethoprim
TSC	Tuberous Sclerosis Complex
TSS	Transformation and Storage Solution
TULIP	Tunable Light-Inducible Dimerization Tags
ULK1	Uncoordinated 51-Like Kinase 1
UVRAG	UV Radiation Resistance-Associated Gene Protein
v-ATPase	vacuolar H^+-ATPase
VAMP	Vesicle-Associated Membrane Protein
Vps34	Vacuolar Protein Sorting 34
Vti1b	Vesicle Transport Through Interaction With t-SNAREs Homolog 1B
WIPI	WD-Repeat Protein Interacting With Phosphoinositides
Zdk	Zdark

Summary

Macroautophagy (autophagy hereafter) is a dynamic cellular recycling process, which is essential to maintain cellular homeostasis and cope with metabolic stress. Central to the process are double-layered vesicles, termed autophagosomes, which form *de novo* and engulf cytoplasmic target material before fusing with lysosomes to become autolysosomes. In the autolysosomes, autophagic cargo is degraded and released back into the cytoplasm as nutrients or metabolic precursors [1,2].

Autophagosome formation and nucleation of the isolation membrane are orchestrated by three protein complexes, mTORC1, ULK1 and PI3KC1 [3]. Two distinct PI3K complexes have been reported, each containing the core components Vps34, p150, Beclin1 and either Atg14L or UVRAG as a fourth subunit [4,5]. Upon autophagy induction, the Atg14L-containing PI3K complex is recruited to the endoplasmatic reticulum (ER). Here, the lipid kinase Vps34 generates phosphatidylinositol 3-phosphate (PI3P) leading to nucleation of a scaffolding platform, termed omegasome, from which the autophagosome is arises [6,7].

UVRAGs exact function in autophagy remains elusive. The UVRAG-containing PI3K complex is supposedly involved in autophagosome formation, but UVRAG also interacts with the HOPS complex to activate the small GTPase Rab7 and stimulate autophagosome-lysosome fusion [4,8,9]. Furthermore, UVRAG plays a role in the generation and trafficking of Atg9 vesicles, supplying membrane to the forming autophagosome [10]. Besides its function in autophagy, UVRAG participates in maintaining genomic stability, retrograde Golgi-ER transport and many other vesicular trafficking or fusion processes [11,12]. Since vesicular transport pathways are naturally intertwined, this makes it even more difficult to pinpoint UVRAGs exact role in autophagy [13].

The controversy about UVRAG's function in autophagy highlights the need for new techniques to study the spatiotemporal context of highly dynamic processes *in vivo*. Traditional techniques are mostly based on altering the gene expression levels by knock out/down or on small molecule modulators of protein function. However, gene silencing is a chronic and global perturbation, which takes hours to days and often alters cellular processes altogether. Chemical inhibitors or inducers allow for fast and efficient perturbations, but many of them lack specificity or show time- and dose-dependent side effects [14]. We thus created the knock off and on approach, which is based on chemically inducible dimerization and facilitates rapid, specific inhibition and re-activation of autophagy *in vivo*. Inducible dimerization systems have become a widespread tool, since dimerization can be induced on a timescale of seconds and with subcellular spatial resolution. The dimerization strategies differ between photoinducible and chemically inducible systems, but the basic principle, remains the same: two proteins are artificially brought into close proximity. Chemically induced dimerization forces proteins into high-affinity interaction through addition of a small molecule, termed dimerizer. Application and dosage control of dimerizers are simple, they can penetrate tissues inaccessible to light, the dimerization kinetics can be rapid and some systems are even reversible [15,16,17].

The SLF'-TMP dimerizer utilized in this thesis is superior to most chemical dimerization systems available to date [18,19]. SLF', a synthetic ligand of the FKBP12, binds with over 1000-fold selectivity to FKBP', the F36V mutant of FKBP12 [20]. Trimethoprim (TMP) is highly selective for the *E.coli* protein

eDHFR. SLF'-TMP dimerizes FKBP'- and eDHFR-fusion proteins rapidly ($t_{1/2} = 44$ s) and is completely bioorthogonal in eukaryotic systems. SLF'-TMP-mediated crosslinking is also rapidly reversible by outcompeting eDHFR-binding with TMP and may be applied orthogonal to rapamycin-based systems. In the knock off and on approach, we employed the SLF'-TMP dimerization system to conditionally mislocalize autophagic target proteins. The knock off and on strategy is based on a bait and prey principle, in which the localization-dependent function of endogenous prey proteins is disrupted by re-routing them to another cellular compartment. Typically, the bait protein is an exogenous FKBP'-fusion protein, which co-localizes with an eDHFR-tagged cellular anchor upon dimerizer addition. Due to its overexpression, the bait protein is highly concentrated, so that mislocalization of the bait-prey complex results in complete depletion and functional disruption of the endogenous prey protein (knock off). Correct localization and function of the prey protein is re-established upon addition of the competitor (knock on). In this study, we modulated the autophagy process by conditionally mislocalizing PI3K complex proteins to the plasma membrane to disrupt their function in autophagosome formation. As a proof of principle, we successfully employed an anti-Vps34 nanobody as bait in knock off/on system, which demonstrates the technique's broad applicability to any protein of interest. By knock off of PI3K complex proteins, we were able to stop the autophagy process during isolation membrane formation and re-activate it through knock on. Using different autophagy markers, we studied the spatiotemporal aspect of PI3K complex function and found that it participates in the early stages of isolation membrane formation, but not in autophagosome transport or maturation. It is interesting to note that the functionality of the complex, i.e. Vps34s kinase activity, is only maintained in presence of the core components, Beclin1 and Atg14L. Furthermore, the complexes function appears to be related to its intracellular localization, as autophagosome formation was enhanced upon re-routing PI3K proteins to the ER. Using the knock off/on approach, we also determined that UVRAG is essential for autophagosome formation and maturation. Based on our observations, we hypothesize that UVRAG is first involved in generation, transport and fusion of Atg9 vesicles to support autophagosome formation and later coordinates trafficking and lysosomal fusion of the closed autophagosome.

Taken together, our results demonstrate that the knock off/on approach is very powerful new tool, especially in combination with traditional autophagy assays. Knock off/on allows to rapidly perturb and monitor autophagosome formation and maturation in live cells, which has not been possible so far.

Zusammenfassung

Makroautophagie (nachstehend Autophagie) ist ein zellulärer Recyclingprozess, der zur Erhaltung der Homöostase und zur Bewältigung von Zellstress dient. Von zentraler Bedeutung sind dabei Doppelmembranvesikel (Autophagosomen), die *de novo* entstehen und das für den Verdau bestimmte, zytoplasmische Zielmaterial umschließen, um dann mit Lysosomen zu Autolysosomen zu verschmelzen. Hier wird das Zielmaterial abgebaut und in Form von Nährstoffen oder metabolischen Vorläufern wieder ins Zytoplasma freigesetzt[1,2].

Die Bildung von Autophagosomen wird hauptsächlich von den drei Proteinkomplexen mTORC1, ULK1 und PI3K gesteuert[3]. Der PI3K-Komplex liegt dabei in zwei Konfiguration vor: Er enthält immer die Kernkomponenten Vps34, p150 und Beclin1 und als vierte Untereinheit Atg14L oder UVRAG[4,5]. Sobald Autophagie induziert wird, lokalisiert der Atg14L-PI3K-Komplex zum endoplasmatischen Retikulum (ER) und die Lipidkinase Vps34 katalysiert die Bildung von mPhosphatidylinositol-3-phosphat (PI3P). Dies führt zur Entstehung von formgebenden Plattformen, den Omegasomen, in denen schließlich das Autophagosom gebildet wird[6,7].

Die Funktion von UVRAG im Autophagieprozess ist noch nicht vollständig erschlossen. Der UVRAG-PI3K-Komplex ist wahrscheinlich an der Entstehung von Autophagosomen beteiligt, aber das Protein interagiert auch mit dem HOPS Komplex , was zur Aktivierung der kleinen GTPase Rab7 führt und so die Fusion von Autophagosomen und Lysosomen einleitet[4,8,9]. Darüberhinaus vermittelt UVRAG die Bildung und den Transport von Atg9-Vesikeln, welche Membranbestandteile zum entstehenden Autophagosom liefern[10]. UVRAG ist außerdem an der Erhaltung der genomischen Stabilität, dem Golgi-ER-Transport und verschiedenen anderen vesikulären Transport- und Fusionsprozessen beteiligt. Dies erschwert es zusätzlich, die genaue Funktion UVRAGs im Autophagieprozess zu definieren[13].

Die Debatte um UVRAGs Funktion unterstreicht die Notwendigkeit für neue Methoden zur Untersuchung hoch dynamischer Prozesse *in vivo* und mit höherer zeitlicher Auflösung. Herkömmliche Methoden konzentrieren sich meist darauf, die Expression bestimmter Gene zu verändern (knock out/down) oder bedienen sich kleiner Moleküle, um einzelne Proteine zu beeinflussen. Das chronische An- oder Ausschalten von Genen kann jedoch einige Stunden oder Tage dauern und betrifft häufig mehr als einen zellulären Prozess. Chemische Modulatoren hingegen wirken innerhalb von Minuten, sind aber häufig unspezifisch und zeigen zeit- und dosisabhängige Nebenwirkungen[14]. Wir haben daher die knock off/on-Strategie entwickelt, welche auf induzierbarer, chemischer Dimerisierung basiert und schnelle, spezifische Inhibition und Reaktivierung von Autophagie ermöglicht. Induzierbare Dimerisierungssysteme sind inzwischen ein weit verbreitetes Werkzeug, da die Dimerisierung innerhalb von Sekunden und mit subzellulärer Auflösung induziert werden kann. Die Dimerisierungsstrategien werden in fotoinduziert und chemisch induziert unterteilt, aber das Grundprinzip bleibt dasselbe: Zwei Proteine werden künstlich in räumliche Nähe gebracht. Chemisch induzierte Dimerisierung zwingt Protein in eine hoch affine Bindung durch Zugabe eines kleines Moleküls, den Dimerisierer. Die Anwendung und Dosierung von Dimerisierern ist einfach, sie können in lichtundurchdringliche Gewebe eindringen, die Dimerisationsgeschwindigkeit ist hoch und einige Systeme sind sogar reversibel[15,16,17].

Der SLF'-TMP-Dimerisierer ist den meisten bekannten Dimerisierungssystemen überlegen[18,19]. SLF', ein synthetischer Ligand von FKBP12, bindet mit über 1000-facher Spezifität an FKBP', die F36V Mutante von FKBP12, während Trimethoprim (TMP) äußerst selektiv an das *E.coli* Protein eDHFR bindet. SLF'-TMP dimerisiert FKBP'- und eDHFR-Fusionsprotein innerhalb von Sekunden ($t_{1/2} = 44$ s) und ist bioorthogonal in eukaryontischen Systemen. SLF'-TMP-basierte Dimerisierung ist zudem innerhalb von Sekunden durch Zugabe von TMP umkehrbar und kann auch parallel zu Rapamycin-basierten Systemen angewandt werden. In der knock off/on Strategie wurde dieses Dimerisierungssystem benutzt, um Fehllokalisierung von Autophagieproteinen zu induzieren. Dabei wurde eine Bait und Prey Strategie angewandt, um endogene Proteine in ein anderes zelluläres Kompartment umzuleiten und damit ihre lokalisationsabhängige Funktion zu inhibieren. Als Bait-Protein wurde ein stark überexprimiertes FKBP'-Fusionsprotein gewählt, das bei Zugabe von Dimerisierer an ein eDHFR-Fusionsprotein bindet, welches als zellulärer "'Anker"' fungiert. Aufgrund der starken Überexprimierung ist das Bait-Protein hochkonzentriert, sodass Fehllokalisierung des Bait-Prey-Komplexes zur totalen Depletion und damit funktionalen Inhibierung des endogenen Zielproteins führt (knock off). Die korrekte Lokalisierung des Zielproteins kann anschließend durch Zugabe von TMP wiederhergestellt werden (knock on).
In dieser Studie wurde der Autophagieprozess durch induzierte Fehllokalisation von Autophagieproteinen zur Plasmamembran gesteuert. Dabei wurde auch ein anti-Vps34 Nanokörper als Bait-Protein eingesetzt, was es ermöglicht, die knock off/on-Methode auf jedes zelluläre Protein anzuwenden. Durch knock off von PI3K-Komplexproteinen, konnten wir den Autophagieprozess während der Induktionsphase erfolgreich stoppen und reaktivieren. Unter Verwendung verschiedener Autophagiemarker wurde die Funktionsweise des PI3K-Komplexes untersucht und es zeigte sich, dass der PI3K-Komplex während der frühen Autophagiestadien sehr wichtig ist, aber während des Transportes und der Fusion von Autophagosomen mit Lysosomen keine Rolle spielt. Interessanter Weise ist die Kinasaseaktivität von Vps34 nur gegeben, wenn alle Kernkomponenten des Komplexes, d.h. Beclin1 und Atg14L, vorhanden sind. Darüberhinaus scheint die Funktion des Komplexes im direkten Zusammenhang mit seiner zellulären Lokalisation zu stehen, da die Bildung von Autophagosomen zunahm, als der PI3K-Komplex an das ER lokalisiert wurde. Unter Verwendung der knock off/on Strategie konnten wir außerdem zeigen, dass UVRAG zur Bildung, aber auch zur Reifung von Autophagosomen benötigt wird. Basierend auf unseren Beobachtungen nehmen wir daher an, dass UVRAG zunächst die Bildung, den Transport und die Fusion von Atg9-Vesikeln reguliert und danach den Transport und die Fusion von autophagischen Vesikeln koordiniert.
Zusammenfassend lässt sich anhand der vorliegenden Ergebnisse feststellen, dass die knock off/on-Strategie ein sehr vielversprechendes, neues Werkzeug darstellt, insbesondere in Kombination mit traditionellen Autophagie-Assays. Knock off/on ermöglicht es die Bildung und Reifung von Autophagosomen zu beeinflussen und gleichzeitig in lebenden Zellen zu beobachten, was bisher so nicht möglich war.

1 Introduction

1.1 Autophagy: An Overview

Living organisms are in constant state of cellular renovation, continuously remodeling, degrading and re-synthesizing the components they are made of. This renovation process is tightly regulated to maintain cellular homeostasis and at the same time guarantee a steady supply of building blocks as well as an efficient clearance of old or dysfunctional material. In eukaryotes, cellular components are degraded by two major systems: the proteasome and the lysosome. Whereas the proteasome is largely responsible for clearance of ubiquitinated substrates, the lysosome is supplied with proteins, organelles and extracellular material by the endocytic or the autophagic pathway. Typically, endocytosis shuttles extracellular material to the lysosome, while cytoplasmic components are delivered by autophagy[21].
The term 'autophagy' is a conglomerate of the Greek words 'auto' (self) and 'phagy' (eating) and is evolutionary conserved throughout all kingdoms of life. Macroautophagy (autophagy hereafter) is crucial to maintain cellular integrity or cope with metabolic stress, which is why malfunction of autophagy has been linked to a wide range of diseases[22,23]. Central to the process, are double-layered vesicles, termed autophagosomes, which form *de novo* and capture cytoplasmic target material before fusing with lysosomes to become autolysosomes[1]. In the autolysosomes, autophagic cargo is degraded and released back into the cytoplasm as nutrients or metabolic precursors[2].
The process is typically divided in three phases: initiation, sequestration and maturation of autophagosomes. In mammalian cells, sequestration and maturation, i.e. formation, closure and lysosomal fusion of the autophagosome are orchestrated by two protein complexes, ULK1 and PI3KC1, and two ubiquitin-like conjugation systems Atg12-5-16L and LC3-PE. Overall autophagic activity is largely controlled by the master regulator mTOR and strongly related to absence or presence of nutrients and growth factors[2,3].
Contrary to popular belief, autophagy was first described in a written report in 1860 and has supposedly been known to the scientific community even longer. However, the cellular process referred to as autophagy nowadays was discovered by Christian de Duve in 1963. Using electron microscopy, de Duve first identified the end point of autophagy, the lysosome, in 1955 and almost a decade later he suggested the existence of an 'autophagic' sequestration pathway, which delivers cytoplasmic material to the lysosome.
In the following four decades, understanding of the autophagy pathway progressed slowly, as most data was obtained from electron microscopy and detection of autophagosomes or lysosomes remained challenging due to their short life time and heterogeneous morphology. A milestone in autophagy research was the identification of autophagy genes in the yeast *Saccharomyces cerevisiae* by Nobel Laureate Yoshinori Ohsumi in the early 1990s and the observation that the process could be initiated by various modes of starvation. This finally provided a readout to monitor autophagy and gave way to a vast number of studies cataloging the yeast autophagy genome. In 1998 Mizushima and co-workers discovered the first autophagy genes in mammalian cells demonstrating that the process is conserved from yeast to mammals and starting the long process of identifying mammalian homologs. Two years later,

the Yoshimori lab found the mammalian homolog of the widespread yeast autophagosome marker Atg8 (LC3) thus paving the way for the development of numerous assays to monitor mammalian autophagy. Since then, understanding of the autophagic pathway has progressed tremendously and the autophagic machinery has been largely identified and extensively characterized[3].

1.1.1 Regulation of Autophagy

Cell homeostasis is of fundamental importance to maintain growth, function and development. To keep an efficient balance between anabolic and catabolic processes, most cell types continiously perform autophagy on a basal level and merely enhance the process upon a starvation or stress signal. Typically, these signals originate from the extracellular space, are detected at the plasma membrane, in the cytosol or in cellular organelles and then forwarded to the autophagic machinery. Here, mTOR is the key regulator activating or inhibiting autophagy depending on the cells nutritional status[24,25].
The mTORC1 complex, comprised of the serine/threonine kinase mTOR, raptor, deptor, PRAS40 and mLST8, positively regulates glycolysis as well as synthesis of proteins, lipids or nucleotides while it suppresses autophagy by inhibiting ULK1s kinase activity. The factors regulating mTORC1 are as diverse as the output it produces: it reacts to levels of oxygen, amino acids, glucose, ATP and growth factors, but also to signals from oncogenes, pathogens or mechanical stress (see Figure 1.1). Autophagy, on the other hand, is mainly governed by the absence or presence of amino acids and growth factors[3].
In general, limited availability of amino acids triggers autophagy by disrupting mTORC1s activity. However, the specific regulatory mechanisms differ, depending on the individual amino acid or their combination. Especially, leucine, arginine and glutamine levels appear to be pivotal for mTORC1 activity. Amino acid sensing via mTORC1 is mediated by the GTPases RagA/B and RagC/D, which form a heterodimer and interact directly with raptor. The Rag GTPases are activated depending on the cellular amino acid levels. If extracellular amino acids are available, L-glutamine is initially shuttled into the cell by its high-affinity membrane transporter SLC1A5. The high L-glutamine levels then facilitate uptake of other essential amino acids through the bidirectional transporter SLC7A5-SLC3A2, which uses the intracellular L-glutamine as an efflux substrate[26].
In presence of high amino acid concentrations RagA/B exchanges guanosine diphosphate (GDP) for guanosine triphosphate (GTP) and consequently assumes its active conformation, while RagC/D exchanges GTP for GDP and is inactivated. The nucleotide exchange is mediated by v-ATPase and a complex termed Ragulator that resides at the lysosome. Subsequently, activated RagA/B forms a heterodimer with inactive RagC/D, which then binds to raptor and sequesters mTORC1 to the lysosomal surface through interaction with the Ragulator complex[27]. Here, mTORs kinase activity is dramatically upregulated through interaction with another small GTPase, termed Rheb, which resides at lysosomes and is a potent activator of mTORC1[28].
Rheb also appears to serve as molecular 'and-gate' integrating growth factor signaling with nutrient sensing. To interact with Rheb, mTORC1 needs to be recruited to lysosomes by the amino acid-sensing Rag-Ragulator pathway. Yet, for subsequent activation of mTORC1, Rheb needs to be activated by growth factor signaling. This mode of signal integration also explains the dominance of amino acid sensing over growth factor signaling: in nutrient-rich conditions cell development may be stimulated, but in starvation conditions mTORC1 is inhibited to induce autophagy and restore intracellular amino acid levels first[26].
In contrast to amino acid-sensing, growth factor signaling communicates the nutritional status of the whole tissue or organism to control proliferation, development and differentiation. mTORC1 is mainly

regulated by growth factors binding to receptor tyrosine kinases or G-protein-coupled receptors (GPCR) at the cell surface. Insulin binding to its GPCR, for instance, triggers a major mTORC1-regulating signaling cascade starting from the phosphatidylinositol-3-OH kinase (PI3KC1a).
Upon growth factor binding, PI3KC1a is activated and generates increased levels of phosphatidylinositol (3,4,5)-triphosphate (PIP_3) at the plasma membrane. This attracts the serine/threonine kinase PDK1, which in turn activates the kinase Akt and thereby disrupts a protein complex termed TSC. The TSC complex consists of the heterodimeric proteins TSC1/2 and exhibits a GAP activity towards Rheb to maintain the GTPase in its inactive conformation. Upon Akt-mediated phosphorylation of TSC2, however, TSCs complex stability and function is perturbed and GTP-bound Rheb can accumulate to stimulate mTORC1 activity. Additionally, several other serine/threonine kinases, like Erk or AMPK, also regulate mTORC1 through phosphorylation of TSC1/2 making it the most essential signaling route in response to growth factor binding[26,27].
Another mTORC1-dependent signaling cascade regulating autophagy responds to the cellular energy state via the energy sensor AMPK. In cells, energy generated by glycolysis or mitochondrial respiration is typically stored by converting adenosine monophosphate (AMP) into adenosine triphosphate (ATP) and monitored by the kinase AMPK. In low energy conditions, i.e. high levels of AMP, AMPK is activated by the kinase LKB1 and stimulates TSCs GAP activity towards Rheb. This induces accumulation of inactive GDP-bound Rheb, which inhibits mTORC1 activity and thus activates autophagy. Apart from AMP/ATP ratios, different stress signals, such as cytoplasmic p53 or nitric oxide (NO), have also been observed to induce autophagy through the AMPK-TSC pathway. In addition AMPK has been reported to directly disrupt mTORC1 by phosphorylating raptor and to enhance autophagy through direct interaction with ULK1 and Beclin1[26].
Apart from mTORC1-dependent pathways, autophagy may also be induced by several other signaling cascades. It appears to be negatively regulated by inositol signaling and also responds intracellular calcium or cAMP levels, for instance. Another level of regulation might be direct activation or inhibition of the ULK1 or PI3K complexes through interaction with their numerous binding partners. One candidate could be the binding platform Beclin1 of the PI3K complex that functionally interacts with more than 50 different proteins of which at least some of them have been linked to autophagy. However, the majority of mTORC1-independent mechanisms and particularly the question, how they integrate with growth factor and amino acid sensing, have not been completely understood yet and remain to be clarified in the future[3,26].

1.1.2 Autophagosome Formation and Maturation

Formation of double-layered membrane vesicles, termed autophagosomes, is a key step of the autophagic pathway and has been extensively studied, first in yeast and later in mammalian systems. The process is coordinated by several autophagy-related 'Atg' proteins and kinases and can be broadly divided into nucleation, elongation and closure of the autophagosome. Nucleation is primarily controlled by the ULK1 and PI3K protein complexes, while the ubiquitin-like conjugation systems Atg12-5-16L and LC3-PE assist elongation and closure. Transport to the lysosome and fusion, i.e. maturation of the autophagosome, are orchestrated by different motor proteins, Rab GTPases, membrane tethers and SNAREs. However, compared to autophagosome formation the understanding of the maturation process is still very limited[7].

1.1.2.1 Autophagosome Nucleation

One of the earliest signaling events in autophagosome formation is translocalization of the ULK1 complex to the endoplasmatic reticulum (ER), where it interacts with the PI3K complex to induce formation of the so-called isolation membrane[29]. In nutrient-rich conditions, the ULK1 complex, comprised of the serine/threonine kinase ULK1, Atg13, Atg101 and FIP200, associates with mTORC1 and its kinase activity is inhibited by mTOR-mediated phosphorylation of ULK1 and Atg13. In starvation or stress conditions, mTOR is inactivated, ULK1 and Atg13 are dephosphorylated and the complex dissociates from mTORC1. ULK1 then becomes autophosphorylated and in turn phosphorylates FIP200 and Atg13, which induces translocalization of the complex to the autophagosome formation site. ULK1 is also phosphorylated by AMPK and acetylated by TIP60, but it is not entirely clear how these postranslational modifications integrate with each other[1,7]. ULK1 also phosphorylates raptor of the mTORC1 complex, which supposedly further activates autophagy by decreasing mTORC1 substrate affinity[3].
The activated ULK1 complex interacts with several downstream proteins like Atg16L or LC3 to initiate and assist isolation membrane nucleation and has been observed to enhance PI3K complex activity. Two distinct PI3K complexes have been reported, each containing the core components Vps34, p150 and Beclin1 and either Atg14L or UVRAG as a fourth subunit[4]. Both PI3K complexes assemble from two protein pairs, the Vps34-p150 heterodimer and the Beclin1-Atg14L/UVRAG heterodimer with Atg14L and UVRAG binding mutually exclusive to Beclin1's coiled-coil domain (CCD)[5].
Upon starvation, Beclin1 dissociates from the inhibitory protein Bcl-2 and the PI3K complex is recruited to the ER by Atg14L. Atg14L associates with the ER membrane through its cysteine-rich N-terminal domain. At the ER, Beclin1 is directly and indirectly (via AMBRA) phosphorylated by ULK1 to enhance the kinase activity of Vps34. The enzyme is additionally phosphorylated by several other kinases, like PKD or AMPK, but their exact function has not been resolved yet. Vps34 is a class III lipid kinase and generates PI3P from phosphatidylinositol, which leads to nucleation of a PI3P-enriched platform, termed omegasome, from the ER. PI3Ps also serve as second messengers recruiting effector proteins like WIPIs and DFCP1 that may support elongation and closure of the isolation membrane[1,3,7].
Several positive feedback loops might additionally stimulate the process. For instance, PI3Ps have been observed to positively interact with Atg13 in the ULK1 complex, which may increase recruitment of the ULK1 complex to the omegasome. Similarly, Atg14L contains a C-terminal 'Atg14L (Barkor in yeast) autophagosome targeting sequence' (BATS) with a high affinity for highly curved, PI3P-rich membranes that may further enhance translocalization of PI3K complexes to the forming autophagosome. The importance of these feedback processes, however, remains to be further investigated[30].

1.1.2.2 Formation and Elongation of the Isolation Membrane

After nucleation of the isolation membrane, two ubiquitin-like conjugation systems, Atg12-5-16L and LC3-PE, accumulate at the omegasome and promote membrane elongation. The Atg12-5-16L complex is recruited first and then supports formation and activity of the LC3-PE system, which is essential for elongation and closure of the autophagosomal membrane.
The Atg12-5-16L complex assembles from Atg12-5 and Atg16L, in an enzymatic process similar to ubiquitin conjugation during which Atg12 is initially conjugated to Atg5 and then binds to Atg16L. In the beginning, Atg12 carries an N-terminal glycin, which is cleaved by the E1-like enzyme Atg7 in order to transfer Atg12 to the E2-like protein Atg10 and later conjugate it to Atg5. Atg12-5 then forms a homodimeric complex with Atg16L at the isolation membrane. The Atg12-5 complex alone shows no distinct membrane localization, but interaction with Atg16L dramatically increases its affinity for

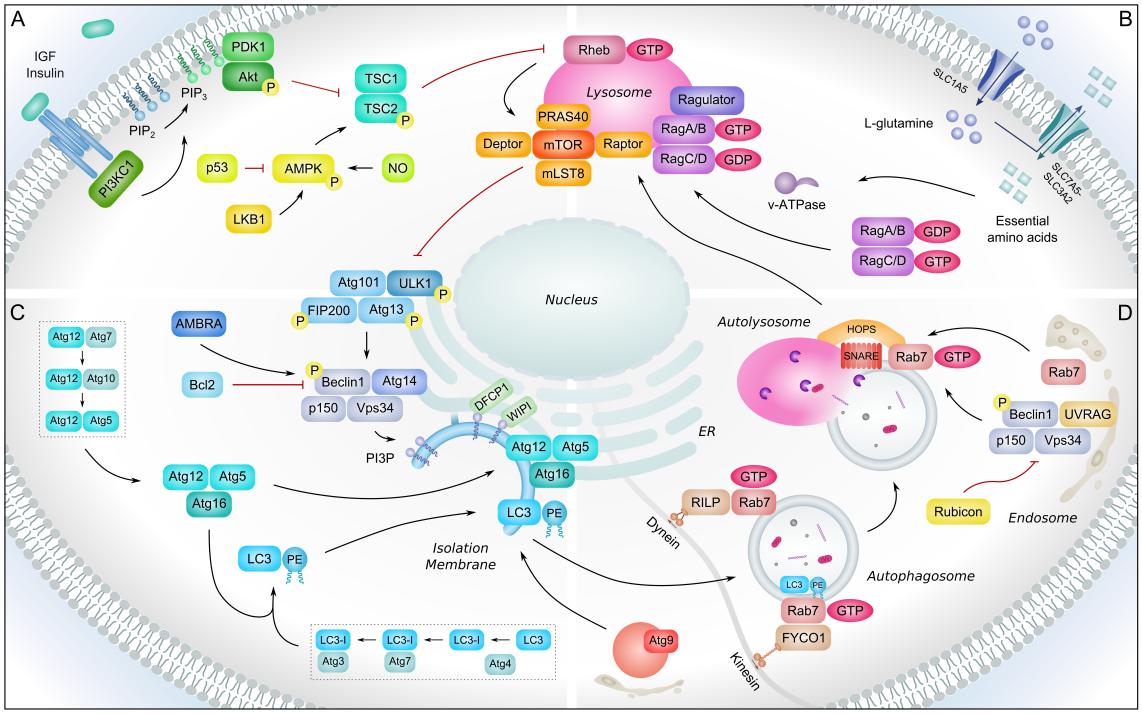

Figure 1.1: Regulation of autophagy induction, autophagosome formation and maturation[1,2,21,27,31]. **A** Regulation of autophagy by growth factors and cellular energy state. mTORC1 is activated through the PI3KC1/Akt/TSC pathway and inhibits autophagy induction. **B** Autophagy is negatively regulated in response to amino acid influx, which activates mTORC1 via Rag GTPases. **C** Autophagosome formation. The ULK1 complex translocates to the ER and stimulates generation of PI3Ps by the PI3K complex. Increased PI3P concentrations attract WIPI and DFCP1 and promote omegasome formation. Two interdependent ubiquitin-like conjugation systems generate Atg12-5-16L and LC3-PE complexes, which support isolation membrane elongation and closure. Atg9 vesicles may provide another membrane source. **D** The closed autophagosome is transported to the lysosome by kinesin or dynein motors, which bind supposedly through RILP- or FYCO1-Rab7 complexes. Lysosomal fusion is most likely orchestrated by a combination of Rabs, HOPS and SNARE complexes and requires the UVRAG-containing PI3K complex. In the autolysosome, the autophagic cargo is degraded and recycled.

the convex surface of the isolation membrane in presence of PI3Ps[32]. Only recently, Mizushima and co-workers proposed that interaction with FIP200 targets Atg16L to the autophagosome formation site by reversing a self-inhibitory effect of Atg16Ls C-terminal WD-repeat domain[33].

Due to its function as E3-like enzyme during LC3-PE conjugation, localization of the Atg12-5-16L complex also determines the site of LC3 lipidation. In mammals, the LC3 family is comprised of seven homologs (LC3A/B/C, GABARAP and GABARAPL1/2/3) with LC3B being the most common isoform within the autophagy process. Similar to Atg12, LC3 is initially expressed with a C-terminal extension that is cleaved by the protease Atg4 so that LC3 can be activated by Atg7 (E1-like enzyme). Afterwards, LC3 is transferred to the E2-like enzyme Atg3 and eventually conjugated to PE supported by Atg12-5-16L's E3-like activity[34]. In contrast to Atg12-5-16L, which dissociates from the isolation membrane upon closure, LC3-PE remains bound to the inner and outer autophagosomal membrane and appears to act as a scaffold for membrane elongation. Accordingly, the complex has also been related to the size of the forming autophagosome and appears to be involved in membrane tethering and closure of the isolation membrane[35,36].

Consistent with these observations, a model of autophagosome biogenesis has been proposed in which Atg12-5-16L is recruited to highly curved isolation membranes and promotes LC3 lipidation. Accumulation of LC3-PE then induces membrane elongation resulting in a decrease of membrane

curvature. Through interaction with LC3-PE, Atg12-5-16L remains associated to the low curvature membrane for stabilization while it simultaneously mediates LC3 lipidation at the highly curved edges of the isolation membrane. In another scenario, LC3-PE is enriched at highly curved membranes by the E2-like enzyme Atg3, which has also been shown to sense membrane curvature. However, both hypothesis have not yet been confirmed *in vivo* and require further clarification[2].
While the function of LC3 family members within autophagosome biogenesis is not entirely clear, they have been shown to interact with different receptor proteins sequestering specific cargo to the autophagosome formation site. Ubiquitinated cargo, for example, is delivered by p62/SQSTM1, NBR1, Optineurin or NDP52 through interaction with LC3/GABARP proteins. This interaction is mostly mediated via a LC3-interacting region (LIR) in the receptor proteins, but it remains to be elucidated whether LIR motifs are a common feature in autophagic receptor proteins and which proteins deliver the remaining autophagic cargo[3].

1.1.2.3 Source of the Isolation Membrane

Another yet unresolved aspect of autophagosome formation is the source of the isolation membrane. Even though LC3-PE is assumed to mediate elongation of the isolation membrane, it is not clear whether a given membrane source is merely elongated or if small vesicles fuse with the isolation membrane to expand it (or a combination of both). In yeast, the transmembrane protein Atg9 catalyzes the delivery of vesicles from the Atg9 compartment to the autophagosome formation site, which is crucial for membrane expansion and closure. Here, Atg9 is recruited by the yeast counterpart of the ULK1 complex and even integrated into the autophagosome membrane. In mammals, Atg9 shuttles between the trans-Golgi network (TGN) and endosomes, but upon starvation it associates with forming autophagosomes. However, while it is necessary for autophagosome formation, it is not required for isolation membrane elongation or closure and also not incorporated in the isolation membrane[2,3,37].
The ER has long been a candidate for the membrane source in mammalian systems and recently, several studies provided direct evidence to support this hypothesis. While other compartments like mitochondria, the plasma membrane, endosomes, the Golgi or ERGIC are also potential sources, the autophagic machinery initially assembles at the ER to create omegasomes[38,39]. Recent EM-based analysis have shown membrane continuity between the ER and the isolation membrane, which led to the proposal of a model where the forming autophagosome is sandwiched between two ER sheets[40,41,42]. However, it has been reported that mitochondria can transfer lipids to the isolation membrane as well and that ERGIC membranes may serve as template for *in vitro* lipidation of LC3[43,44]. Atg9 has also been associated with the TGN and endosomes rather than the ER. Furhtermore, Atg16L can associate with plasma membrane derived vesicles to generate autophagosomes[45]. Based on these observations, it seems most likely that different compartments contribute membrane throughout autophagosome formation[3,37].

1.1.2.4 Closure and Maturation of the Autophagosome

The last phase of autophagy is probably also the most understudied and least understood step of the process. So far, it has been established that autophagosomes must be closed to travel to the lysosome, where they fuse to become an autolysosome and initiate cargo degradation. How theses processes are regulated, however, is not entirely clear yet.
Sealing of the isolation membrane to form a double-membrane vesicle marks the final step of autophagosome biogenesis and seems to be controlled by various members of the LC3 and Atg4 families.

A study in *Caenorhabditis elegans* demonstrated that the homologs of mammalian GABARAP and LC3 are required for closure of the isolation membrane, but could not determine their specific function[46]. Several other suggested an involvement of Atg4 or its family members, which mediate delipidation and subsequent membrane removal of LC3[47,48,49]. The FYVE-domain containing protein FYCO1 has also been associated with the process, but again a complete picture remains elusive[2].

Once the autophagosome is sealed, it is transported from the omegasome to the endocytic system, supposedly along microtubules and actin filaments. In yeast, microtubular destruction showed no effect on autophagy, but in mammals microtubules seem to at least enhance lysosomal fusion as autophagosomes have been observed to move along microtubular tracks[50,51,52,53,54]. In neurons, autophagosomes were observed to travel towards the cell center in a dynein motor-dependent manner and consistently with this observation, loss of dynein has been associated with LC3-PE accumulation and perturbed clearance of autophagic cargo[55,56]. Since lysosomes localize mostly to the perinuclear region, involvement of dynein motors, which move towards the plus end of microtubules, seems not surprising. However, disruption of kinesin motors, which move towards the cell periphery, resulted in autophagy disruption as well[57].

Another unresolved aspect is the transport mechanism of autophagosomes and particularly the connection between the motor proteins and the autophagic vesicle. Rab7, which plays a vital role in endosome trafficking, is one candidate to mediate motor recruitment as it has been observed to interact with FYCO1, which binds to autophagosomes via PI3Ps and LC3. Overexpression of FYCO1 resulted in redistribution of autophagosomes to the cell periphery indicating a functional connection to kinesin-dependent transport[58,59].

Only few studies dealt with the role of actin filaments in autophagy and provided evidence that actin may be important for the fusion process. Lee *et al.* reported that caractin, which regulates actin polymerization, is recruited to autophagosomes via HDAC6 and that loss of actin, coractin or HDAC6 prevents lysosomal fusion in selective autophagy[60]. Similarly, depleting cells of myosin motors perturbed autophagosome turnover[61].

Once the autophagosome arrives at its destination, fusion with the lysosome is supposedly initiated in a cooperative process by Rab GTPases, membrane-tethering complexes and SNAREs[62]. Of the Rab GTPases, Rab7 is again a potentially important regulator, since loss of Rab7 blocks fusion entirely. Rab33b, which interacts with Atg16L, and its GAP OATL1 have also been associated with lysosomal fusion. Still, their exact function remains to be determined[63,64]. The UVRAG-containing PI3K complex may provide another connection to Rab GTPases, as UVRAG interacts with Vps16, a component of the HOPS complex, which controls various membrane tethering and fusion processes. Interaction with UVRAG recruits HOPS to membranes, where the GEF and HOPS subunit Vps39 further activates Rab7. The GTPase then disrupts binding of UVRAG to its inhibitory interaction partner Rubicon, thus liberating additional UVRAG to recruit more HOPS and enhance Rab7 activation[65,66].

Based on their function in other processes, Rab proteins are most probably also involved in the recruitment of tethering factors to the autophagosome. Membrane tethers, like the HOPS complex, have been observed to support fusion processes by bridging membranes and induce formation of SNARE complexes. However, only two tethering factors, HOPS and TECPR1, have been associate with autophagy so far and their function requires further clarification[62].

SNARE proteins are membrane anchors, which mediate vesicle fusion by bringing two membranes into close proximity. Typically, SNARE complexes form at opposing membranes and 'zip up' the so-called donor and acceptor membranes by forming a bridging *trans*-SNARE complex. Only one com-

plete SNARE complex consisting of syntaxin 7, syntaxin 8, Vti1b, VAMP7 and VAMP8 has been indirectly linked to autophagosome-lysosome fusion, because it participates in endosome-lysosome fusion and at least VAMP8 and Vti1b seem to be required during selective autophagy. Syntaxin 17 is the only SNARE protein that appears to be directly involved in autophagy, as loss of syntaxin 17 effectively prevents autophagosomal fusion, but the remaining components of the SNARE complex need to be identified[62].
Lysosomal fusion and delivery of the autophagosomal contents typically marks the terminal point of the autophagic pathway, even though the cargo remains to be degraded and recycled back into the cytoplasm. Degradation of autophagic cargo, however, appears to proceed in a similar manner as recycling of cellular material delivered by the endocytic pathway. Still, the degradation process also remains to be further investigated to completely understand the autophagosomal maturation process.

1.1.3 Studying Self-Digestion: Autophagy Modulation

In order to understand complex processes, such as autophagy, the most common *in vivo* approach, besides mere observation, is to inhibit or enhance the function of one or more components and study the consequences. Traditionally, cells are depleted of a certain protein by genetic knockdown or knockout, while protein function can be enhanced by overexpression or (re-)introduction of dominant negative and constitutively active variants. Especially in the early days of autophagy research, genetic modulation of the process helped to gain a broad understanding of the relationship between autophagy complexes and to identify key regulators[3]. More recently, autophagy modulation with chemical inducers or inhibitors has sparked great interest, as it provides a more dynamic approach to dissect the process experimentally, and because autophagy has become an increasingly important therapeutic target. Dysregulation of autophagy has been associated with various diseases including cancers as well as metabolic, neurodegenerative and infectious conditions. In most of these pathological states, autophagy is inhibited or downregulated. This contributes to obesity or diabetes, but also promotes accumulation of protein aggregates leading to neurodegenerative conditions like Parkinson's or Alzheimer's disease. In cancers, autophagy may be inhibited or enhanced depending on the type of cancer, so that the pharmacological approach modulating autophagy needs to be adjusted to the given conditions[67].
In principle, genetic or chemical perturbation can be applied to any protein, but the choice of candidates is often limited by availability of appropriate functional read-outs or structural information as basis for drug design. Based on the available information, the kinases mTOR, AMPK and Vps34 are popular targets for autophagy modulation. Other targets include Beclin1 or microtubules and lysosomes. However, the functions of mTOR, AMPK or Vps34 are not limited to autophagy and consequently, the majority of chemical modulators lack specificity. Rapamycin, for instance, is a potent mTOR inhibitor and effectively induces autophagy, but also globally affects glycolysis, lipid synthesis and various other metabolic pathways[68].
Popular, but less specific inhibitors of autophagosome sequestration are 3-MA, LY294002 and wortmannin. These drugs target class I and III PI3Ks, which generate PIP_3s and PI3Ps that serve as second messengers and are also required for autophagosome formation. Wortmannin might be the most specific of the three, as it specifically inhibits Vps34. However, amongst other side effects, it also promotes formation of endocytic vacuoles that are easily mistaken for autophagosomes[14].
Besides sequestration inhibitors, a large number of chemical drugs were designed to disrupt microtubular transport or fusion at the lysosome. Particularly for the lysosome, different strategies have been applied to inhibit lysosomal enzymes (e.g. leupeptin, pepstatin, E-64d) or to increase the lysosomal pH by inhibiting v-ATPases with bafilomycinA1 and concanamycinA or with weak base amines like methyl-

or propylamine, chloroquine and Neutral Red. However, protease inhibitors like leupeptin, pepstatin and E-64d also affect cytosolic proteases while modulators increasing the pH might target other acidified compartments as well. Consequently, autophagy inhibitors are mostly applied in combination with other assays or inhibitors in order to identify and exclude unwanted side effects [14].

Besides rapamycin, only few autophagy inducers have been reported to date. Lithium, sodium valproate and carbamazepine are a few examples for inducers that act independently of mTOR by decreasing myo-inositol 1,4,5-triphosphate levels. Other inducers like valproic acid, for instance, inhibit histone deacetylases to stimulate autophagy by yet unknown mechanisms. Much more specific are Beclin1 simulators such as the cell penetrating peptides Tat-Beclin1 or Tat-wtBH3D and Tat-dsBH3D, which disrupt the inhibitory interaction between Beclin1 and Bcl-2. However, similar as for the autophagy inhibitors, the specificity and variety of induces stills needs to be improved to allow for efficient autophagy induction [14].

Apart from chemical modulation, autophagy can also be regulated on a transcriptional level. Overexpression or post-translational activation of TFEB, for example, upregulates biogenesis of autophagosomes and lysosomes. The same applies to the transcription factor CEBPB, which has been successfully activated in order to stimulate autophagy in hepatocytes [69]. In another study, knockdown of the nucleolar transcription factor RRN3/TIF-IA induced autophagy in neurons and MCF7 cells [70,71]. Transcriptional upregulation of Beclin1 expression might be achieved with the anti-cancer drug tamoxifen, however, the effect has only been observed in a few cell lines and needs to be further validated [14,72].

Taken together, only few methods to specifically and dynamically modulate autophagy are currently available. Most known autophagy inhibitors and inducers exert pleiotropic effects and can only be applied in combination with other autophagy assays. Transcriptional control of the autophagic process provides more specific control over distinct proteins and has been successfully applied in many instances, but requires a time frame of hours to days. Chemical biology tools like inducible dimerization could provide an alternative approach to overcome these limitations, but has not been applied to study autophagy yet.

1.2 Inducible Dimerization

Inducible dimerization systems have become a widespread tool with an ever increasing number of biological applications. While the dimerization strategies differ between photoinducible or chemically inducible systems, the basic principle, remains the same: two proteins are artificially brought into close proximity. This approach can be used to induce protein interactions in a controlled manner, to manipulate protein localization, to activate proteins or protein degradation or to reconstitute split proteins. Dimerization can be induced on a timescale of seconds to minutes and with subcellular spatial resolution. In contrast, genetic alteration of protein expression, requires hours to days and interferes with cellular events globally and chronically [15,16,17]. Thus inducible dimerization approaches are often superior when studying dynamic and spatiotemporally confined processes.
Dimerization systems differ according to their dimerization trigger. Chemically inducible dimerization approaches rely on small molecules that are able to interact with two proteins or protein domains simultaneously. If the proteins are identical, the inducers are called homodimerizers, whereas small molecules binding to different proteins are referred to as heterodimerizers [17]. Optogenetic dimerization systems, on the other hand, employ light-sensitive protein domains that undergo a conformational change upon illumination and consequently induce protein interaction. Photoinducible dimerization approaches combine the former systems by using a small molecule dimerizer, which is photocleaved or decaged upon illumination at a specific wavelength [73]. Subsequently, the different approaches and their variations will be introduced in detail.

1.2.1 Chemically Inducible Dimerization

Chemically induced dimerization was the first approach to force proteins into high-affinity interaction through addition of a small molecule, termed 'dimerizer'. Application and dosage control of dimerizers are simple, they can penetrate tissues inaccessible to light, the dimerization kinetics can be rapid and some systems are even reversible. Speed and specificity are essential for the applicability of a dimerizer, but an ideal dimerizer should also be bioorthogonal, cell permeable and feature a high binding affinity. Spatial control of chemically induced dimerization would be another desirable feature, but is almost impossible to achieve [17].

1.2.1.1 Homodimerization Systems

The majority of dimerizers used today has at least partially evolved from natural products and optimized to meet the requirements listed above. The first rationally designed dimerizer was developed by Spencer *et al.* in 1993 and named FK1012. It was derived from the naturally occurring immunosuppressant FK506, which interacts with the proteins calcineurin and FKBP12 (FK506-binding protein of size 12 kD) and paved the way for an entire family of homodimerizers [17,74]. FK1012 was generated by fusing two copies of FK506 via a flexible linker attached to the calcineurin binding site so that FK506-calcineurin interaction would be blocked. Addition of FK1012 thus initiates homodimerization of FKBP12 and any protein of interest fused to FKBP12. The induced dimerization process is rapid, dose-dependent and also reversible by competitive removal of the dimerizer through addition of monomeric FK506 or calcineurin inhibitors like cyclosporin-A. However, FK1012 is not bioorthogonal and interacts with the endogenous form of FKBP12. This may be compensated by administering high concentrations of the dimerizer, but remains problematic due to the high abundance and ubiquity of FKBP12 [74]. Additionally, the chemical structure of FK1012 is rather complex (Figure 1.2), prompting many efforts to generate a

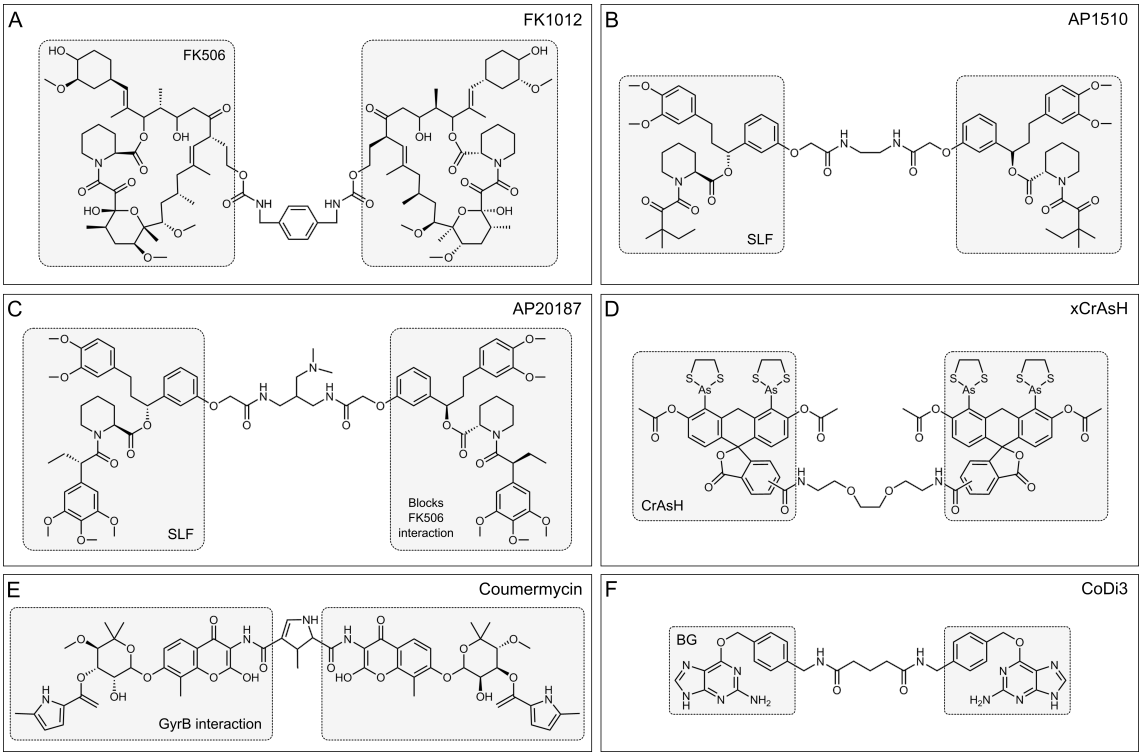

Figure 1.2: Molecular structures of small molecule homodimerizers. **A** FK1012 is comprised of two copies of FK506 and homodimerizes FKBP12 [74]. **B** AP1510 consists of two synthetic FKBP12 ligands (SLFs) [75]. **C** AP20187 is a FKBP12 dimer with high affinity for FKBP' [20]. **D** xCrAsH dimerizes proteins with the sequence motif CCPGCC and exhibits fluorescence upon crosslinking [76]. **E** Coumermycin is a bacterial product that interacts with GyrB proteins [77]. **F** CoDi3 is a member of the CoDi family and crosslinks SNAP-tagged proteins [78].

simplified, bioorthogonal dimerizer for FKBP12.

Holt and colleagues reported several fully synthetic dimerizers originating from AP1510, a non-cyclic, but less affine dimerizer of FKBP12 [75,79]. AP1510 is a symmetric dimer of monomeric synthetic ligands for FKBP12, which was later termed SLF (synthetic ligand of FKBP) and served as the basis for many dimerizers to follow. Since AP1510 and its variants did not adress the specificity problem, Holt and co-workers applied the 'bump and hole' strategy to generate bioorthogonal dimerizers [20]. In the bump and hole approach, presented by Belshawl *et al.*, a space-filling group (bump) is added to the ligand, while a cavity (hole) is engineered into the ligand-binding site of the interacting protein. Consequently, only the modified, but not the native, protein can interact with the ligand [80,81].

After screening different FKBP12 mutants and a panel of SLF analogs with bulky adducts, Holt and colleagues combined a F36V FKBP12 mutant (FKBP' hereafter) with the dimerizers AP1903 and AP20187. The resulting constructs bind to FKBP' with an affinity of 1.8 nM and to FKBP12 with an affinity of 2.9 µM, thus exhibiting over 1000-fold selectivity for the mutated FKBP'. As the compounds differ only in their flexible linkers and AP20187 showed better pharmacological properties, it was made commercially available and is still a widely used FKBP' homodimimerizer [20,82,83].

Shortly after the concept of chemically induced dimerization was first introduced, another non-covalent homodimerizer derived from the bacterial product coumermycin was presented by Farrar *et al.* [77]. Coumermycin acts as a natural dimerizer of the bacterial protein GyrB and is thus bioorthogonal in eukaryotic systems, a major advantage over other available dimerization systems at the time. It is also non-toxic and reversible through addition of the related monomeric antibiotic novobiocin [77,83]. Even

though non-covalent crosslinking of proteins has no fundamental drawbacks, direct detection of protein interaction *in vivo* was challenging at the time and thus several groups focused on covalent homodimerizers.
Johnsson and co-workers generated the CoDi homodimerization system based on the SNAP-tag, which they presented earlier as a method for covalent protein labeling *in vivo*[78,84]. In principle, the SNAP-tag is a mutant of the human DNA repair protein hAGT that forms a covalent bond with the nucleobase O^6-benzylguanine (BG) and its derivatives. BG derivatives were initially conjugated to fluorescent dyes to visualize hAGT-fusion proteins (SNAP-tagged proteins) in cells, but Lemercier *et al.* joined two BG subunits via a flexible linker to generate different covalent homodimerizers. These 'CoDi' dimerizers induce interaction of SNAP-tag fusion proteins. They are bioorthogonal and dimerization can be detected *in vivo* by electrophoresis or microscopy. However, the labeling reaction appears to proceed rather slow (6 hours) and is not reversible[78,83].
The Schulz lab generated another covalent homodimerizer, termed xCrAsH, which was derived from a protein labeling system developed by Tsien and co-workers and features faster kinetics (1 hour labeling), high specificity and reversibility[76,85]. A major advantage of the xCrAsH system is the small size of the dimerization domains, which consist of only twelve amino acids (4cys-tag) and should thus disturb protein activity or localization to a lesser extent than bulky protein tags. Protein crosslinking is achieved through interaction between a dimeric biarsenic derivative of carboxyfluorescein (xCrAsH) and the unique sequence motif CCPGCC that is integrated into the protein of interest. Dimerization can be reversed through addition of dithiols and additionally, the crosslinked proteins emit a fluorescent signal upon dimerization, which can be used during live cell microscopy[76].
Among the inducible homodimerization systems, AP20187 and coumermycin combine probably most of the desirable features of a chemical dimerizer (see table 1.1). However, as all of the homodimerization systems, they also suffer from saturation effects caused by excess dimerizer. To avoid saturation effects, careful optimization of the dimerizer concentration is required. If the dimerizer concentration is too high, each dimerizer molecule binds only one copy of the interacting protein and thus dimerization is limited or completely prevented. Therefore, various labs focused on generation and optimization of heterodimerizers[83,86,87].

1.2.1.2 Heterodimerization Systems

A milestone in the development of chemical heterodimerizers was the discovery and characterization of the bacterial antibiotic rapamycin and its analogs (rapalogs), which remain the most thoroughly studied and widely used dimerizers to date[16,17]. Rapamycin is an immunosuppressant and inhibits the kinase TOR (target of rapamycin) of the TORC1 complex. Since dysregulation of TORC1 has been associated with metabolic diseases, cancer or aging, rapamycin was initially studied as a clinical drug[96,97]. However, as soon as the mechanism of rapamycin-mediated TOR inhibition was discovered, the macrolide sparked interest in the field of chemical biology. In order to block enzymatic activity of TORC1, rapamycin binds to FKBP12 first and the FKBP12-rapamycin complex then binds to TORs FRB domain. Ergo, rapamycin acts as a chemical heterodimerizer of FKBP12 and FRB[17]. In 1996, rapamycin-induced heterodimerization of FKBP12/FRB-fusion proteins was demonstrated for the first time[88,89]. It became quickly apparent that the antibiotic has several other beneficial properties: rapamycin is cell permeable, binds to both FKBP12 and FRB with a low nanonmolar affinity, dimerization occurs within minutes and since the FRB domain interacts only with the FKBP12-rapamycin complex, but not rapamycin alone, it can be applied at high concentrations[98].Then again, rapamycin is not bioorthogonal and causes off-

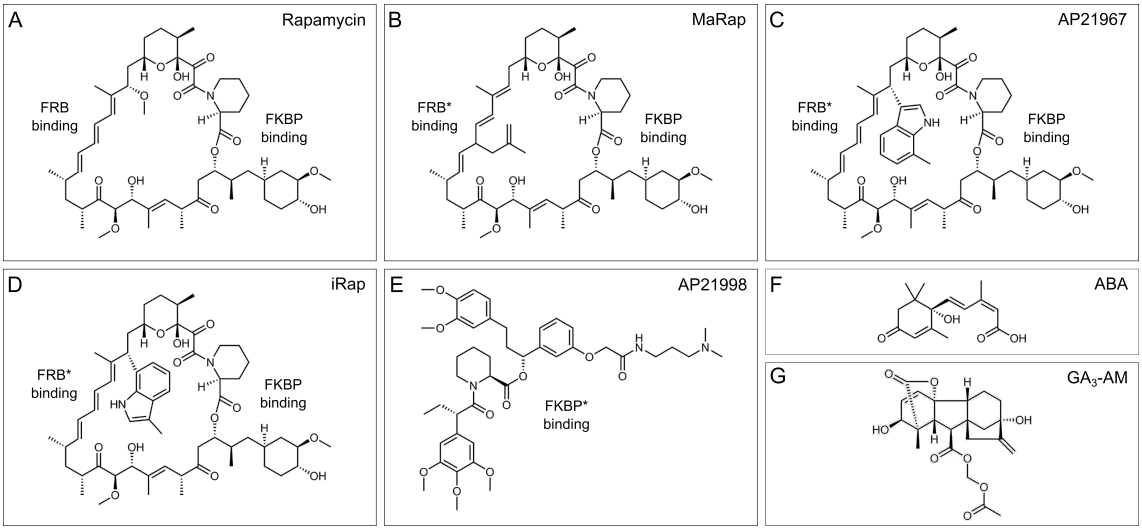

Figure 1.3: Molecular structures of natural chemical heterodimerizers. **A** Rapamycin is a bacterial antibiotic and binds to FKBP and FRB domains[88,89]. **B** MaRap was generated by modification of rapamycins C16 position and dimerizes FKBP with FRB*[90]. **C** AP21967 was generated by indole substitution at C16 and dimerizes FKBP and FRB* with improved pharmacokinetics[91]. **D** iRap was evolved from AP21967 and crosslinks FRP* and FKBP 6-fold faster[92]. **E** AP21998 mediates dissociation of self-associating FKBP* complexes[93]. **F** ABA is phytohormone and dimerizes PP2C and PYL domains[94].**G** The modified phytohormone GA_3-AM induces dimerization of GAI and GID1[95].

target effects leading to cell-cycle arrest and autophagy induction, which may only be avoided by using resistant cell lines[16]. Several studies have attempted to overcome these limitations using the bump-and-hole strategy to generate bioorthogonal rapalogs (Figure 1.3).

Liberles *et al.* introduced bulky substituents to rapamycins FRB-binding site and created MaRap, which binds to the triple mutant FRB*. However, MaRap is difficult to synthesize, unstable and its pharmacokinetic properties needed optimization[90,99]. Based on MaRap, Bayle and co-workers screened different rapalog/FRB combinations in order to mitigate MaRaps drawbacks and identified the FRB*-binding rapalog AP21967. The drug exhibits optimized pharmacokinetics and stability, so that it can be applied *in vivo* and was soon made commercially available[16,91]. Another bumped rapalog, termed iRap, was introduced by Inoue and colleagues and induces dimerization of the mutant FRB* and FKBP12 6-fold faster than AP21967[92]. Rollins *et al.* choose a different approach and presented a reverse dimerization system based on the F36M FKBP12 mutant (FKBP*), which aggregates in absence of the rapalog AP21998. Here, dimerizer addition causes dissociation of the self-associating FKBP* complex[93]. Despite the many benefits of rapalogs developed thus far, several limitations still remain. Synthesis is often complicated and expensive, restricting the accessibility and moreover *in vivo* dimerization is effectively irreversible due to rapamycins high affinity towards its interaction partners. Attempts have been made to address this issue by out-competing FKBP-binding with high concentrations of FK506, but the majority was largely ineffective on a reasonable time scale[16,17,83].

Crabtree and co-workers looked for alternative heterodimerizers and found the phytohormone abscisic acid (ABA), which induces dimerization of PP2Cs (protein phosphatase type 2C) and PYL domains. Similar to rapamycin, it binds initially to the pyrabactin resistance (PYR)/PYR1-like (PYL)/regulatory component of the ABA receptor (RCAR) and the resulting complex then interacts with PP2Cs to block their enzymatic activity. In plants, ABA signaling is fundamentally important for stress response regulation and stimulation of development[94]. ABA-based is orthogonal in mammalian systems, not cytotoxic, in-

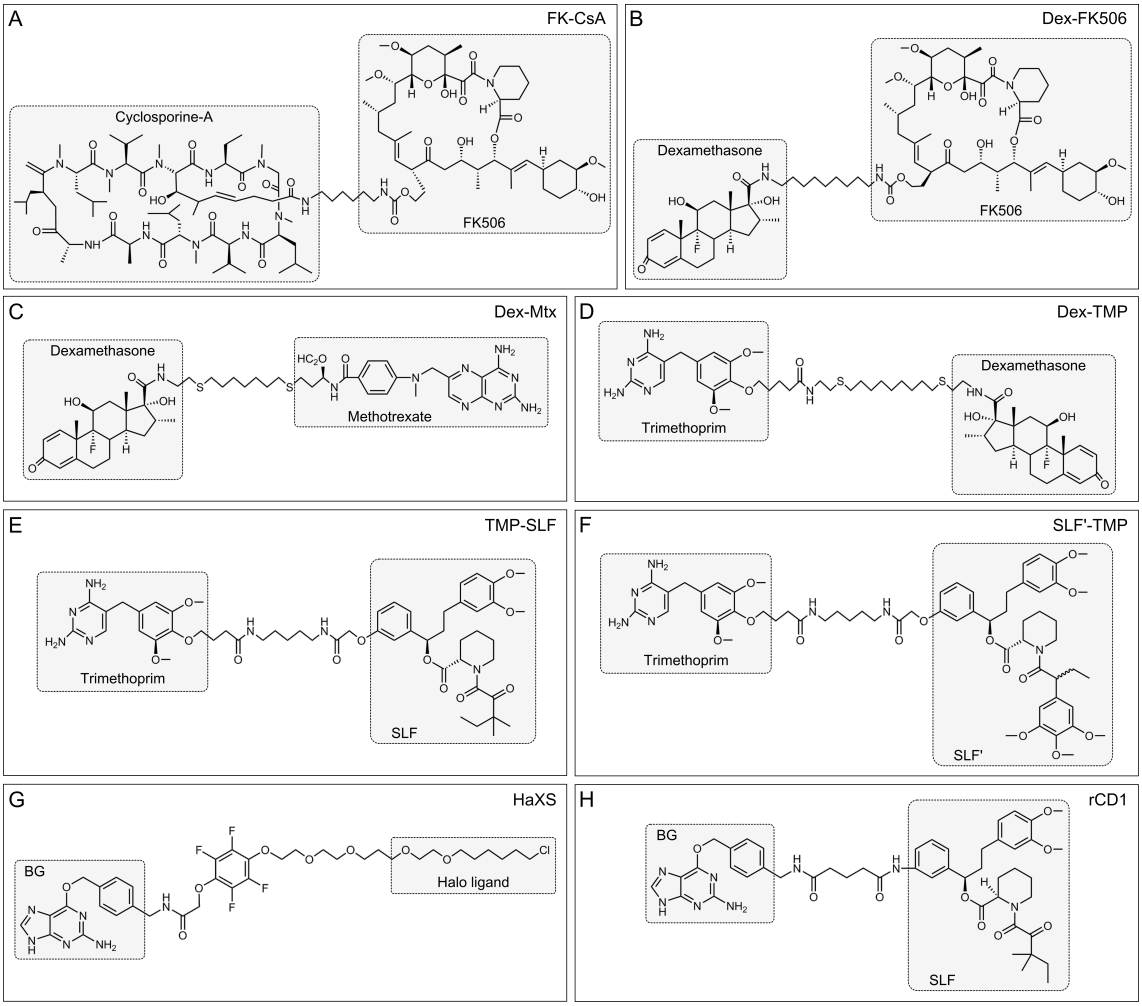

Figure 1.4: Molecular structures of artificial chemical heterodimerizers. **A** FK-CsA is a combination of cyclosporin-A and FK506 that crosslinkes FKBP12 and cyclophilinA[100]. **B** Dex-FK506 combines FK506 with the glucocorticoid hormone dexamethasone to dimerize FKBP and GR[101]. **C** Dex-Mtx is a fusion product of dexamethasone and DHFR-binding methotrexate[102]. **D** In Dex-TMP, dexamethasone was fused to trimethoprim to crosslink GR and eDHFR[103]. **E** TMP-SLF combines trimethoprim with synthetic ligand of FKBP12 to dimerize eDHFR and FKBP12[19]. **F** SLF'-TMP employs a SLF with higher selectivity for the mutant F36V mutant of FKBP and induces rapid dimerization of FKBP' and eDHFR[18]. **G** HaXS combines a Halo ligand with benzylguanine (BG) to dimerize SNAP- and Halo-tags[104]. **H** rCD1 is a fusion of BG and a SLF and crosslinks FKBP' with Halo-tagged proteins[105].

expensive and dimerization can be reversed by washout. On the downside, ABA-mediated dimerization displays slower kinetics than rapamycin-based tools (see table 1.1) and has to be applied in at micromolar concentrations[16,94]. Another inducible dimerization system utilizing plant hormones was introduced by Miyamoto *et al.* and employs the gibberellin GA_3 as a heterodimerizer. Like ABA, GA_3 first forms a complex with gibberellin-insensitive dwarf1 (GID1) prompting a conformational change, which then facilitates interaction of GID1 and gibberellin insensitive (GAI). Initially, GA_3 displayed poor cell permeability due to its negatively charged carboxylic acid moieties. Addition of an acetoxymethyl group (AM) to mask the carboxyl group solved the permeability problem effectively[95]. In the cytoplasm, the AM groups are hydrolyzed by esterases and GA_3s reactivity is re-established. In contrast to ABA, GA_3-AM induces dimerization on a time scale of seconds, but the dissociation kinetics remain comparably slow[16,95].

Recently, the ABA- and GA_3-AM-based dimerization systems were combined with a chemical decaging

Table 1.1: Properties of chemically inducible dimerization systems.

SYSTEM	DIMERIZATION TRIGGER	TIME SCALE	REVERSIBILITY
FK1012s FKBP12-FKBP12	FK1012 (AP1510, AP1903, AP20187) addition	Dimerization: <10 minutes	FK506/Cyclosporin-A addition ($t_{1/2}$ = 15 s)
Coumermycin GyrB-GyrB	Coumermycin addition	Dimerization: 30 seconds	Novobiocin addition
CoDi SNAP-SNAP	CoDi addition	Dimerization: 6 hours	–
xCrAsH CCPGCC-CCPGCC	xCrAsH addition	Dimerization: 1 hour	Dithiol addition (5 min)
Rapamycin FKBP12-FRB	Rapamycin addition	Dimerization: $t_{1/2}$ < 1 min	Washout/Outcompeting with FK506 (hours)
MaRap/AP21967 FKBP12-FRB*	MaRap/AP21967 addition	Dimerization: $t_{1/2}$ = 60 s	Washout/Outcompeting with FK506 (hours)
iRap FKBP12-FRB	iRap addition	Dimerization: $t_{1/2}$ = 10 s	Washout/Outcompeting with FK506 (hours)
ABA PYL-ABI	ABA addition	Dimerization: 30 min	Washout (hours)
GA_3-AM GID1-GAI	GA_3-AM addition	Dimerization: 10-60 s	Washout (hours)
ABA-HP/GA-HP PYL-ABI/GID1-GAI	H_2O_2 induced decaging	Decaging: 5-30 min Dimerization: 10-30 min	–
HaXS SNAP-Halo	HaXS addition	Dimerization: > 15 min	–
rCD1 SNAP-FKBP	rCD1 addition	Dimerization: 10-30 min	FK506 addition ($t_{1/2}$=15 s)
SLF'-TMP FKBP'-eDHFR	SLF'-TMP addition	Dimerization: $t_{1/2}$ = 44 s	TMP addition (1-5 min), redimerization by dimerizer addition

approach to achieve improved temporal control. To this end, ABA and GA_3-AM were modified with a H_2O_2-sensitive boronate ester moiety to mask their dimerization activity. Consequently, the modified dimerizers, termed ABA-HP and GA-HP, only become active upon dose-dependent exposure to exogenous or endogenous H_2O_2, which promotes chemical cleavage of the boronate group [15,106]. Finally, ABA and GA_3-AM or ABA-HP and GA-HP can be used orthogonal to rapamycin-based dimerization tools so that two signaling events can be manipulated independently within a single cell [17].

In addition to dimerizers derived from natural products, several artificial heterodimerizers haven been reported (Figure 1.4). The first artificial, non-covalent heterodimerizer, FK-CsA, was developed in 1996 by Belshaw *et al.* and consists of cyclosporin-A-fused to FK506. FK-CsA crosslinks FKBP12- and cyclophilinA-tagged proteins, but lacks biorthogonality and is thus not much superior to the homodimerizer FK1012 [100]. The same applies to Dex-FK506, which is a fusion product of FK506 and the glucocorticoid hormone dexamethasone and induces proximity of FKBP12 and a glucocorticoid receptor (GR) [101]. Dexamethasone was further combined with the dihydrofolate reductase (DHFR) inhibitor methotrexate to yield Dex-Mtx, a heterodimerizer for DHFRs and GR [102]. However, Dex-Mtx causes many off-target effects due to its interaction with endogenous DHFRs and was thus soon replaced by

Dex-TMP. Trimethoprim (TMP) is another DHFR inhibitor, but in contrast to methotrexate it is highly selective for *E.coli* DHFR (eDHFR), so that Dex-TMP is orthogonal in yeast [103].
The Cornish and Bertozzi labs joined efforts to develop a dimerizer, named TMP-SLF, which combines trimethoprim with a synthetic ligand of FKBP12 and mediates crosslinking of FKBP12 and eDHFR, but is not bioorthogonal [19,83]. Liu *et al.* addressed this challenge by combining TMP with a SLF (SLF') that binds with over 1000-fold selectivity to FKBP', the F36V mutant of FKBP12, and was initially applied for FKBP' homodimerization [20]. SLF'-TMP is thus completely orthogonal in eukaryotic systems and induces rapid dimerization of eDHFR- and FKBP'-fusion proteins. Additionally, SLF'-TMP-mediated crosslinking is rapidly reversible by outcompeting eDHFR-binding with TMP and may be applied orthogonal to rapamycin-based systems, which makes this dimerization tool superior to most available chemical dimerizers [15,18].
The only comparable system in terms of orthogonality and reversibility was presented by Schulz and colleagues, who generated the synthetic rCD1 dimerizer, a fusion of benzylguanine (BG) and another SLF. BG binds covalently to the SNAP-tag and accordingly rCD1 induces dimerization of SNAP- and FKBP'-fusion protein [105]. SNAP and Halo-tags had been employed to generate dimerizers before and Erhart *et al.* even combined both tags in their HaXS heterodimerizer, however even extensive optimization could not mitigate the slow kinetics and saturation effects [104]. rCD1 displays rapid dissociation kinetics, yet dimerization proceeds relatively slow, which presents a serious limitation for some applications.
Taken together, SLF'-TMP appears to be superior to most chemical heterodimerizers in terms of speed, orthogonality and reversibility. It provides improved temporal control of dimerization and dissociation of proteins, especially compared to chemical homodimerizers. Plant hormone based dimerizers, particularly GA_3-AM, feature rapid dimerization kinetics and biorthogonality as well, but their dissociation kinetics remain to be optimized.

1.2.2 Photoinducible Dimerization Systems

Photoinducible dimerization systems provide a spatiotemporal resolution that is unmatched by chemical crosslinking approaches. While the speed of chemically induced dimerization is limited to at least a few seconds by the cellular diffusion rate, photoactivation can be performed within milliseconds or even faster. Moreover, light-induced dimerization can be applied in a spatially defined manner on a subcellular level, which is beneficial when studying spatiotemporally restricted processes. Similar to chemical dimerizers, photodimerizers should ideally be bioorthogonal, non-cytotoxic, and react rapidly, but the photoactivation conditions, i.e. wavelength and intensity, are also decisive factors. Exposure to ultraviolet (UV) light can potentially cause DNA damage and other off-target effects. The same applies to high intensity illumination over a longer period of time [83,114]. Still, most photocleavable caging groups employed to confer photosensitivity to small molecules, react to UV light irradiation, which has to be optimized in the future.
In 2011, two rapamycin-based photosensitive dimerizers were reported: pRap and cRb. Karginov *et al.* generated photocaged rapamycin (pRab) by installing a photocleavable α-methyl-6-nitropiperonyloxycarbonyl (MeNPOC) group at the C-40 position of rapamycin. Like rapamycin, pRab induces interaction of FRB and wild type FKBP12 even in its photocaged form, so that engineering of a pRab-specific FKBP12 mutant, iFKBP, was necessary. Photodecaging can be performed by UV light illumination on a time scale of 1-2 minutes (see table 1.2) and even though dimerization speed was not reported, it should be in an order comparable to rapamycin induced dimerization [107].
Umeda and co-workers chose a different approach and modified rapamycin with a biotin-avidin com-

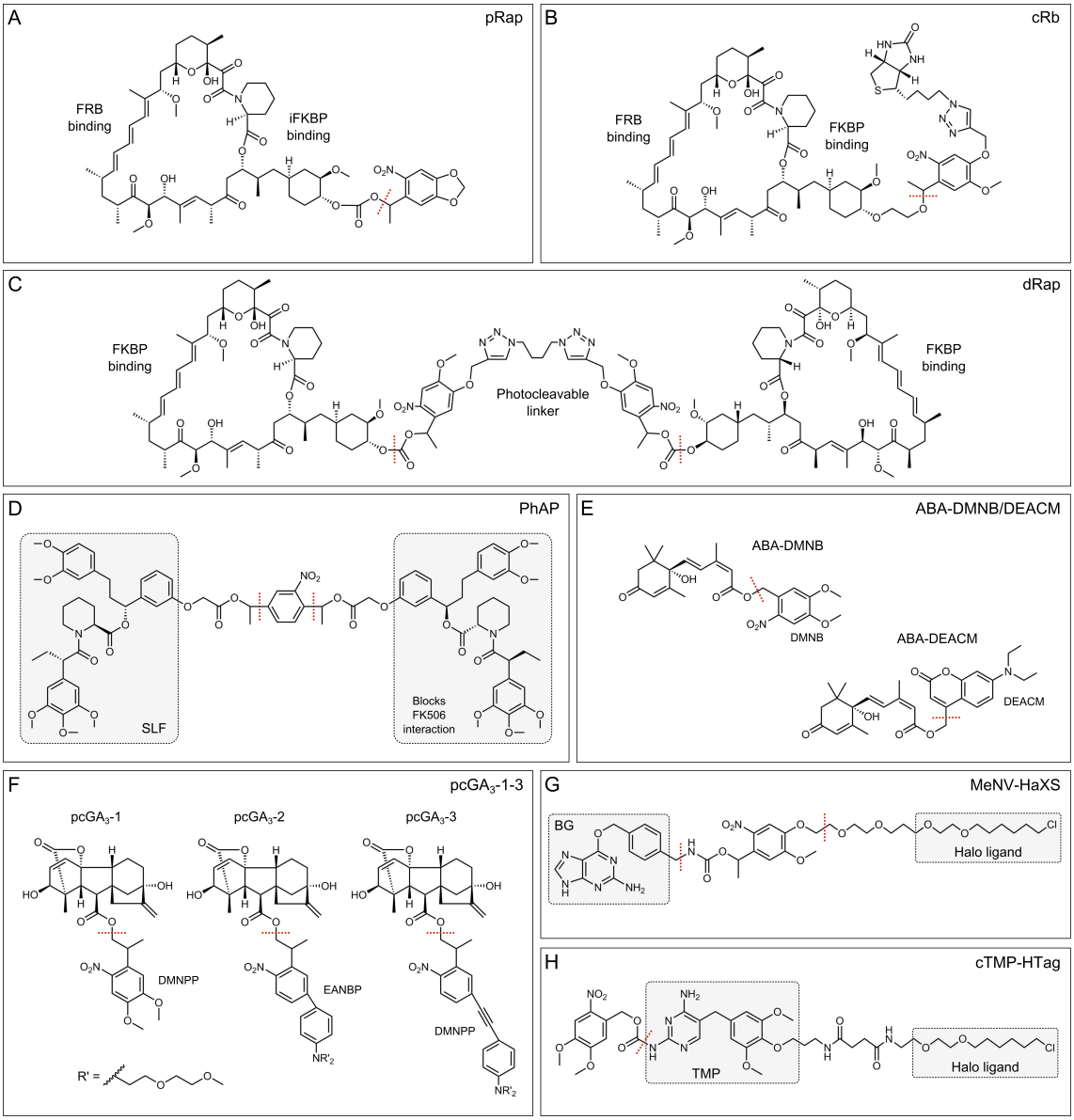

Figure 1.5: Molecular structures of photocaged chemical dimerizers, photocleavage sites are indicated by dotted red lines. **A** pRap has a photocleavable MeNPOC group at rapamycins C-40 position and crosslinks FRB- and iFKBP-domains after decaging at 365 nm [107]. **B** cRb features a biotin-avidin complex attached through a nitrobenzyl linker that is cleaved at 365 nm to dimerize FRB- and FKPB-domains [108]. **C** dRap has a *N*-succinimidyl carbonate at rapamycins C-40 position, which is cleaved at 365 nm to induce homodimerize FKBP-domains [109]. **D** PhAP was developed by inserting a o-nitrobenzyl group into AP20187, which is photocleaved at 365 nm to homodimerize FKBP' [110]. **E** ABA-DMNB/DEACM feature a nitrobenzyl (DMNB) or coumarin (DEACM) group at the carboxylic acid moiety of ABA. DMNB is cleaved at 365 nm and DEACM at 405 nm to crosslink PYL- and ABI-domains [111]. **F** $pcGA_3$-1-3 have a DMNPP ($pcGA_3$-1), EANBP ($pcGA_3$-2) or 2-(*o*-nitro-phenyl)propyl ($pcGA_3$-3) that are photocleaved at 365 nm ($pcGA_3$) or 412/800 nm ($pcGA_3$-2/3) to dimerize GAI- and GID1-domains [112] . **G** MeNV-HaXS combines BG with a Halo ligand and a photocleavable linker (365 nm) to induce dissociation of SNAP- and Halo-fusion proteins [73] . **H** cTMP-Htag is comprised of a Halo ligand and NVOC-caged TMP that is photoactivated at 385-405 nm and dimerizes Halo- and eDHFR-tagged proteins [113].

plex attached through a photocleavable nitrobenzyl linker to yield cRb. Due to the large size of the biotin-avidin group, the dimerizer cannot cross the plasma membrane and is sequestered in the extracellular space until UV light-induced release of rapamycin. Here, dimerization is induced within a

similar time frame as for pRap, but photodecaging can be performed within 0.5 seconds and is thus significantly faster[108]. The most recent modification of rapamycin was presented by Brown *et al.*, who created the UV light-sensitive dimerizer dRap by attaching a *N*-succinimidyl carbonate to rapamycins C-40 position. In contrast to pRap, dRap interacts with wild type FKBP12 while the kinetics of decaging and dimerization are similar[109]. However, none of the rapamycin-based dimerizers is bioorthogonal or reversible and whereas spatial confinement of dimerization is already very limited for pRap and dRab, cRb can only be applied to manipulate processes at the plasma membrane[83].

Ahmed *et al.* developed a photocaged variant of the FKBP' homodimerizer AP20187 by replacing the amine linker with a photosensitive o-nitrobenzyl group. This dimerizer, termed PhAP, crosslinks FKBP'-fusion proteins in their caged state and releases them upon UV light-induced photocleavage[110]. Theoretically, the PhAP system offers better spatiotemporal control than pRap, dRap and cRb, however, this has not been practically demonstrated. Moreover, the required 10 minutes of photodecaging might cause off-target effects.

In a similar approach, Zimmermann and co-workers generated a photocaged version of the Halo-SNAP heterodimerizer HaXS by inserting a photocleavable methyl-6-nitroveratryl (MeNV) group to the core module linking Halo and SNAP moieties. MeNV-HaXS chemically prompts dimerization of Halo- and SNAP-tagged proteins, which can then be reversed through UV light induced photolysis of the dimerizer. Here, spatiotemporal control of the system was extensively demonstrated by releasing proteins from individual vesicles, but the kinetics of dimerization and photodecaging range on a timescale of 10-15 minutes, which is comparably slow[73].

Recently, the plant hormone-based dimerization tools ABA and GA_3-AM have also been modified to become photoactivatable. To generate UV light-sensitive ABA-DMNB, a nitrobenzyl group (DMNB) was attached to the carboxylic acid moiety of ABA, while addition of a coumarin group (DEACM) yielded ABA-DEACM (Figure 1.5). The latter is photoactivatable by 405 nm light, which may be more convenient when experiments are performed on a confocal microscope lacking a UV lamp. The principle of ABA-DMNB/DEACM-regulated dimerization is similar to the pRap and cRb dimerization systems: crosslinking of PYL- or ABI-fusion proteins is induced by photocleavage of the the DMNB and DEACM groups from the ABA dimerizer. Here, photodecaging of the dimerizer can be triggered within a few minutes of illumination, but dimerization is only achieved after about 15 minutes. Still, ABA-DMNB/DEACM synthesis is simpler than generating the rapamycin variants and in theory, the system can be used orthogonal to other, chemically induced dimerization systems as well[15,111].

Based on GA_3-AM, Schelkle *et al.* established three other photoactivatable tools, termed pcGA_3-1-3, that were generated by addition of different caging groups: 2-(4,5-dimethoxy-2-nitrophenyl) propyl (DMNPP), (2-(4'-bis((2-methoxyethoxy)ethyl)amino)-4-nitro-[1,1'-biphenyl]-3-yl)propan-1-ol) (EANBP) and π-extended 2-(*o*-nitro-phenyl)propyl, respectively. Dimerization of GAI- and GID1-tagged proteins is induced upon photoactivation of the dimerizers by one-photon decaging with 405/470 nm light for pcGA_3-1/2 or two-photon decaging of pcGA_3-3 at 800 nm. Due to the red shifted absorption spectra of pcGA_3-2 and pcGA_3-3, they can be applied in parallel to UV light-sensitive tools and similar to ABA-DMNB/DEACM, pcGA_3 dimerizers do not interfere with rapamycin-based chemical dimerization systems. In contrast to most of the photoactivatable dimerizers, pcGA_3-1-3 decaging is completed within 3 seconds and protein crosslinking takes less then 3 minutes, which makes the pcGA_3 dimerizers superior to many others[112]. However, imaging in the commonly used GFP-channel might cause undesired decaging effects of pcGA_3-2/3 dimerizers and both of the plant hormone-based systems still lack reversibility of dimerization[15].

Table 1.2: Properties of photoinducible dimerization systems.

SYSTEM	DIMERIZATION TRIGGER	TIME SCALE	REVERSIBILITY
pRap FRB-iFKBP	Decaging at 365 nm	Decaging: 1-2 min Dimerization: not indicated (30-60 min)	Washout/Outcompeting with FK506 (hours)
cRb FRB-FKBP12	Decaging at 365 nm	Decaging: 0-60 s Dimerization: 2-10 min	Washout/Outcompeting with FK506 (hours)
dRap FRB-FKBP12	Decaging at 365 nm	Decaging: 3 min Dimerization: not indicated (similar to pRap)	Washout/Outcompeting with FK506 (hours)
PhAP FKBP'-FKBP'	Decaging at 365 nm	Decaging: 10 minutes Dimerization: 5-10 min	Washout/Outcompeting with FK506 (hours)
MeNV-HaXS SNAPTag-HaloTag	MeNV-HaXS addition	Dimerization: 2-10 min	Photocleavage of dimerizer at 360 nm (1-60 s)
ABA-DMNB/DEACM PYL-ABI	Decaging at 365/405 nm	Decaging: 1-4 min Dimerization: 15 min	Washout (30 min)
pcGA$_3$-1-3 GID-GAI	Decaging at 405/470 nm and two photon-decaging at 800 nm	Decaging: 2-10 s Dimerization: 30-180 s	–
cTMP-Htag eDHFR-HaloTag	Decaging of cTMP at 365-405 nm	Decaging: 2 s Dimerization: 15-240 s	TMP addition (2-10 min), redimerization after washing (10-30 min)

The most promising photoinducible dimerizer yet was introduced by Ballister *et al.*, who combined NVOC-caged TMP with an uncaged Halo ligand to yield cTMP-Htag. Whereas most of the photocaged dimerizers diffuse throughout the whole cell after photoactivation, cTMP-Htag can be pre-localized prior to decaging and thus provides an improved spatial resolution. The dimerizer is targeted to the compartment of choice via Halo-tagged cellular anchors and only then activated by illumination at 385-405 nm for 2 seconds. Crosslinking of eDHFR-fusion proteins and the pre-localized dimerizer is comparably fast (15-240 s) and the dimerization is also readily reversible by addition of TMP. Additionally, the system is completely bioorthogonal in mammalian cells and yeast, which in summary makes it the best available photoinduced dimerization tool yet[15,113].

1.2.3 Optogenetic Dimerization Systems

Light-responsive regulatory proteins occur naturally throughout all kingdoms of life and orchestrate processes ranging from plant development, gene expression and circadian rhythm to motion of microbes and communication of visual information. Accordingly, the photoreceptor family, comprises proteins with distinct chromophores, spectral ranges and kinetics, which have been utilized in various optogenetic dimerization systems. Six classes of photoreceptors have been identified: rhodopsins, phototropins, cryptochromes, phytochromes, BLUF proteins and photoactive yellow proteins[115]. Rhodopsins were the first photoreceptors used as optogenetic tools to manipulate gene expression or control action potentials in neurons by Shimizu-Sato *et al.* and Zemelman *et al.*, respectively[116,117].
One of the first optogenetic dimerization devices was developed by Yazawa *et al.*[118] based on the phototropin Light-Oxygen-Voltage (LOV) domain, which belongs to the PAS domain family and imparts

blue-light sensitivity[119,120,121]. Phototrophins, BULF proteins and cryptochromes are characterized by their flavin chromophore and the distinct structure of their light-sensing domains, LOV, BLUF and CRY[115]. LOV domains are flavin mononucleotide (FMN) binding photosensors and form a covalent bond to FMN molecules upon photoactivation, which may remain stable for seconds to days (depending on the type of LOV domain)[122].

Yazawa *et al.* generated an inducible dimerization system from the LOV domain containing protein FKF1 of *A. thaliana*, which has been found to interact with the nuclear protein GIGANTEA (GI) in a light-dependent manner. Illumination at 450 nm induces crosslinking of FKF1- and GI-fusion proteins within 5 minutes, but dissociation of the complex proceeds rather slow[118]. However, since the photoreceptors originated from plants, the system is bioorthogonal in mammalian cells and yeast, which indeed applies to the majority of optogenetic tools.

In an attempt to optimize dissociation kinetics, several systems were designed based on the asLOV2 domain of *A. sativa* phototropin 1, which features the characteristic C-terminal helical extension Jα. Photoactivation induces conformational changes in the asLOV2 domain resulting in Jα unwinding and ultimately dissociation. Initially, Hahn and co-workers fused asLOV2-Jα to constitutively active Rac1 in order to sterically block effector binding in the dark state thus yielding a photoactivatable GTPase[123]. Strickland *et al.* then adapted the principle and introduced tunable light-inducible dimerization tags (TULIPs) based on interaction of asLOV2 and engineered variants of the Erbin PDZ domain (ePDZ)[124]. Although many physical properties of LOV domains had already been successfully optimized[125,126,127,128], TULIPs were also among the first approaches to decrease the size of dimerization tags. To this end, Strickland and co-workers fused a ePDZ-binding peptide epitope to the Jα of asLOV2 so that the peptide would be allosterically blocked in the dark state. Photoactivation at 450 nm exposes the peptide and thus facilitates dimerization of the so-called LOVpep domain and the ePDZ domain, which is rapidly reversible in the dark state[122,124]. A very similar approach was developed by Lungu *et al.* based on the same strategy using different peptides (ipaA and SsrA) and their respective interaction domains (vinculin and SspB)[129].

Wang *et al.* developed the LightOn dimerization system employing the smallest LOV domain-containing protein Vivid (VVD) fused to the DNA-binding domain of Gal4 and the p65 activation domain of NF-κB[130]. Due to the VVD LOV domain, this fusion protein, named GAVPO, homodimerizes upon illumination at 450 nm, binds to a promoter and induces transcription of target genes[131]. However, as the initial LightOn system featured slow on/off kinetics and weak dimerization (see table 1.3), different groups evolved the original principle and dimerization/dissociation can now be performed within seconds[131,132,133].

Several other dimerization systems were generated based on the same principle as the LightOn approach: Motta-Mena *et al.* used an optimized version of the LOV domain-containing signaling peptide EL222 of *E. litoralis* with rapid on/off kinetics[134,135,136], Ohlendorf *et al.* presented the Dusk/Dawn system, which evolved from the YtvA system introduced by Möglich *et al.*[119,137,138] and most recently Hahn and colleagues combined asLOV2 with the protein Zdark (Zdk) to yield LOVTRAP. Since Zdk binds selectively to the dark state of asLOV2, illumination of LOVTRAP results in dissociation of the dimerization domains thus releasing the aLOV2- or Zdk-fused target protein[139].

Besides LOV domain-based dimerization systems, many approaches engage the light-sensing domains of cryptochromes, CRY. Photosensitivity of CRY domains is largely conferred through disordered C-terminal extensions that unfold upon photoactivation to expose recognition sites for interaction partners[115]. Kennedy and co-workers combined the CRY2 domain of cryptochrome 2 from *A. thaliana*

with a truncated version of its interacting protein CIB1 to yield a blue light-inducible dimerization system. While dimerization proceeds as fast as in the LOV-based systems, dissociation kinetics are slightly slower, but still on a time scale of minutes[122,140]. Based on CRY2-CIB1 heterodimerization Konermann *et al.* introduced a system termed LITEs (light-inducible transcriptional effectors), which consists of the customizable TALE DNA-binding domain coupled to CRY2 and CIB1 bound to the transcriptional activator VP64[141]. A different approach exploited the recent finding that CRY2 domains form oligomeric clusters independently of CIB1 interaction to generate the homodimerization system CRY2olig[142,143]. However, dissociation kinetics remain slower than observed for LOV-domain mediated dimerization and homodimerization is mostly inferior to heterodimerization approaches.

Another kind of blue light-sensitive photoswitches are BLUF proteins, which also carry a flavin chromophore, but occur predominantly in bacteria and lower eukaryotes[115]. Only few optogenetic dimerization approaches employ BLUF domains and the majority of them is based on photoactivated adenylyl cyclases (PACs), photosensitive enzymes featuring BLUF and enzymatic domains. PACs from *E. gracilis* (euPAC) and *Beggiatoa* (bPAC) have mostly been engineered to photocontrol cyclic adenosine monophosphate (cAMP) levels in neuronal cells of different organisms, but also to manipulate steroid hormone levels in *D. rerio* or in neuromuscular junctions of *C. elegans*[122,144,145,146].

All of the optogenetic dimerization systems mentioned above rely on blue light-sensitive photoreceptors, however, several approaches engage red light-sensitive phytochromes (PHY). Red light can penetrate deeper tissues and has a lower energy content than blue light, which is especially beneficial when probing whole organisms[147]. Phytochromes bind a tetrapyrrole chromophore and photoswitch between the red-sensitive (inactive) and far-red-sensitive (active) conformers Pr and Pfr, respectively. The conformational change from Pr to Pfr is initiated by photoactivation at 650 nm, but can be reversed upon illumination at 750 nm[148]. Five different phytochromes have been identified in plants and microbes (PhyA to PhyE). They interact frequently with constitutively active transcription factors called PIFs (phytochrome-interacting factors)[115]. Of the five, PhyB from *A. thaliana* is the most frequently used optogenetic tool. However, like all phytochromes it requires exogenous addition of a chromophore such as phycocyanobilin. This is beneficial because light protection is not necessary during sample handling. Still, chromophores are difficult to obtain and have a short half-life time in common cell culture media. Therefore Müller and co-workers developed a strategy to produce phycocyanobilin from heme in mammalian cells and thus provide sufficient chromophore levels to support phytochrome function[147].

Shimizu-Sato *et al.* generated a dimerization system based on PhyB-PIF3 interaction, which is photoactivated within seconds of illumination at 650 nm and rapidly reversed by irradiation at 750 nm[116,149]. Even though, the on/off kinetics were already rapid, Müller and colleagues adapted the method to design a PhyB/PIF6 based dimerization system, in which dissociation is induced within milliseconds[150].

Aside from phytochromes, the fluorescent protein Dronpa from stony coral has also been engineered to reversibly photoswitch between the blue light-sensitive active form and the violet light-sensitive inactive form[122,151]. In modified variants of Dronpa conformational conversion is induced rapidly upon illumination, which was exploited by Zhou *et al.* to build photosensitive 'caged' single-chain proteins[151].

Another commonly applied optogenetic dimerization system engages the *A. thaliana* photoreceptor UVR8, which contains a tryptophan-based chromophore and forms a homodimer in the dark state. Upon UV light illumination, the dimer dissociates and the two subunits interact with the WD40 domains of COP1[122,152]. While crosslinking takes only seconds, the dissociation kinetics are very slow thus limiting the applicability of UVR8-based tools. However, Chen *et al.* demonstrated that the slow reassociation kinetics of UVR8 can also be exploited and created a photoinducible protein secretion system

Table 1.3: Properties of optogenetic dimerization systems.

SYSTEM	DIMERIZATION TRIGGER	TIME SCALE	REVERSIBILITY
FKF1-GI	Photoactivation at 450 nm	Dimerization: 5 min	Dark state Dissociation: hours
TULIPs LOVpep-ePDZ	Photoactivation at 450 nm	Dimerization: seconds	Dark state Dissociation: seconds
LightOn/Magnets VVD-VVD	Photoactivation at 450 nm	Dimerization: seconds	Dark state Dissociation: seconds to days
Dusk/Dawn YtvA-YtvA (EL222)	Photoactivation at 450 nm	Dimerization: seconds	Dark state Dissociation: seconds
LOVTRAP aLOV2-Zdk	Photoactivation at 450-490 nm	Dimerization: 1 second	Dark state Dissociation: seconds
LITE CRY2-CIB1	Photoactivation at 450 nm	Dimerization: seconds	Dark state Dissociation: 6 min
CRY2olig CRY2-CRY2	Photoactivation at 450 nm	Dimerization: seconds	Dark state Dissociation: 6-23 min
BLUF PAC-PAC	Photoactivation at 450 nm	Dimerization: seconds	Dark state Dissociation: seconds
PhyB-PIF3	Photoactivation at 650 nm	Dimerization: seconds	Illumination at 750 nm Dissociation: seconds
PhyB-PIF6	Photoactivation at 650 nm	Dimerization: milliseconds	Illumination at 750 nm Dissociation: milliseconds
Dronpa-Dronpa	Photoactivation at 500 nm	Dimerization: seconds	Illumination at 400 nm Dissociation: seconds
UVR8-COP1	Photoactivation at 310 nm	Dimerization: seconds	Illumination at 290 nm Dissociation: 1-4 hours
UVR8-UVR8	Photoactivation at 315 nm	Dimerization: seconds	Illumination at 280 nm Dissociation: 2-24 hours

based on homodimerization of UVR8. Target proteins were fused to UVR8, sequestered into the ER and then released by UV illumination to travel through the secretory pathway [153].
In conclusion, it appears not feasable to determine the most superior optogenetic dimerization system, because their kinetic properties are similar, all of them are bioorthogonal and reversible and many have been designed for specific applications. The PhyB-PIF based systems feature light induced reversibility, which might be beneficial in various aspects, however it also limits the available imaging channels. Only the UVR8 based dimerization tool shows rather slow dissociation rate, but even this potential limitation proved to be valuable for some applications.

1.2.4 Biological Applications of Inducible Dimerization Systems

Due to their versatile nature, inducible dimerization systems have become a powerful technique with numerous applications and many tailor-made variants to tackle specific biological questions. In contrast to traditional methods like RNAi or transfection and overexpression, inducible dimerization facilitates rapid and often reversible manipulation of cellular proteins in spatially defined regions

of interest[17]. Accordingly, induced dimerization has been used to control protein localization and activity. To this end, proteins can be conditionally targeted to cellular anchors, complex formation or dissociation can be induced or split proteins are reconstituted. Especially the most recent generation of dimerization tools provides excellent spatiotemporal resolution and thus applications have become more and more diverse[15,83].

1.2.4.1 Regulation of Biochemical Activity

When the Schreiber and Crabtree groups first introduced chemically induced dimerization, they were actually looking for a technique to regulate a proteins activity without changing its localization. As a result, they developed a broadly applicable concept to manipulate biochemical activity and successfully applied it to study T-cell receptor signaling. It had been observed earlier that dimerization is a key signaling event for many receptors. Accordingly, the T-cell receptor zeta could be activated simply by FK1012-induced homodimerization of FKBP12-fused T-cell-receptors[74]. The principle has since been applied to study the function of various signaling proteins such as the receptor kinases TGF-Beta[154], ErbB[155] or FGFR1[156,157], Raf/MEK/ERK signaling[142,143] as well as the roles of β-arrestin2[158] or AngII AT1 and NE α2C-adrenergic receptors[159] in GPCR signaling.
Dimerization induced activation of signaling pathways has also been exploited to initiate cellular events like proliferation[160,161] or apoptosis. Again, Schreiber and Crabtree established induction of apoptosis by forcing Fas proteins into proximity, but many other proteins like FADD, Asc, Bid and several caspases can also be crosslinked to activate the process[80,162,163,164,165,166].
Another variation of the concept is induction of gene transcription by photoactivated dimerization of DNA-binding domains and transcriptional activators. The LightOn system, for instance, is based on homodimerization of the engineered protein GAVPO, which combines the VVD-fused DNA-binding domain of Gal4 and NF-κBs p65 activation domain[130]. The same principle was applied in the Dusk/Dawn system, where homodimerization of the histidine kinase YF1 and the transcriptional regulator FixJ induces gene expression and also in the LITE system, which relies on crosslinking of the CRY2/CIB1-fused TALE DNA-binding domain and the transcriptional activator VP64[138,141].
All of the approaches mentioned above are based on target proteins functioning in pathways or processes, which already feature dimerization as signaling event. To manipulate the activity of proteins that do not rely on this mechanism, other methods are required[83]. Thus, inducible dimerization has also been extensively used to generate split proteins consisting of two non-functional protein fragments fused to dimerization domains. Upon dimerization, the protein is either reconstituted or conformational change exposes an active site so that the protein can resume its original function. Especially optogenetic dimerization systems are well suited for this approach, since they allow for spatiotemporal confinement of dimerization and thus very focused control of protein activity.
The Hahn lab, for instance, generated a range of activatable kinases by inserting a FKBP (or iFKBP) domain at a conserved position in the catalytic domain to render the protein inactive. Rapamycin-mediated interaction of FKBP with FRB causes a substantial structural alteration and restores the catalytic activity. These 'allosteric switches' were initially based on chemically induced dimerization, but soon after combined with photocaged rapamycin (pRab) to yield photoactivatable kinases[107,167,168,169].
An optimized version of the technique was realized in the 'rapamycin-regulated targeted activation of pathways' (RabR-TAP) system that combines inducible activation with protein translocalization. While

kinase activity is still controlled by photodecaging of rapamycin, the kinase is additionally targeted to FRB-fused effectors or specific cellular compartments. In consequence, kinase activity can be directed to downstream effectors of different signaling pathways, which then become active [15,170].
Another application was introduced by the Bertozzi group, who focused on glycobiology and separated glycotransferases into their catalytic and localization domains to control their activity with the chemical dimerizer SLF-TMP [19]. Two proteases have also been engineered to become chemically activatable: TEV protease and DnaE intein. These enzymes are particularly interesting as they can regulate protein ligation and cleavage, which makes them even more powerful when combined with inducible dimerization [83,171,172,173].
Many split proteins were designed to regulate gene expression. Kennedy *et al.* generated CRY2/CIB1-tagged, split Gal4 and Cre recombinase that prompt DNA transcription or recombination, respectively, upon photoinduced reconstitution [122,140]. Shimizu-Sato *et al.*, on the other hand, developed the first approach to reversibly induce DNA transcription in yeast based on photoinduced PhyB and PIF3 dimerization. As several others afterwards, they created a split version of the transcription factor Gal4 fused to PhyB/PIF3, which activates DNA transcription upon dimerization and is deactivated upon photoinduced dissociation [116]. Later, Müller and colleagues adapted the method to manipulate gene expression in mammalian systems based on PhyB/PIF6 or UVR8 coupled split transcription factors [150,174].
A different approach to manipulate protein activity is steric hindrance of protein interaction by dimerization domains. As mentioned above, Wu *et al.* presented photoactivatable GTPases by introducing asLOV2-Jα to constitutively active RacI and thus block effector binding in the dark [123]. Also engaging an optogenetic dimerization system, Zhou *et al.* fused monomeric DronpaK to one terminus and tetrameric DronpaN to the other terminus of guanine nucleotide exchange factors (GEFs) so that binding of the two Dronpas would block interaction sites and lock the protein in an inactive state. Photoactivation with blue light induces dissociation of the Dronpa multimer and thus activates the caged protein by opening its interaction sites [151].
Similar to activation of proteins, inducible dimerization can also be applied to prompt protein degradation. The concept was first demonstrated in budding yeast by Janse and co-workers, who targeted proteins of interest to the ubiquitin-proteasome pathway by chemically dimerizing them with proteasomal subunits [175]. Pratt *et al.* translated the approach to eukaryotic cells and designed a system termed 'split ubiquitin for the rescue of function' (SURF). Here, proteins are marked for degradation by the proteasome through addition of a N-terminal degron, but can be rescued upon rapamycin-mediated reconstitution of a C-terminally bound split ubiquitin [176]. A similar strategy was pursued by Nishimura *et al.* in an inducible system adapted from the auxin-dependent degradation pathway of plants [177]. In contrast, Stankunas and co-workers demonstrated that dimerization can also be employed to stabilize proteins by destabilizing the glycogen synthase kinase-3 beta through fusion to FRB*, and restoring its stability upon dimerization with FKBP12 [99].

1.2.4.2 Controlling Protein Localization

Protein translocalization is a key signaling event in cells, facilitating communication between organelles, exchange of cellular material and signal transduction throughout regulatory networks. It provides means to rapidly alter intracellular processes and is a crucial factor in the organization of cellular events. To control protein localization through inducible dimerization, typically a protein of interest

is crosslinked with an anchor protein that resides at a specific cellular localization. Since the concept was first introduced by Spencer *et al.* in 1995, proteins have successfully been targeted to the plasma membrane, mitochondria, endoplasmatic reticulum, Golgi apparatus, nucleus, ERGIC, peroxisomes, kinetochores, genomic loci and various other cellular addresses [17,83,178].

Especially the plasma membrane is a popular target, in part because it is comparably easy to address and distinguish, but mostly because it is involved in fundamental cellular processes like cell migration, endocytosis or receptor trafficking [179]. A large number of dimerization probes has been designed to manipulate lipid signaling at the plasma membrane, mostly focusing on the second messengers phosphatidylinositol 4,5-bisphosphate ($PI(4,5)P_2$) and phosphatidylinositol 3-phosphate (PI3P). In 2006, Suh *et al.* and Varnai *et al.* independently introduced a now commonly applied approach to alter $PI(4,5)P_2$ levels: chemically induced recruitment of $PI(4,5)P_2$ 5-phosphatases or 5-kinases to the plasma membrane to decrease or enhance $PI(4,5)P_2$ concentration, respectively [180,181]. 5-phosphatases specifically cleave the phosphate at the C-5 position of $PI(4,5)P_2$ so that a locally increased concentration of 5-phosphatases, like Inp54p, causes a spatially confined depletion of the second messenger. In contrast, kinases such as the PI(4)P 5-kinase, transfer a phosphate group to the 5 position of PI(4)P and thus generate $PI(4,5)P_2$. Suh *et al.* first demonstrated that the activity of the potassium channel KCNQ is tightly associated with $PI(4,5)P_2$ levels and since then the approach has been used to study $PI(4,5)P_2$s function in regulation of other ion channels [182,183], endocytosis [184,185,186], store-operated calcium entry [187,188], PTEN activation [189] and cell movement [190,191]. Fili and co-workers also targeted a phosphatase to Rab5-positive endosomes and observed effects on maturation and structure [192], while Szentpetery *et al.* manipulated $PI(4,5)P_2$ levels in the Golgi membranes [17,179,193].

The most recent approach to alter $PI(4,5)P_2$ concentrations was presented by the Inoue lab and termed $PI(4,5)P_2$ liberation [194]. Here, the amount of free $PI(4,5)P_2$ at the plasma membrane is increased without altering the overall level of $PI(4,5)P_2$ by re-routing the $PI(4,5)P_2$-binding PH domain of PLCδ to the mitochondria. Inoue and co-workers based their $PI(4,5)P_2$ liberation approach on rapamycin induced dimerization of FKBP and FRB domains. The Schulz lab adapted the concept to their rCD1 dimerizer system. Since rCD1-mediated dimerization features rapid reversibility, Schulz and co-workers were able to fine-tune $PI(4,5)P_2$ levels at the plasma membrane with high temporal resolution [15,195].

Another class of proteins that has been extensively studied with inducible dimerization systems are GTPases. GTPases are monomeric G proteins, which switch between an active GTP-bound form and an inactive GDP-bound form [17,122]. Castellano *et al.* were amongst the first to conditionally localize the Rho family GTPase Rac1 to the plasma membrane to elucidate its role in phagocytosis [196,197]. Rho family GTPases interact with distinct effector proteins regulating the organization of the cytoskeleton [122]. Castellano and co-workers chemically induced dimerization of FRB-fused constitutively active Rac1 and the FKBP-tagged cell surface receptor CD25 and observed increased uptake of CD25-bound latex beads through actin-dependent phagocytosis [179]. Inoue *et al.* followed the same principle, but used iRap to target FRB-fused Rho GTPases to plasma membrane localized $Lyn_1$1-FKBP domains. Recruitment of the GTPases Rac1, Cdc42 and RhoA is achieved rapidly due to iRaps optimized kinetic properties and accordingly morphological changes such as membrane ruffling or lamellipodia extension could be observed within minutes after dimerizer addition [92].

As mentioned above, Hahn and co-workers chose a different approach and generated a photoactivatable Rac1 by fusing it to the asLOV2-Jα domain [123]. Here, photoactivation of Rac1 induced membrane ruffling and protusion, which was also reported by Yazawa *et al.* who targeted Rac1 to the plasma membrane through photoinduced dimerization of Rac1-FKF1 and CAAX-GI [118]. Levskaya and co-workers on

the other hand, employed light induced dimerization of PhyB and PIF3 to localize Rac1 and two other Rho-family GTPases (Cdc42 and RhoA) to the plasma membrane by using their GEFs as bait and observed a 'localized lamellipodial bloom' that could even be guided away from the main cell body with a focused laser beam[149].

In general, photoactivatable dimerization systems appear to be advantageous to study morphological effects at the plasma membrane, because they can be applied in a spatially confined fashion. Targeting other organelles, however, is technically challenging, especially when it comes to small or less defined structures like the mitochondria or the ER. Thus, the Inoue lab, amongst others, continued to employ chemical dimerizers (iRap) in order to study the effects of localizing constitutively active Ras to the Golgi, mitochondria, ER or lysosomes[198,199]. Apart from the Rho family, other GTPases, for example in Raf/MEK/ERK signaling, have also been studied with inducible dimerization systems[200,201]. However, the concepts resemble the previously introduced approach of localization-dependent activation of GTPases.

A new combination of the split protein approach and dimerization induced recruitment of proteins was recently presented by Kapitein and co-workers, who employed kinesin, dynein and myosin motors to drive specific cargo transport[202]. Previously, motor proteins were mostly studied with *in vitro* assays rather than in live cells, which presents a serious limitation when studying dynamics and specific cargo preferences. Kapitein *et al.* generated a split kinesin consisting of a constitutively active motor domain fused to FKBP and a series of FRB-tagged kinesin tails. In neuronal cells, the motor domain moves along a microtubule towards the axon or the dendrites, depending on the cargo, while the kinesin tail confers specificity for a certain vesicle. Consequently, rapamycin-induced reconstitution of the motor and the tail, causes mislocalization of the vesicles to the axon or the dendrites. The increases amount of vesicles in a distinct cell region is then used as readout for the kinesin-vesicle interaction[15].

Initially, the assay was only applied in neurons, because their unique organization facilitates an optimal readout, but Bentley and co-workers adapted the method to other cell types[203,204,205]. They engaged a kinesin motor domain that moves towards the plus end of microtubules, i.e. the cell center and a dynein motor, which moves towards the minus end of microtubules or the cell periphery. A series of candidate proteins associating with different vesicles or organelles was then chemically crosslinked to the motor domains and vesicle accumulation in the periphery or central region was used as a readout[15].

To mitigate the limitations of rapalog-induced dimerization and achieve a better spatiotemporal resolution, three recent studies combined the concept with photoactivatable dimerizers. Specifically, the Kapitein and Cui labs employed optogenetic approaches based on blue light induced interaction of LOVpep and ePDZ or CIB1 and CRY2 domains to reconstitute the split motor proteins, while Ballister and co-workers turned to the photocaged cTMP-Htag dimerizer[206,207,208]. All three approaches yielded an improved spatiotemporal resolution and reversibility, but none represents a signifcant improvement.

In the applications presented so far, inducible dimerization was largely employed to activate proteins or pathways, but several approaches were also designed to perturb protein activity. Two methods are predominantly applied, the anchor-away and the knocksideaways technique[209,210]. To 'anchor-away' a protein, it is targeted to highly-expressed cytoplasmic anchor proteins, for example to the ribosome. In yeast, this approach has been extensively applied to deplete the nucleus of certain proteins and study processes like RNA polymerase II termination[211] or fatty acid synthetase (FAS)[212] and to perturb the transcriptional activator Gal4p[213], cell division cycle protein Cdc6[214] or the histone chaperones Spt16/6[15,215]. However, the method is limited to specific nuclear proteins and depends on nuclear export of the respective proteins, which is not the case in the knocksideaways approach. Here, proteins

of interest were knocked down with siRNA and replaced by FKBP-tagged siRNA-resistant proteins that can be targeted to the mitochondria via rapalog-induced dimerization. Depleting the cytoplasm of the engineered proteins led to rapid perturbation of the protein function, but the method is not broadly applicable. Still, knocksideaways was successfully used to study retrograde TGN-to-endosome and also clathrin-coated vesicle-mediated trafficking[15,210,216,217].

A plethora of additional applications has been generated based on inducible dimerization systems and while the diversity is ever increasing, the underlying concepts, remain similar. Recently, photocaged dimerizers generated a lot of attention due to their enhanced spatiotemporal resolution, but only few applications have exploited their unique properties yet. Manipulation of multiple targets by orthogonal application of different dimerization systems is another approach, which holds great potential, but remains to be fully established. Thus, even though inducible dimerization systems experienced a vast improvement over the last 20 years, the will most likely continue to be refined and repurposed over the next few years[83].

2 Materials and Methods

2.1 Materials

2.1.1 Chemicals

All chemicals were purchased from the following companies in the highest purity available.

Table 2.1: Frequently used chemicals and suppliers.

CHEMICAL	SUPPLIER
2-Propanol	J. T. Baker (Deventer, Netherlands)
Acetic acid	Sigma-Aldrich (München, Germany)
Acrylamid/Bisacrylamide (37.5:1, 30 % w/v)	AppliChem GmbH (Darmstadt, Germany)
Agarose	Invitrogen (Darmstadt, Germany)
Ammonium Peroxodisulfate (APS)	Serva (Heidelberg, Germany)
Ammonium persulfate (APS)	Serva (Heidelberg, Germany)
Ampicillin Sodium Salt (Amp)	Gerbu (Gaiberg, Germany)
BafilomycinA1	Sigma-Aldrich (München, Germany)
Bovine serum albumine (BSA)	Biomol (Heidelberg, Germany)
Bradford reagent	BioRad (Hercules, USA)
Bromophenol Blue	Serva (Heidelberg, Germany)
Deoxycholate	AppliChem GmbH (Darmstadt, Germany)
Dimethylsulfoxide (DMSO)	Serva (Heidelberg, Germany)
Ethanol	Thermo Fisher Scientific (Waltham, USA)
Ethylenediaminetetraacetic adic (EDTA)	Gerbu (Gaiberg, Germany)
G418 disulfate salt	Sigma-Aldrich (München, Germany)
Glycerol	Gerbu (Gaiberg, Germany)
Glycine	Carl Roth GmbH (Karlsruhe, Germany)
Kanamycin (Kan)	Gerbu (Gaiberg, Germany)
Low Melting Point Agarose	Thermo Fisher Scientific (Waltham, USA)
Methanol	Sigma-Aldrich (München, Germany)
Milk powder, blotting grade	Carl Roth GmbH (Karlsruhe, Germany)
N,N,N',N'-tetramethylethylendiamin (TEMED)	Serva (Heidelberg, Germany)
NP-40	Sigma-Aldrich (München, Germany)
Orange G	Sigma-Aldrich (München, Germany)
Paraformaldehyde/PBS (4%)	Morphisto (Frankfurt, Germany)

Phenylmethylsulfonylfluoride (PMSF)	Serva (Heidelberg, Germany)
Phosphate buffered saline	Thermo Fisher Scientific (Waltham, USA)
Puromycin	Sigma-Aldrich (München, Germany)
Rapamycin	Biomol (Heidelberg, Germany)
SLF'-TMP	AG Wu (Dortmund, Germany)
Sodium azide	Sigma-Aldrich (München, Germany)
Sodium chloride (NaCl)	Sigma-Aldrich (München, Germany)
Sodium dodecyl sulfate (SDS)	Carl Roth GmbH (Karlsruhe, Germany)
Sucrose	Sigma-Aldrich (München, Germany)
Trimethoprim (TMP)	Sigma-Aldrich (München, Germany)
Tris-(hydroxymethyl)-aminomethan (Tris)	Santa Cruz Biotechnology (Dallas, USA)
Triton X-100	Thermo Fisher Scientific (Waltham, USA)
Tween-20	Serva (Heidelberg, Germany)
Wortmannin	Sigma-Aldrich (München, Germany)
β-Mercaptoethanol	Serva (Heidelberg, Germany)

2.1.2 Enzymes and Standards

The following enzymes and standards were used in this PhD thesis.

Table 2.2: Frequently used enzymes, standards, and suppliers.

ENZYME/STANDARD	SUPPLIER
DpnI	Thermo Fisher Scientific (Waltham, USA)
FastDigest Restriction Enzymes	Fermentas (St. Leon-Rot, Germany)
GeneRuler 1 kb DNA Ladder	Fermentas (St. Leon-Rot, Germany)
Phusion HF PCR Master Mix	Thermo Fisher Scientific (Waltham, USA)
Prestained Protein Marker	New England Biolabs (Frankfurt, Germany)
Protease Inhibitor Cocktail cOmplete	Roche (Grenzach-Wyhlen, Germany)
RedSafe Nucleic Acid Staining Solution	iNtRON Biotechnology (Gyunggi-Do, South Korea)
RedTaq DNA Polymerase	Sigma-Aldrich (München, Germany)
Shrimp Alkaline Phosphatase (SAP)	Fermentas (St. Leon-Rot, Germany)
T4 DNA Ligase	Fermentas (St. Leon-Rot, Germany)

2.1.3 Cell Culture Media and Reagents

All media and reagents were purchased from the following companies in the highest quality available.

Table 2.3: List of frequently used media and reagents and suppliers.

MEDIUM/REAGENT	SUPPLIER
Dulbecco's Phosphate Buffered Saline (DPBS)	Sigma-Aldrich (München, Germany)
Dulbecco's Modified Eagle Medium (DMEM)	Sigma-Aldrich (München, Germany)
Earl's Balanced Salt Solution (EBSS)	Sigma-Aldrich (München, Germany)
Fetal Bovine Serum (FBS)	Thermo Fisher Scientific (Waltham, USA)
Hank's Balanced Salt Solution (HBSS)	Sigma-Aldrich (München, Germany)
Insulin Solution	Sigma-Aldrich (München, Germany)
Minimum Essential Medium Eagle (MEME)	Sigma-Aldrich (München, Germany)
Non-Essential Amino Acid Solution	Sigma-Aldrich (München, Germany)
Opti-MEM Reduced Serum Medium	Life Technologies (Darmstadt, Germany)
Penicillin-Streptomycin	Sigma-Aldrich (München, Germany)
Sodium Pyruvate Solution	Sigma-Aldrich (München, Germany)
Trypsin-EDTA Solution	Sigma-Aldrich (München, Germany)
X-tremeGENE HP DNA Transfection Reagent	Roche (Grenzach-Wyhlen, Germany)

2.1.4 Antibodies

Primary and secondary antibodies were obtained in the highest quality available and selected to meet requirements for immunofluorescence or immunoprecipitation experiments.

Table 2.4: Frequently applied antibodies and suppliers

ANTIBODY	SUPPLIER
Anti-Actin	Merck-Millipore (Darmstadt, Germany)
Anti-Atg14L	BioCat GmbH (Heidelberg, Germany)
Anti-Beclin1	Abcam (Cambridge, United Kingdom)
Anti-GFP	Cell Signalling (Danvers, USA)
Anti-HA	Abcam (Cambridge, United Kingdom)
Anti-His	Cell Signalling (Danvers, USA)
anti-LC3B	Cell Signalling (Danvers, USA)
Anti-mCherry	Abcam (Cambridge, United Kingdom)
anti-PI3K Class III	Abcam (Cambridge, United Kingdom)
anti-tRFP	Evrogen (Moscow, Russia)
Anti-UVRAG	Abcam (Cambridge, United Kingdom)
AlexaFluor488 Goat Anti-Mouse IgG	Jackson ImmunoResearch (Baltimore, USA)
AlexaFluor488 Goat Anti-Rabbit IgG	Jackson ImmunoResearch (Baltimore, USA)
DyLight405 Goat anti-Mouse IgG	Jackson ImmunoResearch (Baltimore, USA)
DyLight405 Goat anti-Rabbit IgG	Jackson ImmunoResearch (Baltimore, USA)
DyLight647 Mouse Anti-Rabbit IgG	Jackson ImmunoResearch (Baltimore, USA)
DyLight649 Rat Anti-Mouse IgG	Jackson ImmunoResearch (Baltimore, USA)

2.1.5 Kits

The following kits were used in this PhD thesis.

Table 2.5: Frequently used kits and suppliers

KIT	SUPPLIER
BigDye Terminator v3.1 Cycle Sequencing Kit	Life Technologies (Darmstadt, Germany)
E.Z.N.A. Cycle Pure Kit	VWR (Darmstadt, Germany)
E.Z.N.A. Gel Extraction Kit	VWR (Darmstadt, Germany)
E.Z.N.A. Plasmid Maxi Kit	VWR (Darmstadt, Germany)
E.Z.N.A. Plasmid Mini Kit	VWR (Darmstadt, Germany)
GFP- and RFP-Trap	Chromotek (Planegg-Martinsried, Germany)
SuperSignal Blotting Detection Reagent	Thermo Fisher Scientific (Waltham, USA)
Western Blotting Detection Reagent	GE Healthcare (München, Germany)

2.1.6 Consumables

All consumables were obtained from the following companies in the highest quality available.

Table 2.6: List of frequently used consumables and suppliers.

CONSUMABLE	SUPPLIER
Cell culture dishes (60 mm, 100 mm, 150 mm)	Sarstedt (Nümbrecht, Germany)
Cell culture flasks (75 cm^2, 175 cm^2)	Sarstedt (Nümbrecht, Germany)
Cell Scraper	Falcon GmbH (Gräfeling-Locham, Germany)
Cloning cylinders (150 µL)	Sigma-Aldrich (München, Germany)
CryoPure Tubes	Sarstedt (Nümbrecht, Germany)
Electroporation cuvettes	Peqlab (Erlangen, Germany)
Eppendorf tube (0.5 mL, 1.5 mL, 2.0 mL, 5.0 mL)	Eppendorf (Hamburg, Germany)
Falcon Tube (50 mL, 15 mL)	Falcon GmbH (Gräfeling-Locham, Germany)
Filter Paper	Thermo Fisher Scientific (Waltham, USA)
Glass Bottom Chambers (4-well , 8-well)	Sarstedt (Nümbrecht, Germany)
Glass Bottom Dishes (35 mm)	MatTek Corporation (Ashland, USA)
Immersion Oil	Olympus (Hamburg, Germany)
Lens Cleaning Tissue	Thorlabs Inc. (Austin, USA)
Multiwell plates (6-well, 12-well, 96-well)	Sarstedt (Nümbrecht, Germany)
Nitrocellulose Membrane	GE Healthcare (München, Germany)
Parafilm	Sigma-Aldrich (München, Germany)
PCR Strips and Tubes	Sarstedt (Nümbrecht, Germany)
Pipette tips (1 - 10 µL, 20 - 200 µL, 100 - 1000 µL)	Nerbe Plus GmbH (Winsen/Luhe, Germany)
Serological pipettes (5 mL, 10 mL, 25 mL)	Sarstedt (Nümbrecht, Germany)
Surgical Disposable Scalpels/Syringes	Braun (Aschaffenburg, Germany)
Syringe Filters (0.22 µm)	Sarstedt (Nümbrecht, Germany)
UltraCruz Autoradiography Film	Santa Cruz Biotechnology (Dallas, USA)
UV Curvettes	Sarstedt (Nümbrecht, Germany)

2.1.7 Instruments

The following instruments were used in the course of this thesis.

Table 2.7: Frequently used instruments.

INSTRUMENT	SUPPLIER
ABI PRISM 3130x1 Genetic Analyzer	Life Technologies (Darmstadt, Germany)
AlphaImager HP	Alpha Innotec (Kasendorf, Germany)
BioPhotometer	Eppendorf (Hamburg, Germany)
Blotting Cassette	GE Healthcare (München, Germany)
Centrifuge 5415C	Eppendorf (Hamburg, Germany)
Centrifuge 5415R	Eppendorf (Hamburg, Germany)
Centrifuge 5424R	Eppendorf (Hamburg, Germany)
Centrifuge 5804R	Eppendorf (Hamburg, Germany)
Easypet Pipetting Aid	Eppendorf (Hamburg, Germany)
EPS 301 Power Supply	GE Healthcare (München, Germany)
FACS Aria Flow Cytometry System	BD Biosciences (Heidelberg, Germany)
Gene Pulser Xcell System	BioRad (Hercules, USA)
Heatable Magenetic Stirrer	IKA (Staufen, Germany)
HORIZON 58 Gel Casting System	Life Technologies (Darmstadt, Germany)
Inverted Microscope Axiovert 40 CFL	Carl Zeiss Microscopy GmbH (Jena, Germany)
Microwave	Siemens (München, Germany)
MilliQ Water/Millipore Advantage A	Merck Millipore (Billerica, USA)
Mini-PROTEAN Tetra Handcast Systems	BioRad (Hercules, USA)
Mini-Trans-Blot Cell	BioRad (Hercules, USA)
NanoDrop 2000c	Thermo Fisher Scientific (Waltham, USA)
New Brunswick INNOVA 4430	Eppendorf (Hamburg, Germany)
OptiMax X-ray Film Processor	PROTEC (Oberstenfeld, Germany)
Pipettes	Gilson Inc. (Middelton, USA)
QBT Block Heater	Grant Instruments (Cambridge, UK)
Safty Cabinet Herasafe HS12	Thermo Fisher Scientific (Waltham, USA)
Shaker ST5	Ingenieurbüro CAT (Staufen, Germany)
Shaking Water Bath SW23	Julabo (Seelbach, Germany)
Standard Power Pack P25	Biometra GmbH (Göttingen, Germany)
Steri-Cycle CO_2 Incubator	Thermo Fisher Scientific (Waltham, USA)
Thermomixer Comfort	Eppendorf (Hamburg, Germany)
T-Personal 48 Thermocycler	Biometra GmbH (Göttingen, Germany)
Tube Rotator	Stuart Equipment (Staffordshire, UK)
Vacusafe Comfort	IBS Tecnomara GmbH (Fernwald, Germany)
Vortex Genie 2	Scientific Industries Inc. (New York , USA)
Water Bath WNB 45	Memmert GmbH (Schwabach, Germany)

2.1.8 Bacterial Strains

The following bacterial strains were used for plasmid expression.

Table 2.8: Bacterial strains.

E. coli STRAIN	GENOTYPE	SUPPLIER
XL-1 Blue	*recA1 endA1 gyrA96 thi-1 hsdR17 supE44 relA1 lac*	Agilent Technologies
	[F' *proAB lacI*^{q}ZΔ*M15* Tn*10* (Tet$_{r}$)]	(Waldbronn, Germany)
SCS110	*rpsL (Str*^{r}*) thr leu endA thi-1 lacY galK galT ara tonA*	Agilent Technologies
	tsx dam dcm supE44 Δ(*lac-proAB*) [F' *traD36 proAB lacI*^{q}ZΔ*M15*]	(Waldbronn, Germany)

2.1.9 Eucaryotic Cell Lines

The following eucaryotic cancer cell lines were obtained from ATCC or generated in this PhD thesis.

Table 2.9: Eucaryotic cell lines.

CELL LINE	ORIGIN	MORPHOLOGY	ATCC NUMBER
HEK293T	Human embryonic kidney	Epithelial (adherent)	CRL-1573
HeLa	Human cervical adenocarcinoma	Epithelial (adherent)	CCL-2
MCF7	Human mammary gland	Epithelial (adherent)	HTB-22

Table 2.10: Stably transfected eucaryotic cell lines.

CELL LINE	EXPRESSED PROTEIN	EXPRESSION PLASMID	FLUORESCENT PROTEIN
HEK293T	Atg14L	w0734 pmCherry-2xFKBP'-Atg14L	mCherry
HEK293T	Beclin1-FKBP'	w0735 pmCherry-2xFKBP'-Beclin1	mCherry
HEK293T	Beclin1Δ143-234–FKPB'	w1420 pmCherry-2xFKBP'-Beclin1 (1-142, 235-451)	mCherry
HEK293T	Beclin1Δ143-272–FKBP'	w1456 pmCherry-2xFKBP'-Beclin1 (1-142, 273-451)	mCherry
HEK293T	mCherry-FKBP'	w0254 pmCherry-2xFKBP'	mCherry
HEK293T	Vps34-Nanobody-FKBP'	w1634 Vps34-Nano-mCherry-2xFKBP	mCherry
MCF7	Atg5	w0356 pEGFP-Atg5	EGFP
MCF7	LC3	w0385 pEGFP-LC3	EGFP
MCF7	LC3	w0606 pmCherry-EGFP-LC3	EGFP/mCherry

2.1.10 Buffers and Growth Media

The following bacterial or mammalian cell culture growth media and buffers were used.

Table 2.11: Composition of used bacterial growth media.

MEDIUM		COMPOSITION
GYT Medium	1 x	30 % (v/v) Glycerin 0.25 % (w/v) Tryptone 0.125 % (w/v) Yeast Extract
LB Medium	1 x	1 % (w/v) Tryptone 1 % (w/v) NaCl 0.5 % (w/v) Yeast Extract
TSS Medium	1 x	10 % (w/v) PEG 5 % (w/v) DMSO 50 mM $MgCl_2$

Table 2.12: Composition of used growth media for mammalian cells.

MEDIUM		COMPOSITION
HeLa Medium	1 x	MEME 10 % (v/v) FBS 1 % (v/v) NEAA 1 mM Sodium Pyruvate
HEK293T Medium	1 x	DMEM 10 % (v/v) FBS 1 % (v/v) NEAA 1 mM Sodium Pyruvate
MCF7 Medium	1 x	MEME 10 % (v/v) FBS 1 % (v/v) NEAA 1 mM Sodium Pyruvate 0.01 mg/mL Insulin

Table 2.13: Composition of used buffers and solutions.

BUFFER		COMPOSITION
BME Buffer	1 x	100 mM BME 62.5 mM Tris-HCl pH 6.8 2 % (w/v) SDS
Dilution Buffer	1 x	10 mM Tris-HCl pH 7.5 150 mM NaCl 0.5 mM EDTA
DNA Loading Buffer	5 x	30 % (w/v) Sucrose 20 % (v/v) Glycerin 0.2 % (w/v) Orange G
Laemmli Buffer	4 x	250 mM Tris-HCl pH 6.8 40 % (v/v) Glycerol 5 % (w/v) SDS 0.005 % (w/v) Bromophenol Blue
Lysis Buffer	1 x	10 mM Tris-HCl pH 7.5 150 mM NaCl 0.5 mM EDTA 0.5 % (v/v) NP–40
RIPA Buffer	1 x	10 mM Tris-HCl pH 7.5 150 mM NaCl 0.5 mM EDTA 0.1 % (w/v) SDS 1 % (w/v) Triton X–100 1 % (w/v) Deoxycholate
SDS Running Buffer	10 x	250 mM Tris-HCl 1.92 mM Glycine 1 % (w/v) SDS
TAE Buffer	50 x	2 M Tris-HCl pH 8.0 1 M Acetic Acid 50 mM EDTA
TBST Buffer	10 x	1.5 M NaCl 200 mM Tris-HCl pH 7.5 1 % (v/v) Tween–20
Transfer Buffer	1 x	190 mM Glycine 25 mM Tris-HCl pH 8.3 20 % (v/v) Methanol

2.1.11 Expression Plasmids

The following mammalian expression plasmids were used in this PhD thesis.

Table 2.14: Expression Plasmids.

EXPRESSION PLASMID	EXPRESSED PROTEIN	SOURCE
w0180 CherryC1-LC3	Cherry-LC3	AG Wu
w0254 pmCherry-2xFKBP	mCherry-FKBP'	AG Wu
w0276 pOPIN(n)EGFP-Atg14L	EGFP-Atg14L	AG Wu
w0323 pcDNA4-Vps34-Flag	Vps34-FLAG	AG Wu
w0356 EGFP-Atg5	EGFP-Atg5	AG Wu
w0359 pTagBFP-2xDHFR-KX	TagBFP-2xeDHFR-CAAX	AG Wu
w0363 pEGFPC1-2xeDHFR-KX	EGFP-2xeDHFR-CAAX	AG Wu
w0385 pEGFP-LC3	EGFP-LC3	AG Wu
w0456 pOPIN-NHis-3C_Vps15	His-Vps15	DPF
w0476 pOPIN-His-MBP_Vps15	His-MBP-Vps15	DPF
w0500 pOPIN(n)Citrine_Beclin1	mCitrine-Beclin1	DPF
w0505 pOPIN(n)EGFP_Beclin1	EGFP-Beclin1	DPF
w0506 pOPIN(n)EGFP_Rubicon	EGFP-Rubicon	DPF
w0507 pOPIN(n)EGFP_UVRAG	EGFP-UVRAG	DPF
w0508 pOPIN(n)EGFP_Vps15	EGFP-Vps15	DPF
w0509 pOPIN(n)EGFP_Vps34	EGFP-Vps34	DPF
w0547 pOPIN(n)Citrine_Vps15	mCitrine-Vps15	DPF
w0548 pOPIN(n)Citrine_Vps34	mCitrine-Vps34	DPF
w0550 pOPIN(n)Cherry_Beclin1	mCherry-Beclin1	DPF
w0571 pOPIN(n)Citrine_UVRAG	mCitrine-UVRAG	DPF
w0599 mKate2-giantin-N1	mKate2-Giantin	AG Wu
w0601 mKate2-Cb5-ER-N1	mKate2-Cb5	AG Wu
w0606 pCherry_EGFP LC3	mCherry-EGFP-LC3	AG Wu
w0734 pCherryC1-2xFKBP-Atg14L	mCherry-2xFKBP'-Atg14L	This Thesis
w0735 pCherryC1-2xFKBPmt-Beclin1	mCherry-2xFKBP'-Beclin1	This Thesis
w0736 pCherryC1-2xFKBPmt-Vps34	mCherry-2xFKBP'-Vps34	This Thesis
w0808 pOPIN(n)Citrine_Atg14L	mCitrine-Atg14L	This Thesis
w0932 pmCherry_2xFKBPmt_N-Vps34	Vps34-mCherry-2xFKBP'	This Thesis
w1135 pCherry-2xFKBPmt-UVRAG	mCherry-2xFKBP'-UVRAG	This Thesis
w1136 mKate2-3xNLS	mKate2-3xNLS	AG Wu
w1155 pOPIN(c)EGFP_Vps34	EGFP-Vps34	DPF
w1156 pOPIN(c)Cherry_Vps34	mCherry-Vps34	DPF
w1220 pEGFP-eDHFR_N23C-L28C-NUC	EGFP-eDHFR-NLS	AG Wu
w1233 pCherryC1-2xFKBPmt-Beclin1 E191L	mCherry-FKBP'-Beclin1_E191L	This Thesis
w1234 pCherryC1-2xFKBPmt-Beclin1 R205L	mCherry-FKBP'-Beclin1_R205L	This Thesis
w1239 pTagBFP-2xeDHFR-Cb5	TagBFP-eDHFR-Cb5	This Thesis
w1290 pCherryC1-2xFKBPmt-Beclin(146-271)	mCherry-FKBP'-Beclin1(1-145, 272-451)	This Thesis
w1338 pCherryC1-2xFKBPmt-Beclin1_mt2	mCherry-FKBP'-Beclin1_E191L_A257L	This Thesis
w1372 pCherryC1-2xFKBPmt-Beclin1_mt3	mCherry-FKBP'-Beclin1_E191L_A219L_A257L	This Thesis

w1402 pCherryC1-HA-2xFKBPmt-Beclin1	mCherry-HA-FKBP'-Beclin1	This Thesis
w1403 pCherryC1-HA-2xFKBP-Beclin1_E191L	mCherry-HA-FKBP'-Beclin1 E191L	This Thesis
w1404 pCherryC1-HA-2xFKBP-Beclin1_R205L	mCherry-HA-FKBP'-Beclin1 R205L	This Thesis
w1405 pCherryC1-HA-2xFKBP-Beclin1_mt2	mCherry-HA-FKBP'-Beclin1_E191L_A257L	This Thesis
w1406 pCherryC1-HA-2xFKBP-Beclin1_mt4	mCherry-HA-FKBP'-Beclin1_E191L_A219L_A257L_E226L	This Thesis
w1408 pCherryC1-2xFKBPmt-Beclin1_mt4	mCherry-FKBP'-Beclin1_E191L_A219L_A257L_E226L	This Thesis
w1420 pmCherry-2xFKBP-Beclin1Δ143-234	mCherry-FKBP'-Beclin1Δ143-234	This Thesis
w1421 pHA-Beclin1	HA-Beclin1	This Thesis
w1422 pHA-Beclin1_E191L	HA-Beclin1 E191L	This Thesis
w1423 pHA-Beclin1_R205L	HA-Beclin1 R205L	This Thesis
w1424 pHA-Beclin1_E191L_A257L	HA-Beclin1 E191L A257L	This Thesis
w1425 pHA-Beclin1_E191L_A219L_A257L_E226L	HA-Beclin1 E191L A219L A257L E321L	This Thesis
w1456 pmCherry-2xFKBP-Beclin1Δ143-272	mCherry-FKBP'-Beclin1Δ143-272	This Thesis
w1457 pmCherryC1-2xFKBP-Beclin1Δ143-278	mCherry-FKBP'-Beclin1Δ143-278	This Thesis
w1518 mCherry-2xFKBP-Beclin1_1-234	mCherry-FKBP'-Beclin1(1-234)	This Thesis
w1519 mCherry-2xFKBP-Beclin1_1-272	mCherry-FKBP'-Beclin1(1-272)	This Thesis
w1520 mCherry-2xFKBP-Beclin1_K265A	mCherry-FKBP'-Beclin1 K265A	This Thesis
w1582 pHA-2xFKBPmt-Beclin1Δ143-234	mCherry-FKBP'-Beclin1Δ143-234	This Thesis
w1583 pHA-2xFKBPmt-Atg14L	HA-FKBP'-Atg14L	This Thesis
w1584 pHA-2xFKBPmt	HA-FKBP'	This Thesis
w1587 mCherry-2xFKBP-Beclin1_267-451	mCherry-FKBP'-Beclin1(267-451)	This Thesis
w1588 mCherry-2xFKBP-Beclin1_N268A	mCherry-FKBP'-Beclin1 N268A	This Thesis
w1593 mCherry-2xFKBP-Beclin1_V269A	mCherry-FKBP'-Beclin1 V269A	This Thesis
w1600 mCherry-2xFKBP-Beclin1_F270A	mCherry-FKBP'-Beclin1 F270A	This Thesis
w1608 mCherry-FKBP-Beclin1_265-72A	mCherry-FKBP'-Beclin1 265-72A	This Thesis
w1615 pTagBFP-2xeDHFR-hERGIC53	TagBFP-eDHFR-ERGIG53	This Thesis
w1616 pTagBFP-2xeDHFR-ActA	TagBFP-eDHFR-ActA	This Thesis
w1634 Vps34-Nano-mCherry-2xFKBP	Vps34-nanobody-mCherry-FKBP'	This Thesis
w1719 mCherry-2xFKBP-Beclin1Δ328-394	mCherry-FKBP'-Beclin1Δ328-394	This Thesis
w1745 FLAG-BecnS	FLAG-BecnS	This Thesis

2.2 Methods

2.2.1 Methods in Molecular Biology

2.2.1.1 Polymerase Chain Reaction

Polymerase chain reaction (PCR) is a popular technique in molecular biology to amplify DNA fragments by several orders of magnitude. The method relies on the enzyme DNA polymerase, which is able to generate new DNA strands complementary to a template DNA. The enzyme is guided by a primer that binds to the template DNA and serves as starting point for amplification. The process itself is controlled by thermal cycling, providing the appropriate temperatures for DNA denaturation, primer annealing and elongation of the new DNA strand by the DNA polymerase. Since the generated DNA fragments serve as templates themselves in the next cycle, amplification proceeds exponentially until the reaction is terminated. This facilitates fast and specific reproduction of DNA fragments for analysis or to create recombinant DNA constructs[218].

2.2.1.1.1 Site-directed Mutagenesis

Site-directed mutagenesis was applied to introduce point-mutations into a DNA sequence. A specific primer was designed and the PCR master mix was prepared according to table 2.15. The PCR programe was performed in a T-Personal 48 Thermocycler as described (see table 2.15). Afterwards the template DNA was removed by digestion with DpnI. 1 µL DnpI (10 U/µL) was added to the PCR product and the mixture was incubated at 37 °C for at least one hour. The PCR product was then purified using a E.Z.N.A. Cycle Pure Kit and transformed into *E.coli* XL1-Blue cells (6 µL). Finally, introduction of the point-mutation was confirmed by DNA sequencing.

Table 2.15: Site-directed mutagenesis PCR master mix composition and programe.

MASTER MIX		V_{tot} = 50 µL	PCR PROGRAM		
Phusion HF PCR Master Mix	2 x	25 µL	98 °C	30 s	
DMSO	100 %	2.5 µL	98 °C	15 s	
Template		20 ng	55 °C	30 s	29 x
Forward primer	100 µM	0.5 µL	72 °C	4 min	
ddH_2O		up to 50 µL	72 °C	10 min	

2.2.1.1.2 Insert Amplification PCR

Polymerase chain reaction was used to amplify DNA fragments for subcloning. Oligonucleotide primers specific for the respective template plasmid were designed and the annealing temperature (T_m) was calculated. The PCR master mix was prepared and the PCR was performed in a Thermocycler (table 2.16). The PCR product was then analyzed by agarose gel electrophoresis and purified with a E.Z.N.A. Cycle Pure Kit.

Table 2.16: Insert amplification PCR composition and program

MASTER MIX		V_{tot} = 50 µL	PCR PROGRAM		
Phusion HF PCR Master Mix	2 x	25 µL	98 °C	30 s	
Template		20 ng	98 °C	8 s	
Forward primer	10 µM	2 µL	T_m	45 s	} 36 x
Reverse primer	10 µM	2 µL	72 °C	45 s	
ddH_2O		up to 50 µL	72 °C	7 min	

2.2.1.1.3 Colony PCR

Colony PCR was used to determine whether plasmid constructs contain the correct DNA insert. The respective construct was transformed into *E.coli* and spread onto agar plates containing an appropriate antibiotic. Single colonies were picked and resuspended in the PCR mix (see table 2.17). In parallel, each of the selected colonies was replicated by streaking it onto a new agar plate. The PCR was performed in a Thermocycler according to the program in table 2.17 and the PCR products were analyzed by agarose gel electrophoresis.

Table 2.17: Colony PCR composition and program.

MASTER MIX		V_{tot} = 20 µL	PCR program		
Bacterial cells			96 °C	4 min	
RedTaq DNA Polymerase	2 x	10 µL	96 °C	30 s	
Forward primer	10 µM	1 µL	55 °C	30 s	} 26 x
Reverse primer	10 µM	1 µL	72 °C	2.5 min	
ddH_2O		up to 20 µL	72 °C	7 min	

2.2.1.1.4 DNA Sequencing

The nucleotide sequence of plasmid constructs was analyzed using the BigDye Terminator v3.1 Cycle Sequencing Kit. The PCR master mix was prepared according to table 2.18 and PCR was performed in a Thermocycler. Afterwards, the DNA was precipitated by adding 50 µL Ethanol, 10 µL ddH_2O, 2 µL EDTA (100 mM) and 2 µL sodium acetate (3 M) and centrifugation at over 13.000 rpm for 20 minutes. The supernatant was then discarded and the pellet was washed with 200 µL 70 % ethanol followed by 10 minutes centrifugation at over 13.000 rpm. The supernatant was again discarded and the pellet was dried at 100 °C for 5 minutes. The DNA sequence was then determined with a ABI PRISM 3130x1 Genetic Analyzer by the service facilities at the Max-Planck-Institute in Dortmund (ZE Biotechnologie).

Table 2.18: Sequencing PCR composition and program.

MASTER MIX		V_{tot} = 10 µL
BigDye Terminator		2 µL
Sequencing Buffer	5 x	2 µL
Template		200 ng
Primer	10 µM	2 µL
ddH_2O		up to 10 µL

PCR program		
96 °C	4 min	
96 °C	10 s	} 26 x
50 °C	5 s	
60 °C	4 min	

2.2.1.2 Agarose Gel Electrophoresis

Agarose gel electrophoresis was performed to determine the length of the DNA fragments or to separate and purify them. Agarose gels with a concentration of 1 % (w/v) were employed for both purposes. The gels were prepared by solubilizing the agarose with RedSafe Nucleic Acid Staining Solution (20 000 x) in TAE buffer (see table 2.13) and allowing the solution to polymerize in a HORIZON 58 gel casting system. DNA loading buffer (see table 2.13) was added to the samples and the gels were run in TAE buffer at 95 V until the fragments were sufficiently separated. GeneRuler 1 kb DNA Ladder served as reference for DNA size and quantity. The gels were analyzed in an AlphaImager HP under UV light at a wavelength of 302 nm.
To purify DNA fragments, the respective band was extracted from the gel and the DNA was isolated with a E.Z.N.A. Gel Extraction Kit.

2.2.1.3 Preparation and Transformation of Competent Cells

Competent bacterial cells are widely used in molecular biology as they are able to take up, multiply and express extracellular DNA. This is termed transformation and typically induced by a heat or electro shock to permeabilize the cellular membrane.

2.2.1.3.1 Electrocompetent Cells

To prepare electrocompetent *E.coli* XL-1 Blue cells, 10 mL LB-medium were inoculated with 100 µL of bacterial culture and incubated overnight at 37 °C shaking at 170 rpm. This starting culture was used to inoculate 1 L LB medium and the cells were returned to the 37 °C shaker until they reached an OD_{600} of 0.5. The bacterial cells were then harvested by centrifugation for 12 minutes at 5000 rcf and 4 °C. The supernatant was discarded and the pellet was washed three times by resuspending it in 10 % glycerol and subsequent centrifugation for 12 minutes at 5000 rcf and 4 °C. Finally, the bacterial pellet was resuspended in icecold 3 mL GYT medium, aliquoted to 80 µL and stored at – 80 °C.
To transform electrocompetent cells, 1 ng to 100 ng DNA were added to the thawed bacterial solution and transferred into a cold electroporation curvette. Membrane permeabilization was induced by exposing the bacteria to a short pulse at 1.8 kV, 200 Ω and 25 µF. The bacterial cells were then incubated in 1 mL LB medium at 37 °C and 170 rpm for 1 h. Finally, the transformed cells were harvested by centrifugation at 10 000 rpm for 1 minute and streaked onto a agar plate containing the appropriate antibiotic.

2.2.1.3.2 Chemically Competent Cells

Chemically competent *E.coli* XL-1 Blue or SCS110 cells were prepared by inoculating 100 mL LB medium with 30 mL overnight culture prepared as previously described and growing the bacterial cells until an OD_{600} of 0.8 was reached. Afterwards the cells were harvested by centrifugation at 2000 rpm and 4 °C for 15 minutes. The pellet was resuspended in 10 mL TSS medium, aliquoted to 300 µL and stored at – 80 °C. For transformation, the chemical competent cells were gently mixed with 1 ng to 100 ng DNA and incubated on ice for 30 minutes. Membrane permeabilization was then achieved by a 1 minute heat shock at 42 °C. The cells were then again incubated on ice for 5 minutes and afterwards transferred into 1 mL LB medium. After 1 h incubation at 37 °C and 170 rpm, the cells were harvested by centrifugation at 10 000 rpm for 1 minute and streaked onto an agar plate containing the appropriate antibiotic.

2.2.1.4 Preparation of Plasmid DNA

Plasmid DNA was isolated from transformed *E.coli* XL-1 Blue or SCS110 cells using the E.Z.N.A. Plasmid Mini Kit or the E.Z.N.A. Plasmid Maxi Kit for larger DNA amounts. Therefore, the plasmid was transformed into bacterial cells and a single colony was picked to inoculate 2 mL to 4 mL LB medium containing the appropriate antibiotic. The culture was incubated at 37 °C for 12 h to 16 h shaking at 170 rpm. The bacterial cells were then harvested by centrifugation at 13.000 rpm for 1 minute and the plasmid DNA was isolated according to the supplier's instructions.
For use in mammalian cells, the plasmid DNA was further purified by ethanol precipitation. To precipitate the DNA, it was initially incubated with 0.1 volumes of sodium acetate (3 M) at room temperature for 30 minutes. Then, two volumes of ethanol were added and the sample was centrifuged at over 13.000 rpm for 20 minutes. The supernatant was discarded and the pellet was washed with 200 µL 70 % ethanol. After 10 minutes of centrifugation at over 13.000 rpm, the supernatant was again discarded and the pellet was dried at 100 °C for 5 minutes. Finally, the pellet was resuspended in ddH_2O and the DNA concentration was determined.

2.2.1.5 Determining DNA Concentration

The concentration of DNA fragments or plasmids was determined by measuring absorbance at 260 nm using a NanoDrop 2000c.

2.2.1.6 Restriction Enzyme Digest

Restriction enzymes are endonucleases that recognize specific, typically palindromic nuleotide sequences of 4 bp to 6 bp and catalyze their cleavage. Restriction enzyme digestion of DNA plasmids or PCR products was performed with FastDigest Restriction Enzymes following the suppliers instructions. Typically, 0.1 µg to 4 µg of the respective DNA sample were incubated with 1 U to 3 U of restriction enzyme for up to 3 h at 37 °C and the enzyme was thermally inactivated afterwards. If only a single restriction enzyme was used, the DNA fragments were additionally dephosphorylated prior to ligation to prevent religation of the vector. To this end, the sample was incubated with 1 U SAP for 30 minutes at 37 °C. Before ligation, the DNA samples were purified by gel extraction or with the E.Z.N.A. Cycle Pure Kit.

2.2.1.7 Ligation of DNA Fragments

DNA ligases are enzymes, which catalyze covalent joining of DNA strands and are widely applied to combine DNA fragments from different sources. For ligation of DNA fragments, T4 DNA Ligase was used according to the suppliers instructions. Usually, DNA vectors were combined with specific inserts in a ratio of 1:3 or 1:6 (vector to insert) and incubated with 1 U ligase for 12 - 16 hours at 16 °C. Afterwards, the ligase was thermally inactivated and the ligation product was transformed into *E.coli* XL-1 Blue cells.

2.2.2 Methods in Cell Biology

All procedures involving direct handling of mammalian cells were performed in a safety cabinet. Media, trypsin-EDTA and DPBS were typically pre-warmed in a 37 °C water bath, whereas the remaining reagents were used at room temperature.

2.2.2.1 Passaging of Cells

Mammalian cells were maintained in complete DMEM (HEK293T) or MEME (MCF7 and HeLa) growth medium supplemented with 10 % heat-inactivated FBS, 1 % glutamine and 1 % non-essential amino acids. MCF7 growth medium further contained 0.1 % insulin solution. For routine subculturing, the cells were seeded into 100 mm cell culture dishes, 75 cm^2 or 175 cm^2 flasks and kept at 37 °C in a humidified 5 % CO_2 / 95 % air atmosphere. Cells were passaged at 80 % confluency by removing the growth medium, washing with 5 - 10 mL DPBS and incubated with 1 mL 0.05 % trypsin-EDTA solution. Once the cells were detached, complete growth medium was added to deactivate the trypsin. The cell number was determined using a Neubauer cell counting chamber and an Axiovert 40 CFL inverted microscope. The cell density was then adjusted according to the cell lines requirements and the cells were transferred into a new culture vessel containing the appropriate growth medium.

2.2.2.2 Cryopreservation of Cells

For crypreservation the cells were trypsinized as previously described (see 2.2.2.1) and resuspended in 5 - 10 mL complete growth medium. The cell suspension was transferred to a falcon tube and the cells were harvested by centrifugation at 200 g for 5 minutes. The supernatant was discarded and the cells were resuspended in complete growth medium containing 10 % cell culture grade DMSO. The cells were then aliquoted to cryovials and frozen slowly to – 80 °C. For long-term storage the cells were transferred to liquid nitrogen.

2.2.2.3 Transient Transfection of Cells

Transfection is a commonly applied method to introduce nucleic acids into eukaryotic cells and express exogenous proteins. Here, plasmid DNA was transiently transfected into mammalian cells using X-tremeGENE HP DNA Transfection Reagent, which employs non-liposomal lipids for DNA delivery. For transfection the cells were harvested as described before (see 2.2.2.1) and approximately 4×10^5 cells were seeded onto 35 mm glass bottom dishes in a total volume of 1.8 mL complete growth medium. A total amount of 2 µg DNA was mixed with 200 µL Opti-MEME reduced serum medium and 1 µL transfection reagent. The mixture was incubated a room temperature for at least 15 minutes and then added dropwise to the cells. The transfected cells were incubated at 37 °C in a humidified 5 % CO_2 / 95 % air atmosphere for 16 - 48 hours before further treatment.

2.2.2.4 Generation of Stable Cell Lines

If permanent expression of DNA constructs was desired, stable cell lines were generated by integrating the respective nucleic acids into the cellular genome. To this end, the nucleic acids were cloned into vectors encoding kanamycin resistance for selection in bacteria and neomycin or puromycin resistance for selection in mammalian cells (table 2.10).
Selective conditions were determined by establishing a dose-response curve. Untransfected cells were seeded onto a 24-well plate and maintained until they reached a confluency of 80 %. The cells were then exposed to increasing concentrations of G418 or puromycin for one week during which the medium was exchanged every 2 - 3 days. Afterwards the number of viable cells was compared between wells and the lowest concentration of antibiotic sufficient to kill the majority of cells per well was determined. For G418 this resulted in a selective concentration of 0.4 mg/mL and 0.5 µg/mL for puromycin.
To generate stable cells, approximately 1×10^6 cells were seeded onto a 100 mm dish and transfection was performed as previously described (see 2.2.2.3). Due to the increased cell number, the total DNA amount was elevated to 10 µg mixed with 1 mL Opti-MEME reduced serum medium and 10 µL transfection reagent. The cells were then incubated for 24 hours at 37 °C in a humidified 5 % CO_2 / 95 % air atmosphere. Afterwards, the growth medium was replaced with fresh medium containing G418 or puromycin at selective concentrations. The cells were then maintained under selective conditions for 2 - 3 weeks until formation of distinct cell colonies could be observed. The colonies were screened for the respective fluorescent marker using an Axiovert 40 CFL inverted microscope and positive colonies were isolated using cloning cylinders. Therefore, the growth medium was completely removed, the cells were washed with 5 - 10 mL DPBS and the cloning cylinders were placed around the positive colonies. The cylinders were stabilized by embedding them in 1 % (w/v) low melting point agarose. Once the agarose was solidified, 40 µL 0.05 % trypsin-EDTA solution were added into each cloning cylinder and the dish was transferred to the 37 °C incubator until the cells detached. Then, each cylinder was filled to capacity with complete growth medium, the cells were resuspended by pipetting up and down and finally the cell suspension was transferred onto a 12-well plate. The were maintained under selective conditions until they reached 80 % confluency before transferring them onto 60 mm dishes and lastly 100 mm dishes [219].
Before further analyzing the stable cells, part of them was cryopreservated as described before (see 2.2.2.2). The remaining cells were kept in culture and the expression level, molecular weight and cellular distribution of the introduced protein were analyzed by western blotting or confocal microscopy as described in section 2.2.3.1 and 2.2.4. Based on the results, cells from one isolated colony were chosen for fluorescence-activated cell sorting (FACS) to separate fluorescent from non-fluorescent cells (see 2.2.2.4.1). The sorted cells were seeded onto a 35 mm dish and grown under selective conditions until sufficient cell numbers for cryopreservation were achieved. Finally, the stably expressed protein was again analyzed by western blotting and confocal microscopy. For routine maintenance, the stable cells were kept in complete growth medium supplemented with reduced concentrations of selection agents, i.e. 0.2 mg/mL G418 and 0.25 µg/mL puromycin.

2.2.2.4.1 Flow Cytometry

Flow cytometry is a powerful method to analyze large numbers of single cells regarding the distribution of certain properties such as viability, cell size and fluorescence. In order to analyze cells by FACS, single cells are channeled past an excitation light source and a fluorescence microscope which measures and records a fluorescence signal for each cell. Based on the acquired data, cells featuring the desired properties are then separated from the remaining population [220]. Here, FACS was applied to isolate cells

permanently expressing a fluorescent marker from non-transfected cells in order to obtain a pure population and homogenous fluorescence, i.e. expression level. Cell sorting was carried out by the FACS facilities at the Max-Planck-Institute in Dortmund using a FACS Aria Flow Cytometry System with appropriate lasers and filter settings for TagBFP (407 nm laser), EGFP (488 nm laser) and mCherry (633 nm laser).

2.2.2.5 Fixation and Immunofluorescence Labeling of Cells

Immunofluorescence labeling of cells is commonly applied to stain specific cellular components with fluorescent labels by targeting them with an antibody. Fixation of cells was applied in order to preserve them for prolonged periods before imaging or to prepare the cells for immunostaining. To this end, the cells were grown in glass bottom dishes or chambers, which provide appropriate optical qualities for confocal microscopy. Fixation, blocking and staining conditions were optimized for each antibody individually, since they are highly dependent on the specificity and stability of the antibody and the properties of the antigen. For fixation, the cells were washed with DPBS and then immobilized by addition of either 4 % PFA/DBPS or ice-cold methanol. PFA-fixed cells were incubated for 10 minutes at room temperature while methanol-fixed cells were incubated at – 20 °C for 10 minutes. After immobilization, the cells were washed three times for 5 minutes with DBPS and then incubated in 0.1 - 0.5 % Triton X-100/DPBS for 10 minutes to permeabilize the cellular membrane. Following permeabilization, the cells were again washed three times in DBPS and then blocked in 1 - 10 % BSA or FBS or both in DPBS for 30 - 60 minutes. For immunostaining, the cells were incubated with the primary antibody in 1 - 3 % BSA or FBS in DPBS for up to 12 hours at RT or 4 °C. Afterwards, the cells were washed three times with DPBS again and then incubated with the secondary antibody for 30 to 60 minutes under the same conditions used for primary antibody labeling. Finally, the cells were washed with DBPS and stored in DBPS at 4 °C.

2.2.2.6 Modulation and Quantification of Autophagy

2.2.2.6.1 Induction and Inhibition of Autophagy

In mammalian cells, autophagy was induced or inhibited by exposing the cells to starvation or targeting specific autophagy phases with autophagy modulators. To induce autophagy, the cells were serum-starved by incubation in EBSS for 1 - 4 hours or in HBSS for 30 minutes to 2 hours. Typically, MCF7 and HeLa cells were starved in EBSS, while HEK293T cells were starved in HBSS.
Autophagosome formation was inhibited by addition of BafilomycinA1, which disturbs vacuolar-type H+-ATPases in the lysosomal membrane and thereby prevents fusion of the autophagosome with the autolysosome. BafilomycinA1 was used at a final concentration of 100 nM for up to 2 hours. In order to inhibit the kinase activity of Vps34 and prevent autophagosome formation, the cells were treated with the non-specific PI3K inhibitor Wortmannin. Wortmannin was applied at a final concentration of 500 nM for up to 2 hours. If starvation-independent autophagy induction was desired, the cells were treated with Rapamycin, which inhibits the kinase mTOR and thus mimics cellular starvation. Rapamycin was applied at a final concentration of 500 nM for up to 4 hours.

2.2.2.6.2 Quantification of Autophagy

Autophagy levels were analyzed by confocal laser scanning microscopy in fixed or living cells or by western blotting for distinctive autophagy marker proteins. In confocal microscopy, autophagy was quantified based on the number and area of autophagosomes and autolysosomes visualized by fluorescently labeled marker proteins. Since the fluorescently tagged autophagic vesicles appear as distinctive puncta within the cytoplasm, these assays are commonly referred to as 'puncta counts'. Several markers were employed to distinguish between the different autophagy phases. The autophagic protein Atg5 is a marker for the isolation membrane, i.e. for the onset of autophagy. EGFP-tagged LC3 was used as marker for autophagosome formation including all processes prior to fusion with the lysosome, while tandem mCherry-GFP-tagged LC3 was employed to monitor autophagic flux. The latter is based on the pH-sensitivity of EGFP, which is quenched in the acidic environment of the lysosome lumen while mCherry remains fluorescent. Thus, tandem mCherry-EGFP-tagged LC3 is often used to distinguish between autophagosomes and autolysosomes and monitor both of them simultaneously. In the fluorescence assay, colocalization of mCherry and EGFP signals represents a compartment which has not fused with the lysosome yet, whereas mCherry fluorescence alone corresponds to autolysosomes[14].
For microscopy-based autophagy assays, stable MCF7 and HeLa cell lines expressing the respective marker proteins were generated (see table 2.10). Typically, the stable cells were additionally transfected with one or more proteins of interest and autophagy was induced or inhibited as previously described (see 2.2.2.6.1). For quantification of autophagy levels based on puncta counts, confocal images were acquired and processed as described in section 2.2.4 and 2.2.4.2.
In addition to the fluorescence assays, autophagy levels were also monitored by western blotting. Here, LC3 and p62 were employed as markers for autophagic flux and autophagic degradation, respectively. LC3 is conjugated to PE during autophagy and while its nonlipidated form LC3-I can be detected in basal conditions as well, the lipidated form LC3-II can only be observed upon autophagy induction. Even though, LC3-II has a higher molecular weight, it shows faster migration than LC3-II during SDS-PAGE, possibly due to its increased hydrophobility. In western blotting, appearance of LC3-II bands corresponds to induction of autophagy and thus autophagy flux can be monitored by detecting LC3-I and LC3-II. In contrast to LC3, p62 or SQSTM1 bind to polyubiquitinated proteins, which in consequence become autophagic cargo and serve as an index of autophagic degradation. Hence, increased levels of p62 correspond to autophagy inhibition, whereas a decrease in p62 represents increased levels of autophagy[14]. For western blot based assays, HEK293T cells stably expressing the proteins of interest were generated (see table 2.10) and treated as previously described (see 2.2.2.6.1). Afterwards, the cell lysates were blotted and endogenous LC3 and p62 were detected with appropriate primary antibodies (see 2.2.3.1).

2.2.2.7 Induction of Heterodimerization

2.2.2.7.1 Chemically Induced Dimerization

Chemically induced dimerization (CID) was applied to localize proteins of interest to the plasma membrane, the mitochondria, ER, ERGIC or Golgi apparatus. To this end, a protein of interest, tagged with the dimerization domain FKBP' and a fluorescent marker protein, was expressed along with a eDHFR-tagged localization signal. Typically, the eDHFR-constructs contained TagBFP as marker, whereas the FKBP'-constructs were labeled with mCherry, mCitrine or EGFP. To target the plasma membrane, the CAAX domain of KRas was used as localization signal, while listerial actin A (ActA) was used for the mi-

tochondria, cytochrome b5 (Cb5) for the ER, hERGIC53 (human ER-Golgi intermediate compartment 53 kDa protein) for the ERGIC and Giantin for the Golgi apparatus. In order to induce dimerization of the eDHFR- and FKBP'-domains, the cells were incubated with 2 µM SLF'-TMP for up to 4 hours either in complete growth medium or in starvation medium. To reverse the dimerization, the cells were treated with 2 µM TMP for up to 4 hours.

2.2.2.7.2 Photoinduced Dimerization

Photoinducible dimerization was used to mislocalize proteins of interest to the plasma membrane. Here, the proteins of interest were modified with a eDHFR-dimerization domain while the localization signal (CAAX domain of KRas) was fused to a HaloTag. To achieve similar expression levels of both components, the proteins were expressed from one vector containing a ribosomal skipping sequence (2A peptide sequence) inbetween the modified proteins. Typically, the eDHFR-constructs were tagged with mCitrine or mTurquoise, whereas the HaloTag-CAAX construct was HA-tagged. In contrast to chemically induced dimerization, the cells were pre-treated with 5 µM Nvoc-TMP-CI in complete growth medium for 1 hour, washed twice with DPBS and incubated for 1 hour in complete growth medium or starvation medium again. Afterwards, the cells were washed with DPBS and dimerization was induced by intensive bleaching with a 405 nm confocal laser. Laser irradiation serves to cleave off the caging group from the TMP moiety of Nvoc-TMP-CI, which can then interact with eDHFR. Dimerization was reversed by addition of 5 µM TMP.

2.2.3 Biochemical Methods

2.2.3.1 Western Blotting

Western blotting is a widespread technique in molecular and cell biology that facilitates specific detection and quantification of proteins. To this end, protein are extracted from cellular lysate, separated based on their molecular weight, transferred onto a membrane and specifically labeled by antibodies.

2.2.3.1.1 Preparation of Cell Lysates

To generate whole cell lysates, cells were cultured in 35 mm, 60 mm, 100 mm or 150 mm dishes until they reached 80 % confluency. To harvest the cells, the dish was placed on ice, growth medium was aspirated and 2 - 5 mL ice-cold DPBS were added. The cells were then scraped off the dish, transferred into a pre-cooled tube and centrifuged at 500 g and 4 °C for 3 minutes. Afterwards, the supernatant was discarded and the cell pellet was gently resuspended in 1 mL ice-cold DPBS. This procedure was repeated twice. After washing, the cells were resuspended in 50 - 200 µL ice-cold lysis or RIPA buffer (see 2.13) supplemented with cOmplete protease inhibitor and 1 mM PMSF. The cell solution was incubated on ice for 30 minutes followed by 15 minutes centrifugation at over 13 000 rpm and 4 °C. Finally, the supernatant was transferred to a pre-cooled tube and stored at – 20 °C until further use.

2.2.3.1.2 Determination of Protein Concentration

A Bradford assay was employed to determine protein concentration in whole cell lysates. The assay relies on the unique properties of the dye Coomassie Brilliant Blue, which shifts its absorption maximum from 465 - 595 nm upon protein binding in acidic solutions. Protein concentration can thus be determined by measuring absorption at 595 nm and relating the result to a BSA standard curve[221].

The assay was performed in UV cuvettes and a BioPhotometer using the respective lysis buffer as control. To determine protein concentrations, 995 µL Bradford reagent were mixed with 5 µL cell lysate and absorbance at 595 nm was measured.

2.2.3.1.3 Immunoprecipitation

Immunoprecipitation was applied to isolate specific proteins and protein complexes from whole cell lysate. Here, immunoprecipitation was performed with GFP- or RFP-Traps by Chromotek according to the manufacturer's instructions. The Traps are based on magnetic agarose beads coupled to nanobodies against GFP or RFP and their derivatives, which facilitates highly efficient isolation of GFP- and RFP-fusion proteins. For immunoprecipitation, whole cell lysate was generated as previously described (see 2.2.3.1.1) and mixed with 300 µL dilution buffer. Afterwards, 10 - 25 µL bead slurry were pipetted into 500 µL ice-cold dilution buffer and magnetically separated. The supernatant was discarded, the beads were washed twice in the same fashion and finally added to the diluted cell lysate. The mixture was tumbled end-over-end for at least 1 hour at 4 °C and then magnetically separated. The beads were washed twice with 500 µL ice-cold dilution buffer, transferred into a fresh tube and resuspended in 30 - 100 µL SDS sample buffer. In order to dissociate the immunocomplex from the beads, the samples were boiled at 100 °C for 10 minutes. Finally, the beads were magnetically separated and the supernatant was analyzed by SDS-PAGE or stored at – 20 °C.

2.2.3.1.4 SDS-PAGE

Sodiumdodecylsulfate-polyacrylamide gel electrophoresis (SDS-PAGE) is a commonly used method to separate proteins based on their molecular weight. SDS is a anionic detergent, which binds to denatured proteins proportionally to their molecular mass and gives them a negative charge. Proteins in complex with SDS are thus attracted towards a positively charged electrode in an electric field. During gel electrophoresis, these proteins migrate through a polyacrylamide gel towards an anode. Due to differing pore sizes in the gel, the migration speed depends on the protein size. Thus, larger proteins migrate slower and can be visualized as higher bands on a polyacrylamide gel, whereas smaller proteins migrate faster and are represented in lower bands.
To prepare samples for SDS-PAGE, cell lysates were generated as previously described and the protein concentration was determined (see 2.2.3.1.1 and 2.2.3.1.2). The protein concentration was adjusted to equal levels by adding ddH_2O and the lysate was mixed with 4 x Laemmli buffer (see 2.13). Afterwards, the samples were boiled at 100 °C for 10 minutes.
SDS-polyacrylamide stacking and separating gels were prepared according to Jiang *et al.*[222] as shown in table 2.19. Typically, 8 % gels were used to analyze larger proteins like p62 and 13.5 % gels were used to visualize smaller proteins like LC3. The gels were prepared with a Mini-PROTEAN® Tetra handcasting system, placed in the tank and covered with SDS running buffer (see 2.13). The samples were loaded onto the gel along with Prestained Protein Marker and the electrophoresis was performed at 90 V until the samples reached the separating gel. Afterwards, the voltage was increased to 120 V and electrophoresis was continued until the desired degree of separation was reached.

2.2.3.1.5 Electroblotting

After SDS-PAGE, the proteins were electrotransferred onto a nitrocellulose membrane in order to make them accessible to antibody staining. As before, an electric current is applied to initiate migration of

Table 2.19: Composition of stacking and separating SDS-Polyacrylamide gels.

STACKING GEL		V_{tot} = 10 mL
ddH_2O		6.8 mL
Acrylamide/ Bisacrylamide	30 % (w/v)	1.7 mL
Tris-HCl pH 6.8	1.0 M	1.25 mL
SDS	10 % (w/v)	100 µL
APS	10 % (w/v)	100 µL
TEMED		10 µL

SEPARATING GEL 8 % / 13.5 %		V_{tot} = 24 mL
ddH_2O		11.04/6.6 mL
Acrylamide/ Bisacrylamide	30 % (w/v)	6.24/10.8 mL
Tris-HCl pH 8.8	1.5 M	6.24 mL
SDS	10 % (w/v)	240 µL
APS	10 % (w/v)	120 µL
TEMED		14.4/9.6 µL

the proteins from the gel onto the membrane. A wet blotting system was employed for the protein transfer and used according to the manufacturer's instructions. Typically, the transfer sandwich was assembled in ice-cold transfer buffer (see 2.13) as follows: sponge, filter paper, SDS-polyacrylamide gel, nitrocellulose membrane, filter paper, sponge. It was then moved to the transfer tank, which was placed on ice and filled to capacity with ice-cold transfer buffer. Electrotransfer was performed at 100 V for 30 - 40 minutes depending on the molecular weight of the transferred protein.

2.2.3.1.6 Blocking and Immunostaining

To prevent unspecific protein binding, the nitrocellulose membrane was blocked with 5 % skim milk in TBST buffer (see 2.13) for 1 hour after electrotransfer. After blocking, the membrane was washed three times for 5 minutes in TBST and then exposed to the primary antibody. Conditions for the immunostaining were highly dependent on the respective primary antibody (see table 2.20). Typically, the membrane was incubated with the primary antibody at 4 °C overnight while gently shaking. The membrane was again washed three times for 5 minutes in TBST and incubated with the secondary antibody at 1:10,000 dilution in 5 % milk/TBST for 1 hour. Depending on the primary antibody, anti-mouse or anti-rabbit HRP was used as secondary antibody. Finally, the membrane was again washed three times for 5 minutes in TBST and stored in TBST buffer until detection.

Table 2.20: Immunostaining conditions of primary antibodies.

Antigen	**Source**	**Dilution**	**Conditions**
Actin	Mouse	1:10,000	0.02 % NaN_3, 4 °C overnight / RT for 1 hour
GFP	Rabbit	1:1000	5 % BSA, 0.02 % NaN_3, 4 °C overnight
LC3B	Rabbit	1:1000	0.02 % NaN_3, 4 °C overnight
mCherry	Mouse	1:1000	5 % Milk, 0.02 % NaN_3, 4 °C overnight
p62	Rabbit	1:10,000	5 % Milk, 0.02 % NaN_3, 4 °C overnight / RT for 1 hour
tRFP (BFP)	Rabbit	1:500	0.02 % NaN_3, 4 °C overnight

2.2.3.1.7 Detection and Quantification

Detection of the western blot membrane was performed by visualizing the HRP-labeled protein through addition of a chemiluminescent substrate, which emits light when exposed to HRP. ECL Blotting Substrate or SuperSignal Blotting Substrate was applied to the membrane according to the manufacturer's

instructions and incubated for 1 - 2 minutes. Afterwards, the membrane was fixed in the film cassette and an autoradiography film was placed on top of the membrane. Depending on the protein concentration and quality of the primary antibody, the film was exposed for up to 1 hour and then developed with an OptiMax X-ray Film Processor. The protein concentration and expression level was then quantified with ImageJ by analyzing the band intensities relative to the intensity of the actin bands, which were typically used as internal control. However, due to variations in loading and transfer efficiency, western blot is considered a semi-quantitative method and provides a relative comparison of protein levels rather then an absolute measure of protein concentrations[223].

2.2.3.1.8 Stripping Western Blot Membranes

Western blot membranes can be stripped off the secondary or primary antibodies in order to detect proteins with a similar molecular weight with antibodies from different source organisms or to re-probe protein bands. If only the secondary antibody needs to be removed, a gentle sodium azide strip is commonly applied, whereas a harsh BME strip is used to remove primary and secondary antibodies. To strip a western blot membrane, it is first washed three times for 5 minutes in TBST and then incubated in either 1 mM sodium azide/TBST for 1 hour at RT or in BME buffer for 30 minutes at 50 °C. Afterwards, the membrane is again washed three times for 5 minutes in TBST and then blocked, stained and detected as previously described (see 2.2.3.1.6 and 2.2.3.1.7).

2.2.4 Microscopy

2.2.4.1 Confocal Laser Scanning Microscopy

Confocal laser scanning microscopy is a widely used technique to image fluorescently labeled macromolecules in fixed or living cells. In contrast to conventional light microscopy, where the whole sample is illuminated, confocal microscopes scan the specimens with a focused laser beam thus optically sectioning the sample. In consequence, only restricted regions of the specimen are illuminated while light from other parts is excluded, leading to an increased maximum lateral and axial resolution[224].
Confocal laser scanning microscopy was routinely applied to analyze subcellular localization, abundance and behavior of proteins of interest in MCF7 or HeLa cells. To this end, the cells were transfected with fluorescently labeled proteins or immunolabeled with appropriate dyes and fixed as previously described (see 2.2.2.3 and 2.2.2.5). Confocal images of fixed and living cells were obtained with a Leica TCS SP5 laser scanning microscope using a 63 x 1.4 NA oil objective. Fixed cells were imaged at room temperature while experiments with living cells were performed in a 37 °C/5 % CO_2 incubator. Typical excitation and detection settings for each fluorescent probe are listed in table 2.21. If combinations of probes with similar excitation and emission maxima were imaged, the detection bandwidth was adjusted to avoid bleed-through. Routinely, images were recorded at 5 - 60 % laser power in sequential mode with a scanning speed of 100 Hz, a line average of one, a frame average of three and a size of 1024 pixel × 1024 pixel. The zoom, gain and pinhole were adjusted for each experiment individually.

2.2.4.2 Data Processing

Data acquired by confocal laser scanning microscopy was analyzed and quantified using ImageJ[225]. Several macros were created and optimized to quantify autophagy levels based on puncta counts and to

Table 2.21: Confocal imaging settings.

PROBE	EXCITATION LASER	DETECTION BANDWIDTH
TagBFP DyLight405 mTurquoise	Diode 405 nm, Model: Cube 1162002/AF	420 - 480 nm
EGFP Alexa488	Argon 488 nm, Model: LGK 7872 ML05	500 - 550 nm
mCitrine	Argon 514 nm, Model: LGK 7872 ML05	530 - 550 nm
mCherry	DPSS 561 nm, Model: YLK 6120 T02	600 - 650 nm
mKate	Helium Neon 594 nm, Model: LGK 7512 P	610 - 650 nm
DyLight647/9	Helium Neon 633 nm, Model: LGK 7654-15	665 - 680 nm

analyze the efficiency of protein mislocalization to the plasma membrane by inducible heterodimerization.

Autophagy levels were estimated from the percentage of puncta area within total cell area. Measuring puncta area proved to be superior to counting the number of puncta, as the size variation of autophagic compartments provides valuable information in itself. Furthermore, certain autophagy modulators (e.g. BafilomycinA1) induced formation of large, clustered autophagosomes that cannot be appropriately separated by thresholding. Analysis of EGFP-LC3 or EGFP-Atg5 puncta area was performed with the 'EGFP Puncta Count' macro (see A.1). The macro initially provides the images as a merge of all channels (e.g. TagBFP-Marker, EGFP-LC3, mCherry-POI), then the region on interest (ROI) is selected for each image individually to exclude non-transfected cells. Afterwards the channels were split, aligned and the puncta area was selected by manually adjusting the threshold in the EGFP channel. In this case, automated thresholding appeared to be disadvantageous due to varying fluorescence intensities. The area of the thresholded particles was then measured and the same procedure was repeated for the cell area. Afterwards, Microsoft Excel and OriginPro were used to calculate the percentage of puncta area in cell area, to determine outliers and to calculate the weighted arithmetic mean and weighted standard error of the mean (SEM). Each dataset contained three replicates of twenty data points, each point representing one cell. The significance level was set to 0.05 (5 %) and statistical significance was tested by performing a Student's *t*-test. All of the data was normalized against a control determined in fed conditions, i.e. prior to autophagy induction.

Autophagic flux was monitored by performing tandem mCherry-EGFP-tagged LC3 puncta counts and quantified with the 'mCherry-EGFP Puncta Count' macro (see A.1). As before, a ROI was selected manually and puncta and cell area were measured by thresholding the mCherry and EGFP channels. Afterwards, binary masks were generated from the thresholded selection of the puncta area. To determine the puncta area of particles exclusively tagged with mCherry, the EGFP channel was subtracted from the mCherry channel and the area of the remaining puncta was analyzed. The number of EGFP-, mCherry- or tandem-tagged particles was determined based on the same principle. Statistical analysis was performed as previously described.

In order to quantify the efficiency of heterodimerization at the plasma membrane, the ratio of mean fluorescence intensity at the plasma membrane to mean fluorescence intensity in the cytoplasm was determined and compared for the POI and a membrane-localized marker protein (see A.1). To this end, the confocal images were transformed into 32-bit images, background fluorescence was subtracted

and a ROI was selected. The plasma membrane was selected by thresholding in the marker channel, a binary mask was generated from the selection and the inverted selection (cytoplasm) and the masks were multiplied with 32-bit images of the POI and marker channel to eliminate background fluorescence. Afterwards, the mean fluorescence intensity and area was measured in the resulting images and membrane-to-cytoplasm ratios of the total fluorescence intensity were calculated and analyzed using Microsoft Excel and OriginPro.

3 Results and Discussion

The aim of this PhD thesis was to develop and apply the knock off/on system to modulate and study the mechanism of autophagosome formation and maturation. To this end, conditional translocalization of target proteins through reversible chemically induced dimerization of bait proteins with cellular anchors was first established and then applied to different autophagic prey proteins. The effects of knock off/on were then analyzed using different autophagy markers as read-out and various cellular anchors. Analysis focused especially on the function of the class III PI3K complex (PI3K complex hereafter) within the autophagy process.

3.1 Establishing the Knock Off and On Strategy

The knock off and on strategy is based on a bait-and-prey principle, in which localization-dependent function of prey proteins is disrupted by re-routing them to another cellular compartment via interaction with bait proteins. Typically, the bait protein is exogenous and overexpressed, so that mislocalization of the bait-prey complex results in depletion of the endogenous prey protein. Here, chemically inducible dimerization of FKBP'- and eDHFR domains was employed to re-route autophagy proteins to the plasma membrane and thus perturb their function within the autophagy process. To this end, target proteins were N-terminally fused to two copies of FKBP' and labeled with a fluorescent protein. The CAAX-domain of KRas was chosen as the plasma membrane anchor and fused to a fluorescent protein as well as two copies of eDHFR. Dimerization was induced by addition of SLF'-TMP, termed 'dimerizer', and reversed by addition of TMP, termed 'competitor', as described above (see 2.2.2.7.1). SLF'-TMP was selected, because it is bioorthogonal in eukaryotic systems, rapidly reversible and has been shown to induce dimerization within less than a minute[18]. The combination of these properties, especially the rapid kinetics, make it superior to most of the chemical heterodimerizers available to date.

Initially, the knock off and on system was tested focusing on the PI3K complex, which is crucial for autophagosome formation and directly participates in isolation membrane formation. The key components of the PI3K complex, Beclin1, Vps34, Atg14L and UVRAG, were fused to FKBP' and the efficiency and speed of membrane recruitment after dimerizer addition were analyzed with confocal laser scanning microscopy. Preliminary experiments confirmed that each of the proteins could be re-routed to the plasma membrane and released from it within less than 10 minutes after addition of SLF'-TMP and TMP, respectively. No cell line-dependent differences in dimerization and dissociation kinetics or transfection efficiency could be observed in HeLa, HEK293T or MCF7 cells. MCF7 cells were chosen for further experiments as they feature a well defined plasma membrane and are very responsive to autophagy induction.

3.1.1 Knock Off Induces Translocalization of Exogenous PI3K Prey Proteins

The knock off and on principle is based on the assumption that inducible translocalization of highly overexpressed bait proteins to the plasma membrane results in re-routing of their endogenous interaction partners (prey) and thus disrupts their local function. In order to confirm that mislocalization of PI3K complex proteins actually perturbed their respective interaction partners, co-localization of bait and prey proteins at the plasma membrane was examined. To this end, PI3K complex bait proteins were fused to mCherry-FKBP' and targeted to the plasma membrane through dimerization with TagBFP-eDHFR-CAAX. Subsequently, localization of different EGFP-tagged PI3K prey proteins was analyzed. Since all PI3K proteins are either cytoplasmic or ER-resident, they only enrich at the plasma membrane through interaction with FKBP'-tagged PI3K proteins.
The dimerization experiments showed that Atg14L and Beclin1 or UVRAG and Beclin1 could function as bait for each other (see Figure 3.1). Vps34 or p150 could neither be used as bait nor translocated to the plasma membrane through interaction with Beclin1, Atg14L or UVRAG (see Figure B.1). However, Vps34 could function as a bait for p150.
Interaction of Beclin1 with Atg14L and UVRAG is well documented in literature and our findings are thus in agreement with previously published results. In fact, Atg14L and UVRAG were first identified as Beclin1 binding proteins in yeast by the Ohsumi group and later in mammalian cells by Mizushima and colleagues, who also established that Atg14L and UVRAG bind mutually exclusive to Beclin1 forming two distinct PI3K complexes[4,226]. Various studies showed that Beclin1 and Atg14L/UVRAG can be co-purified in immunoprecipitation experiments[4,8,9,226,227,228] and that the proteins co-localize in punctate structures upon starvation-induced autophagy[10,38,229,230]. Matsunaga and co-workers also employed a CAAX-domain to target GFP-Atg14L to the plasma membrane of A549 and HEK293T cells and reported translocalization of immunostained endogenous Beclin1. Interestingly, they could also partially attract endogenous Vps34 to the plasma membrane through interaction with GFP-Atg14L-CAAX, which is consistent with various immunoprecipitation experiments confirming interaction of Atg14L/UVRAG and Vps34[4,8,9,227]. The same applies to Beclin1, which binds directly to Vps34 through its ECD domain.
Based on these results, it appears implausible that Vps34 could only serve as a bait for the kinase p150 in the knock off and on system, so we hypothesized that the presence of at least one additional PI3K protein was required to mislocalize the whole complex. This assumption was originally derived from an EM structure of the PI3K complex suggesting that p150 acts as a bridge between Vps34 and Beclin1[231]. However, this could not be confirmed experimentally even though different combinations of PI3K complex proteins with varying baits and preys were tested (see Figure B.1). Finally, a crystal structure of the whole UVRAG-containing PI3K complex, published in 2015, indicated that the complex assembles from a Vps34/p150 heterodimer in combination with a Beclin1 heterodimer containing either Atg14L or UVRAG[5]. This is consistent with our observations, as the different heterodimers could be assembled at the plasma membrane after knock off. To test whether we could induce mislocalization of the whole complex, all PI3K complex proteins were expressed simultaneously with FKBP'-Beclin1 as a bait. Indeed, as shown in Figure 3.1D, expression of four PI3K complex proteins facilitated translocalization of the whole complex to the plasma membrane. This is in agreement with previously published findings and shows that FKBP-tagged bait proteins can be used to re-route their direct and indirect endogenous interaction partners to the plasma membrane.

After establishing that the main PI3K complex proteins could be used as a bait for each other, the analysis was extended to potential PI3K-interacting proteins, such as Rubicon, DFCP1, WIPI or Atg16L. However, while Atg16L could attract Atg12-5 to the plasma membrane, none of the other proteins was

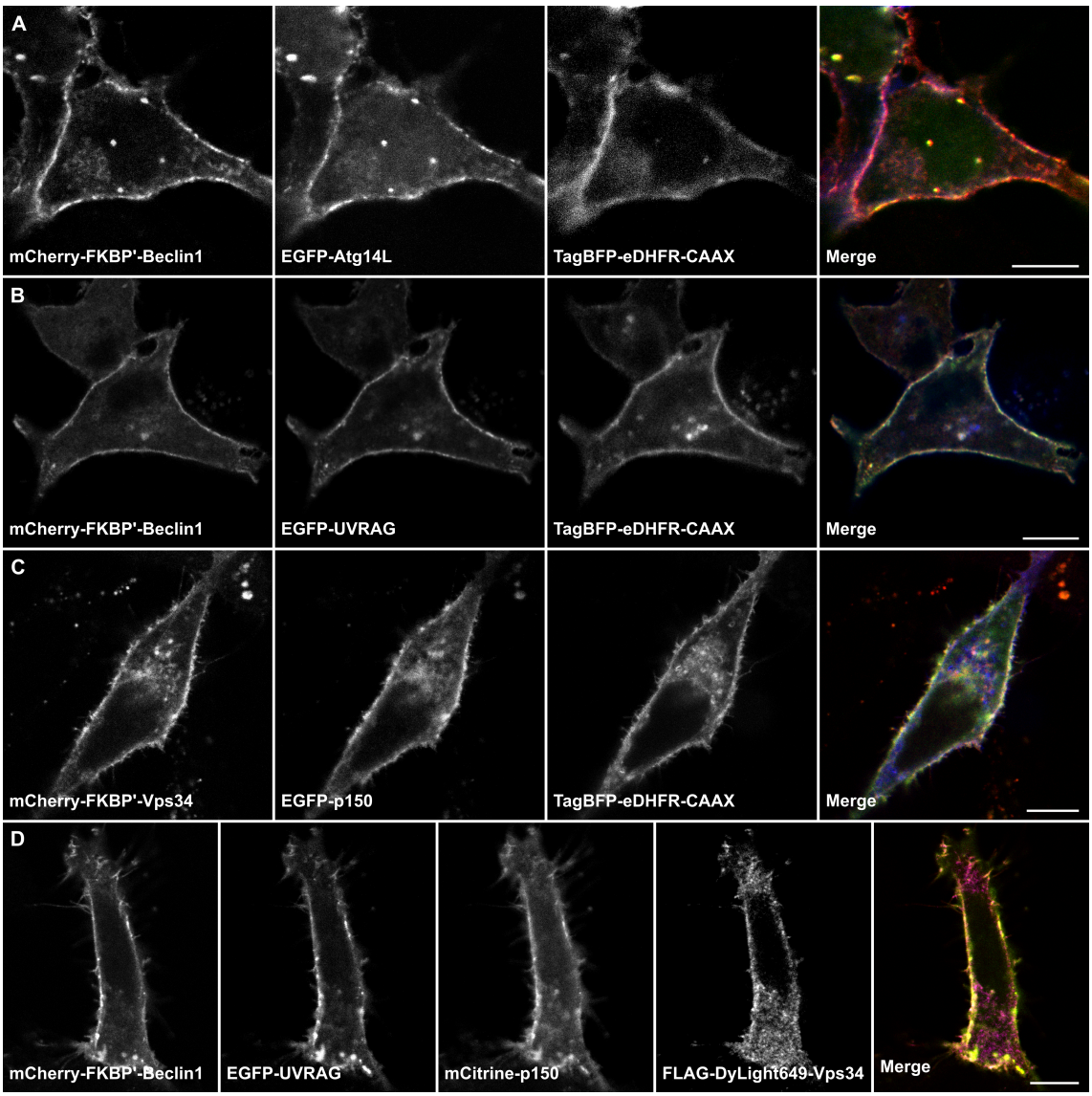

Figure 3.1: Co-localization of exogenous PI3K complex proteins at the plasma membrane of MCF7 cells after 2 hours starvation in EBSS and 30 minutes treatment with SLF'-TMP. Scale bar: 10 µm. **A** FKBP'-Beclin1 attracts Atg14L to the plasma membrane after dimerizer treatment. **B** FKBP'-Beclin1 and UVRAG co-localize at the plasma membrane. **C** FKBP'-Vps34 attracts p150 to the plasma membrane upon SLF'-TMP addition. **D** The whole UVRAG-containing PI3K complex is mislocalized to the plasma membrane using FKBP'-Beclin1 as bait.

re-routed after mislocalization of the PI3K bait proteins (see Table 3.1). Atg12 and Atg5 bind covalently to each other and Atg16L stabilizes this interaction further to form a stable multimeric complex, which has been well characterized in literature[35,232]. Therefore, it is not surprising that Atg16L re-routes Atg12-5 to the plasma membrane and still serves as good proof of principle for the knock off and on system.

Rubicon has been reported to transiently interact with Beclin1 in the UVRAG-containing PI3K complex[228]. Thus we analyzed whether translocalization of UVRAG or Beclin1 also caused Rubicon re-routing. However, neither UVRAG nor Beclin1 could recruit Rubicon to the plasma membrane even if all three proteins were expressed simultaneously. This suggests that Rubicon can only interact with the Beclin1-UVRAG heterodimer within the complete PI3K complex. In order to test this hypothesis, Rubicon, Beclin1, UVRAG, Vps34 and p150 could be expressed simultaneously using one PI3K protein as

Table 3.1: Co-localization of exogenous FKBP'-bait proteins and potential prey proteins at the plasma membrane of MCF7 cells. Autophagy was induced by starvation in EBSS. The cells were treated with SLF'-TMP for at least 30 minutes.

PREY / BAIT	Beclin1	Atg14L	UVRAG	Vps34	Atg16L
Beclin1	–	✓	✓	×	×
Atg14L	✓	–	×	×	×
UVRAG	✓	×	–	×	×
Vps34	×	×	×	–	×
p150	×	×	×	✓	×
Rubicon	×	×	×	×	×
WIPI	×	×	×	×	×
DFCP1	×	×	×	×	×
Atg16L	×	×	×	×	–
Atg12-5	×	×	×	×	✓

FBKP-tagged bait and eDHFR-CAAX as membrane anchor. As demonstrated before, dimerizer addition should induce mislocalization of the PI3K complex to the plasma membrane, which might then attract Rubicon as well. However, expression and imaging of six fluorescently labeled proteins is technically challenging, because the transfection efficiency is presumably low and the choice of fluorescent tags is limited. The latter is due to spectral bleed-through, which occurs between fluorophores with overlapping emission/excitation spectra and causes artifacts that are especially difficult to identify when co-localization is analyzed.

DFCP1 and WIPI bind to the PI3Ps generated by Vps34 [7,233], but were not recruited to the plasma membrane by Vps34, Beclin1, Atg14L or Atg16L mislocalization. This indicates that expression of one PI3K complex component alone is not sufficient to assemble the whole complex and facilitate PI3P generation at the plasma membrane. Similar to Rubicon, DFCP1 and WIPI could potentially be re-routed by attracting the whole PI3K complex to the membrane, but again the analysis are impeded by experimental limitations. Further, binding of DFCP1 and WIPI to PI3Ps may depend on additional factor such as membrane curvature.

3.1.2 Knock Off Induces Mislocalization of Endogenous PI3K Prey Proteins

To confirm that endogenous target proteins are indeed translocalized to the plasma membrane after knock off of PI3K bait proteins, we performed immunofixation and co-immunoprecipitation experiments. Immunofixation was employed to visualize the cellular distribution of endogenous prey proteins in regard to overexpressed FKBP'-PI3K bait proteins before and after dimerizer treatment. Initially, the specificity of anti-Beclin1, anti-UVRAG, anti-Atg14L and anti-Vps34 antibodies was tested by immunostaining fluorescently labeled, overexpressed proteins. To this end, mCherry-FKBP'-tagged Beclin1, UVRAG, Atg14L and Vps34 were introduced into HEK293T cells and immunostained in the presence or absence of the dimerizer. As shown in Figure B.2, all of the tested antibodies co-localize well with their target proteins, which becomes especially clear after mislocalization to the plasma membrane. This confirms that the antibodies are specific for their target proteins in the cellular environment.

Next, FKBP'-Beclin1, -UVRAG and -Atg14L were introduced into different cell lines and immunostain-

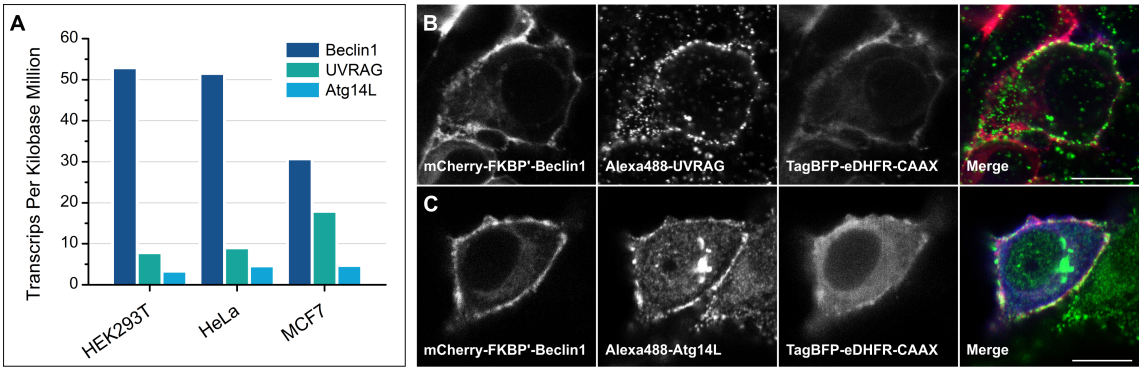

Figure 3.2: Expression and localization of PI3K complex proteins. **A** RNA expression of Beclin1, UVRAG and Atg14L in HEK293T, HeLa and MCF7 cells. Data was provided by The Human Protein Atlas [234,235]. **B** FKBP'-mCherry-Beclin1 is mislocalized to the plasma membrane of HEK293T cells and attracts endogenous UVRAG after 2 hours starvation in EBSS and 30 minutes treatment with SLF'-TMP. **C** Endogenous Atg14L is mislocalized to the plasma membrane of HeLa cells through interaction with FKBP'-mCherry-Beclin1 after 2 hours starvation in EBSS and 30 minutes treatment with SLF'-TMP.

ing was performed against their respective endogenous interaction partners. HEK293T, HeLa and MCF7 cells were chosen since they feature different expression levels of PI3K complex proteins and thus display distinct phenotypes. As shown in Figure 3.2A, Beclin1 expression is significantly higher than UVRAG or Atg14L RNA levels in all cell lines, but reduced in MCF7 cells. In contrast, UVRAG levels higher in MCF7 cells than in HEK293T or HeLa cells, while Atg14L expression is low, but consistent in all three cell lines.

As shown in Figure B.4 immunostaining of endogenous UVRAG indicates that the protein localizes to small punctate structures in HEK293T cells and to the plasma membrane of HeLa and MCF7 cells regardless of dimerizer addition. In HEK293T cells, however, UVRAG translocalizes to the plasma membrane upon addition of SLF'-TMP, even though it still remains in punctate structures (see Figure 3.2B). In contrast to previous studies reporting that UVRAG mainly localizes to puncta in the perinuclear region [4,9,10,11], here puncta could be detected throughout the whole cell and even outside of cells. This suggests that a least part of the observed punctate structures are artifacts from the immunolabeling procedure. The same applies to the immunofluorescence signal at the plasma membrane observed in HeLa and MCF7 cells. In general, immunolabeling outcomes depend heavily on the cell type as well as the fixation and permeabilization procedure and false positive labeling at the plasma membrane has been described on several occasions [236]. Still, endogenous UVRAG was mislocalized to the plasma membrane upon knock off of FKBP'-Beclin1 in HEK293T cells, which is consistent with previous results and indicates that in principle the localization of endogenous target proteins can be regulated by the knock off and on strategy.

In contrast to UVRAG, Atg14L immunofluorescence is very consistent in all three cell lines and shows punctate structures in proximity of the ER or ERGIC region (see Figure B.5), which is in agreement with previously published results [4]. However, upon addition of SLF'-TMP and knock off of FKBP'-Beclin1 to the plasma membrane, Atg14L localization is only affected in HeLa cells. Here, the protein is re-routed to the plasma membrane, which is consistent with the data obtained for exogenous Atg14L (see Figure 3.2C). Similar as for UVRAG labeling, the fixation or permeabilization procedure might have altered the original localization of Atg14L in HEK293T and MCF7 cells so that no immunofluorescence could be detected at the plasma membrane.

Immunostaining against endogenous Beclin1 shows a diffused cytoplasmic distribution with distinct

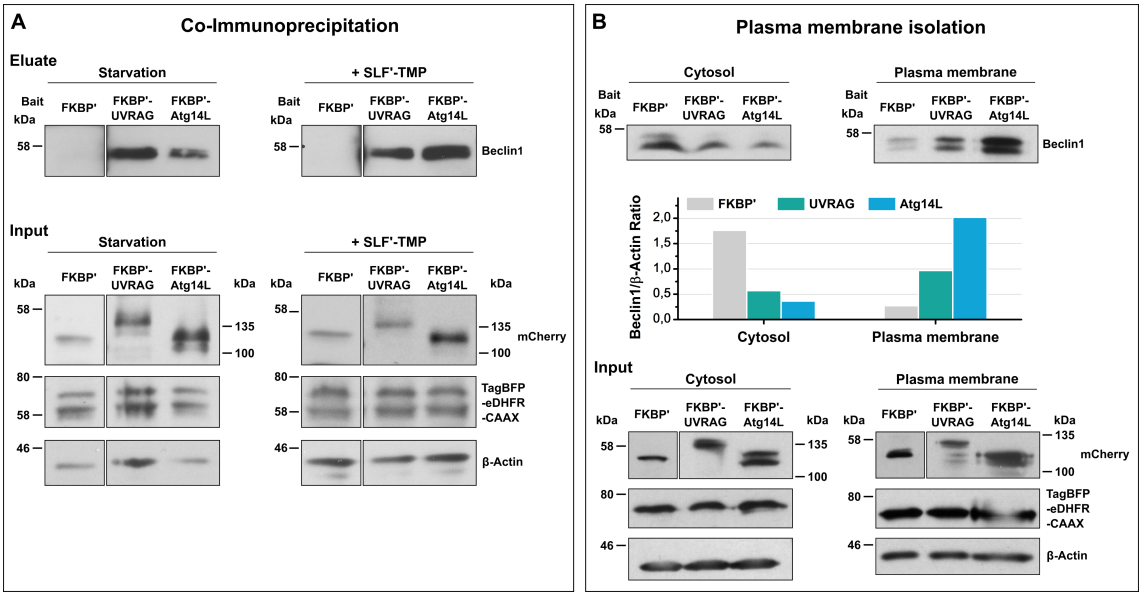

Figure 3.3: Immunoprecipitation and fractionation of HEK293T cell lysates to analyze interaction of PI3K complex proteins. Cells were transfected with TagBFP-eDHFR-CAAX as well as mCherry-FKBP', mCherry-FKBP'-UVRAG and mCherry-FKBP'-Atg14L and starved in EBSS for 2 hours. Scale bar: 10 µm. **A** Co-immunoprecipitation of endogenous Beclin1. FKBP'-UVRAG and -Atg14L, but not mCherry-FKBP', interact with endogenous Beclin1 in the presence or absence of SLF'-TMP. **B** After treatment with SLF'-TMP, endogenous Beclin1 levels are decreased in cytosol fraction of cells expressing FKBP'-UVRAG and -Atg14L while Beclin1 is enriched in the plasma membrane fraction of the same cells.

punctate structures throughout the whole cell, which are most defined in HeLa cells (see Figure B.6) and have been reported before[230,237,238]. Curiously, the subcellular localization of endogenous Beclin1 was not affected by knock off of FKBP'-UVRAG or -Atg14L in any cell line suggesting that the proteins are not interacting or that Beclin1 is trapped in the cytoplasm. However, this would be in stark contrast to previous results where exogenous Beclin1 could be mislocalized to the plasma membrane and appears to bind tightly to UVRAG and Atg14L. Other possible explanations might be immunolabeling artifacts or residual FKBP'-bait proteins in the cytoplasm engaging the majority of endogenous Beclin1. The later appears rather unlikely, since no immunofluorescence whatsoever could be detected at the plasma membrane and even if the fluorescence signal was attenuated by cytoplasmic FKBP'-UVRAG-Beclin1 interaction, it should not be completely abolished. Immunolabeling artifacts cannot be completely excluded and even though different fixation and permeabilization approaches were tested to optimize the immunostaining conditions, the procedure might have altered Beclin1s *in situ* distribution[236]. Therefore, co-immunoprecipitation of FKBP'-UVRAG and Atg14L was employed to investigate whether native Beclin1 could still interact with the modified PI3K proteins.

Co-immunoprecipitation was carried out in HEK293T cells using a RFP-Trap to pull down overexpressed mCherry-FKBP', mCherry-FKBP'-UVRAG and mCherry-FKBP'-Atg14L before and after treatment with SLF'-TMP. Western blotting analysis showed that Beclin1 is indeed pulled down by both, FKBP'-UVRAG and -Atg14L in the presence or absence of the dimerizer (see Figure 3.3A). This confirms that interaction between Beclin1, Atg14L and UVRAG is not disrupted by the mCherry-FKBP'-tag and suggests that FKBP'-UVRAG or -Atg14L should function as Beclin1 baits.

In order to test whether endogenous Beclin1 can be mislocalized by knock off of UVRAG or Atg14L, the plasma membrane of SLF'-TMP treated cells was isolated and Beclin1 levels in the membrane and the cytosol were compared. To this end, lysates of HEK293T cells expressing TagBFP-eDHFR-CAAX and the

mCherry-FKBP'-tagged bait proteins were fractionated using the Minute Plasma Membrane Protein Isolation Kit. Afterwards, the cytosol and plasma membrane fractions were analyzed by western blotting as shown in Figure 3.3B. In the cytosol fraction, Beclin1 levels are decreased by 3-fold in UVRAG knock off cells and by 5-fold in Atg14L knock off cells compared to the control cells expressing only mCherry-FKBP'. In the plasma membrane fraction, however, Beclin1 levels are increased by a factor of three and seven after UVRAG and Atg14L knock off, respectively, whereas it is barely detectable in the control cells. This indicates that most of the Beclin1 population was indeed re-routed to the plasma membrane after knock off of UVRAG and Atg14L.
Taken together, the results suggest that the availability of endogenous target proteins in the cytoplasm can indeed be regulated by knock off of exogenous FKBP'-bait proteins. Knock off of endogenous UVRAG and Atg14L was directly detected by immunostaining, while immunoprecipitation and western blotting confirmed that endogenous Beclin1 can be mislocalized to the plasma membrane.

3.1.3 Nanobodies as Bait in the Knock Off and On System

The knock off and on system employs a bait-and-prey principle that requires relatively stable interaction of the target proteins. However, many proteins bind only transiently to each other or require additional binding partners to stabilize their interaction. Vps34, for instance, binds directly to Beclin1s ECD, but in the knock off/on system the two proteins can only serve as a bait for each other in the presence of the entire PI3K complex. In order to overcome this limitation and target proteins directly and specifically, we tested whether nanobodies can be used as bait to mislocalize autophagy proteins to the plasma membrane.
Typically, mammalian antibodies are comprised of two identical heavy and two light chains featuring variable domains which confer specificity for an antigen. This structural concept is very conserved in mammals, however, *Camelidae* express an additional type of antibodies consisting of only two homodimeric heavy chains with a variable domain, referred to as single-domain antibodies or nanobodies. Compared to the tetrameric antibodies, nanobodies are smaller, easier to obtain, exceptionally stable, soluble in aqueous solutions and can be efficiently expressed in bacterial systems[239,240].
Here, an anti-Vps34 nanobody introduced by Rostislavleva *et al.* was fused to an FKBP' domain to inducibly mislocalize endogenous Vps34[5]. In their report Rostislavleva *et al.* generated a nanobody specific for yeast Vps34 as described by Pardon *et al.* and used it to crystallize the yeast PI3K complex[241]. In the course of their studies, they additionally employed hydrogen-deuterium exchange mass spectrometry to confirm that the nanobody specifically recognizes the helical domain of yeast Vps34, but none of the other PI3K complex proteins (see Figure 3.4). As we intended to target human Vps34, the amino acid sequence of the nanobody was initially optimized for mammalian codon usage and its specificity was analyzed by immunoprecipitation and confocal laser scanning microscopy.
For the confocal microscopy analysis, the FKBP'-tagged nanobody, the membrane anchor TagBFP-eDHFR-CAAX and the target, EGFP-Vps34, were introduced into starved MCF7 cells and dimerization was induced by addition of SLF'-TMP. As shown in Figure 3.5A, most of the exogenous Vps34 was re-routed to the plasma membrane after knock off of the nanobody and only a small fraction remained cytoplasmic. Yet, the translocalization efficiency appears to be lower than in previous analysis with a similar setup (see section 3.1.2), possibly because part of the nanobodies are occupied by endogenous Vps34. This effect was not observed before, but it is likely that the nanobody has a much higher affinity to Vps34 than p150, which was previously used as bait. Taken together, the confocal microscopy data indicates that the anti-Vps34 nanobody binds specifically to Vps34, but we still performed immunopre-

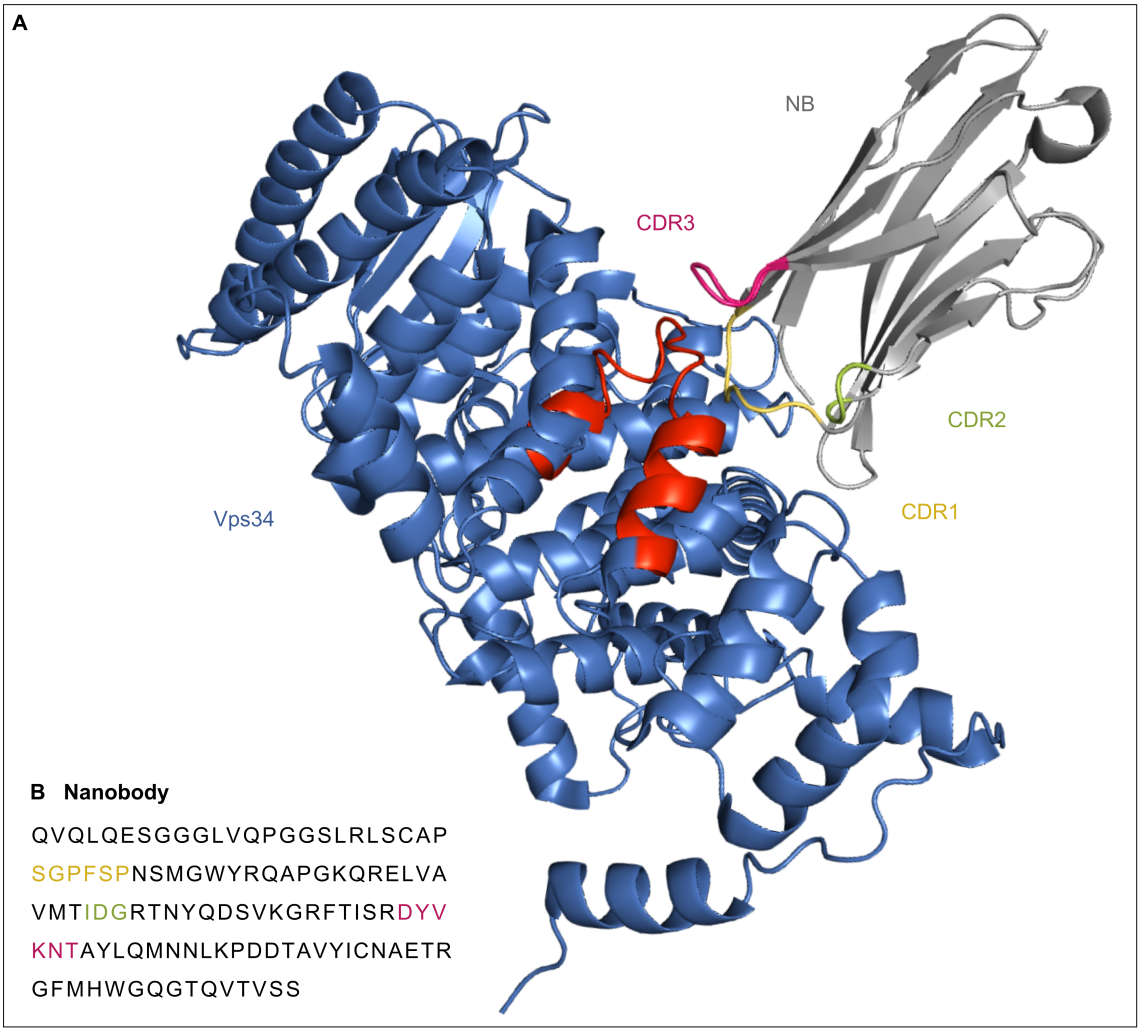

Figure 3.4: The anti-Vps34 nanobody, adjusted from Rostislavleva *et al.*[5]. **A** Vps34-specific nanobody binding to an epitope on the helical domain of Vps34 (red). The interaction is mainly mediated by the complementarity-determining regions CDR1 (yellow) and CDR3 (magenta) with no significant contribution from CDR2 (green).**B** Amino acid sequence of the anti-Vps34 nanobody.

cipitation to obtain an additional confirmation.

Co-immunoprecipitation was performed in lysates of starved HEK293T cells expressing Nano-mCherry-FKBP' and Vps34, which was C- or N-terminally tagged with EGFP. The anti-Vps34 nanobody was employed as bait and the pull down was performed using a RFP-Trap. Subsequent western blotting showed that only the N-terminally tagged variant of EGFP-Vps34 could be pulled down by the nanobody suggesting that the C-terminal EGFP-tag perturbs binding and potentially even Vps34s function. We thus used only N-terminally labeled Vps34 in the subsequent assays. Since N-terminally labeled Vps34 was readily pulled down by the nanobody, we assumed that the nanobody binds specifically to Vps34 in the cell (Figure 3.5B). However, it should be noted that the assay would be even more reliable if the endogenous instead of overexpressed Vps34 was analyzed, but we were not able to obtain an anti-Vps34 antibody of acceptable quality and thus refrained from further analysis. Nevertheless, the combined imaging and co-immunoprecipitation data confirms that the nanobody binds specifically to mammalian Vps34 and thus we proceeded to study the effect of Vps34 mislocalization using the nanobody as bait.

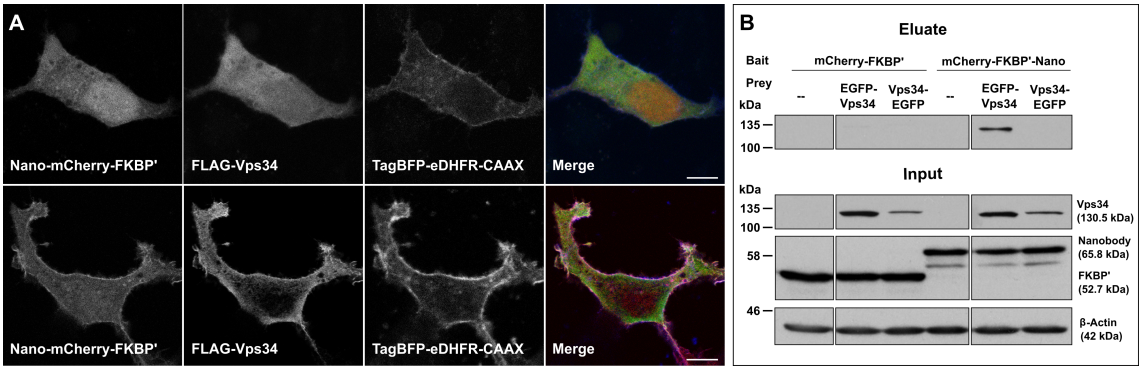

Figure 3.5: Interaction of the anti-Vps34 nanobody with overexpressed Vps34. **A** The nanobody attracts EGFP-Vps34 to the plasma membrane of MCF7 cells that were starved for one hour in EBSS and simultaneously treated with SLF'-TMP. Scale bar: 10 µm. **B** Immunoprecipitation of the Vps34 using the anti-Vps34 nanobody as bait. Only N-terminally EGFP-tagged Vps34 can be immunoprecipitated by the Nano-mCherry-FKBP' construct indicating that the C-terminal tag disrupts the binding and that the nanobody is specific for Vps34. Lysates were generated from HEK293T cells after one hour starvation in EBSS and treatment with SLF'-TMP.

3.2 Modulation of Autophagosome Formation with Knock Off and On

After establishing that endogenous PI3K prey proteins can be re-routed to the plasma membrane through interaction with FKBP'-modified bait proteins, we analyzed whether mislocalization would affect the localization dependent protein function during autophagosome formation. To assess autophagy flux, autophagic structures were labeled with characteristic marker proteins, such as LC3, Atg5 or WIPI and monitored by fluorescence microscopy or immunoblotting.

Fluorescently labeled autophagosomes can be detected as puncta within the cytoplasm and provide a well established read-out for the autophagy level: a large amount of puncta indicates a strong induction of autophagy and a low puncta number represents a basal level of autophagy. The most commonly applied marker to monitor autophagosome formation with fluorescence microscopy is EGFP-LC3, because it remains bound to the inner and outer autophagosomal membrane throughout the entire autophagy process. Initially, we tested whether knock off of FKBP'-Beclin1 affects the amount of EGFP-LC3 puncta in MCF7 cells stably expressing the marker protein. mCherry-FKBP'-Beclin1, the control construct mCherry-FKBP' and TagBFP-eDHFR-CAAX were introduced into the EGFP-LC3-MCF7 cells, autophagy was induced by serum starvation and the autophagy level was assessed in the presence and absence of the dimerizer and competitor. Throughout this thesis, the amount of autophagic puncta was quantified by measuring the percentage of puncta area in cell area as weighted average using an ImageJ macro specifically designed for this purpose as opposed to counting the number of puncta. The latter is often used, but we found the puncta area per cell area to be the most accurate measure for autophagic activity as it accounts for varying cell and puncta sizes.

As shown in Figure 3.6 Beclin1 mislocalization leads to a significant reduction of EGFP-LC3 puncta in the cytoplasm. Quantification of the imaging data shows that the autophagosome population is decreased by more than 50 % within 10 minutes after knock off. Longer exposure to the dimerizer did not lower the amount of autophagic puncta further, suggesting that severe autophagy disruption can be achieved almost immediately after Beclin1 knock off. Similarly, knock on by TMP addition restored the autophagosome level almost completely within a time-frame of 10 minutes. In contrast, mislocalization of the control construct mCherry-FKBP' caused no significant change in the puncta levels, confirming that the previously described effect was indeed caused by knock off and on of Beclin1. Based on these

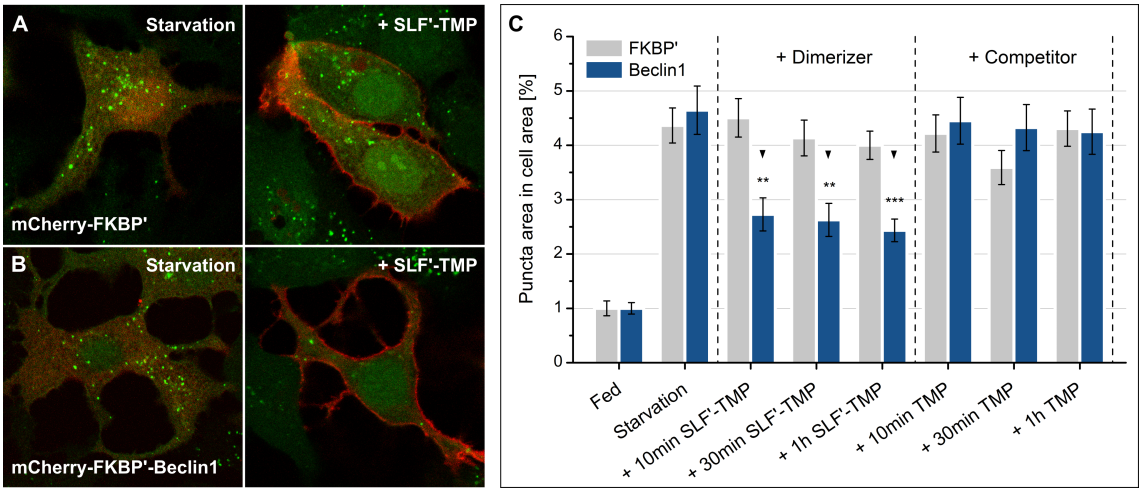

Figure 3.6: Knock off of Beclin1 perturbs autophagosome formation in EGFP-LC3-MCF7 cells. **A** The number of EGFP-LC3 puncta is not affected by mislocalization of the control construct mCherry-FKBP'. **B** The amount of EGFP-LC3 puncta is significantly decreased after knock off of mCherry-FKBP'-Beclin1 and subsequent mislocalization of PI3K complex proteins. **C** Quantification of the percentage of EGFP-LC3 puncta area of total cell area. Beclin1 knock off severely decreases the amount of puncta and autophagosome formation is disturbed. Error bars: weighted mean ± SEM ($n \geq 60$); ** = $p \leq 0.01$; *** = $p \leq 0.001$; statistical significance was determined by pairwise comparison to the starvation condition.

promising results, we extended the analyzes to the remaining PIK3 complex proteins and included EGFP-Atg5 as an additional marker for the early phase of autophagosome formation.

3.2.1 Perturbation of PI3K Proteins Impairs Autophagosome Formation

Our initial experiments showed that mislocalization of FKBP'-Beclin1 significantly decreased the amount of EGFP-LC3 labeled autophagosomes, supposedly due to impaired autophagosome biogenesis. However, due to the dynamic nature of autophagy, the number of autophagosomes at one specific time point is not representative for autophagy flux, but rather corresponds to the ratio between the rate of autophagosome generation and the rate of conversion into autolysosomes[242]. Hence, a decrease in autophagosome number can be caused by autophagy inhibition upstream of autophagosome generation or by acceleration of the autophagosome turnover rate. To distinguish between the two scenarios, we employed the autophagy modulator BafilomycinA1 (see Figure 3.7A), which inhibits the lysosomal V-ATPase and thus prevents autophagosome-lysosome fusion. If autophagosome formation is impaired by mislocalization of PI3K bait proteins, the autophagosome number should also be decreased in the presence of BafilomycinA1.

Initially, BafilomycinA1 treatment was optimized in EGFP-LC3-MCF7 cells expressing FKBP'-Beclin1 and an optimal treatment duration of two hours was determined (see Figure 3.7C). Afterwards, the PI3K bait proteins FKBP'-Beclin1, -Atg14L, and the anti-Vps34 nanobody, were introduced into EGFP-LC3-MCF7 cells, autophagy was triggered by serum starvation and mislocalization was induced by dimerizer addition in the presence or absence of BafilomycinA1. Finally, the amount of autophagosomes was detected by confocal microscopy and quantified with ImageJ as described before.

As shown in Figure 3.8A, knock off of Beclin1, Atg14L and anti-Vps34 nanobody substantially reduced the autophagosome number in untreated and BafilomycinA1-exposed cells, while autophagosome levels remained undisturbed in the presence of the competitor. Mislocalization of FKBP' alone had no

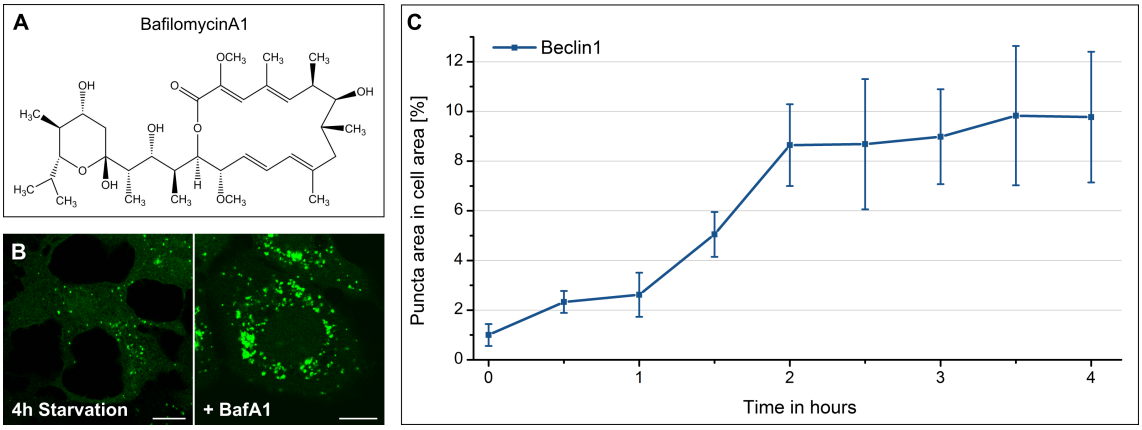

Figure 3.7: BafilomycinA1 prevents lysosomal fusion of autophagosomes. **A** Molecular structure of BafilomycinA1. **B** Treatment with BafilomycinA1 provokes accumulation of large EGFP-LC3 labeled autophagosomes in MCF7 cells. Scale bar: 10 µm. **C** After two hours treatment with BafilomycinA1 no further increase in autophagic activity can be observed.

impact on autophagosome levels regardless of BafiloymycinA1 treatment. This is a strong indication that knock off of PI3K bait proteins indeed disrupts autophagosome formation rather than promoting autophagosome conversion. It further confirms our initial hypothesis that PI3K knock off induces mislocalization of endogenous prey proteins that are essential for autophagosome biogenesis. The autophagic activity was also reduced to a similar extent regardless of which PI3K protein was used as bait, which makes sense since all of the targeted prey proteins function within the same complex.

However, LC3 is a rather unspecific autophagy marker when it comes to differentiating distinct autophagy phases, as it remains bound to the autophagosomal membrane throughout the whole biogenesis process. Atg5, on the other hand, is a very specific marker for the early stages of autophagosome formation as it only localized to the phagophore. In the hierarchy of autophagic complexes, the PI3K complex is upstream of the Atg12-5-16L complex[243] and accordingly, PI3K protein knock off should prevent Atg5 puncta formation. To investigate whether this is actually the case, we performed EGFP-Atg5 puncta counts using the same PI3K bait proteins and treatment conditions as for the LC3 puncta counts. As can be discerned form Figure 3.8B, the Atg5 puncta population is also significantly reduced after mislocalization of FKBP'-Beclin1, Atg14L or the Vps34-specific nanobody, while TMP addition or knock off of FKBP' had no impact. The effect is consistent, even in the presence of BafilomycinA1. This confirms our previous conclusion that knock off of PI3K bait proteins leads to mislocalization of endogenous PI3K proteins and inhibits their localization-dependent function in autophagosome formation.

Compared to results obtained by others with PI3 kinase inhibitors or knock down of PI3K complex proteins, the reduction of autophagic activity achieved by PI3K protein knock off is in a similar range of 50 to 60 % . Wu and co-workers, for instance, reported a 70 % decrease of the GFP-LC3 puncta number in MEFs after three hours treatment with the PI3 kinase inhibitor Wortmannin[244] and Blommart *et al.* observed a 80 to 90 % reduction of autophagosomes in rat hepatocytes after exposure to wortmannin or LY294002, another PI3 kinase inhibitor[245]. This was later confirmed by the Condongo lab, who reported a similar effect in HT-29 cells[246]. However, wortmannin and LY294002 are not specific for the class III PI3 kinase Vps34 and target all PI3 kinases, which might cause unwanted side effects and lead to more severe autophagy disruption. In contrast, knock down of PI3K proteins is very specific and might be more comparable to protein knock off, especially since no specific inhibitors for the PI3K proteins have been reported yet. Matsunaga and colleagues knocked down Atg14L in A549 cells and observed a 50 %

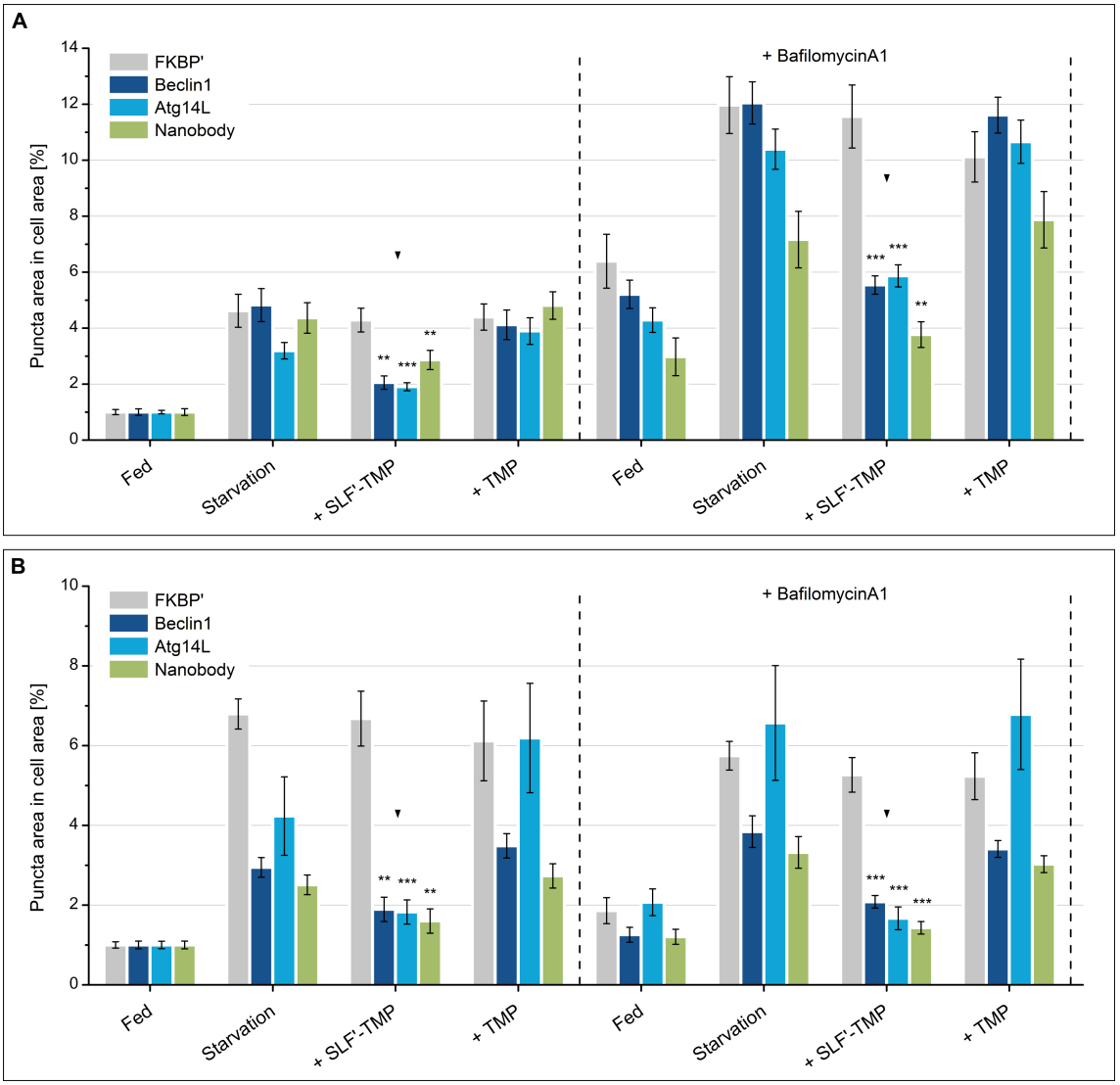

Figure 3.8: Knock off of PIK3 complex proteins perturbs autophagosome formation. Cells were starved in EBSS and/or treated with SLF'-TMP, TMP or BafilomycinA1 for 2 hours. Error bars: weighted mean ± SEM ($n \geq 60$); ** = $p \leq 0.01$; *** = $p \leq 0.001$; statistical significance was determined by pairwise comparison to the starvation condition; data was normalized against the fed condition. **A** The amount of EGFP-LC3 puncta is significantly decreased after knock off of FKBP'-Beclin1, -Atg14L and -anti-Vps34 nanobody in the presence or absence of BafilomycinA1. Mislocalization of FKBP' alone shows no effect. **B** Mislocalization of FKBP'-Beclin1, -Atg14L and -anti-Vps34 nanobody, but not FKBP', causes a significant decrease of Atg5-labeled puncta in the presence or absence of BafilomycinA1. This is a strong indication that knock off of PI3K complex proteins severely disturbs autophagosome formation.

decrease in the GFP-LC3 puncta number[228], which is in agreement with results by Zhong *et al.* showing that Atg14L knock down causes a 40 % reduction in the degradation of long-lived proteins in NIH 3T3 cells[229]. Itakura and co-workers showed that knock down of Atg14L or Vps34 reduced the GFP-LC3 puncta number by approximately 70 % in Hela cells[4], while Kim *et al.* reported a 50 % reduction after Beclin1 knock down in HT22 hippocampal cells[247]. Xing *et al.* found a similar effect of Beclin1 knock down in neuronal cells[248]. Hence, PI3K protein knock off is equally efficient as protein knock down or inhibitor treatment, but much more specific than PI3K inhibitors and less technically challenging then protein knock down. Here, a substantial reduction of autophagic activity was achieved within two hours,

which is on a similar time scale as most inhibitor treatments, but much faster than gene silencing. However, since dimerization of FKBP' and eDHFR domains takes only seconds, we assumed that autophagy disruption can be achieved within a much faster time frame and proceeded to study the dynamics of PI3K protein knock off further.

3.2.2 Dynamics of Autophagosome Formation

The previous analysis established that autophagosome biogenesis can be modulated with the knock off and on system, so we focussed on the temporal and functional aspects of autophagy modulation next. We initially analyzed the dynamics of Beclin1 perturbation and the resulting reduction of EGFP-LC3 puncta and then turned to a more specific PI3K complex marker, WIPI2b.

First, the speed of SLF'-TMP induced FKBP'-Beclin1 translocalization from the cytoplasm to the plasma membrane (PM) was quantified by monitoring the mean fluorescence intensity (MFI) at the plasma membrane by confocal microscopy. mCherry-FKBP'-Beclin1 and EGFP-eDHFR-CAAX were introduced into MCF7 cells, dimerization was induced by SLF'-TMP and the ratio of mean fluorescence intensity in the cytoplasm and at the plasma membrane was determined every minute for half an hour. Afterwards, FKBP'-Beclin1 re-localization was triggered by TMP addition and the MFI was monitored for another 10 minutes. Simultaneously, the amount of EGFP-LC3 puncta was quantified as described before.

The analysis showed that the cytoplasmic pool of FBKP'-Beclin1 was completely translocalized to the plasma membrane within 10 minutes after dimerizer addition and dissociated from the plasma membrane at the same rate upon addition of TMP (see Figure 3.9). Autophagosome formation, however, is effectively inhibited within 6 minutes of FKBP'-Beclin1 mislocalization and completely restored within 4 minutes of competitor addition. This indicates that modulation of about 60 to 70 % of the exogenous FKBP'-Beclin1 population is sufficient to disrupt or restore autophagosome formation. These results demonstrate that the knock off/on approach is suitable to disrupt autophagosome formation on a minute time scale, which is much faster than the traditional knock down/out approach and makes it possible to study the dynamics of autophagosome formation. In order to test whether we can indeed detect differences in the time line of autophagy disruption after knock off of individual PI3K complex proteins, we employed the PI3K activity marker WIPI2b in subsequent analysis.

WIPI2b belongs to an ancient seven-bladed β-propeller protein family and has been proposed to bridge PI3P generation and LC3 lipidation[249]. It is a PI3P effector, which is essential for LC3 lipidation and specifically binds to Atg16L, supposedly to recruit the Atg5-12-16L complex to the forming phagophore[233]. WIPI2b puncta counts have been employed to quantify early autophagy events (upstream of Atg5-12-16L) in previous studies, mostly using stable EGFP-WIPI2b U2OS or HEK293A cell lines. Here, we followed a protocol provided by the Ktistakis lab and immunostained endogenous WIPI2b in MCF7 cells transiently transfected with TagBFP-eDHFR-CAAX and a mCherry-FKBP'-tagged PI3K bait protein[250]. Stable EGFP-WIPI2b HEK293A cells were tested as well, but even after prolonged starvation the dynamic range was not large enough to detect differences in the amount of autophagic puncta. MCF7 cells showed an ample amount of endogenous WIPI2b puncta after moderate starvation and were used for subsequent experiments. The cells were starved for 2 hours before SLF'-TMP induced dimerization and then the amount of puncta was monitored in two-minute-intervals for half an hour.

Figure 3.10 displays the dynamics of autophagy inhibition after knock off of FKBP', FKBP'-Beclin1, FKBP'-Atg14L and the anti-Vps34 nanobody. As expected, knock off of FKBP' alone had no impact on WIPI2b puncta formation (Figure 3.10 A). Perturbation of Beclin1 or its interaction partners (Figure 3.10 B/C) led to a depletion of WIPI2b structures within 4 to 8 minutes. The half-time was estimated

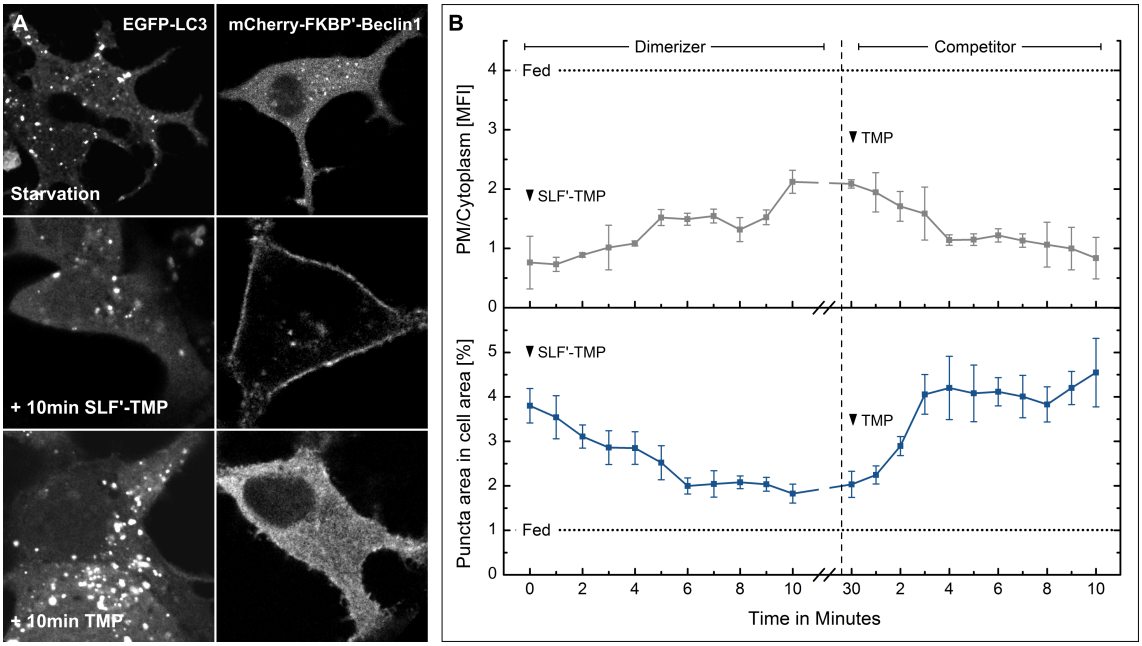

Figure 3.9: Dynamics of Beclin1 knock off. EGFP-LC3-MCF7 cells expressing mCherry-FKBP'-Beclin1 were starved in EBSS for 4 hours and then treated with SLF'-TMP and TMP. Error bars: weighted mean ± SEM (n ≥ 20). **A** FKBP'-Beclin1 is completely mislocalized to the plasma membrane after 10 minutes SLF'-TMP treatment and the EGFP-LC3 puncta number is reduced. After 10 minutes exposure to TMP, FKBP'-Beclin1 re-localizes to the cytoplasm and the EGFP-LC3 puncta level is restored. **B** Quantification of FKBP'-Beclin1 mislocalization and EGFP-LC3 puncta number. Translocalization of FKBP'-Beclin1 to the plasma membrane is completed after 10 minutes treatment with the dimerizer, but autophagosome formation is inhibited within 6 minutes of SLF'-TMP addition. Addition of the competitor releases FKBP'-Beclin1 back into the cytoplasm within 10 minutes, while autophagic activity is restored within 4 minutes.

to $t_{1/2} = 3$ minutes for FKBP'-Beclin1 and $t_{1/2} = 4$ minutes for FKBP'-Atg14L. Interestingly, ectopic plasma membrane localization of endogenous Vps34 using the nanobody as bait (Figure 3.10 D) led to an immediate halt in WIPI2b puncta formation ($t_{1/2} = 2$ minutes). WIPI2b binds to the PI3Ps generated by Vps34, so it should be most sensitive to disruption of the kinase function. However, Vps34s kinase activity appeared to be completely abolished after mislocalization to the plasma membrane or by removing Beclin1 or Atg14L/UVRAG from the PI3K complex. Previous studies showed that 65 % of the cellular PI3P pool are generated by Vps34[251] and that WIPI2b puncta formation is PI3P-dependent[233,252]. Our results suggest that the autophagosomal PI3P pool was severely diminished within minutes after knock off in our setup and could not be recovered even 30 minutes after PI3K protein mislocalization. Dooley *et al.* further showed that ectopic localization of WIPI2b to the plasma membrane is sufficient to attract the Atg12-5-16L complex, induce LC3 lipidation and generate phagophore-like structures[233]. However, formation of WIPI2b structures was not observed at the plasma membrane after knock off so that it appears unlikely that PI3P generation is reestablished at the plasma membrane.

Interestingly, perturbation of different PI3K complex components led to distinct patterns of autophagy inhibition. Mislocalization of endogenous Beclin1, i.e. knock off of Atg14L, caused a partial disruption of WIPI2b puncta formation, whereas perturbation of Beclin1s binding partners or endogenous Vps34 completely inhibited autophagosome formation. These results suggest that the Beclin1-Atg14L heterodimer regulates Vps34 activity and PI3P production at the autophagosome formation site. It has been reported by Zhong and others that Atg14L enhances Vps34 activity in a Beclin1-dependent manner[229,253,254], but our results indicate that Vps34 is only fully functional within the PI3K complex. This is

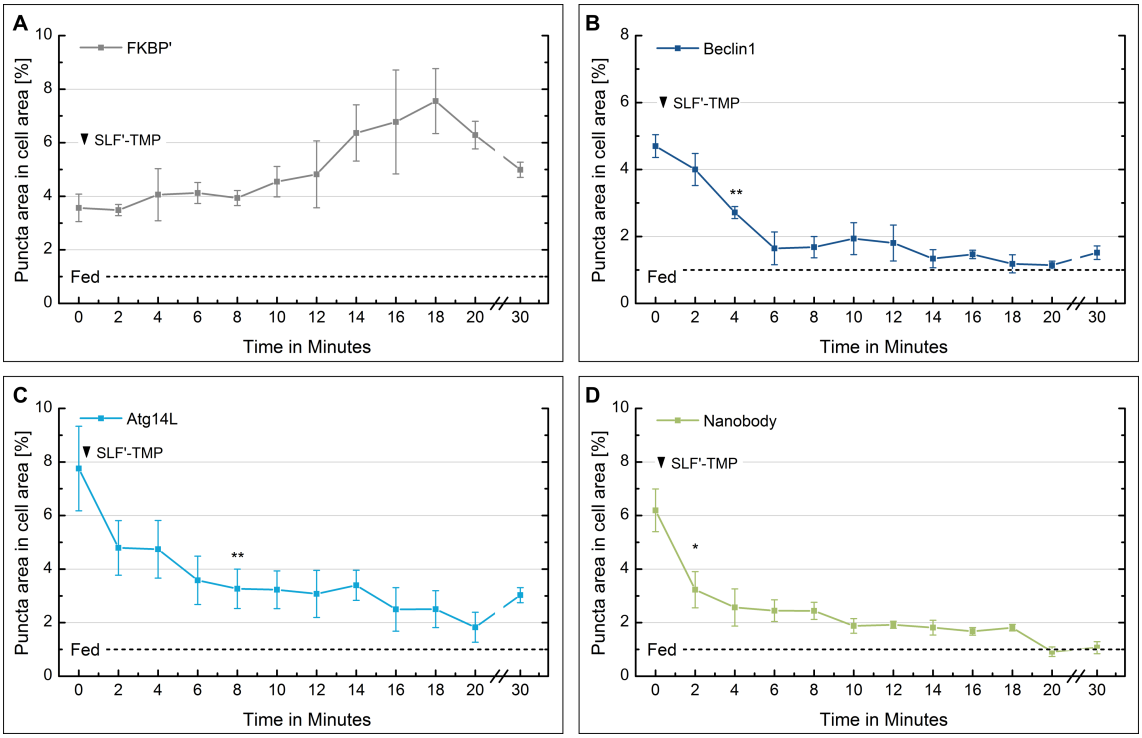

Figure 3.10: Knock off of PIK3 complex proteins perturbs formation of WIPI2b-labeled autophagosomes. MCF7 cells were starved in EBSS for 2 hours and then treated with SLF'-TMP. Error bars: weighted mean ± SEM ($n \geq 20$); * = $p \leq 0.05$, ** = $p \leq 0.01$; statistical significance was determined by student's t-test against the starvation condition; data was normalized against the fed condition. **A** Mislocalization of FKBP' alone has no effect on WIPI2b puncta formation. **B** FKBP'-Beclin1 knock off causes a significant reduction of WIPI2b puncta within 4 minutes after dimerizer addition. **C** -Atg14L knock off. **D** The amount of WIPI2b puncta is significantly decreased within 2 minutes after knock off of FKBP'-anti-Vps34 nanobody.

in agreement with insights obtained from a recently published study on the structure of the UVRAG-containing PI3K complex. Here, the kinase activity of the yeast p150-Vps34 dimer was significantly lower than the activity of the complete PI3K complex and deletion of Vps34s only contact with the Beclin1/UVRAG dimer, the CBR1 loop, resulted in a phenotype similar to Vps34 deletion (see Figure 3.11) [5]. Interestingly, mislocalization of endogenous Beclin1 (see Figure 3.10 C) has a less impact on WIPI2b puncta formation than knock off of Belcin1 interaction partners. This could denote a hierarchy within the PI3K complex in which Beclin1 is least important for PI3P production.

The distinct time lines of autophagy disruption for the individual bait proteins support this hypothesis. In our setup, mislocalization of endogenous Vps34 perturbed autophagosome formation the fastest, followed by the Beclin1 interactome (most likely Atg14L or UVRAG) and Beclin1 alone. However, it remains questionable, whether we can deduce a hierarchical order of PI3K complex protein function from the chronological order of autophagy inhibition. Vps34 is certainly most important for PI3P production, which is in keeping with our observations, but without further evidence it appears presumptuous to conclude that Atg14L or UVRAG are more meaningful to Vps34 function than Beclin1. Problematic in our setup are the fast kinetics of autophagy inhibition and protein knock off making it technically challenging to monitor the events in real time. One simple possibility to slow down the knock off process and stretch the dynamic range would be to apply less dimerizer. Alternatively one could perform the experiment in live cells with a photoinducible dimerizer. Another option may be to slow down cellular processes by lowering the surrounding temperature. This would minimize the chance that the detected

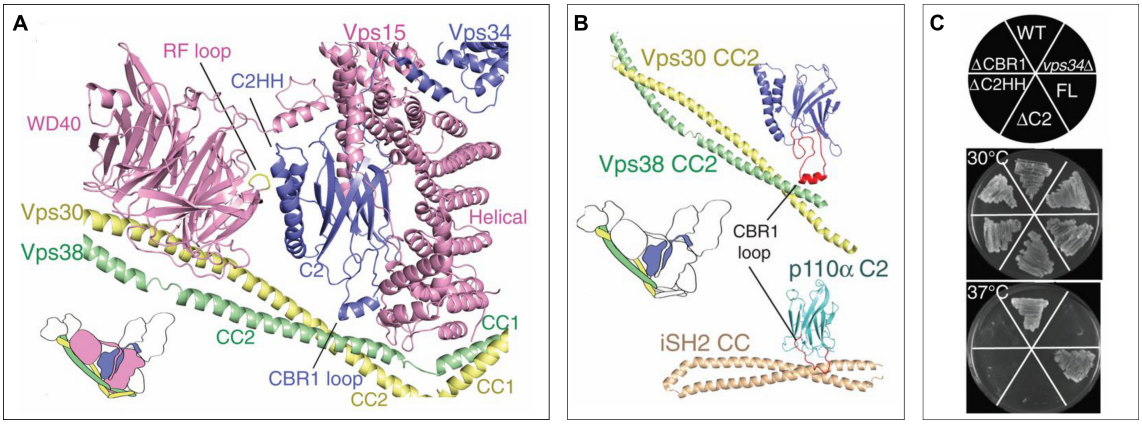

Figure 3.11: Structure of yeast Vps34 in the UVRAG-containing PI3K complex by Rostislavleva *et al.*[5]. **A** Vps34s distinct structural features (C2HH and CBR1 loop). **B** The Vps34 CBR1 loop binds yeast Beclin1/UVRAG CC2. This is similar to the CBR1 loop of class IA PI3Ks contacting the coiled coil (iSH2 CC) of the regulatory subunit. **C** Effects of Vps34 C2 mutants on temperature-sensitive growth. Deletion of Vps34 C2, C2HH or CBR1 prevents growth at 37 °C as opposed to full-length Vps34 (FL) or the wild type strain.

temporal differences are merely due to varying cell culture or fixation conditions and may allow to determine the order of events more reliably.

Taken together, the results presented here show that autophagy can be modulated on a time scale of seconds to minutes with the knock off and on approach. Given the right methodological setup, this makes it feasible to determine not only the hierarchical, but also the spatiotemporal relationship of individual autophagy proteins or protein complexes. Using WIPI2b as a marker, we could further show that the PI3K complex proteins are functionally dependent on each other and potentially also on the cellular environment.

3.2.3 Dynamics of Autophagosome Formation and Maturation

After characterizing the effect of PI3K complex protein mislocalization on autophagosome formation, we focussed on maturation and autophagy flux. To this end we employed an assay developed by Kimura *et al.* The approach is based on tandem mCherry-EGFP-labeled LC3 and exploits the pH sensitivity of EGFP to distinguish between autophagosomes and autolysosomes[255]. Typically, lysosomes feature a pH value of 4 to 5. Due to differences in their chromophores, mCherry fluorescence is stable at pH values below 5, while EGFP fluorescence is quenched in acidic environments. Accordingly, autophagosomes are labeled by both fluorescent proteins and appear yellow, whereas autolysosomes display only mCherry fluorescence and appear red. Thus, an increased number of yellow and red puncta indicates increased autophagy flux. A decreased number of yellow puncta without concomitant decrease of red puncta suggests that lysosomal turnover is blocked, while the opposite scenario indicates inhibition of autophagosome maturation. Based on these patterns, one can apply the tandem LC3 assay to distinguish between autophagy inhibitors and inducers or determine the time point of autophagy modulation. Here, we employed this approach to further characterize the effect of PI3K protein knock off on autophagy flux.

Initially, we performed a preliminary experiment to evaluate the mCherry-EGFP-LC3-MCF7 cell line, the fixation method and the quantification approach. Especially the immunofixation protocol is critical in this assay, since many fixation reagents are basic or neutral and can alter the pH value of the cellular environment. This could dequench EGFP in the lysosome and cause unwanted artifacts. To avoid this,

the immunofixation was carefully optimized prior to conducting any analysis. Afterwards, HA-tagged FKBP' and FKBP'-Beclin1 were introduced into the stable cells and autophagy was induced by starvation. Simultaneously, the cells were treated with dimerizer, competitor or BafilomycinA1. Finally, the amount of autophagosomes and autolysosomes was quantified using an ImageJ macro specifically designed for the purpose (see section A.1.2).
As shown in Figure B.8, the cells responded as expected to nutrient starvation, knock off/on or BafilomycinA1 treatment. The amount of autophagosomes and autolysosomes increased after starvation and was significantly decreased after Beclin1 mislocalization, but remained constant upon FKBP' knock off. Addition of TMP restored autophagy in cells expressing FKBP'-Beclin1, but did not affect the control cells. Upon BafilomycinA1 treatment, the amount of autophagosomes was substantially increased in both setups, while the amount of autolysosomes remained similar to fed conditions. As BafilomycinA1 blocks lysosomal fusion, this phenotype was expected and confirms that the chosen fixation conditions and quantification approach were appropriate.
Since the results suggested that the tandem LC3 assay was functional, we proceeded to study the dynamics of Beclin1 mislocalization. In order to achieve a better temporal resolution, autophagy was induced, Beclin1 was knocked off by dimerizer addition and the amount of autophagic vesicles was monitored every two minutes for half an hour. As a negative control, the analysis was also performed with FKBP' alone. As shown in Figure 3.12, knock off of FKBP' alone had no impact on the autophagosome formation pattern or lysosomal turnover. The amount of both populations increased over time, which is due to the permanent starvation signal.
Knock off of Beclin1, however, almost immediately halted the generation of autophagosomes. This was accompanied by a substantial decrease in autolysosomes, approximately 10 minutes later. The reduction of autolysosomes is probably to due to the reduced supply of autophagosomes. If autolysosomal turnover was impaired by Beclin1 mislocalization as well, the autolysosome number should increase further and eventually remain constant. If the turnover rate was accelerated by Beclin1 mislocalization, the autolysosome number should drop immediately. These results confirm that mislocalization of endogenous Beclin1 interaction partners indeed affects autophagosome formation, but not maturation. This is in keeping with data from previous EGFP-LC3 and -Atg5 puncta counts (see Figure 3.8) and also agrees well with the results of the WIPI2b puncta counts (see Figure 3.10). Knock off of Beclin1 inhibited WIPI2b puncta formation within a similar time frame and to a similar degree as observed for the autophagosome population in the tandem LC3 assay.

The tandem LC3 assay also gives some indication about the lifetime of autophagic structures. After autophagosome formation is inhibited by knock off, it takes about 10 to 15 minutes before the majority of autolysosomes is degraded (see Figure 3.12B). Several studies reported autophagosomal lifetimes of 30 to 40 minutes, depending on the cell lines and starvation conditions[52,54,256,257,258]. However, our assay does not represent the whole autophagosomal lifetime. Since Beclin1 knock off re-routes interacting proteins from forming autophagosomes in all stages, we can only speculate about the fate of these structures afterwards. It remains questionable, whether PI3K complex proteins are required for closure of autophagosomes, what triggers closure and whether autophagosomes can be closed regardless of their size. Several studies suggested that removal of LC3 and PI3Ps from the outer membrane of the closed autophagosome triggers the dissociation of Atg proteins and initiates transport and fusion[259]. As mislocalization of PI3K complex proteins disrupts PI3P generation and LC3 recruitment is ultimately dependent on PI3P effectors, knock off of Beclin1 could have a similar effect. Yet, it appears unlikely that every autophagosomes is fit to mature when Beclin1 mislocalization occurs. Furthermore,

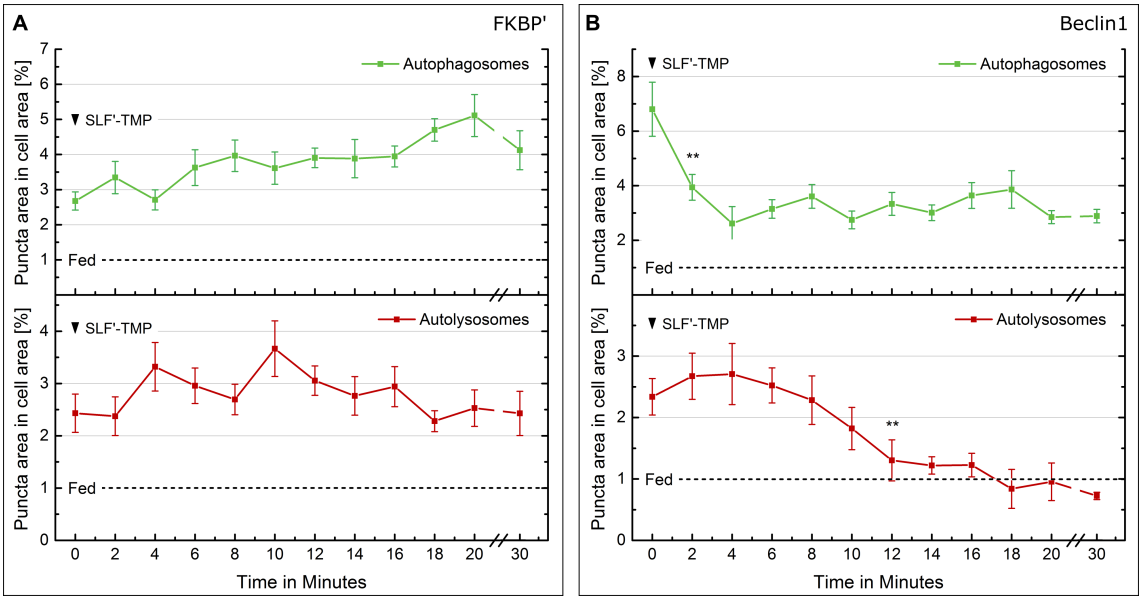

Figure 3.12: Knock off of FKBP'-Beclin1 perturbs formation of autophagosomes. mCherry-EGFP-LC3-MCF7 cells were starved in EBSS for 2 hours and then treated with SLF'-TMP for up to 30 minutes. Error bars: weighted mean ± SEM ($n \geq 40$); ** = $p \leq 0.01$; statistical significance was determined by student's t-test against the starvation condition; data was normalized against the fed condition. **A** Mislocalization of FKBP' alone has no effect on autophagosome or autolysosome formation. **B** FKBP'-Beclin1 knock off causes a significant decrease of autophagosome number within 2 minutes after dimerizer addition. The amount of autolysosomes decreases with a delay of 10 minutes, supposedly due to the lowered supply of autophagosomes.

membrane curvature is a crucial factor in autophagosome elongation and closure. The Atg12-5-16L or LC3-PE complexes, for instance, bind to the highly curved membrane or rim of the phagophore, but not to the flat membrane of the mature autophagosome[260,261,262]. Membrane curvature is, among other factors, dependent on membrane length. Thus, it is likely that the autophagosomal membrane has to overcome a certain threshold before closure is even possible. Since autophagosomes are not generated in a synchronized fashion, only a fraction of autophagic structures can reach this threshold before Beclin1 is mislocalized and membrane elongation is interrupted. Hence, the delay between inhibition of autophagosome formation and clearance of autolysosomes we observed here, is probably more representative for the average time between autophagosome closure and complete lysosomal degradation. It would be interesting to determine the disposition of the unclosed autophagic structures, but this can only be achieved with electron or super-resolution microscopy and remains technically challenging. One could, however, perform the tandem LC3 assay with autophagic proteins representative for specific autophagy phases, such as mTORC1, ULK1 or Atg16L and compare the time span between inhibition of autophagosome generation and completion of lysosomal degradation. If differences are detectable, this could yield further information about dynamics of autophagosome maturation.

Taken together, the tandem LC3 assay delivered valuable information about the impact of Beclin1 mislocalization on autophagy flux. It confirmed that Beclin1 knock off rapidly perturbs autophagosome formation and the results are in agreement with previous experiments. Further, the approach is a valuable addition to the toolbox of autophagy assays, as it allows to monitor the impact of autophagy modulation on autophagosomes and autolysosomes simultaneously.

3.3 UVRAGs Function in Autophagy

A major obstacle in studying autophagy is the highly dynamic nature of autophagosome formation and the accordingly short lifetime of autophagosomes. While traditional techniques like gene knock out or knock down delivered valuable information about hierarchical relationships and spatial distribution of autophagy proteins, they failed to capture the temporal context[263]. An example for the limitations of chronic perturbations is the current debate about the elusive role of UV radiation resistance-associated gene protein (UVRAG) within the autophagy process.

UVRAG was first described in 1990 as cDNA, which partially complements the UV sensitivity of xeroderma pigmentosum cells[264]. More than a decade later, Liang *et al.* identified UVRAG as Beclin1 interaction partner and suggested a role within the autophagic pathway[8,265]. In their study Liang and co-workers observed that autophagosome formation was enhanced by UVRAG overexpression in a Beclin1-dependent manner and severely reduced by UVRAG knockdown. This led to the conclusion that Beclin1 and UVRAG induce autophagy cooperatively. Two years later, Liang *et al.* reported further that UVRAG associates with endosomes and enhances autophagosomal maturation by interacting with the homotypic fusion and vacuole protein sorting (HOPS) complex. Thus, they proposed two distinct functions of UVRAG within the autophagy process: Beclin1-dependent induction of autophagosome formation and C-Vps-dependent promotion of lysosomal fusion[9]. Shortly after, Itakura *et al.* reported that UVARG knock down had no effect on autophagosome formation and suggested that UVRAG functions only in autophagosome maturation[4]. Supporting this notion, they also discovered that Atg14L and UVRAG bind mutually exclusive to Beclin1s CCD domain to generate two distinct PI3K complexes, containing either Atg14L or UVRAG. Since Atg14L had been functionally associated with autophagosome formation in several studies before, Itakura and co-workers proposed a model in which Atg14L initially occupies the common Beclin1 binding side to induce autophagosome formation and is then replaced by UVRAG to promote autophagosome maturation. Contradicting this model, He *et al.* recently observed that UVRAG binds PI3Ps through its C2-domain and is then localized to the ER. Here it interacts with the RINT-1 containing ER-tether to control Golgi-to-ER COPI transport[10]. They suggested that UVRAG dissociates from the tether upon autophagy induction to cooperate with Beclin1 and PI3Ps to initiate Atg9 trafficking. UVRAG has been associated with Atg9 trafficking before[266], as part of the Bif1-containing PI3K complex, but He and co-workers first observed that UVRAG depletion impaired Atg9 translocalization to punctate structures.

Recently, an additional autophagy-related activity of UVRAG was uncovered by Ganley and colleagues. They studied the involvement of the UVRAG-containing PI3K complex in autophagosome-lysosome reformation and identified UVRAG as a target of mTOR1 phosphorylation[267]. They observed that Vps34 activity was enhanced to prevent lysosomal tubulation in response to mTORC1-mediated phosphorylation of UVRAG, while trafficking processes prior to lysosomal fusion remained unimpaired. This suggests a function of the UVRAG-PI3K complex in lysosomal fusion or recovery.

Finally, the recently solved structure of the UVRAG-containing PI3K complex from yeast further indicated different roles of the two PI3K complexes, rather than redundant functions of Atg14L and UVRAG[5]. Here, the kinase activity of the different PI3K complexes on small and large vesicles was compared. While the activities on small vesicles were similar, the UVRAG-PI3K complex showed a substantially higher activity on giant, low-curvature vesicles. This might relate to its function on endosomal membranes or closed autophagosomes, and would suggest a model in which Atg14L and UVRAG exhibit complementary roles in autophagosome formation and maturation, respectively.

Besides its function in autophagy, UVRAG is involved in various other processes, such as maintaining genomic stability, retrograde Golgi-ER transport and many other vesicular trafficking or fusion processes [10,11,12,268]. This makes it even more difficult to pinpoint its exact role in autophagy, since vesicular transport pathways are naturally intertwined [13]. From a methodological point of view, the controversy about UVRAGs function in autophagy further highlights, that traditional techniques like knock down or out have certain limitations, which could be compensated by using an inducible dimerization system. Therefore, we employed the knock off and on system to rapidly mislocalize UVRAG to the plasma membrane and disrupt its localization-dependent function. Afterwards, we used the previously introduced autophagy assays to study the effect of UVRAG knock off on autophagosome progression.

3.3.1 Generation of an UVRAG-specific Beclin1

In order to specifically perturb endogenous UVRAG, we created a UVRAG-specific version of Beclin1 that is deficient in Atg14L-binding. Different strategies to disrupt the Beclin1-Atg14L interaction, like point mutations or truncations, were explored. Interaction of the resulting Beclin1-constructs with Atg14L/UVRAG was analyzed by confocal microscopy and co-immunoprecipitation as described before. Typically, the modified FKBP'-Beclin1 was knocked off to the plasma membrane of MCF7 cells and co-localization with UVRAG or Atg14L was probed by confocal imaging or western blotting. To quantify the imaging data, the mean fluorescence intensity (MFI) at the plasma membrane and in the cytoplasm was calculated and normalized to the bait.
Based on a study by Li *et al.* we initially replaced one to four charged residues in the coiled coil domain of Beclin1 by leucine, which supposedly yields a more stable Beclin1 homodimer and should prevent Atg14L binding while maintaining interaction with UVRAG [269].However, contrary to what Li *et al.* observed, the first two point mutations did not significantly disrupt Beclin1-Atg14L interaction and even the triple or quadruple mutations failed to disrupt the interaction completely (see Figure 3.14A). In fact, the co-immunoprecipitation data indicates that the point mutations rather decreased Beclin1s affinity for UVRAG, while Atg14L binding was left unaffected. The imaging data shows that after dimerizer addition, the MFI of the FKBP'-bait proteins is about three times higher at the plasma membrane than in the

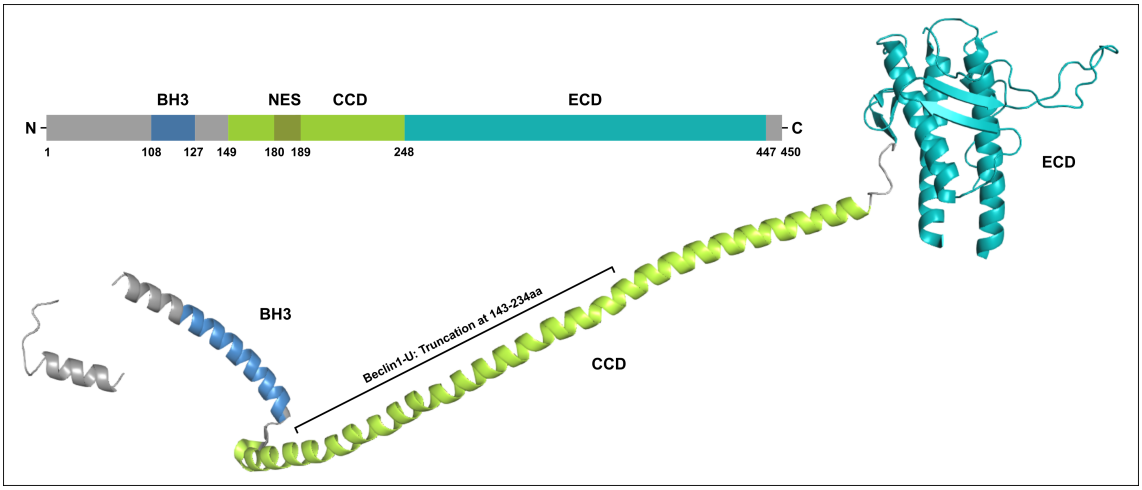

Figure 3.13: Structure of Beclin1, modified from Fu*et al.* [270] and Rostislavleva *et al.* [5]. Beclin1 contains three identified domains, the BH3 domain, the CCD and the ECD. Atg14L and UVRAG interact with Beclin1 via its CCD domain. To generate UVRAG-specific Beclin1-U, the CCD domain was truncated at 143-243aa and the remaining domains were re-connected with a flexible linker.

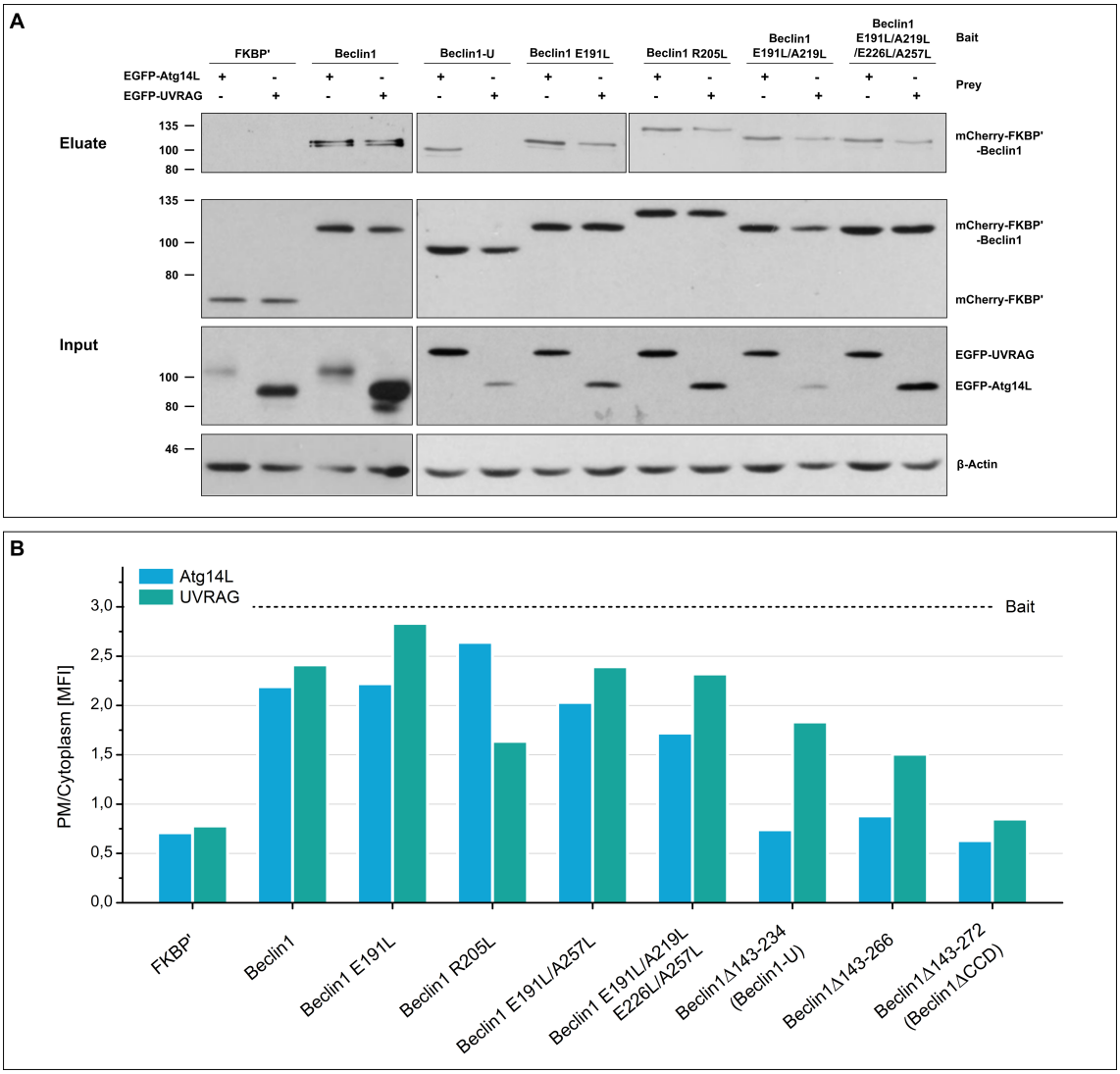

Figure 3.14: Interaction of Beclin1-U and Atg14L or UVRAG in MCF7 cells after 2 hours starvation in EBSS and 30 minutes treatment with SLF'-TMP. **A** FKBP'-Beclin1-U cannot mislocalize Atg14L to the plasma membrane suggesting that the construct is deficient in Atg14L binding. FKBP'-Beclin1-U attracts UVRAG to the plasma membrane indicating that UVRAG binding is maintained regardless of the truncation. **B** FKBP'-Beclin1ΔCCD cannot attract Atg14L or UVRAG to the plasma membrane.

cytoplasm (see Figure 3.14B). If wild type Beclin1 is used as bait, the MFI of Atg14L and UVRAG is about two times higher at the plasma membrane indicating that most of the prey proteins were depleted from the cytoplasm. In keeping with the co-immunoprecipitation results, the MFI of Atg14L/UVRAG is also 1.5 - 2.5 × higher at the plasma membrane if mutated Beclin1 is employed as bait, whereas it is substantially reduced for the non-binding control, i.e. FKBP' alone (see Figure 3.14 A). This confirms further, that the point mutations suggested by Li *et al.* do not prevent Beclin1-Atg14L interaction.

Thus, we proceeded to truncate the CCD of Beclin1 starting at the N-terminal and re-connected the remaining fragments via a flexible glycine-serine linker (see Figure 3.13). Since Beclin1's evolutionary conserved domain (ECD) and the CCD overlap[271], part of the ECD was also truncated in the initial experiments (see Table 3.2). The constructs were tested in the same manner as described before and it turned out that truncating part of the CCD (143-234 aa or 143-266 aa) prevented binding of Atg14L, but merely weakened UVRAG interaction. As shown in Figure 3.14, Beclin1Δ143-234 (Beclin1-U) shows sim-

Table 3.2: Co-localization of exogenous FKBP'-bait proteins and potential prey proteins at the plasma membrane of MCF7 cells. Autophagy was induced by starvation in EBSS and the cells were treated with SLF'-TMP for at least 30 minutes.

BAIT/PREY	Atg14L Interaction	UVRAG Interaction
Beclin1Δ143-234	×	✓
Beclin1Δ143-266	×	✓
Beclin1Δ143-272	×	×
Beclin1Δ265-271 (A)	✓	✓
Beclin1Δ171-272	×	×
Beclin1Δ201-272	✓	✓
Beclin1Δ235-272	✓	✓
Beclin1Δ328-394	✓	✓
Beclin1_1-142	×	×
Beclin1_1-234	✓	✓
Beclin1_1-272	✓	✓
Beclin1_267-451	×	×
Beclin1_1-144 [228]	×	×
Beclin1_88-272 [228]	✓	✓
Beclin1_142-272 [228]	✓	✓
Beclin1_273-450 [228]	×	×
Beclin1_1-148 [229]	×	–
Beclin1_86-267 [229]	✓	–
Beclin1_142-267 [229]	✓	–
Beclin1_142-335 [229]	✓	–
Beclin1_242-448 [229]	×	–
Beclin1_176-266 [269]	✓	✓

ilar MFI ratios for Atg14L as FKBP' alone and cannot be pulled down by EGFP-Atg14L, but is readily by EGFP-UVRAG. In addition, UVRAG co-localizes well with Beclin1-U at the plasma membrane of MCF7 cells after dimerizer addition (see Figure B.9). The MFI ratio of UVRAG is in a similar range as that of Beclin1 indicating that UVRAG-binding is maintained in the truncated construct. Truncation of the whole CCD (143-272 aa) abolished binding of both Atg14L and UVRAG, suggesting that the C-terminal region of Beclin1s CCD is crucial for interaction with UVRAG. This was later confirmed when the structure of the UVRAG-containing PI3K complex was reported [5] and showed that Beclin1 and UVRAG interact along their entire length, but that their CCDs from a heterodimer stabilizing the interaction. Since Beclin1Δ143-234, termed Beclin1-U, served our purpose best, it was employed to specifically mislocalize UVRAG and study the effect on autophagosome formation.

3.3.2 Generation of an Atg14L-specific Beclin1

To distinguish between the effects of UVRAG and Atg14L knock off, we also attempted to generate a Atg14L-specific Beclin1, which is deficient for interaction with UVRAG. Based on our previous observation that the C-terminal region of Beclin1s CCD domain is involved in UVRAG binding, Beclin1s CCD was truncated from the C-terminal to perturb Atg14L binding. The resulting constructs were analyzed by confocal microscopy.

Unfortunately none of the modified Beclin1 baits was specific for Atg14L alone. As show in Table 3.2, truncating the C-terminal part of the CCD (235-272 aa or 201-272 aa) did not affect Atg14L- or UVRAG-binding, while truncation of 171-272 aa abolished interaction with both proteins. Modification of the flexible loop between Beclin1s CCD and ECD had also no effect and the BH3 domain (1-142 aa) or ECD (267-451 aa) alone were not sufficient for Atg14L or UVRAG interaction. Based on a report by Cheng *et al.*, Beclin1 was additionally truncated at 328-394 aa to yield the splice variant BECN1s, which is supposedly specific for Atg14L. However, confocal microscopy showed that all BECN1s constructs can still attract UVRAG to the plasma membrane, indicating that the Beclin1-UVRAG interaction is not substantially perturbed in these constructs.

A high-resolution structure of the Atg14L-containing PI3K complex is not available yet, but the domain organization and length of the CCD domain of UVRAG and Atg14L are similar, suggesting that the interaction of Atg14L with Beclin1 is similar to UVRAG[5]. Furthermore, Li *et al.* determined that UVRAG binds with higher affinity to Beclin1 ($K_d = 0.24 \pm 0.06\,\mu M$) than Atg14L ($K_d = 3.22 \pm 0.95\,\mu M$) and proposed that UVRAG is able to disrupt the Beclin1-Beclin1 homodimer, while Atg14L is not[269]. Consequently, it may not be possible to perturb the Beclin1-UVRAG interaction and simultaneously preserve Atg14L-binding. Thus, we abandoned the idea to employ an Atg14L-specific Beclin1 as bait in the knock off/system. However, as previously demonstrated, nanobodies can be conveniently combined with the knock off/on approach, so that an anti-Atg14L nanobody could be a reasonable alternative to Beclin1 as bait. Unfortunately, an anti-Atg14L-nanobody is not commercially available yet and since generation of customized nanobodies is still rather costly, this approach was not pursued.

3.3.3 UVRAGs Function in Autophagosome Formation and Maturation

To further characterize UVRAG's function in autophagy, we used the UVRAG-specific Beclin1-U as bait to mislocalize endogenous UVRAG and study the effect on autophagosome formation and maturation. EGFP-LC3, -Atg5 and WIPI2 were employed as markers for autophagosome formation in different stages. In addition, the EGFP-mCherry-LC3 assay was utilized to dissect the dynamics of autophagosome generation and maturation.

Initially, FKBP'-Beclin1-U was introduced into stable EGFP-LC3-MCF7 or EGFP-Atg5-MCF7 cells and autophagy was induced by starvation. Simultaneously, knock off was induced or prevented by addition of SLF'-TMP and TMP, respectively. As an additional control, the experiments were performed in the presence and absence of BafilomycinA1. Finally, the amount of autophagic puncta was quantified as previously described.

As shown in Figure 3.15A, perturbation of endogenous UVRAG reduced the amount of EGFP-LC3 puncta significantly. The effect is independent of BafilomycinA1 treatment and phenotypically similar to knock off of Beclin1 or Atg14L. This suggests that UVRAG is required during autophagosome formation, but gives no indication about the exact time point. Thus, we used the isolation membrane marker EGFP-Atg5 to investigate whether UVRAG re-routing affects the very early stages of autophagosome forma-

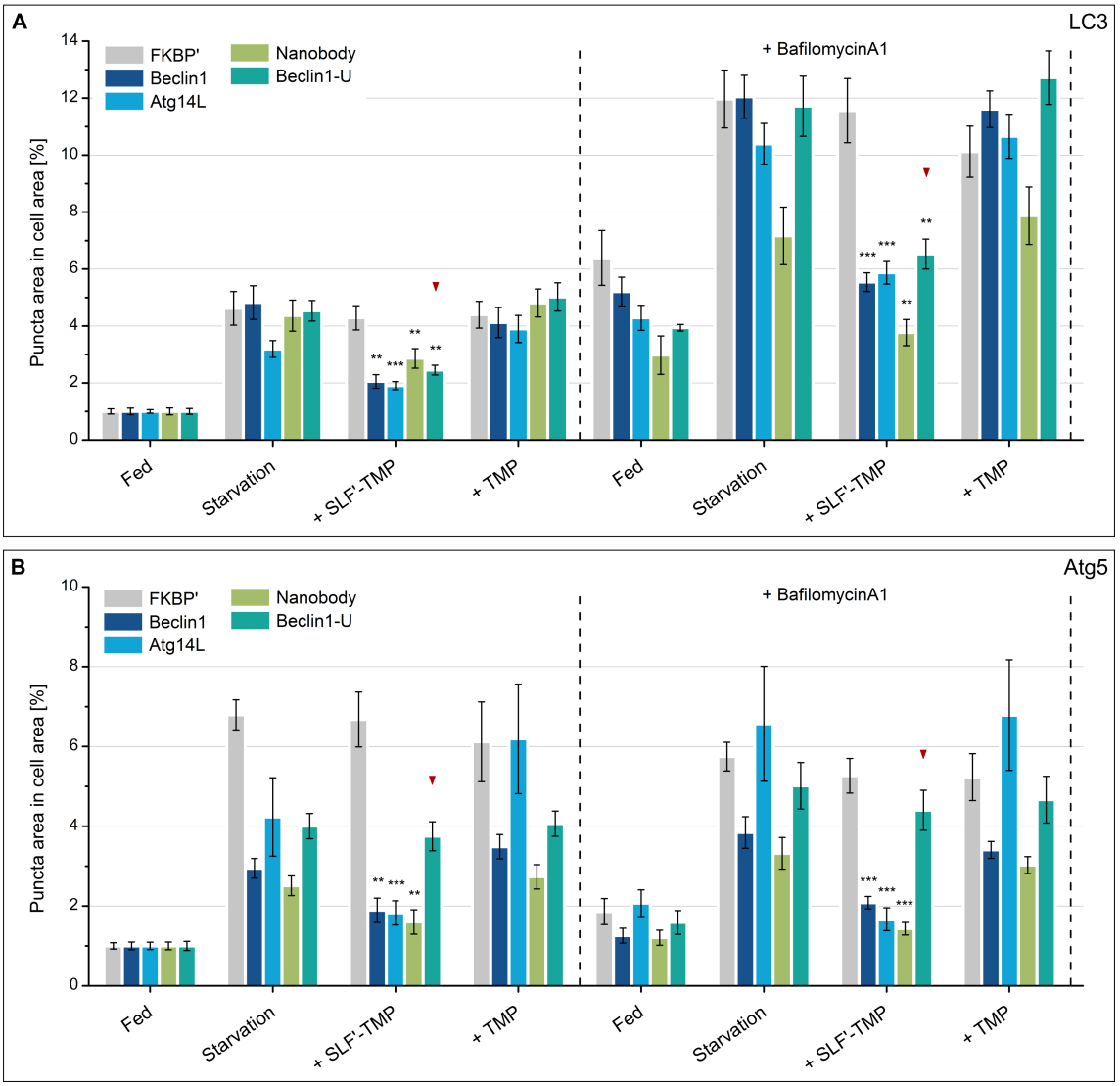

Figure 3.15: Knock off of endogenous UVRAG perturbs late stages of autophagosome formation. Cells were starved in EBSS and/or treated with SLF'-TMP, TMP or BafilomycinA1 for 2 hours. Error bars: weighted mean ± SEM ($n \geq 60$); ** = $p \leq 0.01$; *** = $p \leq 0.001$; statistical significance was determined by pairwise comparison to the starvation condition; data was normalized against the fed condition. **A** The amount of EGFP-LC3 puncta is significantly decreased after knock off of FKBP'-Beclin1-U and in the presence or absence of BafilomycinA1. Mislocalization of the remaining PI3K bait proteins has a similar effect, while knock off of FKBP' alone shows no effect. **B** Mislocalization of FKBP'-Beclin1, -Atg14L and -anti-Vps34 nanobody, but not Beclin1-U or FKBP', causes a significant decrease of Atg5-labeled puncta in the presence or absence of BafilomycinA1. This is a strong indication that UVRAG is not participating in early autophagosome formation.

tion. Interestingly, Beclin1-U knock off had no significant impact on Atg5 puncta formation, regardless of BafilomycinA1 treatment (see Figure 3.15B). This implies that UVRAG is either not involved in formation of the isolation membrane or that its function is redundant. To explore this in more detail, we then evaluated the dynamics of WIPI2b puncta formation in response to UVRAG perturbation. WIPI2b marks an even earlier stage of isolation membrane formation than Atg5 and is specific for the autophagosomal PI3P (see section 3.2.2).

As displayed in Figure 3.16 and B.10A, WIPI2b puncta formation is not impaired by Beclin1-U knock off either. In fact, the phenotype after Beclin1-U knock off is almost identical to the control conditions,

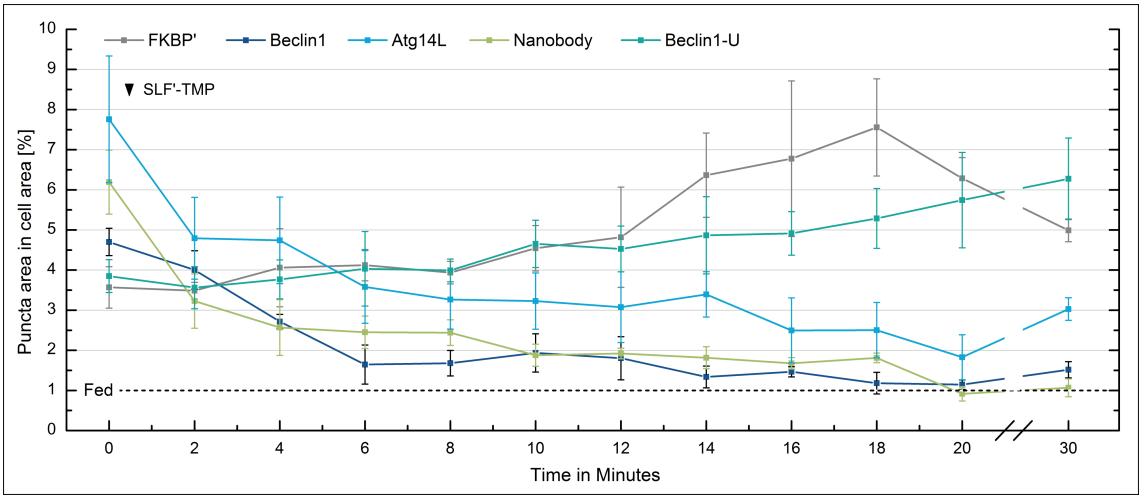

Figure 3.16: Knock off of Beclin1-U has no effect on WIPI2b puncta formation. MCF7 cells were starved in EBSS for 2 hours and then treated with SLF'-TMP for up to 30 minutes. Error bars: weighted mean ± SEM ($n \geq 20$); data was normalized against the fed condition. Mislocalization of Beclin1-U has no effect on WIPI2b puncta formation, similar to FKBP' alone. Knock off of the remaining PI3K bait proteins causes a significant reduction of WIPI2b puncta. This supports the previous observation that UVRAG is not necessary for early autophagosome formation.

where only FKBP' was re-routed to the plasma membrane. This further supports the notion that UVRAG is not involved in isolation membrane formation, but participates in a later stage of autophagosome formation or fusion.

Next, we employed the tandem LC3 assay to monitor the dynamics of autophagosome formation and maturation. Autophagy was induced, Beclin1-U was knocked off and the yellow and red puncta populations were monitored every two minutes for half an hour (see Figure 3.17). Intriguingly, the autolysosome population was instantly affected by UVRAG mislocalization and dropped significantly within two minutes of dimerizer addition. Within four minutes, the amount of autolysosomes was reduced to the basal level and continuously decreased over the course of 30 minutes. The autophagosome population, on the other hand, showed a gradual decline over the whole observation period and was only significantly decreased after 8 minutes. However, dimerizer addition immediately reduced the autophagosome population, suggesting that UVRAG mislocalization directly affects autophagosome generation. Preliminary experiments further showed that autophagosome formation is not recovered for at least two hours after knock off (see Figure B.10B).

The results generated by the tandem LC3 assay can be translated into two scenarios. In the first scenario, UVRAG exhibits a vital function during autophagosome maturation and formation, which is impaired by knock off. Alternatively, UVRAG negatively regulates autolysosome turnover, so that mislocalization accelerates autolysosome clearance. The latter model is supported by the rapid reduction of the autolysosome population instantly after dimerizer addition. This could indicate that absence of UVRAG increases the autolysosome formation and turnover rate. Consequently, autophagosomes are processed faster, while still being generated at the same rate. This would ultimately cause a reduction in the autophagosome population and account for the slow decrease of yellow puncta.

The increased autolysosomal turnover rate might also lead to activation of a feedback loop down-regulating autophagosome generation, for instance, via mTORC1 re-activation due to sufficient replenishment of amino acids[257]. In this model, UVRAG is only involved in autolysosome turnover, but not in the fusion process, which does not integrate well with previously published data and even our own observations.

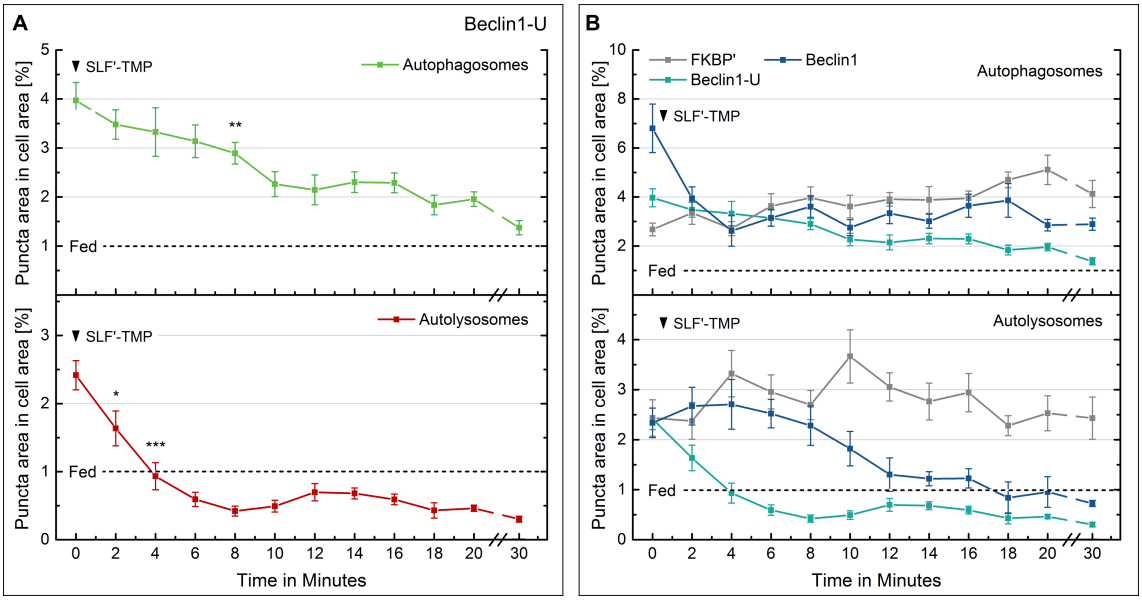

Figure 3.17: Knock off of Beclin1-U modulates autophagosome formation and maturation. EGFP-mCherry-LC3-MCF7 cells were starved in EBSS for 2 hours and then treated with SLF'-TMP for up to 30 minutes. Error bars: weighted mean ± SEM ($n \geq 40$); * = $p \leq 0.05$, ** = $p \leq 0.01$, *** = $p \leq 0.001$; statistical significance was determined by student's t-test against the starvation condition; data was normalized against the fed condition. **A** Mislocalization of endogenous UVRAG causes a significant decrease of autolysosome number within 2 minutes after dimerizer addition. This is accompanied by a concomitant decrease in the autophagosome population. **B** Effect of Beclin1-U knock off on EGFP-mCherry-LC3 puncta formation compared to mislocalization of FKBP' and Beclin1. Knock off of FKBP'-Beclin1 perturbs only formation of autophagosomes while mislocalization of endogenous UVRAG causes a significant decrease in the both populations. Mislocalization of FKBP' alone has no effect on autophagosome or autolysosome formation.

In the EGFP-LC3 puncta counts, we observed that UVRAG mislocalization caused a substantial reduction in the autophagosome population. This was also consistent in the presence of the lysosomal fusion inhibitor BafilomycinA1, which entirely abolishes formation of autolysosomes. Without BafilomycinA1, the reduced autophagosome number might be due to the increased turnover rate or a regulating feedback loop triggered by UVRAG mislocalization. However, upon BafilomycinA1 treatment, re-routing of UVRAG should have no effect and autophagosome formation should proceed normally. Since this is in stark contrast to our observations, it appears unlikely that the reduced autophagosome number is a consequence of UVRAG negatively regulating autolysosome generation and degradation. Moreover, several studies have reported a supporting role of UVRAG in membrane fusion and vesicular transport processes[10,13,266]. Thus it would be surprising if UVRAG exhibited a completely opposed function during autophagosome maturation, which is essentially a combination of transport and fusion.

In an alternative scenario, UVRAG positively regulates the late stages of autophagosome formation, transport and fusion with the lysosome. Several studies support this theory. Liang *et al.* observed early on that UVRAG interacts with the HOPS complex to activate the small GTPase Rab7 and stimulate autophagosome-lysosome fusion[9]. Sun *et al.* and others later determined that this interaction is inhibited by Rubicon, which negatively regulates UVRAG in a mTORC1-dependent manner[65,267,272,273]. Combination of these results yields the following model: In nutrient-rich conditions, UVRAG is phosphorylated by mTORC1. This enhances its interaction with Rubicon, inhibits the lipid kinase activity of Vps34 and prevents UVRAG-HOPS interaction. Upon starvation, mTORC1 is deactivated, UVRAG is dephosphorylated and Rubicon is released[273]. Dissociation from Rubicon facilitates interaction with Vps16, a

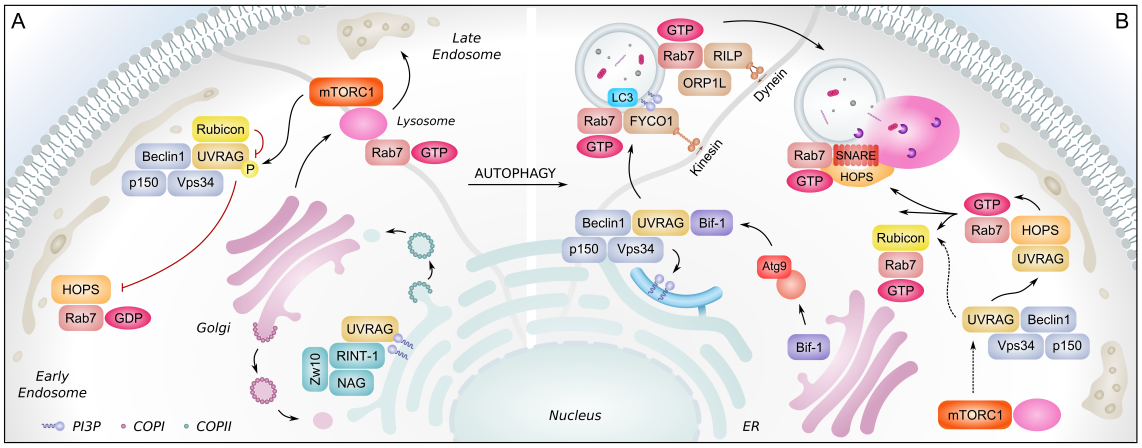

Figure 3.18: Different roles of UVRAG in autophagosome formation and maturation[65,273,274]. **A** In nutrient-rich conditions UVRAG interacts with the PI3K complex at the endosome and is phosphorylated by mTORC1. This enhances interaction with Rubicon, which prevents activation of the HOPS complex. At the Golgi, UVRAG associates with RINT-1-containing ER tether and coordinates COPI vesicle transport. **B** Proposed model for UVRAGs functions in autophagy. Upon autophagy induction, Bif-1 associates with UVRAG and coordinates fusion with Atg9 vesicles to support autophagosome formation. In parallel, phosphorylation of UVRAG by mTORC1 is abolished, Rubicon dissociates from the PI3K complex and UVRAG associates with the HOPS complex. Consequently, HOPS activates Rab7, which regulates transport and lysosomal fusion of autophagosomes.

subunit of the HOPS complex, and activates Rab7[9,65]. Vps39, a component of the HOPS complex serves as a GEF for Rab7, exchanging GDP for GTP to activate the small GTPase and stimulate its localization to late endosomes, lysosomes and late autophagosomes[275,276]. The active, GTP-bound Rab7 exhibits at least three autophagy-related functions. First, it binds to Rubicon to sequester it from UVRAG, which further increases HOPS' GEF activity and enhances Vps34s kinase activity. Second, GTP-bound Rab7 coordinates autophagosome trafficking by connecting autophagosomes with the microtubule motors kinesin and dynein through FYCO1 and ORP1L/RILP, respectively[59,275,277,278]. Finally, active Rab7 is involved in recruitment of SNARE complexes and tethering factors to promote fusion of autophagosomes and lysosomes or late endosomes (see Figure 3.18)[279,280,281,282].

Removing UVRAG from this setup would thus prevent activation of Rab7 via the HOPS complex, which leads to impaired autophagosome trafficking and lysosomal fusion. UVRAG mislocalization should further decrease the kinase activity of Vps34 and therefore reduce production of PI3Ps at the autophagosomal membrane. Since PI3Ps have been shown to attract the tethering factor TECPR1[283] and FYCO1, which is involved in trafficking, this might further impact autophagosome maturation. Consequently, UVRAG mislocalization should almost completely abolish maturation of autophagosomes into autolysosomes. This is in agreement with the results of the tandem LC3 assay, where we observed a dramatic reduction in the autolysosome population immediately after knock off. Assuming autolysosome generation is stopped immediately after UVRAG mislocalization, it further implies that previously existing autolysosomes are cleared within less than four minutes. This is consistent with data by Elrick *et al.*, who determined that the majority of autolysosomes in human dermal fibroblasts is degraded within four minutes[284].

However, this does not entirely explain the concomitant reduction of autophagosomes. The Atg5 and WIPI2b puncta counts showed that UVRAG is probably not involved in early autophagosome formation, so that UVRAG-dependent autophagy disruption at this point appears unlikely. Re-activation of mTORC1 or an alternative feedback loop due to a restored nutrient supply is not a satisfying explanation either, as the cells were continuously exposed to starvation and the autolysosomal turnover rate

should remain constant. In addition, we observed a severe reduction in the autophagosome population in the presence of BafilomycinA1, indicating that UVRAG mislocalization also impairs autophagosome formation. Consistent with this, Liang *et al.* reported that the UVRAG-containing PI3K complex is essential for autophagosome formation and other studies further associated UVRAG with the generation of Atg9 vesicles from the Golgi apparatus[8]. He and co-workers observed that UVRAG positively regulates the RINT-containing ER tethering complex to coordinate Golgi to ER COPI vesicle transport in basal conditions. Upon autophagy induction, UVRAG dissociates from the ER tether and joins the PI3K complex to facilitate Atg9 trafficking[10]. Takahashi *et al.* further determined that Atg9 vesicle formation and trafficking is critically dependent on interaction of the N-BAR-domain-containing protein Bif-1 with UVRAG in the PI3K complex. Bif-1 co-localizes with Atg9 vesicles, but also the Golgi/TGN and phagophore initiation sites. Due to its BAR-domain, it might be involved in generation and fusion of Atg9 vesicles to support autophagosome formation[260,266,285,286]. UVRAG mislocalization should abolish interaction of Bif-1 with the PI3K complex and disturb Atg9 vesicle trafficking and fusion. Since Atg9 is essential for autophagosome formation, this would explain the decreased autophagosome number in absence of UVRAG.

Given the collective evidence, we propose a model in which UVRAG is first involved in generation, transport and fusion of Atg9 vesicles to support autophagosome formation and later coordinates trafficking and lysosomal fusion of the closed autophagosome (see Figure 3.18). How these functions integrate with each other from a spatiotemporal and regulatory perspective remains to be established. Rubicon and mTORC1 appear to be essential regulators of UVRAG activity, but based on current knowledge, they only control part of UVRAGs autophagy-related function. In the future, it would be interesting to dissect this further. For instance, it might be beneficial to determine whether Atg9 and Bif-1 are affected by UVRAG mislocalization and how the cellular distribution of mTORC1 and Rubicon changes. The same applies for Rab7, the HOPS complex or other related fusion factors. The knock off and on system is ideally suited for analysis like this, as it allows to modulate and monitor cellular events in real time and in live cells. It may thus be a powerful tool to finally resolve UVRAGs elusive role in autophagy.

3.4 Spatial Organization of Autophagosome Biogenesis

Aside from targeting proteins to the plasma membrane for autophagy disruption, the knock off and on system can also be employed to localize proteins to other cellular compartments, such as the ER, ERGIC, Golgi or mitochondria. All of these compartments have been linked to autophagy as potential membrane sources or autophagosome formation sites, but the actual origin of the autophagosome remains to be determined (see section 1.1.2.3).

Recently, accumulating evidence promoted the ER as the principle autophagosome formation site. The Yoshimori and Ktistakis labs, for instance, observed generation of omegasomes, cup-shaped, PI3P-enriched structures, at the ER membrane[38,39]. Most reports agree further, that the autophagosome originates from omegasomes, which may arise from all ER membranes, including ER exit sites[287] and mitochondria-ER-contact sites[40]. In keeping with this, several groups demonstrated membrane continuity between the ER or the outer mitochondrial membrane and the autophagosomal membrane[40,41,42]. However, it has also been shown, that Golgi and ERGIC can contribute lipids to the isolation membrane[43,44] and interact with Atg9-vesicles, which are essential for membrane elongation and closure in yeast[2,3,37].

To investigate, which compartments are actually involved in the process, we recruited part of the autophagic machinery to the ER, ERGIC, Golgi or mitochondria and studied the effect on autophagosome formation. Cellular anchors featuring an eDHFR domain were created for each compartment and the knock off and on system was employed to re-route FKBP'-modified Beclin1 towards the anchor proteins. The minimal ER targeting domain cytochrome b_5 (Cb5) was chosen as the ER anchor[288], ERIG53 for the ERGIC[289], the Golgi membrane protein Giantin for the Golgi[290] and the bacterial protein ActA for the mitochondria[291]. As shown in Figure B.11, all of the targeting domains could efficiently localize TagBFP-eDHFR to the respective compartments, where it co-localized well with the specific markers.

In the next step, Beclin1 was re-routed to the cellular anchors and the effect on LC3 puncta formation was analyzed. mCherry-FKBP'-Beclin1 and the negative control mCherry-FKBP' were introduced into EGFP-LC3-MCF7 cells and dimerization or dissociation were induced by addition of SLF'-TMP or TMP, respectively.

As an initial test, FKBP'-Beclin1 was localized to the ER without induction of autophagy to determine whether the presence of PI3K proteins attracted by Beclin1 would be sufficient to stimulate autophagosome formation. However, as shown in Figure 3.19 the number of autophagosomes after Beclin1 mislocalization remained similar to control levels and significantly lower than after serum starvation. These results indicate that autophagosome formation cannot be induced by translocalization of PI3K proteins alone and suggests that upstream signals are required for successful autophagy initiation.

A potential upstream regulator missing in our setup might be the kinase ULK1, which has been shown to phosphorylate Beclin1 on Ser14 to enhance the activity of Atg14L-containing PI3K complexes and is crucial for autophagosome formation[292]. In fact, several studies showed that autophagosome biogenesis is severely impaired after knock out/down of ULK1 in yeast and mice[294,295,296,297]. Moreover, a study by Itakura and Mizushima analyzing the hierarchy of mammalian Atg proteins during autophagosome biogenesis showed that Atg14L and ULK1 appear simultaneously at the autophagosome formation site to generate the phagophore, which then becomes an autophagosome[243,293]. It would be of interest to translocalize both, the ULK1 and PI3K complexes, to the ER and study the effect on autophagy induction in order the define the minimal core machinery required for autophagosome generation.

In this study, however, we focused on the spatial organization of autophagosome formation. Autophagy

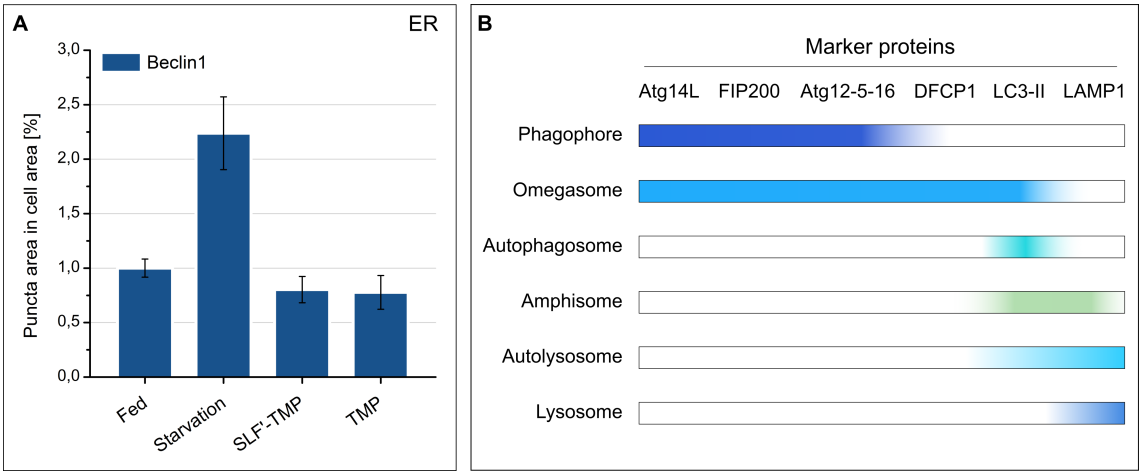

Figure 3.19: Hierarchy of autophagy protein complexes. **A** Re-routing PI3K complex proteins to the ER using FKBP'-Beclin1 as bait. Autophagosome formation was evaluated by quantification of EGFP-LC3 puncta in MCF7 cells and autophagy was induced by 2 h starvation in EBSS. No effect on autophagosome formation could be detected. Error bars: weighted mean ± SEM ($n \geq 60$). **B** Order of marker proteins recruited to distinct autophagic structures based on data obtained in yeast and mammalian cells[293].

was induced by serum starvation in the subsequent experiments and the analysis were extended to the remaining compartments. As shown in Figure 3.20, no significant effect on LC3 puncta formation could be detected after re-routing exogenous Beclin1 to the ERGIC, Golgi or mitochondria, whilst the autophagy level was substantially increased after targeting FKBP'-Beclin1 to the ER in starvation conditions. In combination with the observations from previous experiments showing a severe disruption of autophagosome formation after mislocalization of PI3K proteins to the plasma membrane, these results give new insights into the 'hierarchy' of autophagosome formation sites. The ER appears to be the principal site of autophagosome biogenesis, while the ERGIG, Golgi and mitochondria can serve as secondary autophagosome formation sites. Only the plasma membrane cannot serve as autophagosome initiation site, even in severe starvation conditions.

In the literature, all of these compartments have been proposed as potential membrane source or autophagosome formation site and experimental evidence can be found to support any scenario. Mari *et al.* attempted to reconcile the contradictory results in a single model and proposed that the membrane source and autophagosome formation sites are specific to certain tissues, cells types and stress stimuli[293]. Depending on the given conditions, the autophagosome is then assembled from the most optimal reservoir. This would grant a sufficient supply of lipids without affecting the cell or tissue function.

Alternatively, Mari *et al.* suggested that the phagophore may be derived from a certain compartment and is later supplied with lipids from various other membranes or Atg9-positive vesicles[293]. For the cell, this setup provides the highest flexibility and guarantees that autophagy can progress even if one membrane source is exhausted by prolonged starvation.

However, both of these models neglect the role of the ER-specific omegasome, which appears to be required as a scaffolding membrane during pre-autophagosomal membrane assembly[6]. The ER is also one of the major cellular lipid sources, along with mitochondria and lipid droplets, which are highly connected with the ER. Thus, it seems sensible that the compartment is a major lipid contributor during autophagosome biogenesis. In line with this, the Ktistakis and Yoshimori labs determined that Atg14L, a crucial part of the PI3K complex, localizes mostly to the ER[38,39]. Further, ER-resident proteins, like the

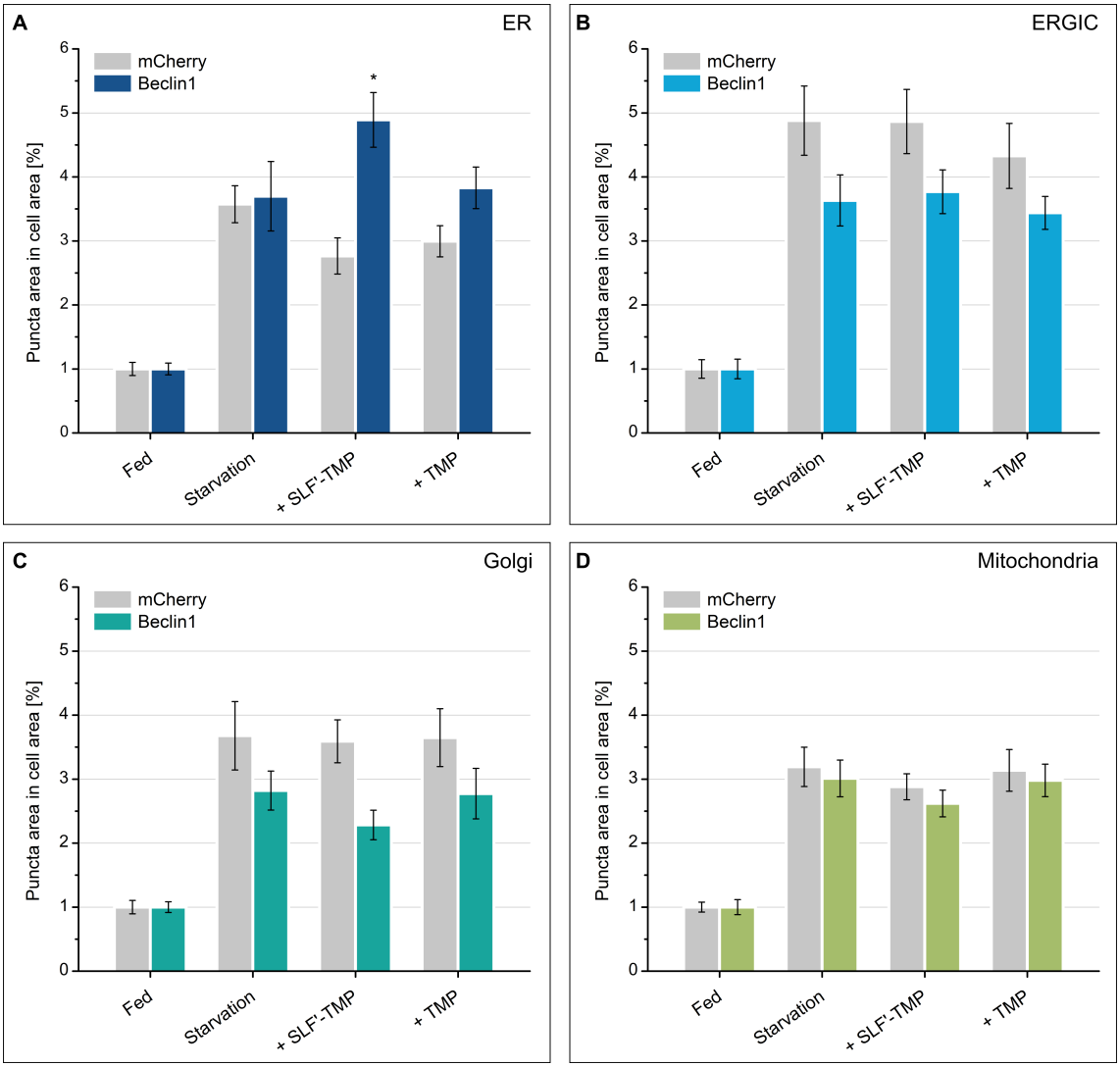

Figure 3.20: Re-routing PI3K complex proteins to different compartments using FKBP'-Beclin1 as bait. Autophagosome formation was evaluated by quantification of EGFP-LC3 puncta in MCF7 cells. Autophagy was induced by 3 h starvation in EBSS. Error bars: weighted mean ± SEM ($n \geq 60$); * = $p \leq 0.05$. **A** ER targeting of FKPB'-Beclin1 causes a significant increase in LC3-puncta. **B** Re-routing of PI3K complex proteins to the ERGIC has no significant effect on autophagosome formation. **C** Induced Golgi localization of FKBP'-Beclin1 does not affect LC3-puncta formation. **D** Autophagosome formation is not influenced by increased PI3k protein concentrations at the mitochondria.

Beclin1 interaction partner VMP1, have been directly associated with generation of autophagosomes from omegasomes[298,299]. Taken together, this yields a third possible scenario in which phagophores are exclusively assembled within omegasomes at the ER. Afterwards, the phagophore is supplied with lipids from the remaining compartments or associates with different membrane sources before becoming a closed autophagosome[293].

Our results support all three hypothesis to some extent, but point mostly towards the latter model. We observed that autophagosomes can be assembled from the ER, ERGIC, Golgi and mitochondria. However, the ER appeared to be the primary site of autophagosome formation - at least under the given conditions. It remains to be determined, whether the effect is consistent in different cell lines or starvation conditions. Our data contradicts the second model stating that autophagosomes assemble from

a specific a site. If there was one exclusive site of autophagosome formation, translocalization of PI3K complex proteins to the other compartments should disrupt the process in a similar fashion as mislocalization to the plasma membrane. Based on our results, it appears likely that autophagosomes are most efficiently generated at the ER, but may originate from other compartments as well. Yet, this would also imply that omegasomes are either not entirely ER-specific or not absolutely necessary for autophagosome biogenesis. This is further complicated by the fact, that the ER is not spatially constricted and in transient contact with all other compartments[6].

In order to determine, whether the ER is indeed the principal autophagosome formation site, one could repeat the experiment in different cell or tissues types and also vary the stress signals. If the autophagosome formation site is specific to certain tissues or stimuli, different conditions should enhance autophagosome formation from distinct compartments in a consistent manner. In addition, it would be of interest to target the ULK1 and PI3K complexes simultaneously to the each tested compartment as described above. In any case, inducible translocalization of autophagy complexes to different cellular compartments is a valuable tool to study the spatial organization of autophagosome formation. In future, it will be of interest to dissect the autophagy process further using inducible localization.

4 Conclusions and Perspectives

The knock off and on system is the first attempt to modulate autophagy with inducible chemical dimerization. A major advantage of this technique are the fast dimerization and dissociation kinetics of SLF'-TMP-mediated dimerization as well as the broad applicability and the simple application. In contrast to altering gene expression, chemical autophagy modulators or other dimerization systems, knock off/on facilitates rapid, tunable and specific perturbation of the autophagy process *in vivo*. In this study, autophagosome formation could be inhibited on a time scale of minutes, but the dimerization speed could probably be even faster at higher concentrations of SLF'-TMP or with an optically pure compound. Similar results can only be achieved with small molecule inhibitors (or inducers) and many of those lack specificity or show time- and dose-dependent side effects[14]. The knock off/on approach can also be customized to target virtually any cellular protein of interest, especially in combination with nanobodies. In this study, we successfully employed an anti-Vps34 nanobody as bait for endogenous Vps34. This gives rise to a range of new applications and is only limited by the high cost of generating customized nanobodies at present.

Here, we applied the knock off/on strategy to disrupt the localization-dependent function of the PI3K complex during autophagosome formation. Using the autophagy markers EGFP-Atg5, -LC3, -WIPI2b and EGFP-mCherry-LC3, we monitored the dynamics of PI3K complex mislocalization and studied the effect on autophagy progression. It turned out that the Atg14L-containing PI3K complex is essential for formation of the isolation membrane and the autophagosome, as knock off of any PI3K complex protein completely abolished autophagosome biogenesis. This PI3K complex is, however, not required for lysosomal fusion or degradation of the autolysosome. Since the main function of the Atg14L-PI3K complex is the generation of PI3Ps, we suppose that the depletion of the PI3P pool at the autophagosome formation site is the underlying cause of the autophagy inhibition we observed. Since the phenotype was also stable for several hours, we further assume that the PI3Ps required for autophagosome formation are exclusively generated by Vps34. In order to confirm this hypothesis, one could target a PI3P-phosphatase, like MTM1, to the autophagosome formation site and thus deplete it of PI3P. Alternatively, the anti-Vps34 nanobody could be employed to recruit Vps34, or its kinase domain to the formation site and generate an excess of PI3Ps. If the only function of the PI3K complex is to provide PI3Ps and PI3P concentration is the only regulatory signal, this should inhibit or enhance autophagosome formation, respectively.

Interestingly, we also observed that Beclin1 and Atg14L or UVRAG are required to maintain Vps34s kinase activity, which has not been reported before. It would be of interest to determine whether the Vps34-p150 heterodimer is sufficient to generate PI3Ps at the autophagosome formation site or if the whole PI3K complex needs to be assembled. This would give some insight on the functional and temporal relationship between the individual proteins within the complex. If assembly and translocalization of the Vps34-p150 heterodimer are sufficient to generate PI3Ps and induce autophagosome formation, the Beclin1-Atg14L heterodimer would merely serve as localization signal and to maintain complex stability. However, given that Beclin1 is a binding platform interacting with a number of regulatory proteins,

this option appears unlikely.
In order to completely understand the signaling events leading to autophagosome formation, the knock off/on strategy could be extended to other protein complexes, like mTORC1 or the ULK1 complex. mTORC1 is a master regulator involved in various processes, so that mislocalization of mTORC1 or its components would probably affect cellular events globally. Yet, it would be possible to target upstream nutrient-sensing proteins or complexes like RagA/B or Rheb. This may also be an option to artificially create specific stress or starvation signals. To dissect the nature and dynamics of ULK1 and PI3K complex interaction, the SLF'-TMP dimerization system could be combined with another dimerization approach to recruit the complexes sequentially to potential autophagosome formation sites.
Another yet unresolved aspect of autophagosome formation is the spatial organization of the process. We observed that autophagosomes are primarily formed at the ER, but also at the ERGIC, Golgi and mitochondria. Considering that omegasomes are mostly ER-localized, this raises the question how and under which conditions autophagosomes are generated at the other compartments. To investigate this further, the experimental conditions could be varied to explore if certain stress stimuli induce autophagosome biogenesis from different localizations, maybe even in a tissue- or cell-specific fashion. Further, one could attempt to re-create an omegasome-like platform at the ERGIC, Golgi or mitochondria by targeting Vps34 or other kinases and phosphatases to the compartments and modulating the lipid composition on the membrane. In line with this, inducible chemical dimerization could be employed to determine the minimally required autophagosome formation machinery at a specific cellular localization. To this end, the SLF'-TMP system could be used in combination with other dimerization systems to progressively recruit different complexes or even single proteins to the different compartments. Another option would be to mislocalize several autophagy complexes to the plasma membrane and then gradually release them.
Employing the knock off/on approach, we also gained valuable insights on UVRAGs autophagy-related function. Based on our observations, we propose a model in which UVRAG is first involved in generation, transport and fusion of Atg9 vesicles to support autophagosome formation and later coordinates trafficking and lysosomal fusion of the closed autophagosome. Here, we analyzed the effect of UVRAG mislocalization on autophagy using common autophagy markers. However, one could dissect UVRAGs function further by studying the effect on potential interaction partners like mTORC1, Bif-1, Rubicon, HOPS or Atg9 vesicles. Again, it might also be conclusive to monitor the lipid synthesis at the omegasome or the autophagosome, since UVRAG features a lipid-binding domain[10] and may be regulated by changes in the lipid composition of autophagosomal membranes.
Taken together, the results presented in this study show that the knock off and on approach is a versatile new strategy to modulate and study the spatiotemporal interaction of proteins or protein complexes in autophagy. In the future, we hope to apply and expand the strategy further to explore the details of autophagosome formation and maturation. However, it also remains worth mentioning, that the knock off and on system is by far not limited to autophagy and can be applied to any cellular process of choice.

Bibliography

[1] M. Wirth, J. Joachim, and S. A. Tooze. Autophagosome formation–the role of ULK1 and Beclin1-PI3KC3 complexes in setting the stage. *Semin Cancer Biol*, 23(5):301–9, 2013.

[2] A. Abada and Z. Elazar. Getting ready for building: signaling and autophagosome biogenesis. *EMBO reports*, 15(8):839–852, 2014.

[3] N. T. Ktistakis and S. A. Tooze. Digesting the Expanding Mechanisms of Autophagy. *Trends in Cell Biology*, 26(8):624–635, 2016.

[4] E. Itakura, C. Kishi, K. Inoue, and N. Mizushima. Beclin 1 forms two distinct phosphatidylinositol 3-kinase complexes with mammalian Atg14 and UVRAG. *Mol Biol Cell*, 19(12):5360–72, 2008.

[5] K. Rostislavleva, N. Soler, Y. Ohashi, L. Zhang, E. Pardon, J. E. Burke, G. R. Masson, C. Johnson, J. Steyaert, N. T. Ktistakis, and R. L. Williams. Structure and flexibility of the endosomal Vps34 complex reveals the basis of its function on membranes. *Science*, 350(6257):aac7365, 2015.

[6] D. Molino, N. Zemirli, P. Codogno, and E. Morel. The Journey of the Autophagosome through Mammalian Cell Organelles and Membranes. *Journal of Molecular Biology*, 429(4):497–514, 2017.

[7] R. Roberts and N. T. Ktistakis. Omegasomes: PI3P platforms that manufacture autophagosomes. *Essays Biochem*, 55:17–27, 2013.

[8] C. Liang, P. Feng, B. Ku, I. Dotan, D. Canaani, B. H. Oh, and J. U. Jung. Autophagic and tumour suppressor activity of a novel Beclin1-binding protein UVRAG. *Nat Cell Biol*, 8(7):688–99, 2006.

[9] C. Liang, J. S. Lee, K. S. Inn, M. U. Gack, Q. Li, E. A. Roberts, I. Vergne, V. Deretic, P. Feng, C. Akazawa, and J. U. Jung. Beclin1-binding UVRAG targets the class C Vps complex to coordinate autophagosome maturation and endocytic trafficking. *Nat Cell Biol*, 10(7):776–87, 2008.

[10] S. He, D. Ni, B. Ma, J. H. Lee, T. Zhang, I. Ghozalli, S. D. Pirooz, Z. Zhao, N. Bharatham, B. Li, S. Oh, W. H. Lee, Y. Takahashi, H. G. Wang, A. Minassian, P. Feng, V. Deretic, R. Pepperkok, M. Tagaya, H. S. Yoon, and C. Liang. PtdIns(3)P-bound UVRAG coordinates Golgi-ER retrograde and Atg9 transport by differential interactions with the ER tether and the beclin 1 complex. *Nat Cell Biol*, 15(10):1206–19, 2013.

[11] Z. Zhao, S. Oh, D. Li, D. Ni, S. D. Pirooz, J. H. Lee, S. Yang, J. Y. Lee, I. Ghozalli, V. Costanzo, J. M. Stark, and C. Liang. A dual role for UVRAG in maintaining chromosomal stability independent of autophagy. *Dev Cell*, 22(5):1001–16, 2012.

[12] J. M. Park, D. Tougeron, S. Huang, K. Okamoto, and F. A. Sinicrope. Beclin 1 and UVRAG confer protection from radiation-induced DNA damage and maintain centrosome stability in colorectal cancer cells. *PLoS One*, 9(6):e100819, 2014.

[13] J.-H. Son, E. C. Hwang, and J. Kim. Systematic analyses of the ultraviolet radiation resistance-associated gene product (UVRAG) protein interactome by tandem affinity purification. *Archives of Pharmacal Research*, 39(3):370–379, 2016.

[14] D. J. Klionsky. Guidelines for the use and interpretation of assays for monitoring autophagy (3rd edition). *Autophagy*, 12(1):1–222, 2016.

[15] S. Voss, L. Klewer, and Y.-W. Wu. Chemically induced dimerization: reversible and spatiotemporal control of protein function in cells. *Curr Opin Chem Biol*, 28:194–201, 2015.

[16] R. Rakhit, R. Navarro, and Thomas J. Wandless. Chemical Biology Strategies for Posttranslational Control of Protein Function. *Chemistry & Biology*, 21(9):1238–1252, 2014.

[17] M. Putyrski and C. Schultz. Protein translocation as a tool: The current rapamycin story. *FEBS Lett*, 586(15):2097–105, 2012.

[18] P. Liu, A. Calderon, G. Konstantinidis, J. Hou, S. Voss, X. Chen, F. Li, S. Banerjee, J. E. Hoffmann, C. Theiss, L. Dehmelt, and Y. W. Wu. A bioorthogonal small-molecule-switch system for controlling protein function in live cells. *Angew Chem Int Ed Engl*, 53(38):10049–55, 2014.

[19] J. L. Czlapinski, M. W. Schelle, L. W. Miller, S. T. Laughlin, J. J. Kohler, V. W. Cornish, and C. R. Bertozzi. Conditional glycosylation in eukaryotic cells using a biocompatible chemical inducer of dimerization. *J Am Chem Soc*, 130(40):13186–7, 2008.

[20] T. Clackson, W. Yang, L. W. Rozamus, M. Hatada, J. F. Amara, C. T. Rollins, L. F. Stevenson, S. R. Magari, S. A. Wood, N. L. Courage, X. Lu, Jr. Cerasoli, F., M. Gilman, and D. A. Holt. Redesigning an FKBP-ligand interface to generate chemical dimerizers with novel specificity. *Proc Natl Acad Sci U S A*, 95(18):10437–42, 1998.

[21] N. Mizushima and M. Komatsu. Autophagy: renovation of cells and tissues. *Cell*, 147(4):728–41, 2011.

[22] J. O. Pyo, J. Nah, and Y. K. Jung. Molecules and their functions in autophagy. *Exp Mol Med*, 44(2):73–80, 2012.

[23] G. V. Helgason, T. L. Holyoake, and K. M. Ryan. Role of autophagy in cancer prevention, development and therapy. *Essays Biochem*, 55:133–51, 2013.

[24] P. Musiwaro, M. Smith, M. Manifava, S. A. Walker, and N. T. Ktistakis. Characteristics and requirements of basal autophagy in HEK 293 cells. *Autophagy*, 9(9):1407–17, 2013.

[25] A. R. Ariosa and D. J. Klionsky. Autophagy core machinery: overcoming spatial barriers in neurons. *Journal of Molecular Medicine*, 94(11):1217–1227, 2016.

[26] C. C. Dibble and B. D. Manning. Signal integration by mTORC1 coordinates nutrient input with biosynthetic output. *Nat Cell Biol*, 15(6):555–564, 2013.

[27] S. Sarkar. Regulation of autophagy by mTOR-dependent and mTOR-independent pathways: autophagy dysfunction in neurodegenerative diseases and therapeutic application of autophagy enhancers. *Biochemical Society Transactions*, 41(5):1103–1130, 2013.

[28] M. J. Groenewoud and F. J. T. Zwartkruis. Rheb and Rags come together at the lysosome to activate mTORC1. *Biochemical Society Transactions*, 41(4):951–955, 2013.

[29] E. Karanasios, E. Stapleton, M. Manifava, T. Kaizuka, N. Mizushima, S. A. Walker, and N. T. Ktistakis. Dynamic association of the ULK1 complex with omegasomes during autophagy induction. *Journal of Cell Science*, 126(22):5224–5238, 2013.

[30] W. Fan, A. Nassiri, and Q. Zhong. Autophagosome targeting and membrane curvature sensing by Barkor/Atg14(L). *Proc Natl Acad Sci U S A*, 108(19):7769–74, 2011.

[31] C. A. Lamb, T. Yoshimori, and S. A. Tooze. The autophagosome: origins unknown, biogenesis complex. *Nat Rev Mol Cell Biol*, 14(12):759–74, 2013.

[32] N. Mizushima, A. Yamamoto, M. Hatano, Y. Kobayashi, Y. Kabeya, K. Suzuki, T. Tokuhisa, Y. Ohsumi, and T. Yoshimori. Dissection of autophagosome formation using Apg5-deficient mouse embryonic stem cells. *J Cell Biol*, 152(4):657–68, 2001.

[33] T. Nishimura, T. Kaizuka, K. Cadwell, M. H. Sahani, T. Saitoh, S. Akira, H. W. Virgin, and N. Mizushima. FIP200 regulates targeting of Atg16L1 to the isolation membrane. *EMBO reports*, 14(3):284–291, 2013.

[34] N. Fujita, M. Hayashi-Nishino, H. Fukumoto, H. Omori, A. Yamamoto, T. Noda, and T. Yoshimori. An Atg4B mutant hampers the lipidation of LC3 paralogues and causes defects in autophagosome closure. *Mol Biol Cell*, 19(11):4651–9, 2008.

[35] J. Geng and D. J. Klionsky. The Atg8 and Atg12 ubiquitin-like conjugation systems in macroautophagy. 'Protein modifications: beyond the usual suspects' review series. *EMBO Rep*, 9(9):859–64, 2008.

[36] H. Nakatogawa. Two ubiquitin-like conjugation systems that mediate membrane formation during autophagy. *Essays Biochem*, 55:39–50, 2013.

[37] S. A. Tooze. Current views on the source of the autophagosome membrane. *Essays Biochem*, 55:29–38, 2013.

[38] K. Matsunaga, E. Morita, T. Saitoh, S. Akira, N. T. Ktistakis, T. Izumi, T. Noda, and T. Yoshimori. Autophagy requires endoplasmic reticulum targeting of the PI3-kinase complex via Atg14L. *J Cell Biol*, 190(4):511–21, 2010.

[39] E. L. Axe, S. A. Walker, M. Manifava, P. Chandra, H. L. Roderick, A. Habermann, G. Griffiths, and N. T. Ktistakis. Autophagosome formation from membrane compartments enriched in phosphatidylinositol 3-phosphate and dynamically connected to the endoplasmic reticulum. *J Cell Biol*, 182(4):685–701, 2008.

[40] M. Hamasaki, N. Furuta, A. Matsuda, A. Nezu, A. Yamamoto, N. Fujita, H. Oomori, T. Noda, T. Haraguchi, Y. Hiraoka, A. Amano, and T. Yoshimori. Autophagosomes form at ER-mitochondria contact sites. *Nature*, 495(7441):389–393, 2013.

[41] P. Yla-Anttila, H. Vihinen, E. Jokitalo, and E. L. Eskelinen. 3D tomography reveals connections between the phagophore and endoplasmic reticulum. *Autophagy*, 5(8):1180–5, 2009.

[42] J. Biazik, P. Yla-Anttila, H. Vihinen, E. Jokitalo, and E.-L. Eskelinen. Ultrastructural relationship of the phagophore with surrounding organelles. *Autophagy*, 11(3):439–451, 2015.

[43] D. W. Hailey, A. S. Rambold, P. Satpute-Krishnan, K. Mitra, R. Sougrat, P. K. Kim, and J. Lippincott-Schwartz. Mitochondria Supply Membranes for Autophagosome Biogenesis during Starvation. *Cell*, 141(4):656–667, 2010.

[44] L. Ge, M. Zhang, and R. Schekman. Phosphatidylinositol 3-kinase and COPII generate LC3 lipidation vesicles from the ER-Golgi intermediate compartment. *Elife*, 3:e04135, 2014.

[45] B. Ravikumar, K. Moreau, L. Jahreiss, C. Puri, and D. C. Rubinsztein. Plasma membrane contributes to the formation of pre-autophagosomal structures. *Nat Cell Biol*, 12(8):747–757, 2010.

[46] M. Manil-Segalen, C. Lefebvre, C. Jenzer, M. Trichet, C. Boulogne, B. Satiat-Jeunemaitre, and R. Legouis. The C.Â elegans LC3 Acts Downstream of GABARAP to Degrade Autophagosomes by Interacting with the HOPS Subunit VPS39. *Dev Cell*, 28(1):43–55, 2014.

[47] H. Nakatogawa, J. Ishii, E. Asai, and Y. Ohsumi. Atg4 recycles inappropriately lipidated Atg8 to promote autophagosome biogenesis. *Autophagy*, 8(2):177–186, 2012.

[48] V. M. S. Betin, B. K. Singleton, S. F. Parsons, D. J. Anstee, and J. D. Lane. Autophagy facilitates organelle clearance during differentiation of human erythroblasts. *Autophagy*, 9(6):881–893, 2013.

[49] J. Ma, C. Becker, C. Reyes, and D. M. Underhill. Cutting Edge: FYCO1 Recruitment to Dectin-1 Phagosomes Is Accelerated by Light Chain 3 Protein and Regulates Phagosome Maturation and Reactive Oxygen Production. *The Journal of Immunology*, 192(4):1356–1360, 2014.

[50] T. Kirisako, M. Baba, N. Ishihara, K. Miyazawa, M. Ohsumi, T. Yoshimori, T. Noda, and Y. Ohsumi. Formation process of autophagosome is traced with Apg8/Aut7p in yeast. *J Cell Biol*, 147(2):435–46, 1999.

[51] R. Kochl, X. W. Hu, E. Y. Chan, and S. A. Tooze. Microtubules facilitate autophagosome formation and fusion of autophagosomes with endosomes. *Traffic*, 7(2):129–45, 2006.

[52] L. Jahreiss, F. M. Menzies, and D. C. Rubinsztein. The itinerary of autophagosomes: from peripheral formation to kiss-and-run fusion with lysosomes. *Traffic (Copenhagen, Denmark)*, 9(4):574–587, 2008.

[53] S. Kimura, T. Noda, and T. Yoshimori. Dynein-dependent movement of autophagosomes mediates efficient encounters with lysosomes. *Cell Struct Funct*, 33(1):109–22, 2008.

[54] E. Fass, E. Shvets, I. Degani, K. Hirschberg, and Z. Elazar. Microtubules Support Production of Starvation-induced Autophagosomes but Not Their Targeting and Fusion with Lysosomes. *Journal of Biological Chemistry*, 281(47):36303–36316, 2006.

[55] S. Maday, K. E. Wallace, and E. L. Holzbaur. Autophagosomes initiate distally and mature during transport toward the cell soma in primary neurons. *J Cell Biol*, 196(4):407–17, 2012.

[56] B. Ravikumar, A. Acevedo-Arozena, S. Imarisio, Z. Berger, C. Vacher, C. J. O'Kane, S. D. Brown, and D. C. Rubinsztein. Dynein mutations impair autophagic clearance of aggregate-prone proteins. *Nat Genet*, 37(7):771–6, 2005.

[57] C. M. Cardoso, L. Groth-Pedersen, M. Hoyer-Hansen, T. Kirkegaard, E. Corcelle, J. S. Andersen, M. Jaattela, and J. Nylandsted. Depletion of kinesin 5B affects lysosomal distribution and stability and induces peri-nuclear accumulation of autophagosomes in cancer cells. *PLoS One*, 4(2):e4424, 2009.

[58] J. M. T. Hyttinen, M. Niittykoski, A. Salminen, and K. Kaarniranta. Maturation of autophagosomes and endosomes: A key role for Rab7. *Biochimica et Biophysica Acta (BBA) - Molecular Cell Research*, 1833(3):503–510, 2013.

[59] S. Pankiv, E. A. Alemu, A. Brech, J. A. Bruun, T. Lamark, A. Overvatn, G. Bjorkoy, and T. Johansen. FYCO1 is a Rab7 effector that binds to LC3 and PI3P to mediate microtubule plus end-directed vesicle transport. *J Cell Biol*, 188(2):253–69, 2010.

[60] J. Y. Lee, H. Koga, Y. Kawaguchi, W. Tang, E. Wong, Y. S. Gao, U. B. Pandey, S. Kaushik, E. Tresse, J. Lu, J. P. Taylor, A. M. Cuervo, and T. P. Yao. HDAC6 controls autophagosome maturation essential for ubiquitin-selective quality-control autophagy. *EMBO J*, 29(5):969–80, 2010.

[61] D. Tumbarello, J. Kendrick-Jones, and F. Buss. Myosin VI and its cargo adaptors - linking endocytosis and autophagy. *Journal of Cell Science*, 126(12):2561–2570, 2013.

[62] I. G. Ganley. Autophagosome maturation and lysosomal fusion. *Essays Biochem*, 55:65–78, 2013.

[63] T. Itoh, N. Fujita, E. Kanno, A. Yamamoto, T. Yoshimori, and M. Fukuda. Golgi-resident Small GTPase Rab33B Interacts with Atg16L and Modulates Autophagosome Formation. *Molecular Biology of the Cell*, 19(7):2916–2925, 2008.

[64] T. Itoh, E. Kanno, T. Uemura, S. Waguri, and M. Fukuda. OATL1, a novel autophagosome-resident Rab33B-GAP, regulates autophagosomal maturation. *J Cell Biol*, 192(5):839–53, 2011.

[65] Q. Sun, W. Westphal, K. N. Wong, I. Tan, and Q. Zhong. Rubicon controls endosome maturation as a Rab7 effector. *Proceedings of the National Academy of Sciences of the United States of America*, 107(45):19338–19343, 2010.

[66] K. Tabata, K. Matsunaga, A. Sakane, T. Sasaki, T. Noda, and T. Yoshimori. Rubicon and PLEKHM1 negatively regulate the endocytic/autophagic pathway via a novel Rab7-binding domain. *Mol Biol Cell*, 21(23):4162–72, 2010.

[67] D. C. Rubinsztein, P. Codogno, and B. Levine. Autophagy modulation as a potential therapeutic target for diverse diseases. *Nat Rev Drug Discov*, 11(9):709–730, 2012.

[68] J. Li, S.Â G. Kim, and J. Blenis. Rapamycin: One Drug, Many Effects. *Cell Metabolism*, 19(3):373–379, 2014.

[69] D. Ma, S. Panda, and J. D. Lin. Temporal orchestration of circadian autophagy rhythm by C/EBP-beta. *EMBO J*, 30(22):4642–51, 2011.

[70] Y. Feng, Z. Yao, and D. J. Klionsky. How to control self-digestion: transcriptional, post-transcriptional, and post-translational regulation of autophagy. *Trends Cell Biol*, 25(6):354–63, 2015.

[71] G. Kreiner, H. Bierhoff, M. Armentano, J. Rodriguez-Parkitna, K. Sowodniok, J. R. Naranjo, L. Bonfanti, B. Liss, G. Schütz, I. Grummt, and R. Parlato. A neuroprotective phase precedes striatal degeneration upon nucleolar stress. *Cell Death and Differentiation*, 20(11):1455–1464, 2013.

[72] P. de Medina, M. R. Paillasse, G. Segala, F. Khallouki, S. Brillouet, F. Dalenc, F. Courbon, M. Record, M. Poirot, and S. Silvente-Poirot. Importance of cholesterol and oxysterols metabolism in the pharmacology of tamoxifen and other AEBS ligands. *Chem Phys Lipids*, 164(6):432–7, 2011.

[73] M. Zimmermann, R. Cal, E. Janett, V. Hoffmann, C. G. Bochet, E. Constable, F. Beaufils, and M. P. Wymann. Cell-permeant and photocleavable chemical inducer of dimerization. *Angew Chem Int Ed Engl*, 53(18):4717–20, 2014.

[74] D. M. Spencer, T. J. Wandless, S. L. Schreiber, and G. R. Crabtree. Controlling signal transduction with synthetic ligands. *Science*, 262(5136):1019–24, 1993.

[75] J. F. Amara, T. Clackson, V. M. Rivera, T. Guo, T. Keenan, S. Natesan, R. Pollock, W. Yang, N. L. Courage, D. A. Holt, and M. Gilman. A versatile synthetic dimerizer for the regulation of protein-protein interactions. *Proceedings of the National Academy of Sciences*, 94(20):10618–10623, 1997.

[76] A. Rutkowska, C. H. Haering, and C. Schultz. A FlAsH-Based Cross-Linker to Study Protein Interactions in Living Cells. *Angewandte Chemie International Edition*, 50(52):12655–12658, 2011.

[77] M. A. Farrar, J. Alberola-lla, and R. M. Perlmutter. Activation of the Raf-1 kinase cascade by coumermycin-induced dimerization. *Nature*, 383(6596):178–181, 1996.

[78] G. Lemercier, S. Gendreizig, M. Kindermann, and K. Johnsson. Inducing and Sensing Protein-Protein Interactions in Living Cells by Selective Cross-linking. *Angewandte Chemie International Edition*, 46(23):4281–4284, 2007.

[79] T. Keenan, D. R. Yaeger, N. L. Courage, C. T. Rollins, M. E. Pavone, V. M. Rivera, W. Yang, T. Guo, J. F. Amara, T. Clackson, M. Gilman, and D. A. Holt. Synthesis and activity of bivalent FKBP12 ligands for the regulated dimerization of proteins. *Bioorganic & Medicinal Chemistry*, 6(8):1309–1335, 1998.

[80] P. J. Belshawl, D. M. Spencer, G. R. Crabtree, and S. L. Schreiber. Controlling programmed cell death with a cyclophilincyclosporin-based chemical inducer of dimerization. *Chemistry & Biology*, 3(9):731–738, 1996.

[81] X. F. Zheng and T. F. Chan. Chemical genomics: a systematic approach in biological research and drug discovery. *Curr Issues Mol Biol*, 4(2):33–43, 2002.

[82] W. Yang, L. W. Rozamus, S. Narula, C. T. Rollins, R. Yuan, L. J. Andrade, M. K. Ram, T. B. Phillips, M. R. van Schravendijk, D. Dalgarno, T. Clackson, and D. A. Holt. Investigating protein-ligand interactions with a mutant FKBP possessing a designed specificity pocket. *J Med Chem*, 43(6):1135–42, 2000.

[83] E. R. Ballister. *Inducible Protein Dimerization: New Tools And Applications To Understanding The Mitotic Checkpoint*. Thesis, University of Pennsylvania, 2014.

[84] A. Keppler, S. Gendreizig, T. Gronemeyer, H. Pick, H. Vogel, and K. Johnsson. A general method for the covalent labeling of fusion proteins with small molecules in vivo. *Nat Biotech*, 21(1):86–89, 2003.

[85] B. A. Griffin, S. R. Adams, and R. Y. Tsien. Specific covalent labeling of recombinant protein molecules inside live cells. *Science*, 281(5374):269–72, 1998.

[86] T. W. Corson, N. Aberle, and C. M. Crews. Design and Applications of Bifunctional Small Molecules: Why Two Heads Are Better Than One. *ACS Chem Biol*, 3(11):677–692, 2008.

[87] A. Fegan, B. White, J. C. Carlson, and C. R. Wagner. Chemically controlled protein assembly: techniques and applications. *Chem Rev*, 110(6):3315–36, 2010.

[88] S. N. Ho, S. R. Biggar, D. M. Spencer, S. L. Schreiber, and G. R. Crabtree. Dimeric ligands define a role for transcriptional activation domains in reinitiation. *Nature*, 382(6594):822–826, 1996.

[89] V. M. Rivera, T. Clackson, S. Natesan, R. Pollock, J. F. Amara, T. Keenan, S. R. Magari, T. Phillips, N. L. Courage, Jr. Cerasoli, F., D. A. Holt, and M. Gilman. A humanized system for pharmacologic control of gene expression. *Nat Med*, 2(9):1028–32, 1996.

[90] S. D. Liberles, S. T. Diver, D. J. Austin, and S. L. Schreiber. Inducible gene expression and protein translocation using nontoxic ligands identified by a mammalian three-hybrid screen. *Proc Natl Acad Sci U S A*, 94(15):7825–30, 1997.

[91] J. H. Bayle, J. S. Grimley, K. Stankunas, J. E. Gestwicki, T. J. Wandless, and G. R. Crabtree. Rapamycin Analogs with Differential Binding Specificity Permit Orthogonal Control of Protein Activity. *Chemistry & Biology*, 13(1):99–107, 2006.

[92] T. Inoue, W. D. Heo, J. S. Grimley, T. J. Wandless, and T. Meyer. An inducible translocation strategy to rapidly activate and inhibit small GTPase signaling pathways. *Nat Meth*, 2(6):415–418, 2005.

[93] C. T. Rollins, V. M. Rivera, D. N. Woolfson, T. Keenan, M. Hatada, S. E. Adams, L. J. Andrade, D. Yaeger, M. R. van Schravendijk, D. A. Holt, M. Gilman, and T. Clackson. A ligand-reversible dimerization system for controlling protein-protein interactions. *Proc Natl Acad Sci U S A*, 97(13):7096–101, 2000.

[94] F. S. Liang, W. Q. Ho, and G. R. Crabtree. Engineering the ABA plant stress pathway for regulation of induced proximity. *Sci Signal*, 4(164):rs2, 2011.

[95] T. Miyamoto, R. DeRose, A. Suarez, T. Ueno, M. Chen, T. P. Sun, M. J. Wolfgang, C. Mukherjee, D. J. Meyers, and T. Inoue. Rapid and orthogonal logic gating with a gibberellin-induced dimerization system. *Nat Chem Biol*, 8(5):465–70, 2012.

[96] R. Zoncu, A. Efeyan, and D. M. Sabatini. mTOR: from growth signal integration to cancer, diabetes and ageing. *Nat Rev Mol Cell Biol*, 12(1):21–35, 2011.

[97] L. M. Ballou and R. Z. Lin. Rapamycin and mTOR kinase inhibitors. *Journal of Chemical Biology*, 1(1-4):27–36, 2008.

[98] L. A. Banaszynski, C. W. Liu, and T. J. Wandless. Characterization of the FKBP.rapamycin.FRB ternary complex. *J Am Chem Soc*, 127(13):4715–21, 2005.

[99] K. Stankunas, J. H. Bayle, J. E. Gestwicki, Y.-M. Lin, T. J. Wandless, and G. R. Crabtree. Conditional Protein Alleles Using Knockin Mice and a Chemical Inducer of Dimerization. *Molecular Cell*, 12(6):1615–1624, 2003.

[100] P. J. Belshaw, S. N. Ho, G. R. Crabtree, and S. L. Schreiber. Controlling protein association and subcellular localization with a synthetic ligand that induces heterodimerization of proteins. *Proc Natl Acad Sci U S A*, 93(10):4604–7, 1996.

[101] E. J. Licitra and J. O. Liu. A three-hybrid system for detecting small ligand-protein receptor interactions. *Proc Natl Acad Sci U S A*, 93(23):12817–21, 1996.

[102] H. Lin, W. M. Abida, R. T. Sauer, and V. W. Cornish. Dexamethasone-Methotrexate: An Efficient Chemical Inducer of Protein Dimerization In Vivo. *J Am Chem Soc*, 122(17):4247–4248, 2000.

[103] S. S. Gallagher, L. W. Miller, and V. W. Cornish. An orthogonal dexamethasone-trimethoprim yeast three-hybrid system. *Anal Biochem*, 363(1):160–2, 2007.

[104] D. Erhart, M. Zimmermann, O. Jacques, M. B. Wittwer, B. Ernst, E. Constable, M. Zvelebil, F. Beaufils, and M. P. Wymann. Chemical development of intracellular protein heterodimerizers. *Chemistry & Biology*, 20(4):549–57, 2013.

[105] S. Feng, V. Laketa, F. Stein, A. Rutkowska, A. MacNamara, S. Depner, U. Klingmuller, J. Saez-Rodriguez, and C. Schultz. A rapidly reversible chemical dimerizer system to study lipid signaling in living cells. *Angew Chem Int Ed Engl*, 53(26):6720–3, 2014.

[106] G. Zeng, R. Zhang, W. Xuan, W. Wang, and F. S. Liang. Constructing de Novo H2O2 Signaling via Induced Protein Proximity. *ACS Chem Biol*, 10(6):1404–10, 2015.

[107] A. V. Karginov, Y. Zou, D. Shirvanyants, P. Kota, N. V. Dokholyan, D. D. Young, K. M. Hahn, and A. Deiters. Light regulation of protein dimerization and kinase activity in living cells using photocaged rapamycin and engineered FKBP. *J Am Chem Soc*, 133(3):420–3, 2011.

[108] N. Umeda, T. Ueno, C. Pohlmeyer, T. Nagano, and T. Inoue. A photocleavable rapamycin conjugate for spatiotemporal control of small GTPase activity. *J Am Chem Soc*, 133(1):12–4, 2011.

[109] K. A. Brown, Y. Zou, D. Shirvanyants, J. Zhang, S. Samanta, P. K. Mantravadi, N. V. Dokholyan, and A. Deiters. Light-cleavable rapamycin dimer as an optical trigger for protein dimerization. *Chem Commun (Camb)*, 51(26):5702–5, 2015.

[110] S. Ahmed, J. Xie, D. Horne, and J. C. Williams. Photocleavable dimerizer for the rapid reversal of molecular trap antagonists. *J Biol Chem*, 289(8):4546–52, 2014.

[111] C. W. Wright, Z. F. Guo, and F. S. Liang. Light control of cellular processes by using photocaged abscisic acid. *Chembiochem*, 16(2):254–61, 2015.

[112] K. M. Schelkle, T. Griesbaum, D. Ollech, S. Becht, T. Buckup, M. Hamburger, and R. Wombacher. Light-induced protein dimerization by one- and two-photon activation of gibberellic acid derivatives in living cells. *Angew Chem Int Ed Engl*, 54(9):2825–9, 2015.

[113] E. R. Ballister, C. Aonbangkhen, A. M. Mayo, M. A. Lampson, and D. M. Chenoweth. Localized light-induced protein dimerization in living cells using a photocaged dimerizer. *Nat Commun*, 5:5475, 2014.

[114] D. I. Pattison and M. J. Davies. Actions of ultraviolet light on cellular structures. *Exs*, 96:131–57, 2006.

[115] G. Miesenbock. Optogenetic control of cells and circuits. *Annu Rev Cell Dev Biol*, 27:731–58, 2011.

[116] S. Shimizu-Sato, E. Huq, J. M. Tepperman, and P. H. Quail. A light-switchable gene promoter system. *Nat Biotech*, 20(10):1041–1044, 2002.

[117] B. V. Zemelman, G. A. Lee, M. Ng, and G. Miesenböck. Selective Photostimulation of Genetically ChARGed Neurons. *Neuron*, 33(1):15–22, 2002.

[118] M. Yazawa, A. M. Sadaghiani, B. Hsueh, and R. E. Dolmetsch. Induction of protein-protein interactions in live cells using light. *Nat Biotechnol*, 27(10):941–5, 2009.

[119] A. Pudasaini, K. K. El-Arab, and B. D. Zoltowski. LOV-based optogenetic devices: light-driven modules to impart photoregulated control of cellular signaling. *Front Mol Biosci*, 2:18, 2015.

[120] E. Huala, P. W. Oeller, E. Liscum, I. S. Han, E. Larsen, and W. R. Briggs. Arabidopsis NPH1: a protein kinase with a putative redox-sensing domain. *Science*, 278(5346):2120–3, 1997.

[121] M. Salomon, J. M. Christie, E. Knieb, U. Lempert, and W. R. Briggs. Photochemical and mutational analysis of the FMN-binding domains of the plant blue light receptor, phototropin. *Biochemistry*, 39(31):9401–10, 2000.

[122] H. M. Beyer, S. Naumann, W. Weber, and G. Radziwill. Optogenetic control of signaling in mammalian cells. *Biotechnol J*, 10(2):273–83, 2015.

[123] Y. I. Wu, D. Frey, O. I. Lungu, A. Jaehrig, I. Schlichting, B. Kuhlman, and K. M. Hahn. A genetically encoded photoactivatable Rac controls the motility of living cells. *Nature*, 461(7260):104–8, 2009.

[124] D. Strickland, Y. Lin, E. Wagner, C. M. Hope, J. Zayner, C. Antoniou, T. R. Sosnick, E. L. Weiss, and M. Glotzer. TULIPs: tunable, light-controlled interacting protein tags for cell biology. *Nat Methods*, 9(4):379–84, 2012.

[125] D. Strickland, X. Yao, G. Gawlak, M. K. Rosen, K. H. Gardner, and T. R. Sosnick. Rationally improving LOV domain-based photoswitches. *Nat Methods*, 7(8):623–6, 2010.

[126] M. T. Alexandre, J. C. Arents, R. van Grondelle, K. J. Hellingwerf, and J. T. Kennis. A base-catalyzed mechanism for dark state recovery in the Avena sativa phototropin-1 LOV2 domain. *Biochemistry*, 46(11):3129–37, 2007.

[127] B. D. Zoltowski, B. Vaccaro, and B. R. Crane. Mechanism-based tuning of a LOV domain photoreceptor. *Nat Chem Biol*, 5(11):827–34, 2009.

[128] J. M. Christie, S. B. Corchnoy, T. E. Swartz, M. Hokenson, I. S. Han, W. R. Briggs, and R. A. Bogomolni. Steric interactions stabilize the signaling state of the LOV2 domain of phototropin 1. *Biochemistry*, 46(32):9310–9, 2007.

[129] O. I. Lungu, R. A. Hallett, E. J. Choi, M. J. Aiken, K. M. Hahn, and B. Kuhlman. Designing photoswitchable peptides using the AsLOV2 domain. *Chemistry & Biology*, 19(4):507–17, 2012.

[130] X. Wang, X. Chen, and Y. Yang. Spatiotemporal control of gene expression by a light-switchable transgene system. *Nat Meth*, 9(3):266–269, 2012.

[131] X. Chen, X. Wang, Z. Du, Z. Ma, and Y. Yang. Spatiotemporal control of gene expression in mammalian cells and in mice using the LightOn system. *Curr Protoc Chem Biol*, 5(2):111–29, 2013.

[132] Z. Ma, Z. Du, X. Chen, X. Wang, and Y. Yang. Fine tuning the LightOn light-switchable transgene expression system. *Biochem Biophys Res Commun*, 440(3):419–23, 2013.

[133] F. Kawano, H. Suzuki, A. Furuya, and M. Sato. Engineered pairs of distinct photoswitches for optogenetic control of cellular proteins. *Nat Commun*, 6:6256, 2015.

[134] L. B. Motta-Mena, A. Reade, M. J. Mallory, S. Glantz, O. D. Weiner, K. W. Lynch, and K. H. Gardner. An optogenetic gene expression system with rapid activation and deactivation kinetics. *Nat Chem Biol*, 10(3):196–202, 2014.

[135] B. D. Zoltowski, L. B. Motta-Mena, and K. H. Gardner. Blue light-induced dimerization of a bacterial LOV-HTH DNA-binding protein. *Biochemistry*, 52(38):6653–61, 2013.

[136] G. Rivera-Cancel, L. B. Motta-Mena, and K. H. Gardner. Identification of natural and artificial DNA substrates for light-activated LOV-HTH transcription factor EL222. *Biochemistry*, 51(50):10024–34, 2012.

[137] A. Moglich, R. A. Ayers, and K. Moffat. Design and signaling mechanism of light-regulated histidine kinases. *J Mol Biol*, 385(5):1433–44, 2009.

[138] R. Ohlendorf, R. R. Vidavski, A. Eldar, K. Moffat, and A. Moglich. From dusk till dawn: one-plasmid systems for light-regulated gene expression. *J Mol Biol*, 416(4):534–42, 2012.

[139] H. Wang, M. Vilela, A. Winkler, M. Tarnawski, I. Schlichting, H. Yumerefendi, B. Kuhlman, R. Liu, G. Danuser, and K. M. Hahn. LOVTRAP: an optogenetic system for photoinduced protein dissociation. *Nat Meth*, 13(9):755–758, 2016.

[140] M. J. Kennedy, R. M. Hughes, L. A. Peteya, J. W. Schwartz, M. D. Ehlers, and C. L. Tucker. Rapid blue-light-mediated induction of protein interactions in living cells. *Nat Methods*, 7(12):973–5, 2010.

[141] S. Konermann, M. D. Brigham, A. E. Trevino, P. D. Hsu, M. Heidenreich, L. Cong, R. J. Platt, D. A. Scott, G. M. Church, and F. Zhang. Optical control of mammalian endogenous transcription and epigenetic states. *Nature*, 500(7463):472–6, 2013.

[142] S. Wend, H. J. Wagner, K. Muller, M. D. Zurbriggen, W. Weber, and G. Radziwill. Optogenetic control of protein kinase activity in mammalian cells. *ACS Synth Biol*, 3(5):280–5, 2014.

[143] L. J. Bugaj, A. T. Choksi, C. K. Mesuda, R. S. Kane, and D. V. Schaffer. Optogenetic protein clustering and signaling activation in mammalian cells. *Nat Meth*, 10(3):249–252, 2013.

[144] S. Schroder-Lang, M. Schwarzel, R. Seifert, T. Strunker, S. Kateriya, J. Looser, M. Watanabe, U. B. Kaupp, P. Hegemann, and G. Nagel. Fast manipulation of cellular cAMP level by light in vivo. *Nat Methods*, 4(1):39–42, 2007.

[145] M. Stierl, P. Stumpf, D. Udwari, R. Gueta, R. Hagedorn, A. Losi, W. Gartner, L. Petereit, M. Efetova, M. Schwarzel, T. G. Oertner, G. Nagel, and P. Hegemann. Light modulation of cellular cAMP by a small bacterial photoactivated adenylyl cyclase, bPAC, of the soil bacterium Beggiatoa. *J Biol Chem*, 286(2):1181–8, 2011.

[146] R. J. De Marco, A. H. Groneberg, C. M. Yeh, L. A. Castillo Ramirez, and S. Ryu. Optogenetic elevation of endogenous glucocorticoid level in larval zebrafish. *Front Neural Circuits*, 7:82, 2013.

[147] K. Muller, R. Engesser, J. Timmer, F. Nagy, M. D. Zurbriggen, and W. Weber. Synthesis of phycocyanobilin in mammalian cells. *Chemical Communications*, 49(79):8970–8972, 2013.

[148] K. Zhang and B. Cui. Optogenetic control of intracellular signaling pathways. *Trends in Biotechnology*, 33(2):92–100, 2015.

[149] A. Levskaya, O. D. Weiner, W. A. Lim, and C. A. Voigt. Spatiotemporal control of cell signalling using a light-switchable protein interaction. *Nature*, 461(7266):997–1001, 2009.

[150] K. Muller, R. Engesser, S. Metzger, S. Schulz, M. M. Kampf, M. Busacker, T. Steinberg, P. Tomakidi, M. Ehrbar, F. Nagy, J. Timmer, M. D. Zubriggen, and W. Weber. A red/far-red light-responsive bistable toggle switch to control gene expression in mammalian cells. *Nucleic Acids Res*, 41(7):e77, 2013.

[151] X. X. Zhou, H. K. Chung, A. J. Lam, and M. Z. Lin. Optical control of protein activity by fluorescent protein domains. *Science*, 338(6108):810–4, 2012.

[152] L. Z. Fan and M. Z. Lin. Optical control of biological processes by light-switchable proteins. *Wiley Interdisciplinary Reviews: Developmental Biology*, 4(5):545–554, 2015.

[153] D. Chen, E. S. Gibson, and M. J. Kennedy. A light-triggered protein secretion system. *J Cell Biol*, 201(4):631–40, 2013.

[154] B. R. Stockwell and S. L. Schreiber. Probing the role of homomeric and heteromeric receptor interactions in TGF-beta signaling using small molecule dimerizers. *Curr Biol*, 8(13):761–70, 1998.

[155] S. K. Muthuswamy, M. Gilman, and J. S. Brugge. Controlled dimerization of ErbB receptors provides evidence for differential signaling by homo- and heterodimers. *Mol Cell Biol*, 19(10):6845–57, 1999.

[156] B. E. Welm, K. W. Freeman, M. Chen, A. Contreras, D. M. Spencer, and J. M. Rosen. Inducible dimerization of FGFR1: development of a mouse model to analyze progressive transformation of the mammary gland. *The Journal of Cell Biology*, 157(4):703–714, 2002.

[157] M. Grusch, K. Schelch, R. Riedler, E. Reichhart, C. Differ, W. Berger, A. Ingles-Prieto, and H. Janovjak. Spatio-temporally precise activation of engineered receptor tyrosine kinases by light. *The EMBO Journal*, 33(15):1713–1726, 2014.

[158] S. Terrillon and M. Bouvier. Receptor activity-independent recruitment of betaarrestin2 reveals specific signalling modes. *EMBO J*, 23(20):3950–61, 2004.

[159] M. Bellot, S. Galandrin, C. Boularan, H. J. Matthies, F. Despas, C. Denis, J. Javitch, S. Mazeres, S. J. Sanni, V. Pons, M. H. Seguelas, J. L. Hansen, A. Pathak, A. Galli, J. M. Senard, and C. Gales. Dual agonist occupancy of AT1-R-alpha2C-AR heterodimers results in atypical Gs-PKA signaling. *Nat Chem Biol*, 11(4):271–9, 2015.

[160] L. Jin, N. Siritanaratkul, D. W. Emery, R. E. Richard, K. Kaushansky, T. Papayannopoulou, and C. A. Blau. Targeted expansion of genetically modified bone marrow cells. *Proceedings of the National Academy of Sciences of the United States of America*, 95(14):8093–8097, 1998.

[161] K. Okazuka, B. C. Beard, D. W. Emery, K. Schwarzwaelder, M. R. Spector, G. E. Sale, C. von Kalle, B. Torok-Storb, H. P. Kiem, and C. A. Blau. Long-term regulation of genetically modified primary hematopoietic cells in dogs. *Mol Ther*, 19(7):1287–94, 2011.

[162] D. M. Spencer, P. J. Belshaw, L. Chen, S. N. Ho, F. Randazzo, G. R. Crabtree, and S. L. Schreiber. Functional analysis of Fas signaling in vivo using synthetic inducers of dimerization. *Curr Biol*, 6(7):839–47, 1996.

[163] L. Fan, K. W. Freeman, T. Khan, E. Pham, and D. M. Spencer. Improved Artificial Death Switches Based on Caspases and FADD. *Human Gene Therapy*, 10(14):2273–2285, 1999.

[164] V. O. Mallet, C. Mitchell, J.-E. Guidotti, P. Jaffray, M. Fabre, D. Spencer, D. Arnoult, A. Kahn, and H. Gilgenkrantz. Conditional cell ablation by tight control of caspase-3 dimerization in transgenic mice. *Nat Biotech*, 20(12):1234–1239, 2002.

[165] S. M. Srinivasula, J. L. Poyet, M. Razmara, P. Datta, Z. Zhang, and E. S. Alnemri. The PYRIN-CARD protein ASC is an activating adaptor for caspase-1. *J Biol Chem*, 277(24):21119–22, 2002.

[166] U. B. Pajvani, M. E. Trujillo, T. P. Combs, P. Iyengar, L. Jelicks, K. A. Roth, R. N. Kitsis, and P. E. Scherer. Fat apoptosis through targeted activation of caspase 8: a new mouse model of inducible and reversible lipoatrophy. *Nat Med*, 11(7):797–803, 2005.

[167] A. V. Karginov, F. Ding, P. Kota, N. V. Dokholyan, and K. M. Hahn. Engineered allosteric activation of kinases in living cells. *Nat Biotechnol*, 28(7):743–7, 2010.

[168] A. V. Karginov and K. M. Hahn. Allosteric activation of kinases: design and application of RapR kinases. *Curr Protoc Cell Biol*, Chapter 14:Unit 14 13, 2011.

[169] A. V. Karginov, K. M. Hahn, and A. Deiters. Optochemical Activation of Kinase Function in Live Cells. *Methods in molecular biology (Clifton, N.J.)*, 1148:31–43, 2014.

[170] A. V. Karginov, D. Tsygankov, M. Berginski, P. H. Chu, E. D. Trudeau, J. J. Yi, S. Gomez, T. C. Elston, and K. M. Hahn. Dissecting motility signaling through activation of specific Src-effector complexes. *Nat Chem Biol*, 10(4):286–90, 2014.

[171] M. C. Wehr, R. Laage, U. Bolz, T. M. Fischer, S. Grunewald, S. Scheek, A. Bach, K.-A. Nave, and M. J. Rossner. Monitoring regulated protein-protein interactions using split TEV. *Nat Meth*, 3(12):985–993, 2006.

[172] D. C. Gray, S. Mahrus, and J. A. Wells. Activation of Specific Apoptotic Caspases with an Engineered Small-Molecule-Activated Protease. *Cell*, 142(4):637–646, 2010.

[173] T. Sonntag and H. D. Mootz. An intein-cassette integration approach used for the generation of a split TEV protease activated by conditional protein splicing. *Mol Biosyst*, 7(6):2031–9, 2011.

[174] K. Muller, R. Engesser, S. Schulz, T. Steinberg, P. Tomakidi, C. C. Weber, R. Ulm, J. Timmer, M. D. Zurbriggen, and W. Weber. Multi-chromatic control of mammalian gene expression and signaling. *Nucleic Acids Res*, 41(12):e124, 2013.

[175] D. M. Janse, B. Crosas, D. Finley, and G. M. Church. Localization to the proteasome is sufficient for degradation. *J Biol Chem*, 279(20):21415–20, 2004.

[176] M. R. Pratt, E. C. Schwartz, and T. W. Muir. Small-molecule-mediated rescue of protein function by an inducible proteolytic shunt. *Proceedings of the National Academy of Sciences*, 104(27):11209–11214, 2007.

[177] K. Nishimura, T. Fukagawa, H. Takisawa, T. Kakimoto, and M. Kanemaki. An auxin-based degron system for the rapid depletion of proteins in nonplant cells. *Nat Methods*, 6(12):917–22, 2009.

[178] D. M. Spencer, I. Graef, D. J. Austin, S. L. Schreiber, and G. R. Crabtree. A general strategy for producing conditional alleles of Src-like tyrosine kinases. *Proceedings of the National Academy of Sciences of the United States of America*, 92(21):9805–9809, 1995.

[179] R. DeRose, T. Miyamoto, and T. Inoue. Manipulating signaling at will: chemically-inducible dimerization (CID) techniques resolve problems in cell biology. *Pflugers Arch*, 465(3):409–17, 2013.

[180] B. C. Suh, T. Inoue, T. Meyer, and B. Hille. Rapid chemically induced changes of PtdIns(4,5)P2 gate KCNQ ion channels. *Science*, 314(5804):1454–7, 2006.

[181] P. Varnai, B. Thyagarajan, T. Rohacs, and T. Balla. Rapidly inducible changes in phosphatidylinositol 4,5-bisphosphate levels influence multiple regulatory functions of the lipid in intact living cells. *J Cell Biol*, 175(3):377–82, 2006.

[182] J. Yao and F. Qin. Interaction with Phosphoinositides Confers Adaptation onto the TRPV1 Pain Receptor. *PLoS Biol*, 7(2):e1000046, 2009.

[183] V. Lukacs, B. Thyagarajan, P. Varnai, A. Balla, T. Balla, and T. Rohacs. Dual Regulation of TRPV1 by Phosphoinositides. *The Journal of Neuroscience*, 27(26):7070–7080, 2007.

[184] R. Zoncu, R. M. Perera, R. Sebastian, F. Nakatsu, H. Chen, T. Balla, G. Ayala, D. Toomre, and P. V. De Camilli. Loss of endocytic clathrin-coated pits upon acute depletion of phosphatidylinositol 4,5-bisphosphate. *Proceedings of the National Academy of Sciences*, 104(10):3793–3798, 2007.

[185] N. Abe, T. Inoue, T. Galvez, L. Klein, and T. Meyer. Dissecting the role of PtdIns(4,5)P2 in endocytosis and recycling of the transferrin receptor. *Journal of Cell Science*, 121(9):1488–1494, 2008.

[186] F. Nakatsu, R. M. Perera, L. Lucast, R. Zoncu, J. Domin, F. B. Gertler, D. Toomre, and P. De Camilli. The inositol 5-phosphatase SHIP2 regulates endocytic clathrin-coated pit dynamics. *The Journal of Cell Biology*, 190(3):307–315, 2010.

[187] C. M. Walsh, M. Chvanov, L. P. Haynes, O. H. Petersen, A. V. Tepikin, and R.Â D. Burgoyne. Role of phosphoinositides in STIM1 dynamics and store-operated calcium entry. *Biochemical Journal*, 425(1):159–168, 2010.

[188] M. K. Korzeniowski, M. A. Popovic, Z. Szentpetery, P. Varnai, S. S. Stojilkovic, and T. Balla. Dependence of STIM1/Orai1-mediated Calcium Entry on Plasma Membrane Phosphoinositides. *Journal of Biological Chemistry*, 284(31):21027–21035, 2009.

[189] M. Rahdar, T. Inoue, T. Meyer, J. Zhang, F. Vazquez, and P. N. Devreotes. A phosphorylation-dependent intramolecular interaction regulates the membrane association and activity of the tumor suppressor PTEN. *Proceedings of the National Academy of Sciences*, 106(2):480–485, 2009.

[190] T. Inoue and T. Meyer. Synthetic Activation of Endogenous PI3K and Rac Identifies an AND-Gate Switch for Cell Polarization and Migration. *PLoS One*, 3(8):e3068, 2008.

[191] M. Fivaz, S. Bandara, T. Inoue, and T. Meyer. Robust Neuronal Symmetry Breaking by Ras-Triggered Local Positive Feedback. *Current Biology*, 18(1):44–50, 2008.

[192] N. Fili, V. Calleja, R. Woscholski, P. J. Parker, and B. Larijani. Compartmental signal modulation: Endosomal phosphatidylinositol 3-phosphate controls endosome morphology and selective cargo sorting. *Proc Natl Acad Sci U S A*, 103(42):15473–8, 2006.

[193] Z. Szentpetery, P. Varnai, and T. Balla. Acute manipulation of Golgi phosphoinositides to assess their importance in cellular trafficking and signaling. *Proceedings of the National Academy of Sciences*, 107(18):8225–8230, 2010.

[194] T. Ueno, B. H. Falkenburger, C. Pohlmeyer, and T. Inoue. Triggering actin comets versus membrane ruffles: distinctive effects of phosphoinositides on actin reorganization. *Sci Signal*, 4(203):ra87, 2011.

[195] M. Schifferer, S. Feng, F. Stein, C. Tischer, and C. Schultz. Reversible chemical dimerizer-induced recovery of PIP2 levels moves clathrin to the plasma membrane. *Bioorg Med Chem*, 23(12):2862–7, 2015.

[196] F. Castellano, P. Montcourrier, J.-C. Guillemot, E. Gouin, L. Machesky, P. Cossart, and P. Chavrier. Inducible recruitment of Cdc42 or WASP to a cell-surface receptor triggers actin polymerization and filopodium formation. *Current Biology*, 9(7):351–361, 1999.

[197] F. Castellano, P. Montcourrier, and P. Chavrier. Membrane recruitment of Rac1 triggers phagocytosis. *Journal of Cell Science*, 113(17):2955–2961, 2000.

[198] T. Komatsu, I. Kukelyansky, J. M. McCaffery, T. Ueno, L. C. Varela, and T. Inoue. Organelle-specific, rapid induction of molecular activities and membrane tethering. *Nat Methods*, 7(3):206–8, 2010.

[199] T. Komatsu and T. Inoue. A method to rapidly induce organelle-specific molecular activities and membrane tethering. *Methods Mol Biol*, 1174:231–45, 2014.

[200] K. Zhang, L. Duan, Q. Ong, Z. Lin, P. M. Varman, K. Sung, and B. Cui. Light-mediated kinetic control reveals the temporal effect of the Raf/MEK/ERK pathway in PC12 cell neurite outgrowth. *PLoS One*, 9(3):e92917, 2014.

[201] A. Mor and M. R. Philips. Compartmentalized Ras/MAPK signaling. *Annu Rev Immunol*, 24:771–800, 2006.

[202] L. C. Kapitein, M. A. Schlager, W. A. van der Zwan, P. S. Wulf, N. Keijzer, and C. C. Hoogenraad. Probing intracellular motor protein activity using an inducible cargo trafficking assay. *Biophys J*, 99(7):2143–52, 2010.

[203] S. Al-Bassam, M. Xu, T. J. Wandless, and D. B. Arnold. Differential trafficking of transport vesicles contributes to the localization of dendritic proteins. *Cell Rep*, 2(1):89–100, 2012.

[204] B. Jenkins, H. Decker, M. Bentley, J. Luisi, and G. Banker. A novel split kinesin assay identifies motor proteins that interact with distinct vesicle populations. *J Cell Biol*, 198(4):749–61, 2012.

[205] M. Bentley, H. Decker, J. Luisi, and G. Banker. A novel assay reveals preferential binding between Rabs, kinesins, and specific endosomal subpopulations. *J Cell Biol*, 208(3):273–81, 2015.

[206] P. van Bergeijk, M. Adrian, C. C. Hoogenraad, and L. C. Kapitein. Optogenetic control of organelle transport and positioning. *Nature*, 518(7537):111–4, 2015.

[207] L. Duan, D. Che, K. Zhang, Q. Ong, S. Guo, and B. Cui. Optogenetic control of molecular motors and organelle distributions in cells. *Chemistry & Biology*, 22(5):671–82, 2015.

[208] E. R. Ballister, S. Ayloo, D. M. Chenoweth, M. A. Lampson, and E. L. Holzbaur. Optogenetic control of organelle transport using a photocaged chemical inducer of dimerization. *Curr Biol*, 25(10):R407–8, 2015.

[209] H. Haruki, J. Nishikawa, and U. K. Laemmli. The anchor-away technique: rapid, conditional establishment of yeast mutant phenotypes. *Mol Cell*, 31(6):925–32, 2008.

[210] M. S. Robinson and J. Hirst. Rapid inactivation of proteins by knocksideways. *Curr Protoc Cell Biol*, 61:15 20 1–7, 2013.

[211] P. Schaughency, J. Merran, and J. L. Corden. Genome-wide mapping of yeast RNA polymerase II termination. *PLoS Genet*, 10(10):e1004632, 2014.

[212] H. G. Suresh, A. X. da Silveira Dos Santos, W. Kukulski, J. Tyedmers, H. Riezman, B. Bukau, and A. Mogk. Prolonged starvation drives reversible sequestration of lipid biosynthetic enzymes and organelle reorganization in Saccharomyces cerevisiae. *Mol Biol Cell*, 26(9):1601–15, 2015.

[213] T. Nguyen, H. Fischl, F. S. Howe, R. Woloszczuk, A. Serra Barros, Z. Xu, D. Brown, S. C. Murray, S. Haenni, J. M. Halstead, L. O'Connor, G. Shipkovenska, L. M. Steinmetz, and J. Mellor. Transcription mediated insulation and interference direct gene cluster expression switches. *Elife*, 3:e03635, 2014.

[214] M. Kalantzaki, E. Kitamura, T. Zhang, A. Mino, B. Novak, and T. U. Tanaka. Kinetochore-microtubule error correction is driven by differentially regulated interaction modes. *Nat Cell Biol*, 17(4):421–33, 2015.

[215] C. Jeronimo, S. Watanabe, C. D. Kaplan, C. L. Peterson, and F. Robert. The Histone Chaperones FACT and Spt6 Restrict H2A.Z from Intragenic Locations. *Mol Cell*, 58(6):1113–23, 2015.

[216] L. P. Cheeseman, E. F. Harry, A. D. McAinsh, I. A. Prior, and S. J. Royle. Specific removal of TACC3-ch-TOG-clathrin at metaphase deregulates kinetochore fiber tension. *J Cell Sci*, 126(Pt 9):2102–13, 2013.

[217] J. Hirst, G. H. Borner, R. Antrobus, A. A. Peden, N. A. Hodson, D. A. Sahlender, and M. S. Robinson. Distinct and overlapping roles for AP-1 and GGAs revealed by the "knocksideways" system. *Curr Biol*, 22(18):1711–6, 2012.

[218] S. J. Meltzer. *PCR in Bioanalysis*. Humana Press, 1998.

[219] S. Mathupala and A. A. Sloan. An agarose-based cloning-ring anchoring method for isolation of viable cell clones. *Biotechniques*, 46(4):305–7, 2009.

[220] D. Mattanovich and N. Borth. Applications of cell sorting in biotechnology. *Microbial Cell Factories*, 5(1):1–11, 2006.

[221] M. M. Bradford. A rapid and sensitive method for the quantitation of microgram quantities of protein utilizing the principle of protein-dye binding. *Analytical Biochemistry*, 72(1):248–254, 1976.

[222] P. Jiang and N. Mizushima. LC3- and p62-based biochemical methods for the analysis of autophagy progression in mammalian cells. *Methods*, 75:13–8, 2015.

[223] T. Mahmood and P. C. Yang. Western blot: technique, theory, and trouble shooting. *N Am J Med Sci*, 4(9):429–34, 2012.

[224] S. W. Paddock. *Confocal Microscopy - Methods and Protocols*, volume 122. Humana Press, 2014.

[225] C. A. Schneider, W. S. Rasband, and K. W. Eliceiri. NIH Image to ImageJ: 25 years of image analysis. *Nat Methods*, 9(7):671–5, 2012.

[226] S. Kametaka, T. Okano, M. Ohsumi, and Y. Ohsumi. Apg14p and Apg6/Vps30p Form a Protein Complex Essential for Autophagy in the Yeast, Saccharomyces cerevisiae. *Journal of Biological Chemistry*, 273(35):22284–22291, 1998.

[227] A. Kihara, T. Noda, N. Ishihara, and Y. Ohsumi. Two distinct Vps34 phosphatidylinositol 3-kinase complexes function in autophagy and carboxypeptidase Y sorting in Saccharomyces cerevisiae. *J Cell Biol*, 152(3):519–30, 2001.

[228] K. Matsunaga, T. Saitoh, K. Tabata, H. Omori, T. Satoh, N. Kurotori, I. Maejima, K. Shirahama-Noda, T. Ichimura, T. Isobe, S. Akira, T. Noda, and T. Yoshimori. Two Beclin 1-binding proteins, Atg14L and Rubicon, reciprocally regulate autophagy at different stages. *Nat Cell Biol*, 11(4):385–96, 2009.

[229] Y. Zhong, Q. J. Wang, X. Li, Y. Yan, J. M. Backer, B. T. Chait, N. Heintz, and Z. Yue. Distinct regulation of autophagic activity by Atg14L and Rubicon associated with Beclin 1-phosphatidylinositol-3-kinase complex. *Nat Cell Biol*, 11(4):468–76, 2009.

[230] Q. Sun, W. Fan, K. Chen, X. Ding, S. Chen, and Q. Zhong. Identification of Barkor as a mammalian autophagy-specific factor for Beclin 1 and class III phosphatidylinositol 3-kinase. *Proc Natl Acad Sci U S A*, 105(49):19211–6, 2008.

[231] S. Baskaran, L. A. Carlson, G. Stjepanovic, L. N. Young, J. Kim do, P. Grob, R. E. Stanley, E. Nogales, and J. H. Hurley. Architecture and dynamics of the autophagic phosphatidylinositol 3-kinase complex. *Elife*, 3(e05115), 2014.

[232] C. Otomo, Z. Metlagel, G. Takaesu, and T. Otomo. Structure of the human ATG12 ATG5 conjugate required for LC3 lipidation in autophagy. *Nat Struct Mol Biol*, 20(1):59–66, 2013.

[233] H. C. Dooley, M. Razi, H. E. J. Polson, S.E. Girardin, M.I. Wilson, and S.A. Tooze. WIPI2 Links LC3 Conjugation with PI3P, Autophagosome Formation, and Pathogen Clearance by Recruiting Atg12-5-16L1. *Molecular Cell*, 55(2):238–252, 2014.

[234] M. Uhlen, P. Oksvold, L. Fagerberg, E. Lundberg, K. Jonasson, M. Forsberg, M. Zwahlen, C. Kampf, K. Wester, S. Hober, H. Wernerus, L. Bjorling, and F. Ponten. Towards a knowledge-based Human Protein Atlas. *Nat Biotech*, 28(12):1248–1250, 2010.

[235] M. Uhlen, L. Fagerberg, B. o. r. M. Hallström, C. Lindskog, P. Oksvold, A. Mardinoglu, A. Sivertsson, C. Kampf, E. Sjöstedt, A. Asplund, I. Olsson, K. Edlund, E. Lundberg, S. Navani, C. A.-K. Szigyarto, J. Odeberg, D. Djureinovic, J. O. Takanen, S. Hober, T. Alm, P.-H. Edqvist, H. Berling, H. Tegel, J. Mulder, J. Rockberg, P. Nilsson, J. M. Schwenk, M. Hamsten, K. von Feilitzen, M. Forsberg, L. Persson, F. Johansson, M. Zwahlen, G. von Heijne, J. Nielsen, and F. Ponten. Tissue-based map of the human proteome. *Science*, 347(6220):1260419, 2015.

[236] U. Schnell, F. Dijk, K. A. Sjollema, and B. N. G. Giepmans. Immunolabeling artifacts and the need for live-cell imaging. *Nat Meth*, 9(2):152–158, 2012.

[237] A. I. Fogel, B. J. Dlouhy, C. Wang, S. W. Ryu, A. Neutzner, S. A. Hasson, D. P. Sideris, H. Abeliovich, and R. J. Youle. Role of membrane association and Atg14-dependent phosphorylation in beclin-1-mediated autophagy. *Mol Cell Biol*, 33(18):3675–88, 2013.

[238] W. Huang, W. Choi, W. Hu, N. Mi, Q. Guo, M. Ma, M. Liu, Y. Tian, P. Lu, F. L. Wang, H. Deng, L. Liu, N. Gao, L. Yu, and Y. Shi. Crystal structure and biochemical analyses reveal Beclin 1 as a novel membrane binding protein. *Cell Res*, 22(3):473–89, 2012.

[239] S. Muyldermans. Nanobodies: natural single-domain antibodies. *Annu Rev Biochem*, 82:775–97, 2013.

[240] C. Deffar, H. Shi, L. Li, X. Wang, and X. Zhu. Nanobodies - the new concept in antibody engineering. *African Journal of Biotechnology*, 8(12):2645–2652, 2009.

[241] E. Pardon, T. Laeremans, S. Triest, S. G. Rasmussen, A. Wohlkonig, A. Ruf, S. Muyldermans, W. G. Hol, B. K. Kobilka, and J. Steyaert. A general protocol for the generation of Nanobodies for structural biology. *Nat Protoc*, 9(3):674–93, 2014.

[242] N. Mizushima, T. Yoshimori, and B. Levine. Methods in Mammalian Autophagy Research. *Cell*, 140(3):313–326, 2010.

[243] E. Itakura and N. Mizushima. Characterization of autophagosome formation site by a hierarchical analysis of mammalian Atg proteins. *Autophagy*, 6(6):764–76, 2010.

[244] Y. T. Wu, H. L. Tan, G. Shui, C. Bauvy, Q. Huang, M. R. Wenk, C. N. Ong, P. Codogno, and H. M. Shen. Dual role of 3-methyladenine in modulation of autophagy via different temporal patterns of inhibition on class I and III phosphoinositide 3-kinase. *J Biol Chem*, 285(14):10850–61, 2010.

[245] E. F. Blommaart, U. Krause, J. P. Schellens, H. Vreeling-Sindelarova, and A. J. Meijer. The phosphatidylinositol 3-kinase inhibitors wortmannin and LY294002 inhibit autophagy in isolated rat hepatocytes. *Eur J Biochem*, 243(1-2):240–6, 1997.

[246] A. Petiot, E. Ogier-Denis, E. F. C. Blommaart, A. J. Meijer, and P. Codogno. Distinct Classes of Phosphatidylinositol 3'-Kinases Are Involved in Signaling Pathways That Control Macroautophagy in HT-29 Cells. *Journal of Biological Chemistry*, 275(2):992–998, 2000.

[247] M. Kim, J. Fekadu, E. Maronde, and A. Rami. Alleviation of autophagy by knockdown of Beclin-1 enhances susceptibility of hippocampal neurons to proapoptotic signals induced by amino acid starvation. *Histochem Cell Biol*, 139(1):99–108, 2013.

[248] S. Xing, Y. Zhang, J. Li, J. Zhang, Y. Li, C. Dang, C. Li, Y. Fan, J. Yu, Z. Pei, and J. Zeng. Beclin 1 knockdown inhibits autophagic activation and prevents the secondary neurodegenerative damage in the ipsilateral thalamus following focal cerebral infarction. *Autophagy*, 8(1):63–76, 2012.

[249] T. Proikas-Cezanne, Z. Takacs, P. DÃ¶nnes, and O. Kohlbacher. WIPI proteins: essential PtdIns3 effectors at the nascent autophagosome. *Journal of Cell Science*, 128(2):207–217, 2015.

[250] E. Karanasios, E. Stapleton, M. Manifava, and N. T. Ktistakis. *Imaging Autophagy*, volume 69, book section 12.34, pages 1–16. John Wiley & Sons, Inc., 2001.

[251] K. Devereaux, C. Dall'Armi, A. Alcazar-Roman, Y. Ogasawara, X. Zhou, F. Wang, A. Yamamoto, P. De Camilli, and G. Di Paolo. Regulation of Mammalian Autophagy by Class II and III PI 3-Kinases through PI3P Synthesis. *PLoS One*, 8(10):e76405, 2013.

[252] H. E. Polson, J. de Lartigue, D. J. Rigden, M. Reedijk, S. Urbe, M. J. Clague, and S. A. Tooze. Mammalian Atg18 (WIPI2) localizes to omegasome-anchored phagophores and positively regulates LC3 lipidation. *Autophagy*, 6(4):506–22, 2010.

[253] J. Kim, Y. C. Kim, C. Fang, R. C. Russell, J. H. Kim, W. Fan, R. Liu, Q. Zhong, and K. L. Guan. Differential regulation of distinct Vps34 complexes by AMPK in nutrient stress and autophagy. *Cell*, 152(1-2):290–303, 2013.

[254] B. Ma, W. Cao, W. Li, C. Gao, Z. Qi, Y. Zhao, J. Du, H. Xue, J. Peng, J. Wen, H. Chen, Y. Ning, L. Huang, H. Zhang, X. Gao, L. Yu, and Y.-G. Chen. Dapper1 promotes autophagy by enhancing the Beclin1-Vps34-Atg14L complex formation. *Cell Research*, 24(8):912–924, 2014.

[255] S. Kimura, T. Noda, and T. Yoshimori. Dissection of the autophagosome maturation process by a novel reporter protein, tandem fluorescent-tagged LC3. *Autophagy*, 3(5):452–60, 2007.

[256] U. Pfeifer. Inhibition by insulin of the formation of autophagic vacuoles in rat liver. A morphometric approach to the kinetics of intracellular degradation by autophagy. *J Cell Biol*, 78(1):152–67, 1978.

[257] N. T. Ktistakis, S. Andrews, and J. Long. What is the advantage of a transient precursor in autophagosome biogenesis? *Autophagy*, 7(1):118–22, 2011.

[258] N. T. Ktistakis, E. Karanasios, and M. Manifava. Dynamics of autophagosome formation: a pulse and a sequence of waves. *Biochem Soc Trans*, 42(5):1389–95, 2014.

[259] F. Reggiori and C. Ungermann. Autophagosome Maturation and Fusion. *Journal of Molecular Biology*, 429(4):486–496, 2017.

[260] N. Nguyen, V. Shteyn, and T. J. Melia. Sensing Membrane Curvature in Macroautophagy. *Journal of Molecular Biology*, 429(4):457–472, 2017.

[261] S. Nath, J. Dancourt, V. Shteyn, G. Puente, W. M. Fong, S. Nag, J. Bewersdorf, A. Yamamoto, B. Antonny, and T. J. Melia. Lipidation of the LC3/GABARAP family of autophagy proteins relies on a membrane-curvature-sensing domain in Atg3. *Nat Cell Biol*, 16(5):415–424, 2014.

[262] N. Fujita, T. Itoh, H. Omori, M. Fukuda, T. Noda, and T. Yoshimori. The Atg16L complex specifies the site of LC3 lipidation for membrane biogenesis in autophagy. *Mol Biol Cell*, 19(5):2092–100, 2008.

[263] Y. Chen and D. J. Klionsky. The regulation of autophagy - unanswered questions. *J Cell Sci*, 124(Pt 2):161–70, 2011.

[264] T. Teitz, M. Penner, D. Eli, M. Stark, M. Bakhanashvili, T. Naiman, and D. Canaani. Isolation by polymerase chain reaction of a cDNA whose product partially complements the ultraviolet sensitivity of xeroderma pigmentosum group C cells. *Gene*, 87(2):295–8, 1990.

[265] B. Perelman, N. Dafni, T. Naiman, D. Eli, M. Yaakov, T. L. Feng, S. Sinha, G. Weber, S. Khodaei, A. Sancar, I. Dotan, and D. Canaani. Molecular cloning of a novel human gene encoding a 63-kDa protein and its sublocalization within the 11q13 locus. *Genomics*, 41(3):397–405, 1997.

[266] Y. Takahashi, C. L. Meyerkord, T. Hori, K. Runkle, T. E. Fox, M. Kester, T. P. Loughran, and H.-G. Wang. Bif-1 regulates Atg9 trafficking by mediating the fission of Golgi membranes during autophagy. *Autophagy*, 7(1):61–73, 2011.

[267] M. J. Munson, G. F. Allen, R. Toth, D. G. Campbell, J. M. Lucocq, and I. G. Ganley. mTOR activates the VPS34-UVRAG complex to regulate autolysosomal tubulation and cell survival. *EMBO J*, 34(17):2272–90, 2015.

[268] S. D. Pirooz, S. He, T. Zhang, X. Zhang, Z. Zhao, S. Oh, D. O'Connell, P. Khalilzadeh, S. Amini-Bavil-Olyaee, M. Farzan, and C. Liang. UVRAG is required for virus entry through combinatorial interaction with the class C-Vps complex and SNAREs. *Proc Natl Acad Sci U S A*, 111(7):2716–21, 2014.

[269] X. Li, L. He, K. H. Che, S. F. Funderburk, L. Pan, N. Pan, M. Zhang, Z. Yue, and Y. Zhao. Imperfect interface of Beclin1 coiled-coil domain regulates homodimer and heterodimer formation with Atg14L and UVRAG. *Nat Commun*, 3:662, 2012.

[270] L. L. Fu, Y. Cheng, and B. Liu. Beclin-1: autophagic regulator and therapeutic target in cancer. *Int J Biochem Cell Biol*, 45(5):921–4, 2013.

[271] N. Furuya, J. Yu, M. Byfield, S. Pattingre, and B. Levine. The evolutionarily conserved domain of Beclin 1 is required for Vps34 binding, autophagy and tumor suppressor function. *Autophagy*, 1(1):46–52, 2005.

[272] Q. Sun, J. Zhang, W. Fan, K. N. Wong, X. Ding, S. Chen, and Q. Zhong. The RUN domain of rubicon is important for hVps34 binding, lipid kinase inhibition, and autophagy suppression. *J Biol Chem*, 286(1):185–91, 2011.

[273] Y.-M. Kim, C. H. Jung, M. Seo, E. K. Kim, J.-M. Park, S.S. Bae, and D.-H. Kim. mTORC1 Phosphorylates UVRAG to Negatively Regulate Autophagosome and Endosome Maturation. *Molecular Cell*, 57(2):207–218, 2015.

[274] S. Nakamura and T. Yoshimori. New insights into autophagosome-lysosome fusion. *Journal of Cell Science*, 130:1209–1216, 2017.

[275] M. G. Gutierrez, D. B. Munafo, W. Beron, and M. I. Colombo. Rab7 is required for the normal progression of the autophagic pathway in mammalian cells. *Journal of Cell Science*, 117(13):2687–2697, 2004.

[276] S. Jäger, C. Bucci, I. Tanida, T. Ueno, E. Kominami, P. Saftig, and E.-L. Eskelinen. Role for Rab7 in maturation of late autophagic vacuoles. *Journal of Cell Science*, 117(20):4837–4848, 2004.

[277] R. H. Wijdeven, H. Janssen, L. Nahidiazar, L. Janssen, K. Jalink, I. Berlin, and J. Neefjes. Cholesterol and ORP1L-mediated ER contact sites control autophagosome transport and fusion with the endocytic pathway. *Nature Communications*, 7:11808, 2016.

[278] I. Jordens, M. Fernandez-Borja, M. Marsman, S. Dusseljee, L. Janssen, J. Calafat, H. Janssen, R. Wubbolts, and J. Neefjes. The Rab7 effector protein RILP controls lysosomal transport by inducing the recruitment of dynein-dynactin motors. *Current Biology*, 11(21):1680–1685, 2001.

[279] E. Itakura, C. Kishi-Itakura, and N. Mizushima. The Hairpin-type Tail-Anchored SNARE Syntaxin 17 Targets to Autophagosomes for Fusion with Endosomes/Lysosomes. *Cell*, 151(6):1256–1269, 2012.

[280] P. Jiang, T. Nishimura, Y. Sakamaki, E. Itakura, T. Hatta, T. Natsume, and N. Mizushima. The HOPS complex mediates autophagosome-lysosome fusion through interaction with syntaxin 17. *Molecular Biology of the Cell*, 25(8):1327–1337, 2014.

[281] J. Diao, R. Liu, Y. Rong, M. Zhao, J. Zhang, Y. Lai, Q. Zhou, L. M. Wilz, J. Li, S. Vivona, R. A. Pfuetzner, A. T. Brunger, and Q. Zhong. ATG14 promotes membrane tethering and fusion of autophagosomes to endolysosomes. *Nature*, 520(7548):563–566, 2015.

[282] Z. Wang, G. Miao, X. Xue, X. Guo, C. Yuan, Z. Wang, G. Zhang, Y. Chen, D. Feng, J. Hu, and H. Zhang. The Vici Syndrome Protein EPG5 Is a Rab7 Effector that Determines the Fusion Specificity of Autophagosomes with Late Endosomes/Lysosomes. *Molecular Cell*, 63(5):781–795, 2016.

[283] D. Chen, W. Fan, Y. Lu, X. Ding, S. Chen, and Q. Zhong. A Mammalian Autophagosome Maturation Mechanism Mediated by TECPR1 and the Atg12-Atg5 Conjugate. *Molecular Cell*, 45(5):629–641, 2012.

[284] M. J. Elrick, T. Yu, C. Chung, and A. P. Lieberman. Impaired proteolysis underlies autophagic dysfunction in Niemann-Pick type C disease. *Human Molecular Genetics*, 21(22):4876–4887, 2012.

[285] Y. Takahashi, D. Coppola, N. Matsushita, H. D. Cualing, M. Sun, Y. Sato, C. Liang, J. U. Jung, J. Q. Cheng, J. J. Mule, W. J. Pledger, and H. G. Wang. Bif-1 interacts with Beclin 1 through UVRAG and regulates autophagy and tumorigenesis. *Nat Cell Biol*, 9(10):1142–51, 2007.

[286] Y. Takahashi, N. Tsotakos, Y. Liu, M. M. Young, J. Serfass, Z. Tang, T. Abraham, and H.-G. Wang. The Bif-1-Dynamin 2 membrane fission machinery regulates Atg9-containing vesicle generation at the Rab11-positive reservoirs. *Oncotarget*, 7(15):20855–20868, 2016.

[287] M. Graef, J. R. Friedman, C. Graham, M. Babu, and J. Nunnari. ER exit sites are physical and functional core autophagosome biogenesis components. *Molecular Biology of the Cell*, 24(18):2918–2931, 2013.

[288] P. K. Kim, C. Hollerbach, W. S. Trimble, B. Leber, and D. W. Andrews. Identification of the Endoplasmic Reticulum Targeting Signal in Vesicle-associated Membrane Proteins. *Journal of Biological Chemistry*, 274(52):36876–36882, 1999.

[289] H. P. Hauri, F. Kappeler, H. Andersson, and C. Appenzeller. ERGIC-53 and traffic in the secretory pathway. *J Cell Sci*, 113 (Pt 4):587–96, 2000.

[290] A. D. Linstedt and H. P. Hauri. Giantin, a novel conserved Golgi membrane protein containing a cytoplasmic domain of at least 350 kDa. *Molecular Biology of the Cell*, 4(7):679–693, 1993.

[291] S. Pistor, T. Chakraborty, K. Niebuhr, E. Domann, and J. Wehland. The ActA protein of Listeria monocytogenes acts as a nucleator inducing reorganization of the actin cytoskeleton. *The EMBO Journal*, 13(4):758–763, 1994.

[292] R. C. Russell, Y. Tian, H. Yuan, H. W. Park, Y. Y. Chang, J. Kim, H. Kim, T. P. Neufeld, A. Dillin, and K. L. Guan. ULK1 induces autophagy by phosphorylating Beclin-1 and activating VPS34 lipid kinase. *Nat Cell Biol*, 15(7):741–50, 2013.

[293] M. Mari, S. A. Tooze, and F. Reggiori. The puzzling origin of the autophagosomal membrane. *F1000 Biology Reports*, 3:25, 2011.

[294] E. Y. W. Chan, S. Kir, and S. A. Tooze. siRNA Screening of the Kinome Identifies ULK1 as a Multidomain Modulator of Autophagy. *Journal of Biological Chemistry*, 282(35):25464–25474, 2007.

[295] E.-J. Lee and C. Tournier. The requirement of uncoordinated 51-like kinase 1 (ULK1) and ULK2 in the regulation of autophagy. *Autophagy*, 7(7):689–695, 2011.

[296] H. Cheong, T. Lindsten, J. Wu, C. Lu, and C. B. Thompson. Ammonia-induced autophagy is independent of ULK1/ULK2 kinases. *Proceedings of the National Academy of Sciences*, 108(27):11121–11126, 2011.

[297] F. McAlpine, L. E. Williamson, S. A. Tooze, and E. Y. W. Chan. Regulation of nutrient-sensitive autophagy by uncoordinated 51-like kinases 1 and 2. *Autophagy*, 9(3):361–373, 2013.

[298] J. Calvo-Garrido, J. S. King, S. Munoz-Braceras, and R. Escalante. Vmp1 regulates PtdIns3P signaling during autophagosome formation in Dictyostelium discoideum. *Traffic*, 15(11):1235–46, 2014.

[299] M. I. Molejon, A. Ropolo, A. L. Re, V. Boggio, and M. I. Vaccaro. The VMP1-Beclin 1 interaction regulates autophagy induction. *Sci Rep*, 3:1055, 2013.

Appendices

A Methods and Materials

A.1 ImageJ Macros

A.1.1 EGFP Puncta Count

```
macro "EGFP Puncta Count [F5]" {
run("Bio-Formats");
dir = getDirectory("Choose an output directory");
path = dir;
MergeDir = path + "Merge" + File.separator;
File.makeDirectory(MergeDir);
setBatchMode(true);
ids=newArray(nImages);
for (i=0;i<nImages;i++) {
           selectImage(i+1);
       title = getImageID;
       ids[i]=getImageID;
       saveAs("tif", MergeDir+title);
           path = dir;
           ROIDir = path + "ROI" + File.separator;
           File.makeDirectory(ROIDir);
           path = dir;
           ResultsDir = path + "Results" + File.separator;
           File.makeDirectory(ResultsDir);}
setBatchMode(false);
imgArray = newArray(nImages);
for (i=0; i<nImages; i++) {
           selectImage(i+1);
           imgArray[i] = getImageID();}
for (i=0; i< imgArray.length; i++) {
           selectImage(imgArray[i]);
           myImageID = getImageID();
           setTool("freehand");
           waitForUser("Selection", "Select ROI, then click OK.");
           selectImage(myImageID);
           run("Make Inverse");
           run("Set...", "value=NaN");
           getNumber("How many cells?", 0);
           newDir = ROIDir;
           selectImage(myImageID);
           title = getTitle;
```

```
            saveAs("tif", newDir+title);
            run("Close");}
setBatchMode(true);
path = ROIDir
filename = getFileList(path);
for (i=0; i<filename.length; i++) {
        if(endsWith(filename[i], ".tif")) {
        open(path+filename[i]);
            run("Split Channels");}}
path = dir
newDir = path + "Split" + File.separator;
File.makeDirectory(newDir);
ids=newArray(nImages);
for (i=0;i<nImages;i++) {
        selectImage(i+1);
        title = getTitle;
        saveAs("tif", newDir+title);}
run("Close All");
setBatchMode(false);
list=getFileList(newDir);
for(i=0;i<list.length;i++){
            showProgress(i+1, list.length);
            filename = newDir + list[i];
            if(endsWith(list[i],".tif")&&indexOf(list[i],"C2")>=0){
            open(filename);}}
imgArray = newArray(nImages);
for (i=0; i<nImages; i++) {
            selectImage(i+1);
            imgArray[i] = getImageID();}
for (i=0; i< imgArray.length; i++) {
            selectImage(imgArray[i]);
            myImageID = getImageID();
            run("Threshold...");
            waitForUser("Threshold", "Set threshold to select CELL AREA, then click OK.");
            selectImage(myImageID);
            rename("Cell Area");
            run("Analyze Particles...", "size=300-Infinity pixel circularity=0.00-1.00
                show=[Overlay Outlines] display summarize");
            selectImage(myImageID);}
dir = ResultsDir;
selectWindow("Summary");
saveAs("Text", dir +"Cell Area.txt");
selectWindow("Cell Area.txt");
run("Close All");
list=getFileList(newDir);
for(i=0;i<list.length;i++){
            showProgress(i+1, list.length);
            filename = newDir + list[i];
```

```
            if(endsWith(list[i],".tif")&&indexOf(list[i],"C2")>=0){
            open(filename);}}
imgArray = newArray(nImages);
for (i=0; i<nImages; i++) {
            selectImage(i+1);
            imgArray[i] = getImageID();}
for (i=0; i< imgArray.length; i++) {
            selectImage(imgArray[i]);
            myImageID = getImageID();
            run("Threshold...");
            waitForUser("Threshold", "Set threshold to select GREEN PUNCTA AREA, then
                click OK.");
            selectImage(myImageID);
            name = getTitle;
            rename("Green Puncta Area");
            run("Analyze Particles...", "size=3-Infinity pixel circularity=0.00-1.00
                show=[Overlay Outlines] display summarize");}
dir = ResultsDir;
selectWindow("Summary");
saveAs("Text", dir +"Green Puncta Area.txt");
selectWindow("Green Puncta Area.txt");
selectWindow("Results");
run("Close");
run("Close All");
selectWindow("Log");
saveAs("Text", dir +"Cell Number.txt")}
```

A.1.2 mCherry-EGFP Puncta Count

```
macro "mCherry-EGFP Puncta Count [F6]"{
run("Bio-Formats");
dir = getDirectory("Choose an output directory");
path = dir;
MergeDir = path + "Merge" + File.separator;
File.makeDirectory(MergeDir);
setBatchMode(true);
ids=newArray(nImages);
for (i=0;i<nImages;i++) {
        selectImage(i+1);
        title = getImageID;
        ids[i]=getImageID;
        saveAs("tif", MergeDir+title);
            path = dir;
            MaskGreenDir = path + "MaskGreen" + File.separator;
            File.makeDirectory(MaskGreenDir);
            path = dir;
            ROIDir = path + "ROI" + File.separator;
```

```
            File.makeDirectory(ROIDir);
            path = dir;
            AlignedDir = path + "Aligned" + File.separator;
            File.makeDirectory(AlignedDir);
            path = dir;
            ResultsDir = path + "Results" + File.separator;
            File.makeDirectory(ResultsDir);
            path = dir;
            Masks2Dir = path + "Masks2" + File.separator;
            File.makeDirectory(Masks2Dir);}
setBatchMode(false);
imgArray = newArray(nImages);
for (i=0; i<nImages; i++) {
            selectImage(i+1);
            imgArray[i] = getImageID();}
for (i=0; i< imgArray.length; i++) {
            selectImage(imgArray[i]);
            myImageID = getImageID();
            setTool("freehand");
            waitForUser("Selection", "Select ROI, then click OK.");
            selectImage(myImageID);
            run("Make Inverse");
            run("Set...", "value=NaN");
            getNumber("How many cells?", 0);
            newDir = ROIDir;
            selectImage(myImageID);
            title = getTitle;
            saveAs("tif", newDir+title);
            run("Close");}
dir1 = ROIDir;
list = getFileList(dir1);
for (i=0; i<list.length; i++) {
            showProgress(i+1, list.length);
            filename = dir1 + list[i];
            if (endsWith(filename, "tif")) {
            run("Bio-Formats", "open=filename autoscale color_mode=Default view=Hyperstack
                stack_order=XYCZT");}}
imgArray = newArray(nImages);
for (i=0; i<nImages; i++) {
            selectImage(i+1);
            imgArray[i] = getImageID();}
for (i=0; i< imgArray.length; i++) {
            selectImage(imgArray[i]);
            myImageID = getImageID();
            run("StackReg ", "transformation=[Rigid Body]");
            newDir = AlignedDir;
            selectImage(myImageID);
            title = getTitle;
```

```
            saveAs("tif", newDir+title);
            run("Close");}
setBatchMode(true);
path = AlignedDir
filename = getFileList(path);
for (i=0; i<filename.length; i++) {
        if(endsWith(filename[i], ".tif")) {
        open(path+filename[i]);
            run("Split Channels");}}
path = dir
newDir = path + "Split" + File.separator;
File.makeDirectory(newDir);
ids=newArray(nImages);
for (i=0;i<nImages;i++) {
        selectImage(i+1);
        title = getTitle;
        saveAs("tif", newDir+title);}
run("Close All");
setBatchMode(false);
list=getFileList(newDir);
for(i=0;i<list.length;i++){
            showProgress(i+1, list.length);
            filename = newDir + list[i];
            if(endsWith(list[i],".tif")&&indexOf(list[i],"C2")>=0){
            open(filename);}}
imgArray = newArray(nImages);
for (i=0; i<nImages; i++) {
            selectImage(i+1);
            imgArray[i] = getImageID();}
for (i=0; i< imgArray.length; i++) {
            selectImage(imgArray[i]);
            myImageID = getImageID();
            run("Threshold...");
            waitForUser("Threshold", "Set threshold to select CELL AREA, then click OK.");
            selectImage(myImageID);
            rename("Cell Area");
            run("Analyze Particles...", "size=300-Infinity pixel circularity=0.00-1.00
                show=[Overlay Outlines] display summarize");
            selectImage(myImageID);}
dir = ResultsDir;
selectWindow("Summary");
saveAs("Text", dir +"Cell Area.txt");
selectWindow("Cell Area.txt");
run("Close");
run("Close All");
list=getFileList(newDir);
for(i=0;i<list.length;i++){
            showProgress(i+1, list.length);
```

```
            filename = newDir + list[i];
            if(endsWith(list[i],".tif")&&indexOf(list[i],"C2")>=0){
            open(filename);}}
imgArray = newArray(nImages);
for (i=0; i<nImages; i++) {
            selectImage(i+1);
            imgArray[i] = getImageID();}
for (i=0; i< imgArray.length; i++) {
            selectImage(imgArray[i]);
            myImageID = getImageID();
            run("Threshold...");
            waitForUser("Threshold", "Set threshold to select GREEN PUNCTA AREA, then
                click OK.");
            selectImage(myImageID);
            name = getTitle;
            rename("Green Puncta Area");
            run("Analyze Particles...", "size=3-Infinity pixel circularity=0.00-1.00
                show=[Overlay Outlines] display summarize");
            run("Convert to Mask");
            rename(name);}
// get image IDs of all open images
dir = Masks2Dir;
ids=newArray(nImages);
for (i=0;i<nImages;i++) {
            selectImage(i+1);
            name = getTitle;
        ids[i]=getImageID;
        saveAs("tiff", dir + name);}
run("Close All");
list=getFileList(newDir);
for(i=0;i<list.length;i++){
            showProgress(i+1, list.length);
            filename = newDir + list[i];
            if(endsWith(list[i],".tif")&&indexOf(list[i],"C1")>=0){
            open(filename);}}
// get image IDs of all open images
dir = Masks2Dir;
ids=newArray(nImages);
for (i=0;i<nImages;i++) {
        selectImage(i+1);
            name = getTitle;
        ids[i]=getImageID;
        saveAs("tiff", dir + name);}
dir = ResultsDir;
selectWindow("Summary");
saveAs("Text", dir +"Green Puncta Area.txt");
selectWindow("Green Puncta Area.txt");
run("Close");
```

```
run("Close All");
nucleiName = "C1";
cytoplasmName = "C2";
inputFolder = Masks2Dir;
var allImages;
allImages = getFileList(inputFolder);
var numberOfImages = 0;
numberOfImages = countNucleiImages();
nucleiImages = getImagesContaining(nucleiName);
function countNucleiImages() {
count = 0;
for(i=0; i<allImages.length; i++) {
           if (indexOf(allImages[i], nucleiName) !=-1 )
           count++;}
return count;}
function getImagesContaining(text) {
result = newArray(numberOfImages);
index = 0;
for (i=0; i<allImages.length; i++) {
           if (indexOf(allImages[i], text) != -1) {
           result[index] = allImages[i];
           index++;}}
return result;}
for (i=0; i<nucleiImages.length;i++) {
           inputPath = inputFolder + nucleiImages[i];
           open(inputPath);
           rename("Red");
           run("8-bit");
           open(inputFolder + replace(nucleiImages[i], nucleiName, cytoplasmName));
           rename("Green");
           run("8-bit");
           imageCalculator("Subtract create", "Red","Green");
           selectWindow("Green");
           run("Close");
           selectWindow("Red");
           run("Close");}
// get image IDs of all open images
dir = MaskGreenDir;
ids=newArray(nImages);
for (i=0;i<nImages;i++) {
       selectImage(i+1);
           name = getImageID;
       ids[i]=getImageID;
       saveAs("tiff", dir + name);}
run("Close All");
list=getFileList(MaskGreenDir);
for(i=0;i<list.length;i++){
           showProgress(i+1, list.length);
```

```
            filename = MaskGreenDir + list[i];
            if(endsWith(list[i],".tif")>=0){
            open(filename);}}
imgArray = newArray(nImages);
for (i=0; i<nImages; i++) {
            selectImage(i+1);
            imgArray[i] = getImageID();}
for (i=0; i< imgArray.length; i++) {
            selectImage(imgArray[i]);
            myImageID = getImageID();
            run("Threshold...");
            waitForUser("Threshold", "Set threshold to select RED PUNCTA AREA, then click
                OK.");
            selectImage(myImageID);
            name = getTitle;
            rename("Red Puncta Area");
            run("Analyze Particles...", "size=2-Infinity pixel circularity=0.00-1.00
                show=[Overlay Outlines] display summarize");
            selectImage(myImageID);}
run("Close All");
path= ResultsDir;
list=getFileList(path);
for(i=0;i<list.length;i++){
        open(path+list[i]);}
dir = ResultsDir;
selectWindow("Results");
run("Close");
selectWindow("Summary");
saveAs("Text", dir +"Red Puncta Area.txt");
dir = ResultsDir;
selectWindow("Log");
saveAs("Text", dir +"Cell Number.txt")}
```

B Results and Discussion

B.1 Establishing the Knock Off and On Strategy

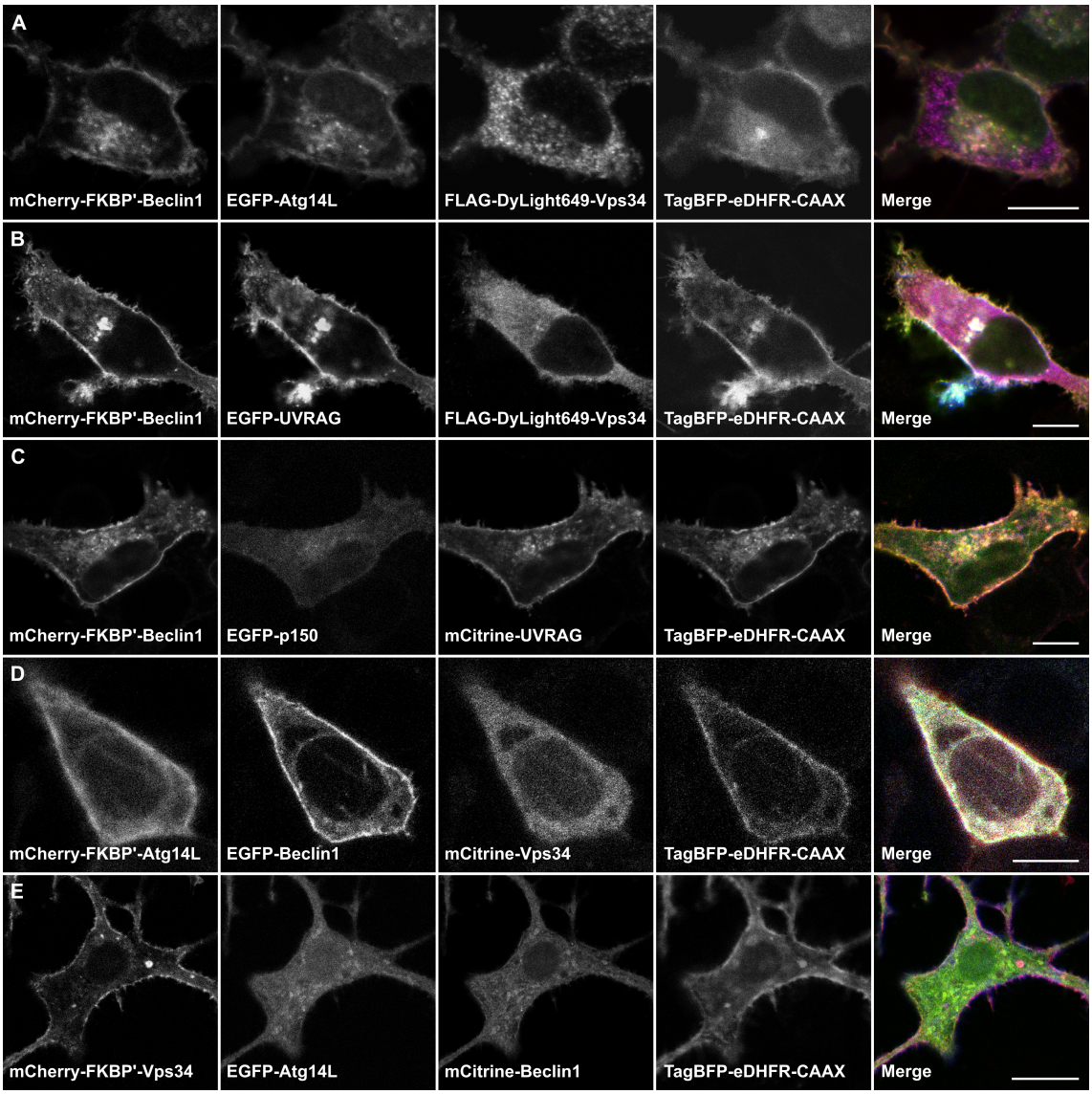

Figure B.1: Co-localization of exogenous autophagy proteins at the plasma membrane of MCF7 cells after 2 hours starvation in EBSS and 30 minutes treatment with SLF'-TMP. Scale bar: 10 µm. **A** FKBP'-Beclin1 attracts Atg14L to the plasma membrane, but not Vps34. **B** FKBP'-Beclin1 and UVRAG co-localize at the plasma membrane, but Vps34 remains cytoplasmic. **C** FKBP'-Beclin1 attracts UVRAG to the plasma membrane, but not p150. **D** Beclin1 is mislocalized to the plasma membrane through interaction with FKBP'-Atg14L, but Vps34 is not attracted. **E** FKBP'-Vps34 cannot serve as a bait for Atg14L or Beclin1.

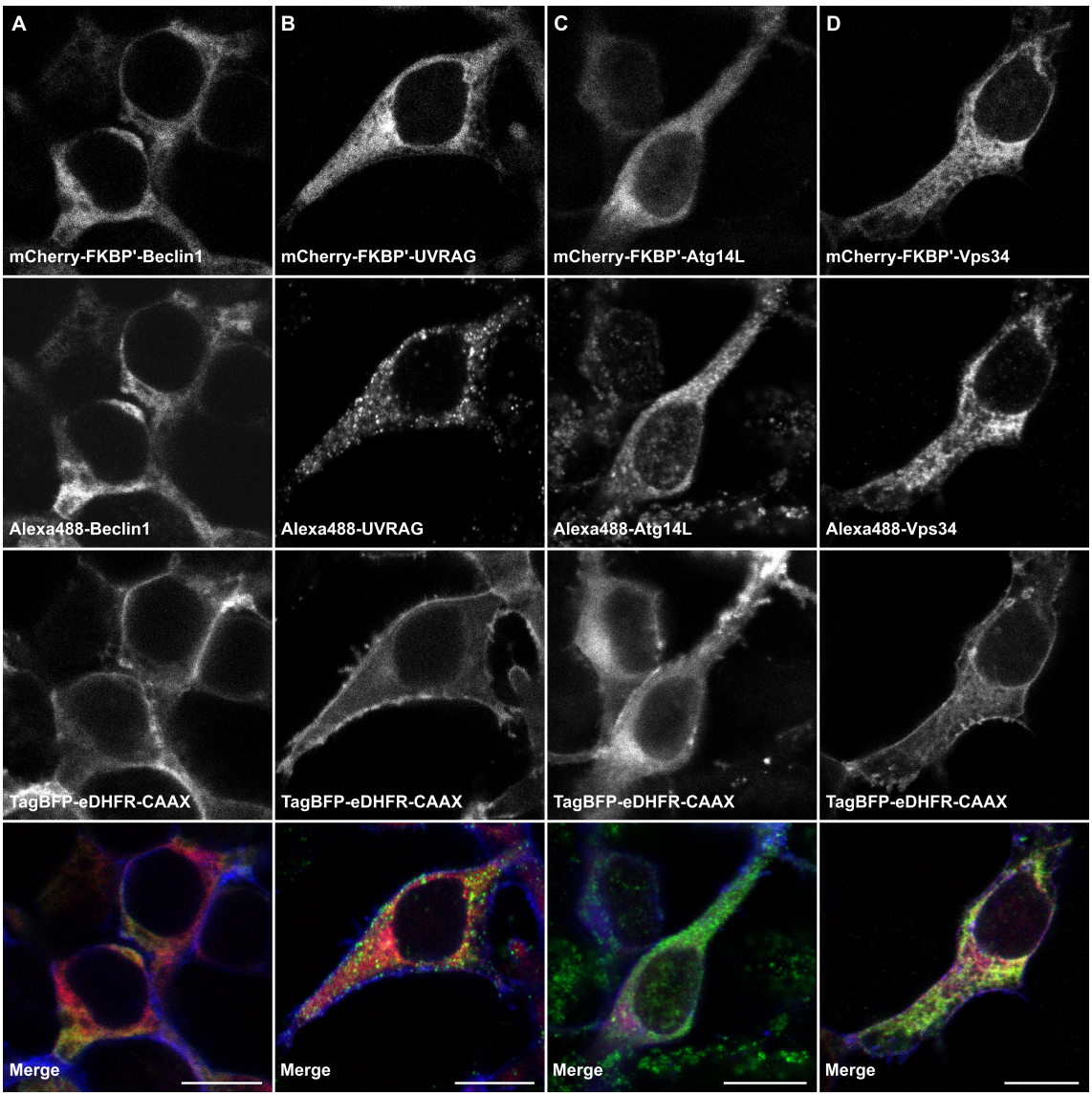

Figure B.2: Co-localization of overexpressed and endogenous PI3K complex proteins at the plasma membrane of HEK293T cells after 1 hour starvation in EBSS. Scale bar: 10 µm. **A** Co-localisation of exogenous and endogenous Beclin1. **B** Co-localisation of exogenous and endogenous UVRAG. **C** Co-localisation of exogenous and endogenous Atg14L. **D** Co-localisation of exogenous and endogenous Vps34.

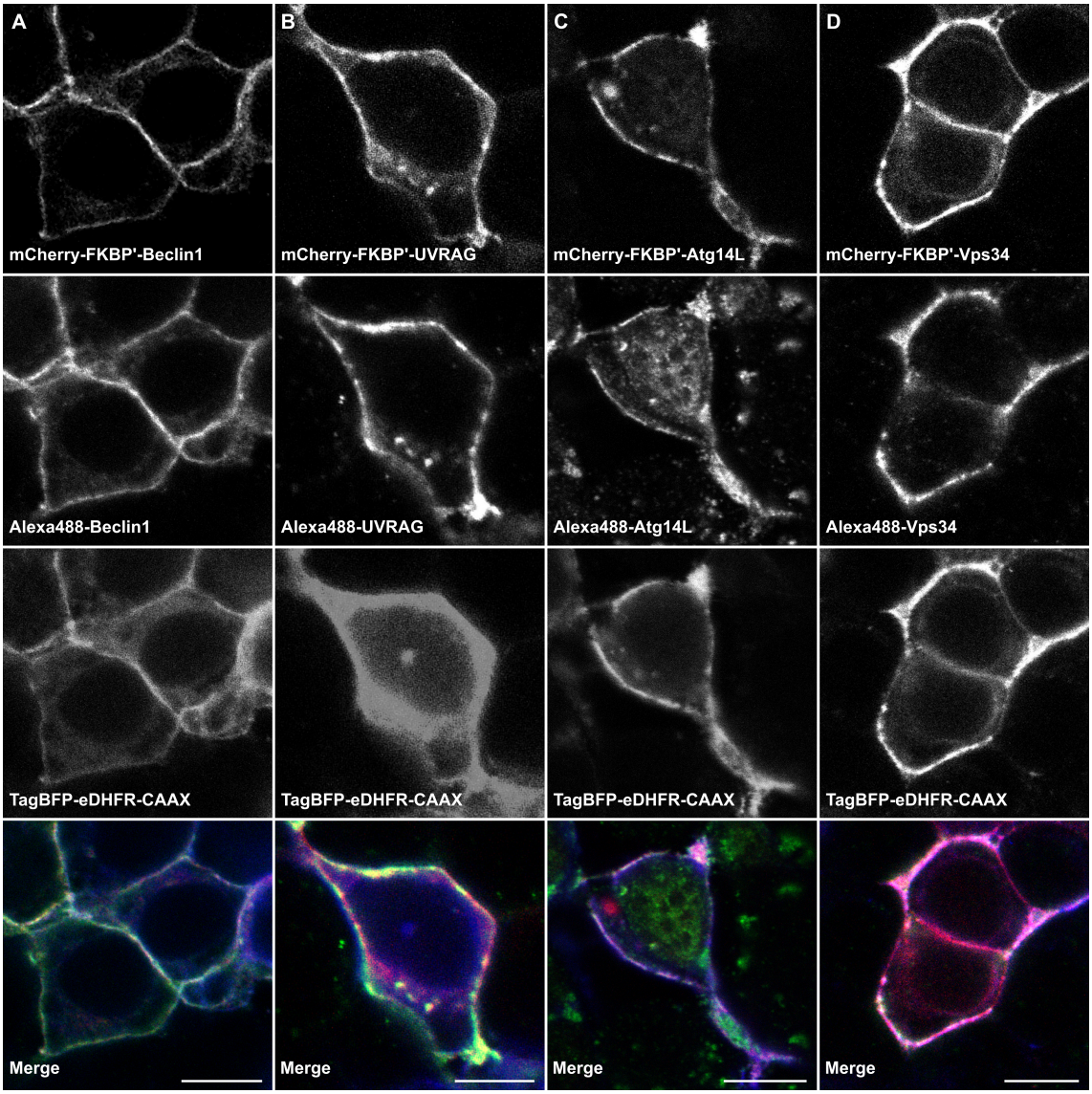

Figure B.3: Co-localization of overexpressed and endogenous PI3K complex proteins at the plasma membrane of HEK293T cells after 1 hour starvation in EBSS and treatment with SLF'-TMP. Scale bar: 10 µm. **A** Co-localisation of exogenous and endogenous Beclin1. **B** Co-localisation of exogenous and endogenous UVRAG. **C** Co-localisation of exogenous and endogenous Atg14L. **D** Co-localisation of exogenous and endogenous Vps34.

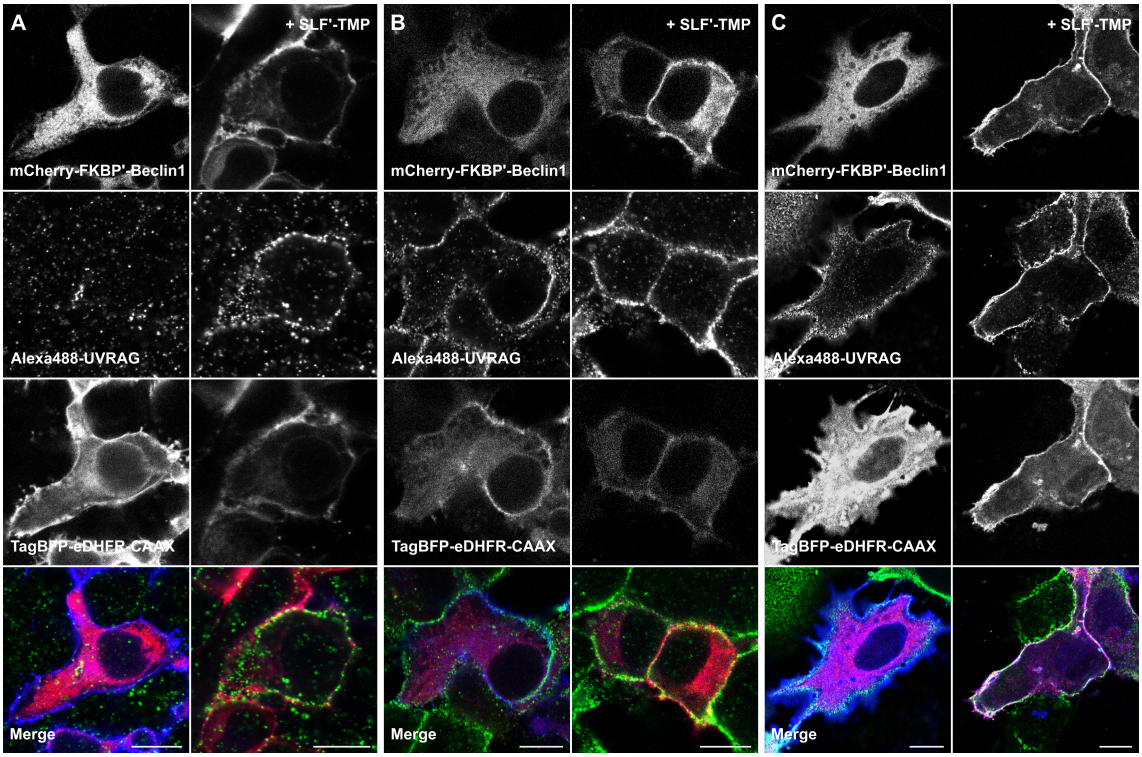

Figure B.4: Cellular localization of overexpressed FKBP'-Beclin1 and immunostained endogenous UVRAG. Cells were starved in EBSS for 1 hour in presence or abscence of SLF'-TMP. Scale bar: 10 µm. **A** FKBP'-Beclin1 attracts endogenous UVRAG to the plasma membrane of HEK293T cells. **B** In HeLa cells, immunostained UVRAG appears to localize to the plasma membrane regardless of SLF'-TMP treatment. **C** In MCF7 cells immunostained UVRAG displays a similar phenotype as in HeLa cells.

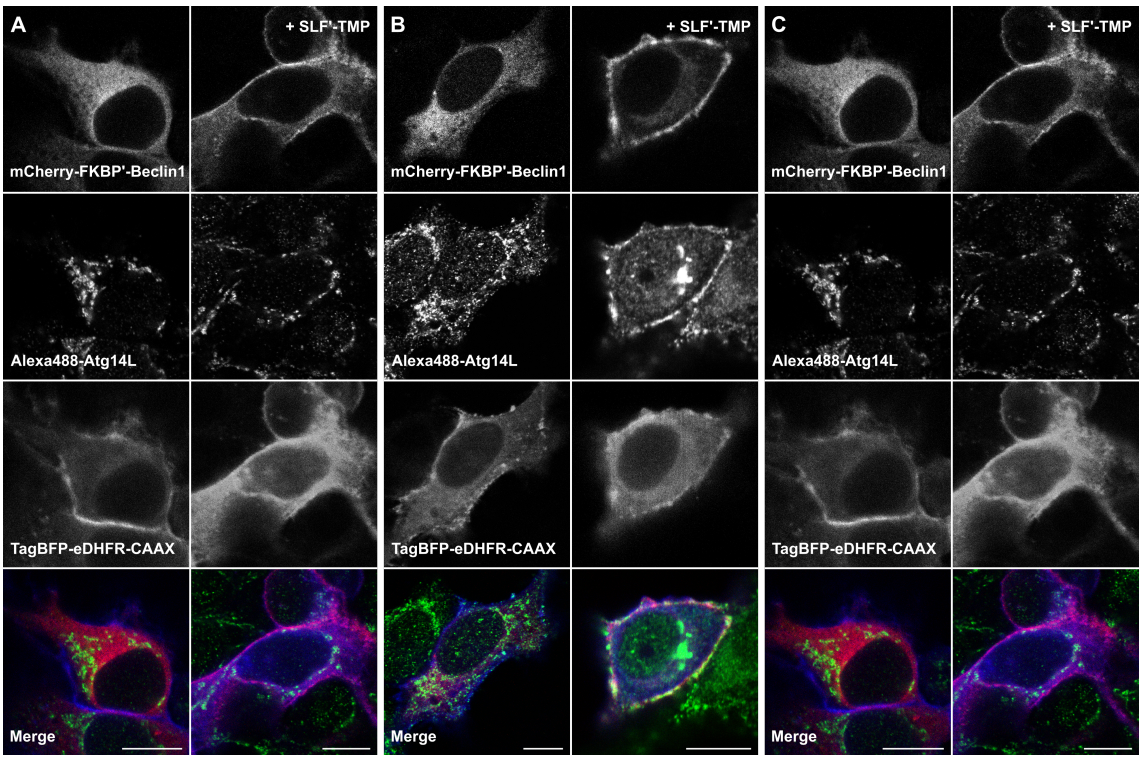

Figure B.5: Cellular distribution of overexpressed FKBP'-Beclin1 and immunostained endogenous Atg14L. Cells were starved in EBSS for 1 hour in presence or abscence of SLF'-TMP. Scale bar: 10 µm. **A** In HEK293T cells, immunostaining for Atg14L shows punctate structures close to the plasma membrane, but no co-localization of FKBP'-Beclin1 and Atg14L. **B** FKBP'-Beclin1 attracts endogenous Atg14L to the plasma membrane of HeLa cells. **C** In MCF7 cells, immunostained Atg14L displays a similar phenotype as in HEK293T cells and appears to localize to punctacte structures.

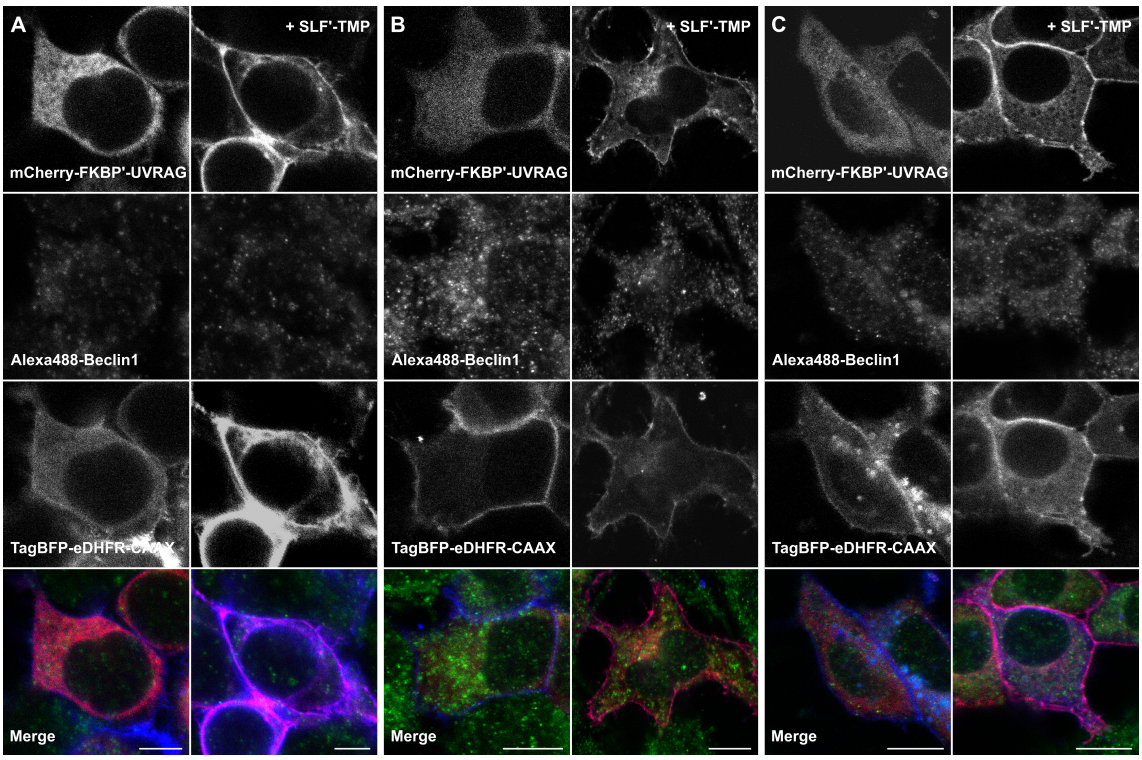

Figure B.6: Cellular distribution of overexpressed FKBP'-UVRAG and immunostained endogenous Beclin1. Cells were starved in EBSS for 1 hour in presence or abscence of SLF'-TMP. Scale bar: 10 µm. **A** In HEK293T cells, immunostaining for Beclin1 shows diffused punctate structures and indicates no co-localization of FKBP'-UVRAG and Beclin1. **B** In HeLa cells, immunostaining for Beclin1 shows more definded punctate structures, but no co-localization of FKBP'-UVRAG and Beclin1 could be detected. **C** In MCF7 cells, immunostaining for Beclin1 indicates diffuse cytoplasmic localization and punctate structures, but no co-localization of FKBP'-UVRAG and Beclin1.

B.2 Modulation of Autophagosome Formation with Knock Off and On

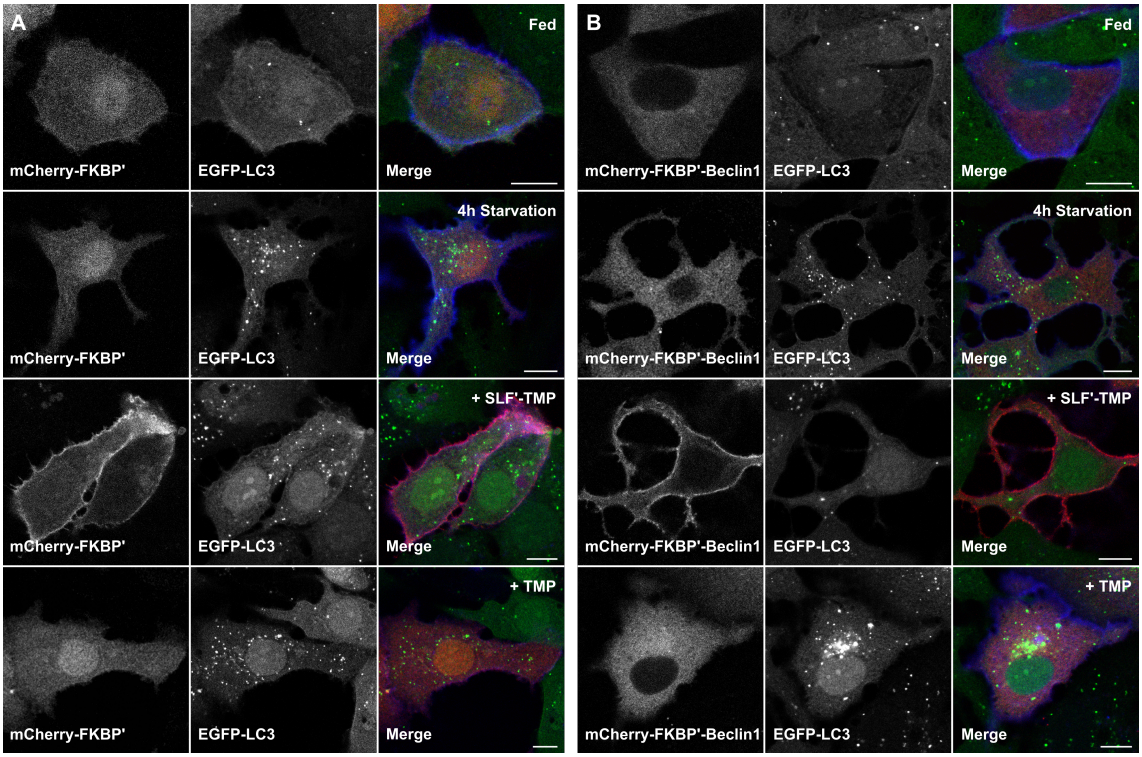

Figure B.7: Knock off of Beclin1 perturbs autophagosome formation in EGFP-LC3-MCF7 cells. **A** MCF7 expressing the control construct mCherry-FKBP' show no reaction to dimerizer addition and autophagosome formation is not affected. **B** Autophagosome formation is inhibited after dimerizer addition in MCF7 cells transfected with mCherry-FKBP'-Beclin1.

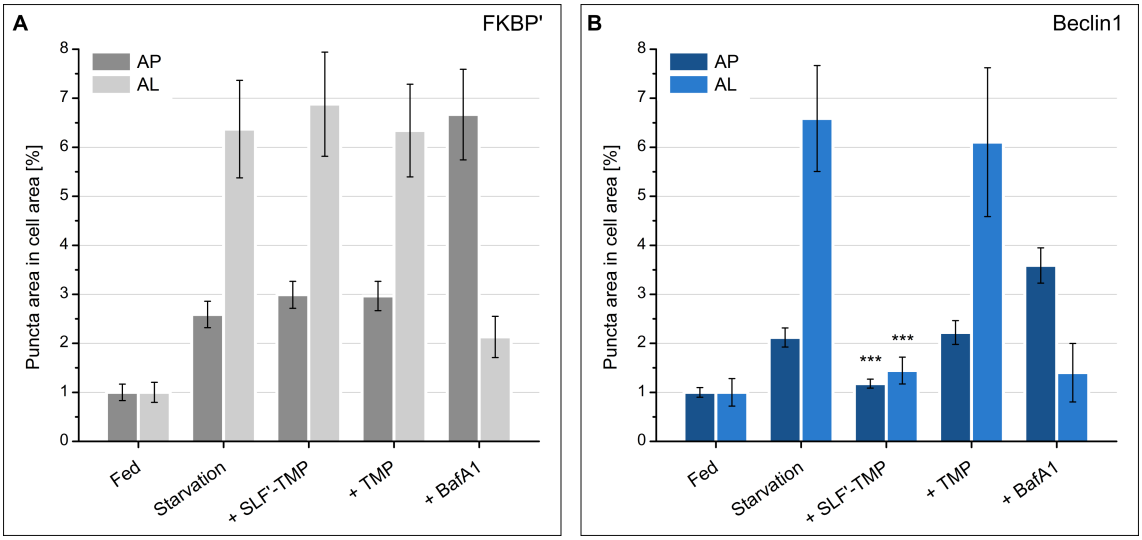

Figure B.8: Knock off of FKBP'-Beclin1 perturbs autophagy flux. mCherry-EGFP-LC3-MCF7 cells were starved in EBSS for 2 hours and simultaneously treated with SLF'-TMP, TMP or BafilomycinA1. AP = Autophagosomes, AL = Autolysosomes. Error bars: weighted mean ± SEM ($n \geq 40$); *** = $p \leq 0.001$; statistical significance was determined by student's t-test against the starvation condition; data was normalized against the fed condition. **A** Mislocalization of FKBP' alone has no effect on autophagosome formation or maturation. BafilomycinA1 treatment causes an increase autophagsomes, but a decrease in autolysosomes indicating blockage of autophagosome maturation. **B** FKBP'-Beclin1 knock off causes a significant reduction of yellow and red puncta suggesting that overall autophagy flux is impaired. The effect can be reversed by addition of TMP. BafilomycinA1 treatment produces the same phenotype as in the control cells expressing only FKBP'.

B.3 UVRAGs Function in Autophagy

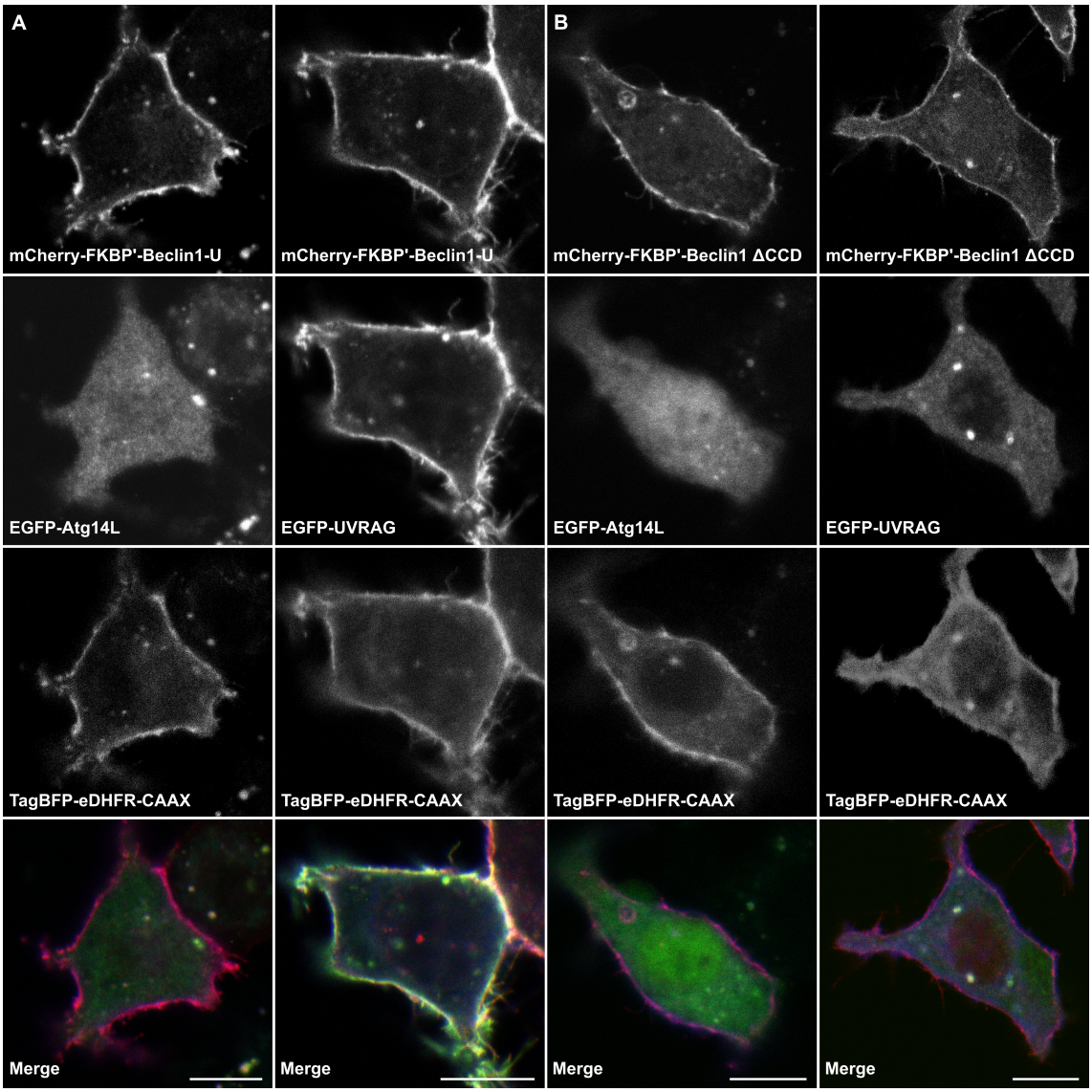

Figure B.9: Interaction of Beclin1-U and Atg14L or UVRAG in MCF7 cells after 2 hours starvation in EBSS and 30 minutes treatment with SLF'-TMP. Scale bar: 10 µm. **A** FKBP'-Beclin1-U cannot mislocalize Atg14L to the plasma membrane suggesting that the construct is deficient in Atg14L binding. FKBP'-Beclin1-U attracts UVRAG to the plasma membrane indicating that UVRAG binding is maintained regardless of the truncation. **B** FKBP'-Beclin1ΔCCD cannot attract Atg14L or UVRAG to the plasma membrane.

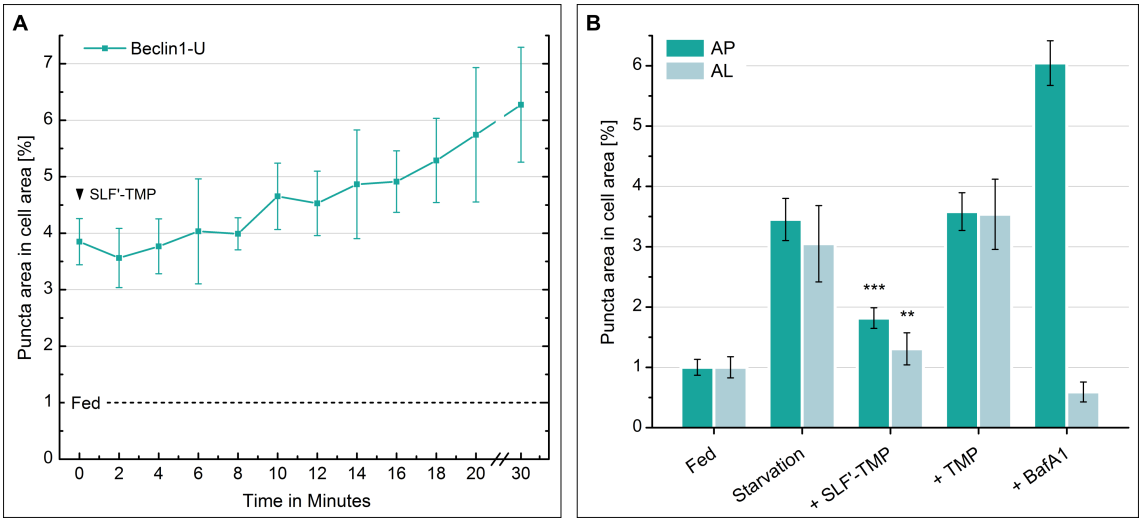

Figure B.10: Mislocalization of enodgenous UVRAG does not affect early autophagosome formation, but modulates autophagosome maturation. Error bars: weighted mean ± SEM ($n \geq 20$ for WIPI assay, $n \geq 40$ for EGFP-mCherry-LC3 assay); ** = $p \leq 0.01$, *** = $p \leq 0.001$; statistical significance was determined by student's t-test against the starvation condition; data was normalized against the fed condition. **A** Knock off of Beclin1-U has no impact on WIPI2b puncta formation. **B** FKBP'-Beclin1-U knock off causes a significant reduction of autophagosomes (AP) and autolysosmes (AL) suggesting that overall autophagy flux is impaired. The effect can be reversed by addition of TMP. BafilomycinA1 treatment produces the same phenotype as in the control cells expressing only FKBP'. mCherry-EGFP-LC3-MCF7 cells were starved in EBSS for 2 hours and simultaneously treated with SLF'-TMP, TMP or BafilomycinA1.

B.4 Spatial Organization of Autophagosome Biogenesis

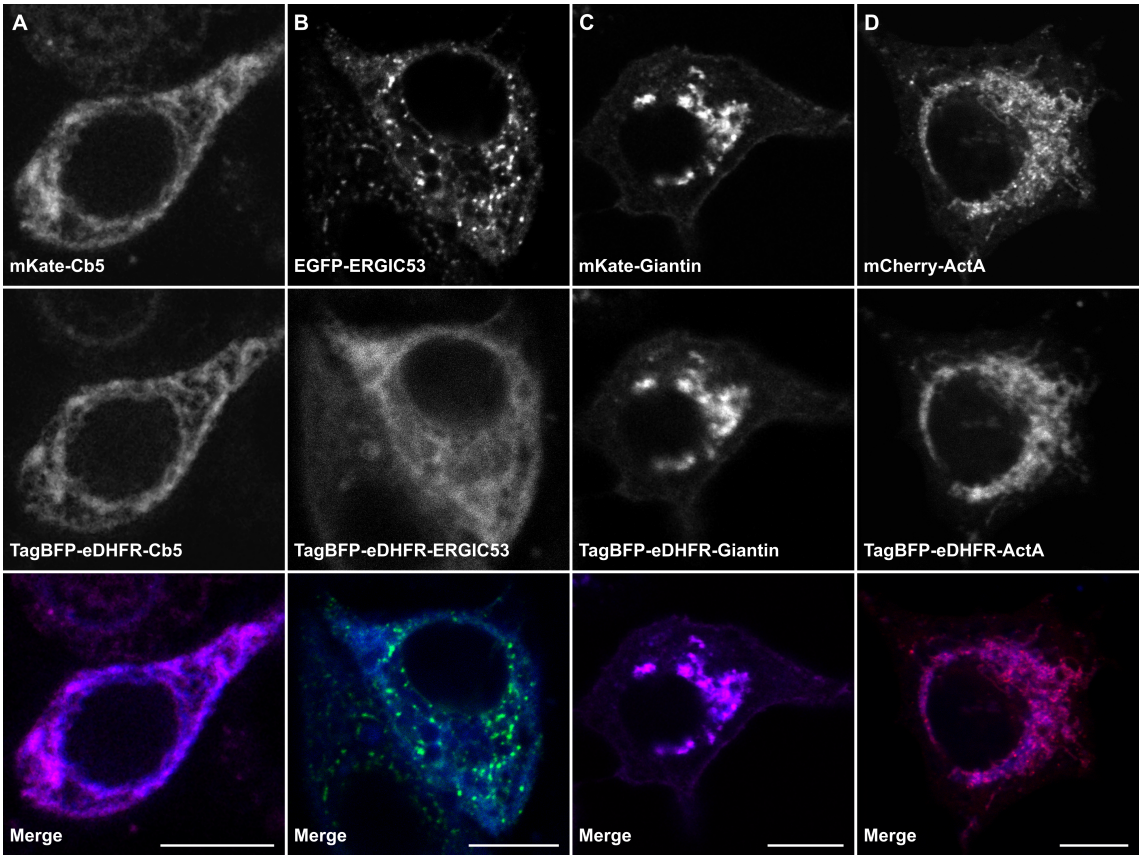

Figure B.11: Bait proteins co-localizing with specific organelle markers. Scale bar: 10 µm. **A** mKate-Cb5 was used to label the ER and co-localizes with TagBFP-eDHFR-Cb5. **B** TagBFP-eDHFR was targeted to the ERGIC using ER-GIC53. **C** mKate-Giantin was employed to visualize the Golgi and TagBFP-eDHFR-Giantin served as cellular Golgi anchor. **D** Mitochondria were labeled with mCherry-ActA and co-lolcalizes with TagBFP-eDHFR-ActA.

Acknowledgments

First, I have to acknowledge my supervisor Dr. Yaowen Wu for giving me the opportunity to join his laboratory, gain a diverse range of experiences and become part of 'Team Autophagy'.

I would also like to express my gratitude to Prof. Dr. Roger S. Goody, who kindly agreed to serve as first examiner of my thesis. Further, I would like to thank Prof. Dr. Philippe Bastiaens for taking the time to serve as second examiner and for being an active member of my thesis advisory committee along with Prof. Dr. Leif Dehmelt. Their feedback and input on the project were very valuable and highly appreciated.

A special thanks goes out to all past and present group members of AG Wu for sharing their expertise, advise and reagents with me. In particular, I would like thank Steffi and my office gang for many fruitful scientific (and not so scientific) discussions and their support during the ups and downs of my PhD. This altogether created a great working-environment.

I am also very thankful to all the members of the CGC and AG Goody, especially Matthias and Amrita, for the countless lunch and coffee breaks we shared - this saved me from entering autophagy on multiple occasions.

I would like to express my deepest gratitude to the IMPRS for financial aid, but most importantly for the opportunity to participate in numerous educational and (on many levels) inspiring meetings, events and workshops. My sincere thanks also goes out to Christa Hornemann, who swiftly removed all administrative obstacles and offered moral support during the trying times of this undertaking.

I am very grateful for the assistance of my master student Ira Schulz and the recurring help of our lab rat Neele Kleffner, whose passion for minipreps and chemistry nicely complemented my indifference towards both.

Further, I wish to thank Petra Geue, Nathalie Bleimling and Dr. Sven Müller for their excellent technical assistance, especially in the beginning of this project.

Finally, the most heartfelt thank you is directed towards Sprockhövel: I am more than grateful to my friends, family and soon-to-be husband for their love, patience, encouragement and distraction throughout the years. I could not have done it without you.

Affidavit (Eidesstattliche Versicherung)

KLEWER, Laura	163846
Name, Vorname (Surname, first name)	Matrikel-Nr. (Enrolment number)

Belehrung:

Wer vorsätzlich gegen eine die Täuschung über Prüfungsleistungen betreffende Regelung einer Hochschulprüfungsordnung verstößt, handelt ordnungswidrig. Die Ordnungswidrigkeit kann mit einer Geldbuße von bis zu 50.000,00 €geahndet werden. Zuständige Verwaltungsbehörde für die Verfolgung und Ahndung von Ordnungswidrigkeiten ist der Kanzler/die Kanzlerin der Technischen Universität Dortmund. Im Falle eines mehrfachen oder sonstigen schwerwiegenden Täuschungsversuches kann der Prüfling zudem exmatrikuliert werden, §63 Abs. Hochschulgesetz NRW.

Die Abgabe einer falschen Versicherung an Eides statt ist strafbar.

Wer vorsätzlich eine falsche Versicherung an Eides statt abgibt, kann mit einer Freiheitsstrafe bis zu drei Jahren oder mit Geldstrafe bestraft werden, §156 StGB. Die fahrlässige Abgabe einer falschen Versicherung an Eides statt kann mit einer Freiheitsstrafe bis zu einem Jahr oder Geldstrafe bestraft werden, §161 StGB.

Die oben stehende Belehrung habe ich zur Kenntnis genommen:

Official notification:

Any person who intentionally breaches any regulation of university examination regulations relating to deception in examination performance is acting improperly. This offence can be punished with a fine of up to 50,000.00 €. The competent administrative authority for the pursuit and prosecution of offences of this type is the chancellor of the TU Dortmund University. In the case of multiple or other serious attempts at deception, the candidate can also be unenrolled, Section 63, paragraph 5 of the Universities Act of North Rhine-Westphalia.

The submission of a false affidavit is punishable.

Any person who intentionally submits a false affidavit can be punished with a prison sentence of up to three years or a fine, Section 156 of the Criminal Code. The negligent submission of a false affidavit can be punished with a prison sentence of up to one year or a fine, Section 161 of the Criminal Code.

I have taken note of the above official notification.

Dortmund, 23.06.2017	
Ort, Datum (Place, date)	Unterschrift (Signature)

Titel der Dissertation:
(Title of the thesis): **Knock off and on: a novel approach to autophagy modulation**

Ich versichere hiermit an Eides statt, dass ich die vorliegende Dissertation mit dem Titel selbstständig und ohne unzulässige fremde Hilfe angefertigt habe. Ich habe keine anderen als die angegebenen Quellen und Hilfsmittel benutzt sowie wörtliche und sinngemäße Zitate kenntlich gemacht.

Die Arbeit hat in gegenwärtiger oder in einer anderen Fassung weder der TU Dortmund noch einer anderen Hochschule im Zusammenhang mit einer staatlichen oder akademischen Prüfung vorgelegen.

I hereby swear that I have completed the present dissertation independently and without inadmissible external support. I have not used any sources or tools other than those indicated and have identified literal and analogous quotations.

The thesis in its current version or another version has not been presented to the TU Dortmund University or another university in connection with a state or academic examination.*

*Please be aware that solely the German version of the affidavit ("Eidesstattliche Versicherung") for the PhD thesis is the official and legally binding version.

Dortmund, 23.06.2017	
Ort, Datum (Place, date)	Unterschrift (Signature)